The effect of ApoE4 on Neurovascular Coupling in the Visual Cortex

Orla Bonnar
School of Psychology
University of Sussex

Submitted for the degree of
Doctor of Philosophy
August 2020

Declaration

I hereby declare that this thesis has not been and will not be submitted in whole or in part to another University for the award of any other degree.

Signature:

Orla Bonnar

UNIVERSITY OF SUSSEX

Orla Bonnar

Submitted for the degree of

Doctor of Philosophy

Summary

Neurovascular coupling (NVC) is the process whereby the brain increases local blood supply in response to neuronal activity, providing neurons with energy. Disruptions to NVC have been implicated in Alzheimer's disease (AD), so a better understanding of how NVC goes wrong, and when, is imperative for better understanding the disease and assisting in the identification of therapeutic targets. The main genetic risk factor for developing AD, expression of Apolipoprotein $\epsilon 4$ (APOE4), is associated with vascular deficits, including pericyte damage and impaired cerebral blood flow. I tested whether expression of APOE4 affected NVC, by studying neuronal activity and vascular responses in visual cortex.

To investigate this, mice with humanised APOE4 or APOE3 were crossed with mice expressing a genetically-encoded calcium indicator or with labelled pericytes. Mice were implanted with a cranial window over visual cortex and neuronal and vascular activity was recorded using two-photon microscopy. Baseline and stimulus evoked measurements were taken to determine the effect of ApoE4 on basal energy balance and on the ability of the brain to deliver adequate energy to neurons.

Results suggest that there were some baseline alterations in APOE4 mice that may result in a lower energy supply. Compounding this,I found there to be a mismatch in energy supply and demand during sensory stimulation, where neuronal demand was greater, but blood supply was less reliable in APOE4 mice.

Together these data suggest that there could be an energy deficit in APOE4 carriers. In vivo studies investigating the role of ApoE4 in NVC are few and the study of individual vessels and neurons across different age points, as done in this body of work, is a novel and unique approach. By better understanding how ApoE4 modulates neurovascular function, we can better understand its role in AD pathology and possibly identify therapeutic targets in the future.

Acknowledgements

To begin with, Catherine you deserve a world of thanks and more. You have been amazing in so many ways and I feel so incredibly lucky to have had you guide me through my PhD. To have a mentor like you who is not only incredibly clever, driven and successful but also kind and approachable, who takes the time to care for their students both academically and personally - I feel like I won the supervisor lottery! You have taught me to believe in myself and have provided me with so many opportunities that I am so grateful for. Thank you for all of this and more, you have been, and will continue to be a great inspiration to me.

Then to my 5D15 friends, what a spectacular bunch of people you are, I could never in my wildest hopes have wished for a better ensemble of lab mates. Kira - what can I say, the two headed beast that is us has been a joy, not only because we both love company, but because you have been the most helpful, patient person throughout my PhD. I know we always joke about "paying it forward" but I truly will never forget how much you have done to aid me in this process. You have also been such a good friend and support to me - I can't think how many hours we have spent together chatting about our lives, our mutual scardey-cat tendencies, yummy food, data, analysis, blood vessels and about how much we hate the 25X (I would have hated it 100 times more without you) and literally EVERYTHING else in between. Thank you 10000 times over. Dori, my lovely pal. You have been a treat and I am so glad we have become such good friends - you have taught me so much, both about science-y things and about life as well, I truly believe I am a better person (and coder!) because of you. My years at Sussex would have been far less special without you in them. Katie, as you know, I think you are the funniest person on planet earth, you kept me laughing SO much during the joyous 2 years we had in the office together. Of course you are so much more than funny, you are also extremely kind, clever and a really excellent friend. I feel so lucky to have had you right from the beginning - it would not have been anywhere near as wonderful without you. Devin, you are just the most excellent human. Over the years you have inspired and amazed me with your hard work and drive (and with you commitment to beds of frozen vegetables!). Thank you for

being such a grounding and calming presence during my PhD and for being such a pro in the karaoke booth, you are a gem. Laura, how would I have managed without you during these years? You have been such a help and have always been so generous with your time in teaching us your skills, I am so grateful for that. You are amazing and I am so glad we got to work together for so long. Silvia, to have someone as great as you join us has been such a treat and you have brought so much to our group! You have been really thrown into things this year and have coped better than I ever could have - I am amazed and inspired by you and hope I can learn as quickly when I move to my new lab. Harry - as I write this we have met only once in person! All I can say is that I hope you love being part of this wonderful group as much as I have, I am positive you will. Thank you for your help with my analyses and for all the amazing work I'm sure you will do for Hall lab in the future.

To the members of the DTC - being part of this group has been such a pleasure. Not only has it been so exciting to be part of an ever growing group of ApoE researchers, but it has been such a valuable learning environment for me. To have people to talk to about all things ApoE4 has been truly exceptional and I thank all of you for being part of my PhD experience. Jenny and Louise, you have both been wonderful leaders of the group, thank you for assembling such an exceptional bunch of people and for doing such a great job of making everyone feel enthused, supported and valued. Thank you for all you have done for me personally, I have always felt an extra layer of support as a part of the DTC. Thank you to the BRF for the help and hard work in looking after my animals and for teaching me so much with kindness and patience.

To Sussex Neuroscience, for having such excellent PG support available, your generous funding enabled me to attend two of my most memorable PhD events, thank you so much.

To OC, my soulmate best friend sister! As with all my endeavours you have been as supportive as is humanly possible to be, cheering me on, asking for constant updates and being generally fabulous. Your presence in my life makes me able to cope when things get hard- you are a lifeline to me. I will eternally love you 2π and will always be the Frankie to your Grace.

Mattie, where do I even start? You have provided more support to me than I could have ever hoped for, thank you for endlessly believing in me and for being such a kind and amazing human. You've been there for me when it felt like too much and, importantly, you've always known when to turn on Queer Eye and let the Fab 5 work their magic.

PhDs are notoriously stressful and I am so sure mine would have been 100 times harder without you, you have carried some of that stress alongside me and I feel just too lucky to have you in my life. Thank you so much for being next to me through all of it.

Finally, to my parents, my original and greatest cheerleaders. I would never have embarked on this PhD journey without your support and love, throughout my life you have made me feel like I could do and achieve anything, that the world really was my oyster. I truly think it is only this belief that you both instilled in me that gave me the confidence to apply for this PhD. For that and so many other things I am so grateful.

Contents

List of Tables

List of Figures

List of Abbreviations

20-HETE 20-Hydroxy-icosatetraenoic Acid
Ach Acetylcholine
ATP Adenosine Triphosphate
αSMA Alpha Smooth Muscle Actin
AD Alzheimer's disease
APP Amyloid Precursor Protein
ALS Amyotrophic Lateral Sclerosis
Aβ Amyloid Beta
APOE Apolipoprotein E
APOE-KI APOE- Knock In
AA Arachidonic Acid
AUC Area Under the Curve
BBB Blood Brain Barrier
CBF Cerebral Blood Flow
CAA Cerebral Amyloid Angiopathy
$CMRO_2$ Cerebral Metabolic Rate of Oxygen
CNS Central Nervous System
CV Coefficient of Variation
cGMP Cyclic Guanosine Monophosphate
COX-1 Cyclooxygenase -1
CSF Cerebrospinal fluid
CypA Cyclophilin A
EOAD Early Onset Alzheimer's Disease
ET_A Endothelin A
FFT Fast Fourier Transform
FITC dextran fluorescein isothiocyanate-dextran
FTD Frontotemporal Dementia
FWHM Full Width at Half Maximum
GABA Gamma aminobutyric acid
GUI Graphical user interface
HbD Deoxygenated Haemoglobin
HbO Oxygenated Haemoglobin
HbT Total Haemoglobin
HDL High-density Lipoproteins.
hiPSCs Human Induced Pluripotent Stem Cells
$K_{IR}2$ Inward Rectifier Potassium Channel
LRP Lipoprotein receptor related protein-1
LDF Laser Doppler Flowmetry
LFP Local Field Potential
LOAD Late Onset Alzheimer's Disease
NA Noradrenaline
NG2 Neuron-Glial Antigen 2

NMDA N-methyl-D-aspartate
nNOS Neuronal Nitric Oxide Synthase
NO Nitric Oxide
NOR Novel Object Recognition
NPY Neuropeptide Y
NVU Neurovascular Unit
NVC Neurovascular Coupling
NVCi Neurovascular Coupling Index
OEF Oxygen Extraction Fraction
SO_2 Oxygen Saturation
PBS Phosphate-buffered-saline
PDGFRβ Platelet Derived Growth Factor Receptor Beta
PFA Paraformaldehyde
PG Prostaglandin
PGE_2 Prostaglandin E_2
PPM Peaks per Minute
PSD-95 Postsynaptic density protein 95
PSEN Presenilin
RAGE Receptor for Advanced Glycation End Products
RBCV Red Blood Cell Velocity
ROI Region of Interest
ROS Reactive Oxygen Species
SEM Standard Error of the Mean
SMC Smooth Muscle Cell
SNAP s-notroso-N-acetylpenicillamine
SOR Spatial Object Recognition
VLDL Very-low-density Lipoprotein.

Chapter 1

Introduction

Disruptions to the neurovasculature have been implicated in a number of conditions, including Alzheimer's Disease (AD), yet the details of how and when these may occur are poorly understood. Carriers of the $\epsilon 4$ allele of the Apolipoprotein E gene, are at an increased risk of developing AD, and evidence shows there to be a myriad of deleterious interactions between ApoE4 and the vasculature early in the disease process (Zlokovic, 2013). Therefore, a better understanding of how ApoE4 might modulate vascular function is imperative for furthering our understanding of its role in AD pathophysiology and thus aid in the identification of potential therapeutic targets.

One of the key functions of the neurovasculature is to increase local blood supply, and therefore energy delivery, in response to neuronal activity, a process called neurovascular coupling (NVC). In this chapter I will discuss the importance of NVC in the healthy brain, how neurons communicate with the vasculature to induce dilatations and how the dilations are conducted along the vasculature.

There is plentiful evidence to suggest that there is vascular dysfunction in AD and that it may be one of the earliest features of the disease, indeed many of the risk factors for developing AD have a vascular component and also increase the risk of developing cardiovascular diseases (Livingston et al., 2017). I will discuss, in brief, the main characteristics of AD, alongside evidence that shows vascular dysfunction to be a key player in the disease process. This includes disruption to the vascular anatomy, cerebral blood flow, altered neurovascular coupling and interactions between the vasculature and the two pathological hallmarks of AD - amyloid beta and hyperphosphorylated tau.

As vascular dysfunction is thought to first occur early in the disease trajectory, prior to the accumulation of amyloid beta and hyperphosphorylated tau (Iturria-Medina et al., 2016), it is essential that we understand how deficits occurs in the absence of these proteins and

how they might facilitate disease progression. The biggest greatest risk for going on to develop AD is the APOE4 gene, and evidence shows that disruption to vascular function is an early feature of ApoE4 pathophysiology (Zlokovic, 2013). I will discuss the physiological role of APOE in the healthy brain before exploring the existing evidence showing the role of ApoE4 in AD and, importantly, how it interacts with the neurovasculature in a manner that is independent from amyloid beta and hyperphosphorylated tau. I suggest that over time, these interactions could lead to an energy imbalance in the brain as a result of inadequate blood supply, leading to neuronal ill-health and eventually the accumulation of amyloid beta and hyper-phosphorylated tau.

This body of evidence supports the "Two Hit Hypothesis of Alzheimer's Disease" proposed by Berislav Zlokovic (Zlokovic, 2011). In this hypothesis he suggests that AD consists of two "hits" that converge. "Hit" one is vascular dysfunction as a result of a risk factor such as ApoE4. The downstream effects of this vascular dysfunction facilitate "hit" two, the production of amyloid beta and pathological tau, eventually leading to the neurodegeneration and cognitive decline observed in AD.

It is the hope that the presentation of this existing evidence demonstrates that, in agreement with the two hit hypothesis, investigation into the effect of ApoE4 on the neurovasculature and the functional hyperaemia response, as is carried out in this thesis, is a valuable and important research avenue.

1.1 Neurovascular Coupling

The brain has a limited ability to store energy in the form of oxygen and glucose and so relies upon the delivery of these substrates via the blood, a process termed neurovascular coupling (NVC). In fact, the brain is so energetically demanding, it constitutes only 2% of the body's mass but utilises 20% of its available energy at rest (Attwell et al., 2010; Attwell and Laughlin, 2001). The majority of this energy consumption (50%) is at postsynaptic glutamate receptors, where it is used for the reversal of ions against their electrochemical gradients, with 21% of signalling energy being used on action potentials and 20% on resting potentials (Howarth et al., 2012). This phenomenon of neurovascular coupling was first described in the late 1800's in humans by Mosso (1880) and in animals by Roy and Sherrington (1890). Despite a paucity of interest in the field in the following decades, NVC is now a process that is widely researched and is accepted as one of the brain's many fundamental and critical functions.

This demand for a constant energy supply in response to neuronal activity within the brain, has resulted in a dense network of cerebral vasculature. In neocortex, this network is composed of anatomically heterogeneous blood vessels (see figure 1.2), with large pial arterioles, enwrapped in several layers of smooth muscle cells (SMCs), that are present across the surface of the brain before they dive into the tissue and transition into penetrating arterioles. Penetrating arterioles are encased in astrocytic endfeet, as well as a thinner layer of SMCs. As the SMCs thin to a single layer and the arterioles branch to form a dense capillary network, SMCs are replaced with pericytes, encased within the basement membrane and also enwrapped in astrocytic endfeet. Blood is then drained from the capillaries by venules which transition to ascending veins and then large pial veins (Kisler et al., 2017a; Iadecola, 2017; Mishra, 2017). Much interest exists in how the properties of NVC may vary across this so called vascular tree, and in the cellular mechanisms and signalling pathways that underlie the communication between activated neurons and the vasculature. Despite the wide body of research that exists on this subject, many controversies and uncertainties still abound.

1.1.1 Signalling Pathways

Historically it was believed that this blood flow increase, observed in response to an increase in neuronal activity, was as a result of a negative feedback loop whereby metabolic changes would signal an increase in blood flow. However increasing blood oxygen levels and decreasing blood glucose levels did not alter the increase in blood flow in response to neuronal activity (Powers et al., 1996; Lindauer et al., 2010). Numerous studies, such as those demonstrating blood flow changes in response to glutamate (Fergus and Lee, 1997), have enabled us to conclude that it is, in fact, a primarily feed forward mechanism that results in blood flow increases following the release of vasoactive messengers. Various mechanisms have been identified in this process, both direct neuronal effects on the vasculature, as well as astrocyte-mediated pathways. Despite the multitude of studies that exist, uncertainty still prevails when it comes to identifying the exact pathways involved, the timing and the site of action.

Effect of pial innervation and subcortical inputs on vascular tone: Pial arteries are highly innervated by peripheral nerves which can release vasoactive substances, and in the cortex, the vasculature receives input from subcortical areas (basal forebrain, locus correleus, raphe nucleus), resulting in the release of vasoactive substances such as acetylcholine (Ach), noradrenaline (NA) and serotonin respectively. These innervations are thought to affect cerebral blood flow (CBF) over large regions and likely contribute more to resting vascular tone rather than the neurovascular coupling response (Hamel, 2006; Mishra, 2017; Iadecola, 2017).

Excitatory neuronal control of vascular tone: Glutamate has been long been shown to cause local vascular dilations (Fergus and Lee, 1997) and this combined with the knowledge that much of the energy supply used by the brain is at postsynaptic glutamate receptors (Howarth et al., 2012), means that the mechanism behind glutamate evoked vascular responses is of particular interest. Direct neuronal effects on the vasculature occur as a result of glutamatergic activation of postsynaptic N-methyl-D-aspartate (NMDA) receptors. The subsequent rise in intracellular Ca^{2+} activates nitric oxide synthase (nNOS) to produce nitric oxide (NO), resulting in a vasodilation in SMCs as a result of the produced cyclic guanosine monophosphate (cGMP) (Attwell et al., 2010; Busija et al., 2007). As well as this primary pathway, direct neuronal modulation of the vasculature arises from the release of the SMC relaxant adenosine, as a result of ATP hydrolysis (Ko et al., 1990; Lovatt et al., 2012) and the release of potassium from neurons during the repolarisation phase of the action potential via a variety of K^+ channels. The

potassium acts upon the vasculature to hyperpolarise the SMCs present on arterioles, causing a vasodilation (Longden et al., 2017).

Astrocytic control of vascular tone: Glutamate also modulates vascular tone via astrocytic signalling. Astrocytes are well positioned to mediate the neurovascular coupling response as their endfeet are wrapped around much of the vasculature. In response to neuronal glutamate release, there is an increase in astrocytic calcium and a downstream modulation of vascular activity. However some debate exists over the timing of the astrocytic response, with some groups reporting calcium changes in astrocytes that occur after vascular dilation (Nizar et al., 2013), suggesting they would be too slow to be responsible for the functional hyperaemia response. Other groups have found rapid calcium signalling in astrocytes (Lind et al., 2013), as well as the slow responses, that mean they could indeed play a role in the neurovascular coupling response, see Mishra (2017) for a review. A study from Mishra et al. (2016) has helped to shed light on the specific, previously unclear, mechanisms underlying astrocytic control of vascular tone by identifying that astrocytes are essential for signalling to capillaries but that this identified signalling pathway did not contribute to vascular changes observed at the arteriole level. In this elegant study, calcium increases in the astrocyte (that were found to be independent of calcium increases in the neuron as a result of NMDA receptor activation), as a result of glutamatergic synaptic activity and subsequent post synaptic ATP release, were found to be necessary for dilation of capillaries but not arterioles. This dilation was found to be mediated by the activation of the $P2X_1$ receptor on astrocytes, not the activation of mGluR1 or mGluR5 receptors that were originally thought to be involved. Following the increase in Ca^{2+}, arachidonic acid (AA) was produced via a phospholipase D2-phosphatidic acid-diacylglycerol (PLD_2-PA- DAG) pathway. The AA was metabolised to the vasodilator prostaglandin E_2 (PGE_2) by cyclooxygenase -1 (COX1) and thus acted on the EP_4 receptor present on pericytes, resulting in vasodilation. This pathway was found to be distinctly different to that which mediates arteriolar dilations, blocking the NMDA receptors and NOS strongly reduced arteriolar dilations, unlike capillary dilations, and chelation of astrocytic calcium, which diminished capillary dilation, had no effect on the observed arteriolar dilation. This study demonstrated two distinct pathways by which glutamate signals to the capillaries and arterioles. They also suggested that AA may also be metabolised to epoxyeicosatrienoic acids (EETs) or prostaglandins (PGs) that could act on the arteriolar component (Mishra et al., 2016). AA itself may also directly act on vascular SMCs to produce the vasoconstrictor 20-hydroxy-eicosatetraenoic

acid (20-HETE) although its formation is inhibited by NO. Similar to the mechanism described above following neuronal K^+ release, there is also thought to be a dilatory effect due to the release of K^+ from astrocytic endfeet, ensuing an increase in intracellular calcium, and the resultant activation of large conductance Ca^{2+}-activated K^+ channels. This K^+ acts upon the vasculature to hyperpolarise the vascular SMCs (Filosa et al., 2006).

Interneuron control of vascular tone: In addition to glutamate released from excitatory neurons, evidence is emerging highlighting a role for inhibitory interneurons in the neurovascular coupling response via the vasodilator NO and the vasoconstrictor neuropeptide Y (NPY) (Cauli et al., 2004; Cauli and Hamel, 2010). A study using optogenetic activation of interneurons, induced an increase in CBF similar to that seen in response to a sensory stimulation as well as producing a constriction that was attributed to NPY (Uhlirova et al., 2016). In addition, it has been demonstrated that the selective activation of nNOS- or SST-expressing interneurons results in haemodynamic changes, showing that there is a role for interneurons in modulating vascular tone (Lee et al., 2020) .

Low oxygen levels modulate vascular tone: Oxygen levels also affect NVC, at low $[O_2]$ there is an increase in lactate release by monocarboxylate transporters, preventing the reuptake of the vasodilatory PG, resulting in vasodilation (Gordon et al., 2008)). There is also an increase in adenosine production, which itself is vasodilatory and also inhibits the vasoconstrictor 20-HETE. Low $[O_2]$ may also limit the amount of NO and 20-Hydroxy-icosatetraenoic Acid (20-HETE) that is produced (Attwell et al., 2010). Finally, low oxygen levels cause red blood cells to increase their deformability and thus increasing flow through capillaries (Wei et al., 2016), demonstrating the varied roles $[O_2]$ levels have in modulating the neurovascular coupling response. Interestingly, these studies show that, although the trigger for the functional hyperaemia is likely feed forward as discussed above, there may also be a metabolic feedback modulation of the response.

*The role of Caveolae:*A recent study from Chow et al. (2020), showed the presence of caveolae, small "pits" in the plasma membrane, in arteriole endothelial cells that are absent in capillary endothelial cells. The primacy of these caveolae in the arteriolar dilation in response to a sensory stimulation was highlighted, however their exact role remains unclear. The investigators demonstrated that the mechanism is independent of NO signalling and given the ability of caveolin 1 deficient mice (that lack caveolae in the arteriolar endothelial cells) to vasodilate in response to NO, it is unlikely that the caveolae provide a membrane reservoir to facilitate vasodilation, as postulated previously.

The authors suggest that it is likely that the caveolae may cluster ion channels that play a role in NVC and this may aid the transmission of vasodilatory signals to smooth muscle cells, but ultimately the mechanism and cell signalling pathways remain unknown(Chow et al., 2020).

In summary, the signalling pathways involved in neurovascular coupling are complex and multifaceted and depend on a number of variables such as the vascular compartment involved and $[O_2]$ levels. See figure 1.1 for a summary.

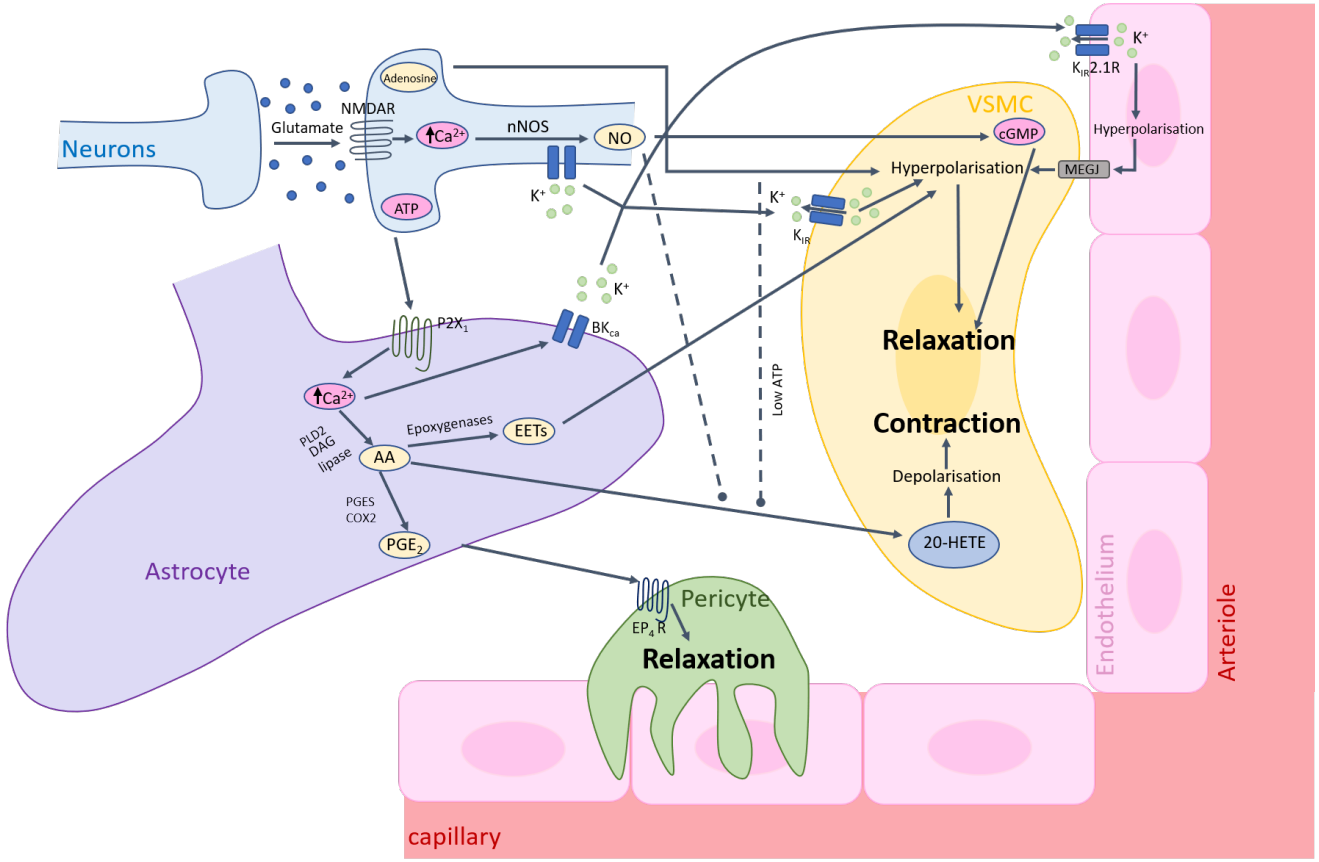

Figure 1.1: **NVC signalling pathways** Following the release of glutamate, neurons signal directly to arterioles via the release of the vasodilators NO and adenosine. Post synaptic ATP release activates the $P2X_1$ on astrocytes resulting in the downstream release of the vasoactive AA, PGE_2 and EETs. PGE_2 acts on the EP_4 receptor on pericytes to cause a relaxation, whilst EETs may hyperpolarise VSMCs, leading to a relaxation and a vascular dilation. AA itself is metabolised to the vasoconstrictor 20-HETE in VSMCs, however this synthesis is inhibited by NO and adenosine. Potassium released from neurons and astrocytes activate inward rectifying potassium channels on VSMCs or endothelial cells, resulting in the efflux of potassium from the cell, causing hyperpolarisation. Endothelial depolarisation travels to VSMCs via myodendothelial gap junctions. (NMDAR = N-methyl-D-aspartate (NMDA) receptors, ATP = Adenosine triphosphate, nNOS = nitric oxide synthase, NO= nitric oxide, cGMP = cyclic guanosine monophosphate, $K_{IR}2$ = Inward rectifier potassium channel , 20-HETE = 20-hydroxy-eicosatetraenoic acid, $P2X_1$ = P2X purinoceptor 1 , PGE_2 = Prostaglandin E_2 , AA = arachidonic acid , EETs = epoxyeicosatrienoic acids, PLD2 = phospholipase D2, DAG lipase = diacylglycerol lipase, PGES = Prostaglandin E synthase, COX2= Cyclooxygenase 2, BKtextsubscriptca = Ca^{2+}-activated K^+ channelsm MEGJ = myoendothelial gap junctions.) Adapted from Attwell et al. (2010); Kisler et al. (2017a); Mishra et al. (2016)

1.1.2 Propagation of Signals

These vasoactive messengers produced following neuronal activation within the brain tissue are unlikely to have the ability to travel the relatively long distances to the large surface pial arteries and arterioles. Nevertheless, these vessels are important in the execution of the neurovascular response, dilating in response to neuronal activity, supporting the idea that there must be a degree of signal propagation from somewhere else in the vascular tree (Kisler et al., 2017a). In contrast to the pial arteries and arterioles, brain capillaries are, on average, <15μm from the closest neuronal cell body (Tsai et al., 2009a), meaning they are ideally positioned to sense signals released by neuronal activation and communicate these dilations upstream. In 1997, a study in rats demonstrated that stimulation of cerebellar fibres produced an increase in vascular diameter and CBF upstream from the activated area, in the absence of local field potential (LFP) changes next to these upstream vessels (Iadecola et al., 1997). This idea of a retrograde conduction of vascular signals from the activated area to upstream vessels was bolstered by Chen et al. (2014) who demonstrated the critical role endothelial cells play in conducting this response by selectively disrupting endothelial cells in a single pial arteriole that had previously dilated in response to sensory stimulation. This disruption resulted in an attenuated response to stimulation, showing the key role for endothelial cells in the propagation of these signals (Chen et al., 2014). Evidence shows that inward rectifier potassium channels (K_{IR}), specifically those from the $K_{IR}2.1$ subfamily, are key mediators in propagating the dilatory response. Capillary endothelial cells are enriched with $K_{IR}2.1$ channels, which are sensitive to K^+ released from neighbouring synapses or from the encasing astrocytic endfeet. In one study, when K^+ was applied to capillaries, a robust dilation was recorded in upstream arterioles as a result of the rapid activation of the $K_{IR}2.1$ channels and a subsequent retrograde transmission of a hyperpolarising signal to upstream arteriolar smooth muscle via myoendothelial gap junctions. In vivo studies further buttressed the role of $K_{IR}2.1$ channels as key players in the propagation of this hyperpolarising signal, as increases in CBF in response to the application of K^+ and haemodynamic responses to sensory stimulation were blunted in endothelial cell $K_{IR}2.1^{-/-}$ mice, as well as in the presence of the relatively specific $K_{IR}2$ blocker, barium (Longden et al., 2017).

In light of this evidence, it is likely that the functional hyperaemia response consists of two elements, the local response following the release of vasoactive messengers from nearby astrocytes and neurons as well as a propagated component originating from downstream vessels.

1.1.3 Site of signal initiation

As well as propagating signals, a further role for capillaries in the functional hyperaemia response is a source of much debate in the field, specifically whether or not they themselves actively dilate in response to neuronal activity, and what role pericytes play in this. Pericytes are cells which are present along the walls of capillaries and whose roles are multifaceted, including maintenance of blood brain barrier (BBB) integrity, angiogenesis, glial scar formation and blood flow control in the brain (Attwell et al., 2016; Hall et al., 2014). Canonically, the neurovascular coupling response was thought to be as a result of arteriolar smooth muscle dilation, however a convincing body of evidence has emerged endowing brain capillaries with the ability to actively dilate to increase blood flow, as a result of the relaxation of capillary pericytes (Peppiatt et al., 2006; Kisler et al., 2017b; Hall et al., 2014; Mishra et al., 2016). Pericytes actively respond to synaptic activation with calcium decreases (Rungta et al., 2018), capillaries that branch directly off penetrating arterioles (termed 1st order capillaries) dilate to sensory stimulation before the connected arteriole, suggesting that they actively dilate, rather than in response to upstream pressure changes (Kisler et al., 2017b; Hall et al., 2014; Cai et al., 2018) and dilations have been shown to be more frequent and larger at pericyte locations compared to locations where pericytes are absent (Kisler et al., 2017b; Hall et al., 2014). In a mouse model of pericyte deficiency, Kisler et al. (2017b) found neurovascular coupling responses to be blunted and hypoxic pockets were observed in the parenchymal tissue (Kisler et al., 2017b), however in a similar study from (Watson et al., 2020) the only difference they observed in the same pericyte deficient model was an increase in blood flow through the capillary bed. It is thought that these incongruous findings could be attributed to differences in mouse background and therefore severity of the pericyte loss (Watson et al., 2020). Indeed in a recent preprint from the same laboratory, they use optogenetic approaches to conclude that pericytes may indeed contribute to the slow regulation of flow within capillaries (Hartmann et al., 2020). Despite this body of work, arguments against there being an active role for pericytes in the dilation of capillaries and modulation of CBF in response to neuronal activity, still exist (Wei et al., 2016; Fernández-Klett et al., 2010; Hill et al., 2015).

A large share of this debate exists due to disagreement over the nomenclature of pericytes. Pericytes are morphologically heterogeneous (Attwell et al., 2016; Grant et al., 2019) with smooth muscle cells on the arteriolar side which posses wide processes and no visible cell body. The SMCs transition to pericytes with visible soma and circumferential processes,

with classically termed "bump on a log" morphology, these processes become increasingly longitudinal and eventually become stellate in their morphology at the venular side (Attwell et al., 2016). These various pericyte subtypes are not only morphologically varied but they also differ in their contractile machinery, with the circumferential processes on lower branching orders (i.e. those closer to the penetrating arterioles) containing more smooth muscle α-actin (αSMA) (Attwell et al., 2016; Grant et al., 2019). In one study, these αSMA containing pericytes were reclassified as "pre-capillary smooth muscle cells", leading researchers to inevitably conclude that pericytes were non-contractile and therefore did not play a role in the control of blood flow in the brain (Hill et al., 2015). In an attempt to standardise the semantics used when describing pericytes, subtypes have been termed "ensheathing pericytes", which are present on lower order branches (i.e. those closer to the penetrating arteriole), have a high level of vessel coverage, posses αSMA and are generally accepted to be contractile. "Mesh pericytes" are present on higher order branches with intermediate vessel coverage and no αSMA and finally, "thin-strand" pericytes, also on higher branch orders with long thin processes and again, posses no αSMA (Grant et al., 2019). As aforementioned, it is a subject of controversy whether or not the mesh and thin strand pericytes have the ability to contract or dilate capillaries and indeed debate exists on whether or not capillaries even actively dilate, rather than their diameter change being a passive response to an upstream dilation. Several groups refute the evidence previously discussed, and have failed to see the dilation of capillaries (Hill et al., 2015; Wei et al., 2016; Longden et al., 2017). Perhaps this was due to methodological differences such as animal preparation, imaging resolution or the presence of a pericyte on the imaged capillary sections, or perhaps these differences in results arise from variations in the nomenclature used to define vessels, highlighting the need for careful interpretation of results and a clearer definition of where an arteriole transitions into a capillary. Although reported capillary dilations are small, they were estimated to account for 84% of the flow increase in response to neuronal activation (Hall et al., 2014) and unsurprisingly they offer the greatest resistance across the vascular tree (Gould et al., 2017), making them important mediators of the NVC response. A further role for pericytes in the alteration of vascular tone was proposed by Longden et al. (2017), who suggested pericytes could amplify the electrical signals from K_{IR} signalling during their transmission to the arteriole upstream (Longden et al., 2017).

In summary, neurovascular coupling is a complex process that is modulated by many factors that differ across the vascular tree (see figure 1.2 for summary) but, together, allow for the fine control of local blood supply in response to synaptic activity, facilitating the delivery of the oxygen and glucose required to maintain neuronal function and health. Disruptions to this delicate control of blood supply are thought to play a role in pathological disease states such as amyotrophic lateral sclerosis (ALS), Parkinson disease and several dementias, including Alzheimer's disease, which is the focus of this thesis (Iadecola, 2017).

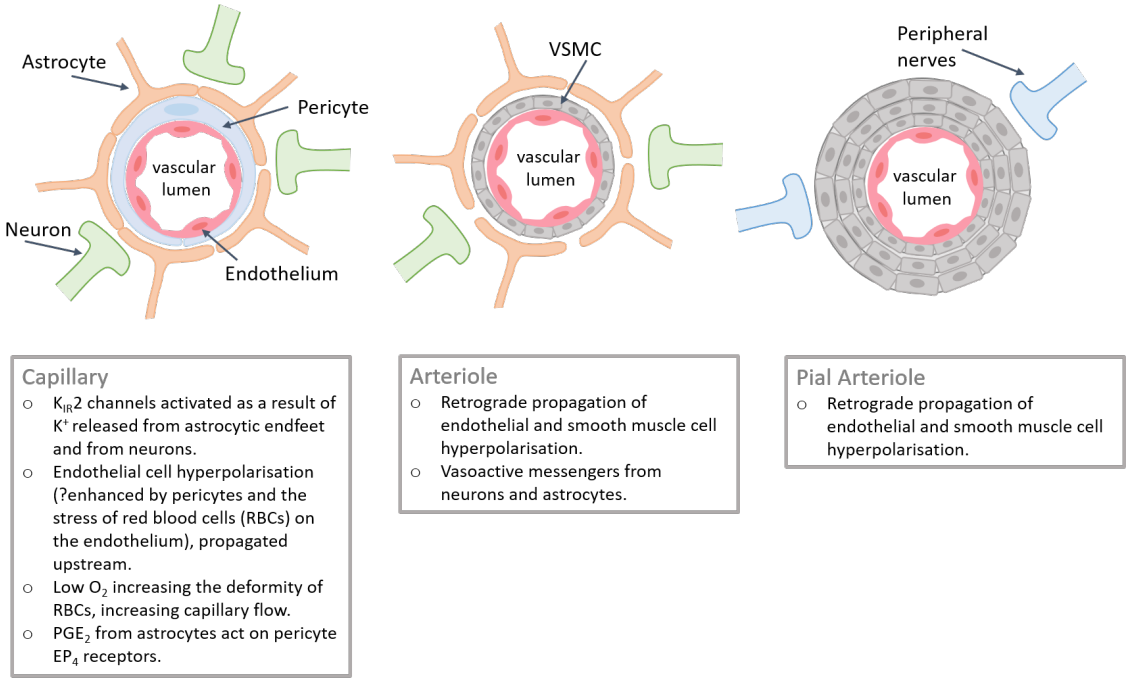

Figure 1.2: **Neurovascular coupling mechanisms vary across the vascular tree**. Adapted from (Iadecola, 2017).

1.2 Alzheimer's Disease

Alzheimer's Disease (AD) is the most common form of dementia with most cases presenting in older adults (termed "late onset AD" (LOAD)) however a small number of cases do occur in early life ("Early onset AD" (EOAD)). In the UK, there are estimated to be 850,000 people living with dementia and this number is expected to rise to two million by 2050, with one in three people born this year expected to go on to develop dementia in their lifetime (ARUK, 2019). Needless to say, it is an enormous social and economic issue, with little available in the way of therapeutics. AD is characterised by memory loss

and cognitive decline, brain atrophy, neuronal damage and specifically, by two pathological hallmarks, β-amyloid (Aβ) extracellular deposition, and the intracellular deposition of hyperphosphorylated tau (De Strooper and Karran, 2016). One of the multitude of challenges faced by AD researchers is the insidious nature of the preclinical phase of the disease, with changes to the brain's structure and function, as well as the deposition of the aforementioned pathological hallmarks of the disease, Aβ and hyperphosphorylated tau, occurring many years prior to symptom onset (Long and Holtzman, 2019). The existence of this preclinical phase highlights the importance of investigations into the early stages of AD and may offer the best window for therapeutic intervention.

1.2.1 Pathological features of AD

Amyloid Beta

Aβ is produced in neurons as a result of the proteolytic cleavage of amyloid precursor protein (APP) by β- and γ-secretases, in the amyloidogenic pathway (Haass, 2004). Alternatively, in the non-amyloidogenic pathway, APP is cleaved in the middle of the Aβ region by α-secretase (Haass et al., 2012; Esch et al., 1990; Wang et al., 1991). As these two pathways compete with each other, α-secretase has been identified as a potential therapeutic target to reduce Aβ production (Coman and Nemeş, 2017). Aβ is prone to aggregation, forming oligomers and fibrils, eventually depositing as plaques (Long and Holtzman, 2019). Aβ has canonically been the focus of much AD research and it was suggested by Hardy and Higgins (1992), in the amyloid cascade hypothesis, that this deposition of Aβ in the brain may be the initial trigger in AD, leading to a cascade of pathological events such as tau hyperphosphorylation and cognitive decline. Since then however, it has become clear that despite its unequivocal role in the disease process, there are many more factors at play as various anti-amyloid drugs have failed in clinical trials to improve the impairments seen in AD (Karran et al., 2011). Additionally the degree of deposition of Aβ does not correlate with cognitive decline (Nelson et al., 2012) however, it does seem to be important in the initiation of the disease process, with tau pathology being dependent on Aβ deposition (Price and Morris, 1999; Price et al., 2009).

Tau

Tau is a soluble, natively unfolded protein that is expressed in neurons and is thought to be physiologically important in microtubule assembly and transport, as well as axonal stability (Dixit et al., 2008; Weingarten et al., 1975). Under certain conditions, tau becomes

phosphorylated, aggregating into oligomers, then paired helical filaments and finally forming tangles (Goedert et al., 2017; Mandelkow et al., 2007). This aggregated tau behaves in a prion-like manner, where it seeds the aggregation of unfolded tau. In addition, it is secreted as a result of electrical activity and so can travel synaptically to connected regions (Goedert et al., 2017; Calafate et al., 2015; Long and Holtzman, 2019). Cognitive decline is observed when tau pathology spreads to the neocortex from the entorhinal cortex, (Aβ pathology is required for this transition) (Price and Morris, 1999; Price et al., 2009; Wang et al., 2016) and from there tau correlates well with cognitive deficits, for that reason it is thought to be an important driver in the disease process (Nelson et al., 2012).

1.2.2 Risk Factors for AD

There are a number of factors that can increase or decrease the risk of going on to develop AD. The greatest risk is age, the older you become the more likely you are to develop the disease (ARUK, 2019). As well as this, there are a number of genetic risk factors that are also currently considered "non-modifiable". These include mutations that result in early onset AD such as PSEN (presenilin)1, PSEN2 and APP mutations (Silva et al., 2019; Livingston et al., 2017). As presenilin is a subunit of the γ-secretase, these mutations are thought to involve aberrant APP processing (De Strooper and Karran, 2016). The greatest genetic risk factor for developing late onset Alzheimer's Disease, is the ϵ4 allele of the Apolipoprotein E gene (Corder et al., 1993; Livingston et al., 2017), which has multiple effects that may explain why it elevates the risk of developing AD, including effects on the vasculature. In addition to genetic risk factors there are also many factors that are considered to be potentially"modifiable", many of which have a vascular component and are also risk factors for cardiovascular disease. These modifiable risk factors include diabetes mellitus, hypertension, obesity, smoking, poor diet, depression and dyslipidaemia (Crous-Bou et al., 2017; Livingston et al., 2017; Silva et al., 2019).

1.2.3 Alzheimer's Disease and the Vasculature

Many risk factors for AD are shared risk factors for cardiovascular diseases and there is a convincing body of evidence to suggest that there is vascular dysfunction in Alzheimer's disease. Vascular perturbations are observed early in the disease process, before early mild cognitive impairment, with studies reporting vascular disruptions prior to the metabolic, functional, structural, pathological and cognitive changes observed in AD (Iturria-Medina et al., 2016).

Hypoperfusion in the early phase of AD has been shown to follow a similar pattern to Aβ deposition in the parenchyma (Love and Miners, 2016). Capillary blood flow stalling in a small number of capillaries ($\sim$2%) has been shown to contribute to a global reduction in CBF observed in mouse models with APP overexpression (Cruz Hernández et al., 2019), this stalling was shown to be as a result of neutrophils adhering in these segments. Astonishingly, clearing these few stalled capillaries resulted in a 13% increase in CBF, bringing the mice to around two-thirds of the normal flow, showing that capillary stalling is likely to contribute to a significant portion of the CBF deficits we see in APP over-expressing mouse models. On top of these transient blockages that were noted in capillaries, there is also an increase in the number of "string" vessels in the brains of AD patients. String vessels are devoid of endothelial cells and therefore cannot support blood flow (Brown, 2010).

The blood brain barrier is a specialised structure that plays an essential role in the protection of neurons from blood-derived products, however in AD patients and in mouse models that mimic elements of the disease, proteins such as fibrinogen, prothrombin, albumin and immunoglobulin have been found to leak into the brain parenchyma from the blood (Ryu and McLarnon, 2009; Zipser et al., 2007; Sweeney et al., 2018b; Montagne et al., 2017). Many of these blood-derived proteins are neurotoxic and so contribute to the neurodegeneration seen in AD (Sweeney et al., 2018b).

As well as providing a physical barrier between the blood and the parenchyma, the BBB also plays an important role in the clearance of Aβ from the brain, a process that is inhibited in AD (Mawuenyega et al., 2010). Transportation of Aβ from the brain parenchyma to the blood, in order to be cleared away, is primarily via the low density lipoprotein receptor related protein-1 (LRP1 receptor) (Deane et al., 2004; Shibata et al., 2000), however in AD brains and as a direct result of Aβ, there is a decrease in LRP1 in microvessels (Donahue et al., 2006; Shibata et al., 2000), and LRP1 has been shown to be oxidised in AD (Owen et al., 2010) which may result in a loss of function. Conversely, the receptor for advanced glycation end products (RAGE), which is responsible for the transport of Aβ in the opposite direction, i.e. from the blood into the parenchyma (Cai et al., 2016), is upregulated in AD brains (Donahue et al., 2006).

Clearance of Aβ across the BBB is only one of several clearance mechanisms utilised by the brain, it is also cleared via a para- /peri- vascular pathway (Iliff et al., 2012; Bacyinski et al., 2017; Carare et al., 2020), a process which has been shown to be defective in AD and in cases of cerebral amyloid angiopathy (CAA; where Aβ deposits around blood

vessels (Vinters, 1987)) (van Veluw et al., 2019; Weller et al., 2009; Peng et al., 2016; Arbel-Ornath et al., 2013; Di Marco et al., 2015). Although this clearance process is not completely understood and many controversies involving the underlying mechanisms exist, the oscillation of blood vessels is thought to be important, as an interruption of vascular oscillations results in a reduction clearance (Iliff et al., 2013) and may lead to an increase in Aβ accumulation (Garcia-Alloza et al., 2011). Oscillations at ~0.1Hz are called vasomotion and is key in this clearance mechanism as demonstrated by van Veluw et al. (2019). They showed reduced clearance in mice with CAA compared to WT mice, that correlated strongly with the power at the vasomotion frequency (0.1Hz) (van Veluw et al., 2019). Overall this reduction in Aβ clearance contributes to a build up of the protein and eventually the deposition of plaques.

Many studies have used both mouse models and human subjects to examine the relationship between Aβ, vascular tone and the functional hyperaemia response. One elegant study from Nortley et al. (2019), demonstrated that the addition of Aβ to human tissue resulted in a marked constriction of capillaries but not arterioles. Using pharmacological methods, they gleaned that this constriction was as a result of the generation of reactive oxygen species and the downstream release of endothelin-1 which acted on ET_A receptors present on pericytes, evoking a capillary constriction. This effect of Aβ was reinforced by the finding that blood vessels in both animal and human tissue with Aβ present, had diameters that increased as a function of pericye soma distance, in direct contrast to tissue that had no Aβ deposits (Nortley et al., 2019). Further evidence that there is an interaction between pericytes and Aβ comes from Sagare et al. (2013), where pericyte deficient mice were crossed with mice overexpressing the Swedish mutation of human Aβ-precursor protein (Pdgfr$\beta^{+/-}$ $APP^{sw/0}$). When compared with mice that had normal pericyte coverage, the Pdgfr$\beta^{+/-}$$APP^{sw/0}$ mice displayed a plethora of deleterious effects including a reduction in pericyte coverage, accelerated Aβ pathology, the development of tau pathology and cognitive deficits. In addition, it was found that Aβ accumulated in pericytes, and if this occurred in excess, lead to cell death (Sagare et al., 2013).

The importance of pericytes in the neurovascular coupling response has been previously highlighted, so unsurprisingly a number of functional studies have shown the neurovascular coupling response to be attenuated in a mouse models of Aβ deposition (van Veluw et al., 2019; Niwa et al., 2000; Iadecola et al., 1999; Zhang et al., 1997). The role of pericytes in the blunting of these responses has yet to be fully elucidated and various other mechanisms have been suggested, such as a reduction in vascular smooth muscle

cell density (van Veluw et al., 2019), superoxide production (Iadecola et al., 1999) and NADPH oxidase production which was shown to result in endothelial damage (Park et al., 2014, 2005).

Thus far, much of the focus of research into vascular dysfunction in AD has centred around the effects of Aβ, with tau, the other pathological hallmark of the disease, being largely ignored. Some studies have utilised the Tg4510 tauopathy mouse model (which carries a mutation associated with frontal temporal dementia (FTD)) to probe the question - how does tau affect the neurovasculature? One study found this mouse model to have increased angiogenesis with an upregulation of a specific gene, PAI-1, that is important in extracellular remodelling during vascular formation (Bennett et al., 2018), and another group has reported BBB leakage in the same model that was ameliorated upon the suppression of tau (Blair et al., 2015). Further, analysis of human tissue has shown that tau oligomers accumulate in the cerebrovasculature of AD patients (Castillo-Carranza et al., 2017) and that vascular remodelling takes place in a manner that correlates with Braak tau pathology (Merlini et al., 2016). Recent work from Park et al. (2020) has taken the first step to elucidate the effect of tau on the neurovascular coupling response. In this novel study it was found that pathological tau (in mouse models associated with FTD) disrupted the association between nitric oxide synthase and postsynaptic density protein 95 (PSD95), the protein that enables the coupling of NMDA receptor activation and nNOS production, leading to a vasodilation as a result of the produced NO. This disruption between PSD95 and nNOS results in an inhibition in the NO production and so a reduction in the neurovascular coupling response. Despite this finding, more evidence is required to fully understand the impact tau has on the neurovasculature and the functional hyperaemia response, particularly in the presence of non-mutated tau, as in AD (Bonnar and Hall, 2020).

This wide body of work provides indisputable evidence that there is vascular dysfunction in AD, across different compartments of the vascular tree, and attests the importance of further research in this field. In addition to the demonstrable negative effects of AD pathology on the vasculature, understanding how the APOE4 gene increases the risk of developing AD, in the absence of Aβ and pathological tau, and understanding if effects on the blood vessels contribute to this risk, will be essential in bettering our understanding of the disease.

1.3 apolipoprotein E

The presence of the gene encoding for apolipoprotein E (APOE) 4 is the greatest genetic risk factor for going on to develop late onset AD (Corder et al., 1993). Three APOE isoforms exist, $\epsilon 2$, $\epsilon 3$ and $\epsilon 4$, with two alleles of $\epsilon 4$ increasing disease risk 9-15 fold (Yamazaki et al., 2019; Farrer, 1997), despite an $\epsilon 4$ allele frequency of 14% in healthy individuals, it is over represented in AD patients with a frequency of 38% (Yamazaki et al., 2019; Corder et al., 1993). ApoE is a 34kDa protein, consisting of 299 amino acids and each isoform differs by only one amino acid at two residues. ApoE2 has a cysteine at position 158 and 112, ApoE3 has a cysteine at position 112 and arginine at 158 and ApoE4, an arginine at 112 and 158. These polymorphisms impact the structure and function of each ApoE isoform (Bu, 2006). Peripheral ApoE is produced mainly in the liver and in the central nervous system (CNS) it is produced primarily by astrocytes but also by vascular mural cells, microglia and neurons under stress conditions (Xu et al., 2006; Bu, 2006; Casey et al., 2015). ApoE plays an important role in the transport of cholesterol and other lipids to neurons, mediated by receptors of the LDL family. ApoE mostly exists in association with lipids, something that functionally important as its lipidation is essential for its binding with the LDL receptors (Hauser et al., 2011).

The role of APOE in the pathobiology of AD is still not completely understood but its stature as the greatest known genetic risk factor for the development of AD makes it of great interest to researchers. Much existing research implicates APOE4 in the facilitation of Aβ aggregation and the prevention of its clearance, however in addition to these effects, there is also a clear interaction between APOE and the brain's vasculature.

1.3.1 APOE and Aβ

Evidence shows that ApoE and Aβ are inextricably linked with the influence of ApoE on the deposition of Aβ suggested by the finding that the low levels of cerebrospinal fluid (CSF) ApoE, as seen in ApoE4 carriers (Cruchaga et al., 2012), correlates with increased Aβ deposition, suggesting that low ApoE levels may promote this deposition. With regards to ApoE binding, it has been suggested that Aβ may compete with lipids (Kanekiyo et al., 2014) and may affect its ability to transport lipids properly, something that is essential for synaptic health (Bu, 2006).

APOE4 carriers have been shown to have an increased Aβ plaque burden (Kok et al., 2009; Polvikoski et al., 1995), elevated levels of oligomeric Aβ (Koffie et al., 2012) and increased CAA (Nelson et al., 2013; Pfeifer et al., 2002), when compared to APOE3 or

APOE2 carriers, as well as an increased quantity of Aβ per affected vessel, increasing the chances of vessel rupture (Alonzo et al., 1998). This is thought to be mostly as a result of altered Aβ clearance as well as the increased propensity of Aβ to aggregate in the presence of ApoE4 (Castano et al., 1995; Ma et al., 1994). As previously mentioned, the BBB and paravascular clearance pathways are important in the clearance of Aβ, it can also be cleared by enzymatic degradation, by neprilysin and insulin degrading enzyme, as well as by lysosomal breakdown in glial cells (Safieh et al., 2019).

ApoE affects Aβ clearance in an isoform dependent manner (Castellano et al., 2011), firstly when looking at the clearance of Aβ across the BBB, ApoE4 binds to LRP1 with poor affinity (Bell et al., 2012) meaning that the clearance of APOE4 and Aβ complexes are redirected to the VLDL receptor where they are cleared at a slower rate across the BBB when compared to ApoE2-Aβ and ApoE3- Aβ complexes which are cleared by both the LRP1 and VLDL receptors (Bell et al., 2007; Deane et al., 2008). Additionally, paravascular clearance of Aβ was found to be disrupted in ApoE4 mice, compared to ApoE3 mice, as injected Aβ accumulated in the clearance pathways in APOE4 mice (Hawkes et al., 2012).

Glial degradation of Aβ is also reduced in APOE4 carriers. In a study examining pericytes co-cultured with astrocyte-derived ApoE3 or ApoE4, it was shown that pericyte uptake and clearance of Aβ is isoform dependent, with the clearance of Aβ in the presence of ApoE4 reduced, compared to ApoE3 (Ma et al., 2018). In addition to pericytes, astrocytes also uptake Aβ, contributing to its clearance. However it has been shown that APOE4 iPSC-derived astrocytes are less efficient at taking up Aβ_{42} compared to APOE3 iPSC-derived astrocytes (Lin et al., 2018). The degradation of Aβ by neprilysin in microglia is also less efficient in the presence of ApoE4-containing high-density lipoprotein (HDL) particles, compared to ApoE2- or ApoE3-containing particles (Jiang et al., 2008) and ApoE4 reduced levels of insulin-degrading enzyme compared to ApoE2 or ApoE3 (Cook et al., 2003; Du et al., 2009). These studies converge to show that the presence of ApoE4 facilitates the accumulation and aggregation of Aβ, primarily due to the failure of a number of clearance mechanisms.

1.3.2 APOE and Tau

Evidence suggests that ApoE and Tau interact in an isoform dependent manner, ApoE4 expression in neurons results in tau phosphorylation to a greater extent than ApoE3 (Brecht et al., 2004), and post-mortem studies of human tissue have shown that APOE4

carriers have a greater number of tau aggregates than non-carriers but only in the presence of Aβ (Tiraboschi et al., 2004). In vitro studies using cultured hiPSC-derived neurons, showed that neurons derived from APOE4 homozygotes produced more phosphorylated tau than APOE3 neurons (Wang et al., 2018). In a study from Shi et al. (2017), a human ApoE knock in (APOE-KI) mouse model was crossed with a tauopathy model, P301S, that is associated with frontotemporal dementia. They showed by 3 months of age, P301S/E4 mice had higher levels of tau present, as well as going on to develop greater levels of brain atrophy and inflammation at 9 months than P301S/E2 or P301S/E3 mice (Shi et al., 2017). One mechanism that has been suggested to explain the increase in tau accumulation in ApoE4 carriers, is that ApoE4 is less effective than ApoE3 in binding to non-phosphorylated tau and preventing its subsequent hyperphosphorylation (Safieh et al., 2019). Neuronal ApoE4 is also more vulnerable to proteolytic cleavage, which results in the production of neurotoxic fragments, these can cause mitochondrial damage and disruption to the cytoskeleton (Mahley et al., 2006). In addition, evidence suggests that they also promote the phosphorylation of tau resulting in the formation of tangle-like structures (Huang et al., 2001; Brecht et al., 2004). In contrast to the findings of Shi et al. (2017), another study observed that upon injecting AAV- Tau^{P301L}, it was in fact, the APOE2-knock in mice that had the greatest amount of tau pathology and deficits in behavioural tests (Zhao et al., 2018). These discordant findings have been attributed to differences in experimental model and levels of tau expression (Najm et al., 2019; Yamazaki et al., 2019).

These studies show that there is extensive interplay between APOE and the two pathological features of AD, highlighting its integral role in the disease process.

1.3.3 APOE and the Cerebrovasculature

APOE genotype and cardiovascular risk factors interact to affect cognition and long term memory. APOE4 carriers have been found to have greater long term memory impairments that are associated with cardiovascular risk factors (Caselli et al., 2011) and a small rise in blood pressure in APOE4 carriers is associated with reduced regional brain volumes and cognitive deficits (Bender and Raz, 2012). In addition, there is an isoform dependent increase in the risk of developing coronary artery disease and myocardial infarction (e4 >e3) (Belloy et al., 2019). It is possible that dysfunction of the cardiovascular system associated with ApoE4 may contribute to or even instigate the cognitive decline and

neurodegeneration observed in AD.

In the prefrontal cortex of human APOE4 carriers, capillary basement membrane area is lower than that of APOE3 carriers (Salloway et al., 2002). Basement membrane thinning is thought to be indicative of blood brain barrier leakage and indeed, another study found lower levels of phosphorylated occludin at Thr residues in an in vitro BBB model with astrocytes prepared from ApoE4-KI mice compared with those prepared from ApoE-3 KI mice (Nishitsuji et al., 2011). Phosphorylation of occludin at Thr residues is essential for its assembly into the tight junctions of the BBB. A multitude of studies have corroborated these findings and have shown that the BBB is leaky in an isoform dependent (e4 >e3) manner in humans, in vitro and in mouse models. This has been measured by increased prothrombin leakage in the prefrontal cortex of patients carrying at least one APOE4 allele (Zipser et al., 2007) and increases in extravascular IgG and fibrin in the cortex of APOE4 carriers with AD (Halliday et al., 2016; Hultman et al., 2013). In the aforementioned in vitro BBB, it was more permeable when astrocytes were prepared from APOE4 mice, compared to APOE3 mice (Nishitsuji et al., 2011) and in mouse studies, similar results have been observed. In one seminal study by Bell et al. (2012), utilising different humanised APOE mouse models, they showed a reduction in BBB integrity resulting in the deposition of the neurotoxic proteins thrombin and fibrin in mice expressing humanised ApoE4. This was shown to be as a result of the upregulation of a proinflammatory Cyclophilin A (CypA)-nuclear factor (NF)-κB-matrix-metalloproteinase-9 (MMP-9) pathway in capillary pericytes. It was demonstrated that ApoE4 was unable to suppress this pathway, unlike ApoE2 and ApoE3, due to its low interaction with LRP1. They accompanied these results with reports of reduced microvascular length, reduced pericyte coverage, DNA fragmentation in pericytes and endothelial cells and regional blood flow reductions that, importantly, preceded any neuronal alterations (Bell et al., 2012). A recent study from the same group confirmed that this pro-inflammatory mechanism was also present in human APOE4 carriers. APOE4 subjects had increased BBB leakage that correlated with CSF levels of the pericyte injury marker, soluble PDGFRβ (Montagne et al., 2020). In addition, levels of CSF MMP-9 and CypA were increased in APOE4 carriers, highlighting the potential importance of this pathway in the breakdown of the BBB observed in APOE4 animals and humans.

Congruous with these observations, several other groups have also reported interactions between ApoE and capillary pericytes. Human pericytes cultured from APOE4 carriers

were found to be more susceptible to damage when co-incubated with Aβ, than those cultured from non-carriers (Wilhelmus, 2005) and a reduction in capillary coverage by pericytes in APOE4 carriers has been reported by other groups in humans (Halliday et al., 2016), and in mice (Koizumi et al., 2018). One interesting study from Casey et al. (2015), observed that in the absence of pericytic ApoE, pericyte migration increases dramatically, an effect that is reversed upon application of exogenous ApoE3 but not ApoE4. This migration was found to depend on LRP1 and the activation of the protein RhoA, which has been shown to regulate cell adhesion and migration. Although this migration is important in the formation of glial scars and angiogenesis, an excess response may result in depletion of pericytes on capillaries which could alter CBF.

Much of the focus of existing work outlining the interplay between ApoE on pericytes has focused on the effect on BBB integrity and the putative role this plays in neurodegeneration as a result of the extravasation of neurotoxic substances from the blood stream. However few groups have investigated the effect of this pericyte damage on the neurovascular coupling response, in which pericytes have previously been shown to play a key role. One study that has begin to address this question is from Koizumi et al. (2018). They use the APOE-TR model, and find, similarly to what was reported by others, a reduction in pericyte coverage, a reduction in vascular density in 3-4 month old mice, reductions in cortical CBF and interestingly, a reduced functional hyperaemia response, as measured by laser Doppler flowmetry, to whisker stimulation. They propose that the effect of ApoE4 on net CBF responses is endothelium dependent as superfusion with the endothelium-dependent vasodilators acetylcholine and bradykinin resulted in the attenuated response observed with the whisker stimulation, however superfusion with the smooth muscle relaxant adenosine and NO donor s-notroso-N-acetylpenicillamine (SNAP) did not show an attenuated response in APOE4 mice. They also used three-photon microscopy to record from the corpus collosum, and showed increased vulnerability of APOE4 mice to vascular alterations in response to bilateral carotid stenosis (Koizumi et al., 2018).

A more detailed probe into the neurovascular dysfunction would determine if deficits occur at a single vessel level, if so, where in the vascular tree they occur and how this effect is modulated by age. In addition, an examination of neuronal activity in these animals would help to determine if any changes in the haemodynamics are as a result of neuronal alterations in APOE4 mice .

1.3.4 APOE and Neurons

In functional hyperaemia, blood flow increases are commensurate with neuronal demand and so in order to assess this response in its entirety, it is important to study neuronal behaviour. Various effects of ApoE4 on the neurons have been observed, although it remains unclear how these effects interact with the vasculature and the NVC response.

The GABAergic system is an inhibitory system in the brain and regulation of its inhibition is essential for normal brain function. These interneurons also play an important role in learning and memory, as well as preventing hyperexcitability of excitatory neurons (Najm et al., 2019). A reduction in GABA has been shown in post mortem brains of AD patients and a resulting disinhibition may be responsible for the seizures sometimes observed in the disease (Lanctôt et al., 2004; Najm et al., 2019). Neurotoxic fragments generated from the proteolytic cleavage of ApoE4 are particularly damaging to GABAergic neurons (Li et al., 2009). In a knock-in mouse model of APOE, removing tau rescued the effects of ApoE4 on interneuron loss, as well as behavioural deficits (Andrews-Zwilling et al., 2010), demonstrating the interplay between tau and ApoE in this interneuron loss. In neurons derived from APOE3 or APOE4 hiPSCs, there was no difference in the generation of dopaminergic or glutamatergic neurons, however there was a degeneration of GABAergic neurons in ApoE4 vs ApoE3 (Wang et al., 2018), again highlighting the selective vulnerability of these neurons to ApoE4. Intriguingly, the cellular source of ApoE seems to be important in this interneuron loss, as deletion of neuronal ApoE4 in GABAergic interneurons prevents the GABAergic neuron loss, however deletion of astrocytic ApoE4 does not have the same effect (Knoferle et al., 2014).

This selective vulnerability of GABAergic neurons to ApoE4 mediated damage has effects on network function and results in hyperactivity. ApoE4 patients are at a greater risk of developing seizures, including those as a result of previous trauma (Johnson et al., 2018; Diaz-Arrastia et al., 2003) and hyperactivity has been observed in the entorhinal cortex of APOE-KI mice (Nuriel et al., 2017) and in human subjects a greater level of entorhinal activation during learning is observed compared to non-carriers (Dickerson et al., 2005). This collection of evidence demonstrates the selective susceptibility of GABAergic interneurons to ApoE4 mediated damage, and that there is a critical role for tau in this process. As a result, hyperactive phenotypes are exhibited among APOE4 carriers and can affect task performance and memory.

ApoE4 has also been associated with a reduction in dendritic spine density, in both human carriers (Ji et al., 2003) and in APOE4 mouse models (Ji et al., 2003; Rodriguez

et al., 2013; Dumanis et al., 2009). As well as this, human carriers have shown reduced synaptic plasticity (Arendt et al., 1997), fewer synaptic markers and a reduced post synaptic density in healthy APOE4 carriers (Love and Miners, 2016) and a reduced number of glutamate receptors (Sweet et al., 2016). In line with these findings, mouse models have shown ApoE4 to be associated with a reduction in synaptic proteins e.g. vGLUT the presynaptic glutamatergic vesicular transporter (Liraz et al., 2013), reduced synaptic transmission (Wang et al., 2005), and reduced neurite outgrowth possibly as a result of lower activation of LRP1 by ApoE4 (Nathan et al., 2002). Demonstrating that ApoE4 has an array of deleterious effects on the synapse which is likely to be strongly associated with the cognitive decline observed in AD.

It is clear that ApoE4 may increase the the risk of AD via a number of harmful mechanisms (see figure 1.3 for a summary) that are likely to converge and result in the neurodegeneration observed in AD. Although it is clear that there is a role for vascular dysfunction among this, it remains to been seen exactly how the NVC is modulated by ApoE and what downstream effects may result.

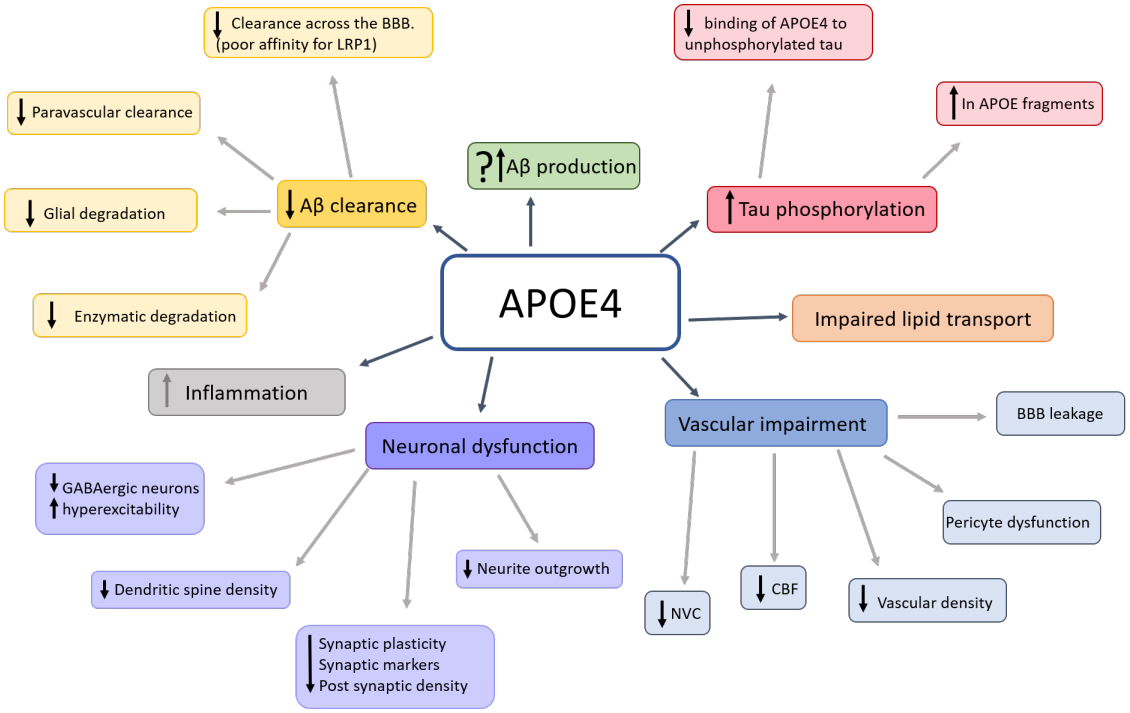

Figure 1.3: Various APOE4 pathways that likely contribute to the neurodegeneration and cognitive decline observed in AD. Modified from Safieh et al. (2019).

1.4 Hypoxia

Altered NVC and CBF could, over time, result in a deficient supply of oxygen within the brain. There are a multitude of detrimental downstream effects of hypoxia, including the facilitation of tau hyperphosphorylation (Fang et al., 2010; Chen et al., 2003) and Aβ accumulation (Sun et al., 2006; Zhang and Le, 2010), disruptions to BBB integrity (Ueno et al., 2002; Pluta, 2005) and increased neuroinflammation (Liu et al., 2001; Gerhard et al., 2000), all of which are known to contribute to the neurodegeneration observed in Alzheimer's disease.

1.5 Two Hit Hypothesis of Alzheimer's Disease

This extensive body of evidence pointing towards a significant contribution of vascular dysfunction to AD has led to the proposition of the vascular two hit hypothesis by Berislav Zlokovic. In this hypothesis he suggests that there are two "hits" contributing to the pathological cascade involved in AD, "hit" one is Aβ independent and involves vascular dysfunction such as BBB dysfunction, CBF dysregulation and hypoperfusion as a result of risk factors such as CV disease, diabetes mellitus, hypertension or the presence of an APOE4 allele. Hit one facilitates the accumulation of Aβ and inhibits its clearance, resulting in a build up of Aβ pathology in the brain. This is "hit 2" of the hypothesis, with Aβ exerting neurotoxic effects and triggering tau pathology , finally resulting in the cognitive decline we see in AD (Zlokovic, 2011) (see figure 1.4) .

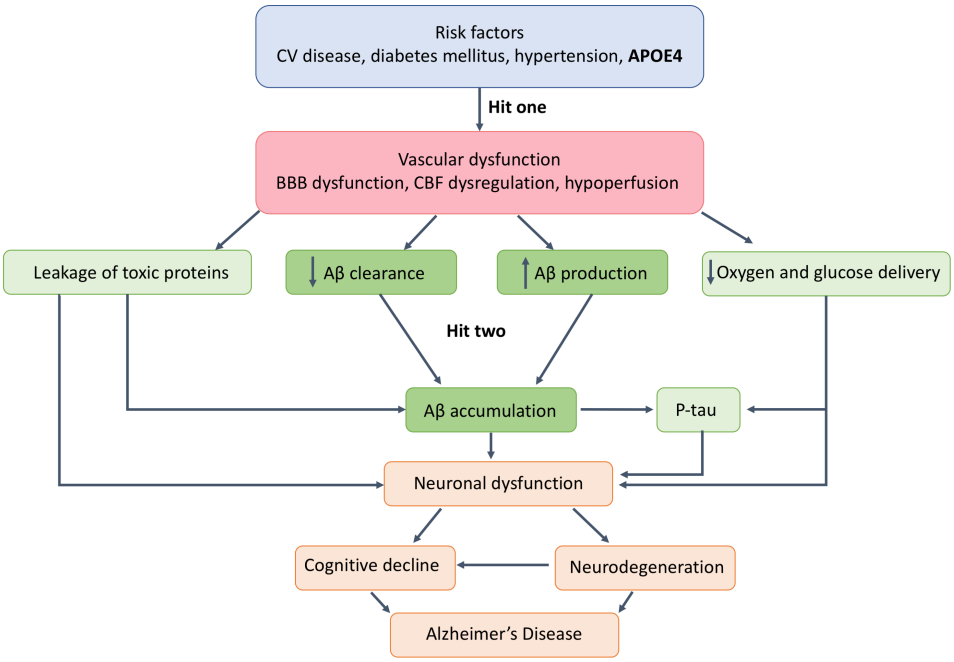

Figure 1.4: **Two Hit Hypothesis of Alzheimer's Disease**. Hit one: Aβ independent vascular dysfunction which leads to Hit 2: Aβ mediated neurodegeneration and cognitive decline, finally resulting in AD. Adapted from Zlokovic (2011).

AD research has classically focused upon Aβ pathology and neuronal damage, however the evidence outlined above supports the central postulate of perturbed vascular function in the disease process. The idea that vascular factors could be an early, or even an initial, trigger of the disease is undoubtedly a credible one and the body of work presented in this thesis aims to answer some of the outstanding questions relating to the role of ApoE in the NVC response and how this may contribute to the neurodegeneration and cognitive decline observed in AD.

In light of the evidence explored in this chapter, it is clear that there are many knowledge gaps in our understanding of the effect of ApoE4 on the neurovasculature and how these interactions might promote AD. Given that previous work suggests APOE4 animals may exhibit vascular dysfunction in early life, an in depth exploration into neuronal and vascular function in young animals, at a single vessel and neuronal level, would provide invaluable information to the field. In order to assess this, resting state conditions first need to be examined, to determine if APOE4 animals are existing with basal deficits upon which the functional hyperaemia response is elicited. Following this, the vascular and neuronal responses to sensory stimulation can be measured, to estimate how energy demand (from active neurons) and energy supply (via the blood supply) is balanced in ApoE4 animals. Finally, how these effects might change with age is of great interest, so tracking these parameters across a section of the lifespan would provide an interesting insight and help to identify where and when dysfunctions might occur.

Hypothesis: ApoE4 disrupts pericyte function, altering the blood brain barrier, even in young animals. I predict that this alteration in pericyte function will also disrupt baseline cerebral blood flow and neurovascular coupling responses to neuronal stimulation. Because blood brain barrier function deteriorates with time, any observed deficits in neurovascular effects are also expected to deteriorate with age.

With this in mind, this body of work aims to answer three core questions:

1. Does ApoE4 modulate resting neuronal or vascular properties in young animals?

2. Does ApoE4 affect the ability of the brain to elicit the functional hyperaemia response in young animals?

3. How does age interact with ApoE4 when considering neurovascular function?

Chapter 2

Methods

2.1 Animals

All animal procedures in the outlined methods were carried out in accordance with the guidelines of the UK Animals (Scientific Procedures) Act 1986.

All mice were bred in house from targeted replacement (TR) APOE mice, where exons 2-4 of murine APOE were replaced with exons 2-4 of human APOE, resulting in the production of human ApoE in these animals (Sullivan et al., 1997; Knouff et al., 1999). APOE3-TR or APOE4-TR homozygotes were subsequently bred with mice expressing DsRed under the control of NG2 promoter (NG2DsRedBAC) (Zhu et al., 2008), allowing for the visualisation of vascular mural cells, or with mice expressing GCaMP6f under the control of the Thy1 promoter (C57BL/6J-Tg(Thy1-GCaMP6f)GP5.5Dkim/J), which primarily leads to GCaMP expression in subsets of pyramidal neurons (Chen et al., 2012; Dana et al., 2014) (see table 2.1). These mice were then subsequently backcrossed for several generations to produce APOE-TR homozygotes and Thy1-GCaMP6f heterozygotes or APOE-TR homozygotes and NG2DsRed heterozygotes. APOE-TR, NG2DsRed and Thy1-GCaMP6f founder mice were generously gifted by Sarah King, David Attwell and Leon Lagnado, respectively. NG2DsRed and Thy1-GCaMP6f animals of the same APOE genotype were grouped together in all analyses as they did not exhibit robust genotype differences in the neurovascular parameters measured (see appendix B.5) although group sizes were not balanced.

Both male and female mice were used and were categorised into three age groups at the time of experimentation (see table 2.1 for groups and animal weight). Prior to surgery, mice were group housed in a temperature controlled room (22+/-2°C) with a 12 hour light/dark cycle and *ad libitum* access to food and water. Following the post-surgery

monitoring period outlined here, mice were singly housed under the same temperature conditions and with the same access to food and water as before, but under a reverse 12 hour light/dark cycle and with access to a running wheel to aid with habituation to the imaging rig.

Genotype	Age Groups
APOE4/4 NG2DsRed APOE3/3 NG2DsRed	Young (3-4 months) Weight range: 20.6g – 33.3g
	Middle (6-7 months)
APOE4/4 Thy1GCaMP6f APOE3/3 Thy1GCaMP6f	Old (12-13 months) Weight range: 23g – 55.9g

Table 2.1: **Mouse genotypes and age categories** Experimental mice genotypes and age categories are outlined above. Not all experiments had data for each genotype at each age point. Experimental group sizes are specified in Appendix A under each individual experiment.

2.2 Surgical Preparation

All animals used in in vivo experiments underwent an aseptic surgical procedure to implant both a glass cranial window over the primary visual cortex (V1) and titanium head bars atop the skull which allowed for head fixation.

Isoflurane 4% was used to induce anaesthesia in a chamber, after which animals were moved to a stereotaxic frame. Here anaesthesia was maintained with ∼1.5 - 2% isoflurane, delivered via a nose cone (Kopf) and body temperature was kept at 37°C by a homeothermic monitoring system (PhysioSuite, Kent Scientific Corporation). Reflexes and breathing rates were monitored throughout, and levels of anaesthesia were adjusted accordingly. Animals underwent subcutaneous injections of saline 0.9% (400μL) to prevent dehydration, buprenorphine (1.2μg, Vetergesic, Ceva), an analgesic for pain relief, meloxican (6.2 μg, Metacan, Boehringer Inglehim), an anti-inflammatory and dexamethasone (120μg, Dexadreson, MSD Animal Health), an anti-inflammatory steroid. Eye gel (Viscotears Liquid Gel, Novartis) was periodically applied to prevent drying or damage from particulates.

Hair from the skull area was cut as much as possible using curved scissors before the application of hair removal cream to reveal the skin below. Ethanol 70% and the antiseptic, betadine (Purdue Product, USA) was applied to clean the area. A large, round incision

was made to revel the entire dorsal surface of the skull below, with a small amount of neck muscle and any exposed periosteum removed to ensure only bone was exposed. The edges of the incision were sealed with a tissue adhesive (Vetbond, 3M), and the 3mm craniotomy site was marked using surgical calipers (Fine Science Tools) and a bone pen (see figure 2.1) for position). To increase the surface area for head bar adhesion, deep grooves were made in the skull using a scalpel blade before the head was tilted to lay the craniotomy site flat. The entire skull surface, excluding the marked site of the craniotomy and ∼1mm of the surrounding area, was then coated in dental cement (Unifast TRAD, GC; mixed 1:15 with black ink), ensuring thicker layers were added wherever necessary to provide a flat surface for the placement of the head bars (see figure 2.1 for placement). After a few moments, the cement hardened and the bars were then fixed in place. The craniotomy was then made using a 3mm biopsy punch (Kai Medical), by slowly twisting the punch over the marked site it was possible to entirely remove the desired section of skull. If necessary a microdrill (OmniDrill 35, World Precision Instruments) with a fine drill bit (0.5mm, Fine Science Tools) was used to drill through any remaining segments of bone. When using the microdrill, regular applications of saline to the skull were necessary to prevent heating of the underlying brain. Following removal of the skull flap, the exposed brain was immediately covered with gelfoam (Avitene Ultrafoam, Bard Davol Inc., US) to keep the underlying brain from becoming dry, to keep the area sealed and to control any bleeding. The dura was carefully removed using super fine forceps (Fine Science Tools) and the area was again moistened with gelfoam. Glass windows were made from two 3mm layers of glass coverslip, affixed to a single 5mm coverslip (Harvard Apparatus). The 3mm side of the window was used to plug the craniotomy with a tight seal and was held in place temporarily with a glass rod while tissue adhesive and dental cement was applied around the edges to secure the window in place. Finally, two small rubber rings were glued and cemented to the outer rim of the head bars to later facilitate the use of a water-based objective. The level of isoflurane was slowly reduced and the animal was placed in a heat box at 38°C to recover. Once awake, grooming and exploring the new home cage, animals were returned to a temperature controlled recovery room where they were monitored regularly for three days post-operatively. Animals were administered oral meloxicam (10μg, Boehringer Ingelheim) in food and weighed daily during this period. At the end of this three day period, animals were moved to a room with a reverse light/dark cycle and were allowed a minimum of 1 week of recovery before habituation.

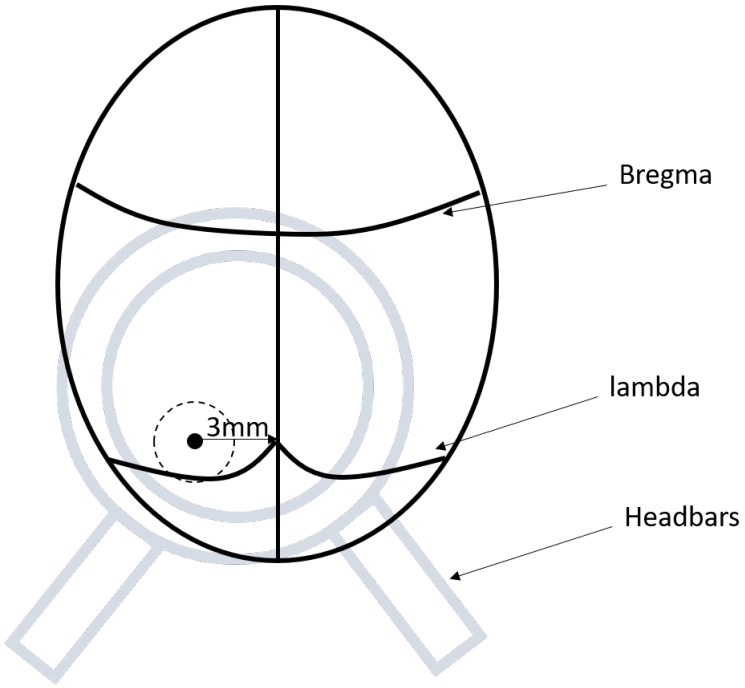

Figure 2.1: **Schematic of craniotomy site and head bar placement** Craniotomy site marked (dashed line), 3mm from the intersection of lambda and the midline. Grey solid line depicts approximate placement of head bars.

2.3 Habituation

Mice were slowly habituated to head fixation to ensure minimal stress for the animal during imaging. Habituation occurred over the course of approximately 1 week, depending on the animal. Initially mice were placed upon the imaging cylinder without head-fixation so that the environment would become familiar. They would then be briefly head fixed and gradually the restraint period would increase in duration until the animals could comfortably walk on the cylinder for extended periods of time.

2.4 In Vivo Experiments

2.4.1 Data Collection

During imaging mice were head-fixed atop a running cylinder as mentioned above, (see Figure 2.2) where they were free to engage with locomotion. To record locomotion the cylinder was equipped with a rotary encoder (Kuebler) and this was positioned under a two-photon microscope (Scientifica) or a combined laser Doppler flowmetry haemoglobin spectroscopy probe (Oxy-CBF probe) (Moor instruments) that allowed for the measurement of net haemodynamic parameters across the cranial window. In front of the mice were two screens (Asus, ∼17cm from the mouse) which displayed visual stimuli

(delivered using Psychopy) when required.

Two experimental paradigms were employed throughout, a "visual stimulation" paradigm and a "no visual stimulation" paradigm. The "visual stimulation" paradigm consisted of the presentation of 20 trials of a drifting grating. The grating was angled at 315°, made up of alternating trials with a spatial frequency of either 0.04 cycles per degree or 0.2 cycles per degree (10 trials each), a temporal frequency of 2Hz and sized at 220 degrees of visual space (i.e. a full screen stimulus). The grating was presented for 5 seconds with an inter stimulus interval of 20 seconds. The "no visual stimulation" paradigm meant the mouse was not presented with the gratings described above, but was allowed to engage with voluntary locomotion while the screens were dark.

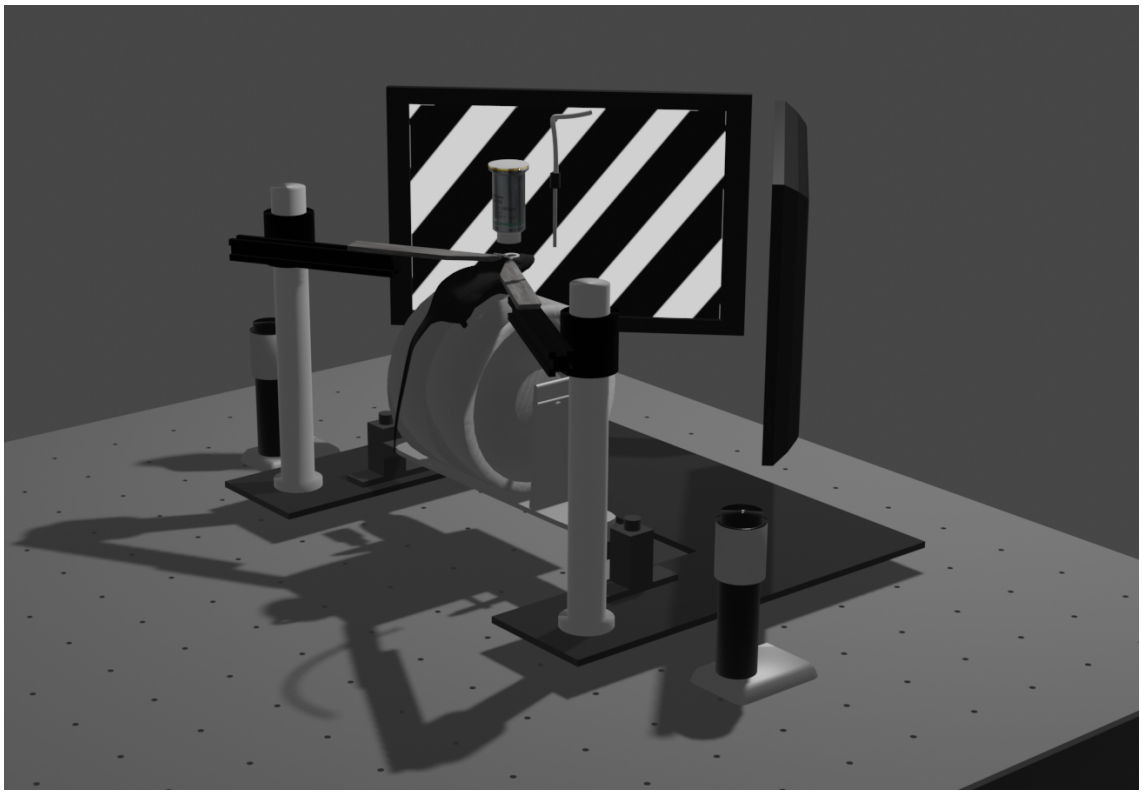

Figure 2.2: **Schematic of *in vivo* imaging set up** Mice were head fixed atop a cylindrical running cylinder, underneath a two-photon objective or Oxy-CBF probe and in front of two screens displaying visual stimuli, when required. Imaged generated by Dori Grijseels and used with permission.

Two-photon Microscopy

Prior to two-photon recordings, mice were injected with a fluorescent dextran. Those with green fluorescence (i.e. GCaMP6f in excitatory neurons) were injected with 2.5 %Texas Red (neutral, Invitrogen) either subcutaneously (3kDa) or intravenously (70kDa), and those with red fluorescence (i.e.DSred in vascular mural cells) were injected intravenously with 2.5% fluorescein isothiocyanate-dextran (FITC-dextran), to allow visualisation of the vasculature. To aid with intravenous injection, mice were placed in a heated box (38°C) for 10 minutes, before being restrained and injected. Vasculature was recorded +/- fluorescently labelled neurons, using a 20x (XLUMPlanFL N, Olympus) or 16x (LWD, Nikon) water immersion objective and a mode-locked Ti-sapphire multiphoton laser (Chameleon, Coherent). Tissue was excited at either 940nm or 970nm and red and green light was collected using SciScan (Scientifica) software. Images were captured at an acquisition rate of 3.8 - 7.6 frames per second for whole vessel (average pixel size : 0.424 μm) or neuronal population (average pixel size : 1.28 μm) recordings (XY movies), and high speed line scans were used to concurrently record vascular diameter and red blood cell velocity of small vessels (average pixel size : 0.195 μm) at an average acquisition rate of 1221 lines per second. Typically, a large pial arteriole that dilated to visual stimulation would be identified within the window. The ability of the vessel to dilate helped to confirm where the active region was and also to confirm the vessel's identity as an arteriole, rather than a vein. The presence of fluorescent smooth muscle cells in some cases as well as the morphology (the size and position relative to the large pial veins) of the vessel would also aid in its identification as a pial arteriole. Each branch of the arteriole was imaged (under both experimental paradigms) until a branch began to dive into the parenchyma, in which case, the vessel was no longer considered to be pial, but instead, a penetrating arteriole. Capillaries branching off the penetrating arterioles and beyond, were imaged using high speed line scans, again under both experimental conditions (i.e. +/- visual stimulation). If excitatory neurons were labelled with GCaMP6f, a recording would be taken at the cell body layer of the cortex (layer 2/3 ($\sim$ z =-150μm), in the area proximate to the imaged vasculature. Z-stacks were taken to aid in identification of vessels within the network, as well as to enable the characterisation the vascular anatomy (average frames per plane: 4, average pixel size:1.28 μm , average z-step: 1.09μm).

Oxy-CBF probe

Net measurements of the haemodynamic parameters, total haemoglobin (HbT), oxy-(HbO) and deoxy-(HbD) haemoglobin and oxygen saturation (SO_2) could be obtained (acquisition rate: 40Hz) from the different absorption spectra of HbO and HbD as described in Kohl-Bareis et al. (2005). Briefly, a white light of wavelength 450nm-700nm was emitted from the probe and reflected light was collected with a spectrometer. A Monte Carlo simulation (Wang et al., 1995) was used to estimate the intensities of the reflected light and based on the knowledge that the absorption coefficients of Hb0 and HbD are 20 and 240 times less than the maximum respectively (Kohl-Bareis et al., 2005), the relative quantities of each were calculated and from these, SO_2 was also calculated using the formula:

$$SO_2 = \frac{HbO}{HbO + HbD}$$

In addition to the haemoglobin spectroscopy, the probe used laser Doppler flowmetry to calculate blood flow (CBF) across the window. Using these parameters, the cerebral metabolic rate of oxygen consumption (CMRO $_2$) was calculated using the following equation:

$$CMRO_2 = CBF \times \frac{HbD}{HbT}$$

The probe was placed against the glass of the cranial window and net measurements were taken during both experimental paradigms described above.

2.4.2 Data Analysis

Custom written MATLAB scripts for the extraction of data from raw image files were co-written by Dr Kira Shaw, Dori Grijseels and I.

Any images deemed to be of poor quality were excluded from further analysis. This was primarily due to the dye not being bright enough due to fading or a poor injection or in some cases, areas of the window that were less clear.

Locomotion Detection

Throughout all in vivo experiments, locomotion was detected, as mentioned, by a rotary encoder. Continuous locomotion traces were obtained for each experiment and traces went through a number of processing steps. Firstly, the differential and the absolute values for each locomotion trace were calculated, to remove drift and negative values (from backwards locomotion), respectively. All values below one standard deviation of the entire trace were

deemed to reflect noise, rather than real locomotion, and so were set to zero. Finally, all traces were normalised so that they fell between zero and one, to make them more comparable between sessions (Figure 2.3).

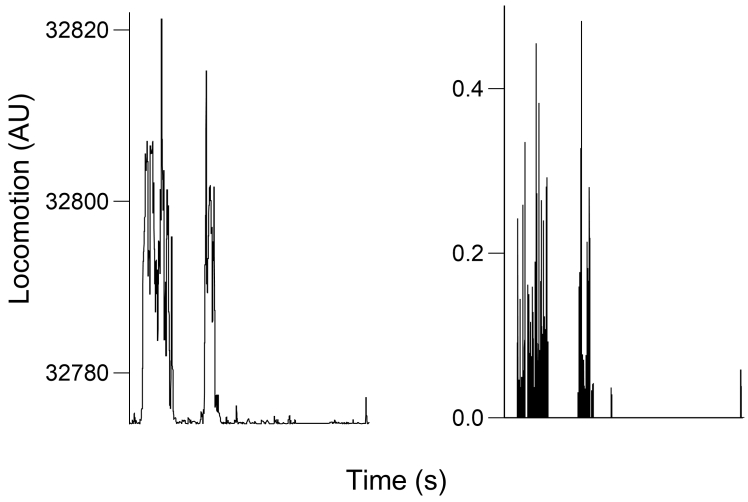

Figure 2.3: **Example Locomotion Traces** Left graph: An example trace of raw locomotion. Right graph: The same locomotion trace that has been processed to remove drift, negative numbers and noise.

Vascular diameter measurements

Using the FIJI distribution of ImageJ (Schindelin et al., 2012), a number of pre-processing steps were taken to improve image quality and consistency between vessels. Namely, wherever required, images were registered to remove motion artefacts, despeckled to remove noise and/or median 3D filtered (X, Y and Z radii = 2) to smooth the image. All images had the "Stack Contrast Adjustment" plug-in applied to brightness match all frames and so eliminating light artefacts in the data. Light artefacts might arise from the visual stimulation presentation (although care was taken to block as much light as possible by shielding the objective with light occluding tape). A custom MATLAB script was written to extract the diameter in a number of steps. As the vessel was brighter than the background, a skeleton could automatically be generated and modified by the user. For every point in the skeleton, a perpendicular line was drawn across the vessel, allowing for an intensity profile to be generated. Intensity profiles were obtained across a sliding window of five pixels at every second point in the skeleton. The full width at half maximum (FWHM) was calculated for each of the five intensity profiles within each window, that is, the distance in pixels between the first time the curve crossed the half maximum

value and the second time it crossed this same value. The five FWHM values were then averaged to give a single value in pixels for each window and diameters were calculated by multiplying by pixel size. All diameters for skeleton points within a single frame were averaged so a continuous diameter trace over time could be extracted (see Figure 2.4). All vascular data traces were inspected by eye for signs of swelling. If swelling occurred the traces were cut to the period before the swelling began.

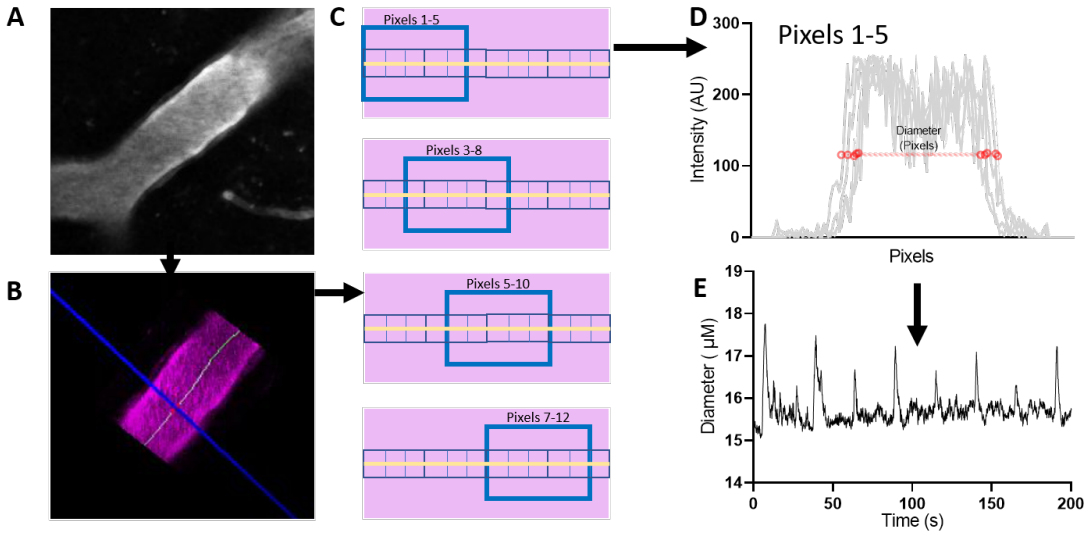

Figure 2.4: **Pipeline for diameter extraction using FWHM** A) Raw vessel file imported into MATLAB B) Vessel is skeletonised and a perpendicular line is drawn across each skeleton point C) A sliding window, that moves in steps of 2 pixels, groups together 5 pixels within each window D) The distance between the FWHM values (red) are taken for each of the five skeleton points per window and averaged to give one diameter measurement per window. E) Averaged values are obtained for each skeleton point per image frame. The skeleton points are then averaged together to give one diameter measurement per frame

Line scan data analysis

Line scan diameter and red blood cell velocity (RBCV) measurements were made using custom MATLAB scripts following the same preprocessing steps in ImageJ as described above. For diameter measurements, a scan path was drawn perpendicular to the vessel (see Figure 2.5) and intensity measurements were taken across a sliding window, but in this case, the window was 40ms of time, rather than in pixels, and the intensity measurements were taken from an average of each time window. The sliding window overlaps by 10ms and the FWHM was calculated from each intensity curve as before.

Red blood cell velocity measurements could be made, as the plasma of injected mice was fluorescent but the individual RBCs were not, meaning they cast a shadow (see Figure 2.5). By defining a scan path that travelled along the vessel (see Figure 2.5, left panel), the

velocity of the shadows (i.e. RBCs) could be measured by calculating the gradient of the shadow in the outputted image. The flatter the shadow, the faster the RBC velocity as it has moved further along the scan path in the time it takes the laser to traverse the path once. To calculate this angle and the velocity, freely available MATLAB code was adapted (Drew et al., 2010a) and the data was split into overlapping time windows of 40ms as described for diameter measurements. The method from Drew et al. (2010a) utilised a radon transform to calculate the average angle of the dark streaks across each 40ms time window, and the tangent of this angle is inversely proportional to the RBCV, allowing for a continuous velocity-time trace to be calculated.

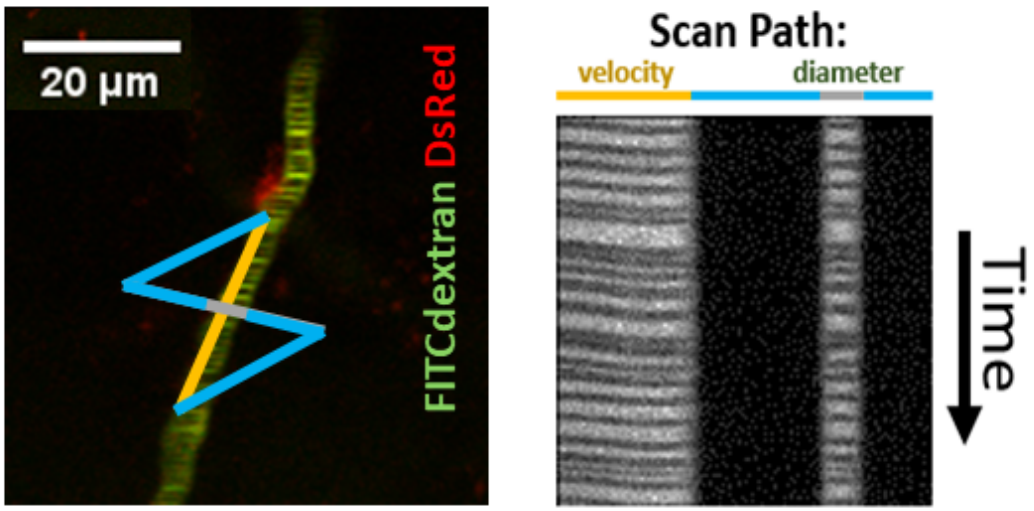

Figure 2.5: **Example line scan path** Left panel: Capillary with streaks of fluorescent plasma labelled with FITC-dextran (green) and red blood cells(black). A scan path was drawn perpendicular to the vessel axis (grey) to measure diameter and along the vessel (yellow) to measure RBCV. Right panel: Image collected in SciScan. Each row represents one traversal of the entire scan path with left section (yellow) depicting the path that travels along the vessel measuring RBCV, and the right section (grey) depicting the section of the scan path path that is perpendicular to the vessel and measures diameter.

Linsecan data processing

Due to the noise present in line scan data, as a result of movement artefacts and the small pixel size, all traces underwent a number of processing steps to minimise this noise. Red blood cell velocity traces underwent three preprocessing steps, firstly, when the angles of RBCs were outputted from the radon transform, angles that were either very large or very small were removed (see Figure 2.6, Step Two), secondly, once converted to velocity, the traces then underwent two iterations of outlier removal so that any points that were greater than three standard deviations above or below the mean of the trace were removed (see Figure 2.6, Steps Three and Four). Line scan diameter traces were less subject to noise and so underwent only the first iteration of outlier removal.

GCaMP signal fluorescence

Mice with a genetically encoded calcium indicator in neurons, such as the thy1-GCaMP6f mice used in this study, have neurons that will change fluorescence as a result of calcium transients (Dana et al., 2014), so by measuring the changes in fluorescence, it is possible to measure neuronal activity. An automated region of interest (ROI) finder, suite2P (Pachitariu et al., 2016), was used to register neuronal recordings, identify ROIs, extract fluorescence traces and remove background signal. ROIs were selected based upon the behaviour of the pixels as well as morphological features such as size (see Figure 2.7 for example ROIs). All pixels in each ROI were connected and did not overlap with any other ROIs. Within the suite2P graphical user interface (GUI), ROIs could be selected or deselected by the user and a round doughnut around each ROI provided a background measure. The fluorescence signal was then extracted from each ROI and at this point (0.7 x the background trace) was subtracted from each ROI to remove any light artefacts, based on the recommendation from the authors of the suite2P package (Pachitariu et al., 2016). Where appropriate, the fluorescence signal was normalised to give a ΔF/F measurement and show fluorescence changes from baseline. The following equation was used:

$$\Delta F/F = \frac{F - F_{\min}}{F_{\max} - F_{\min}}$$

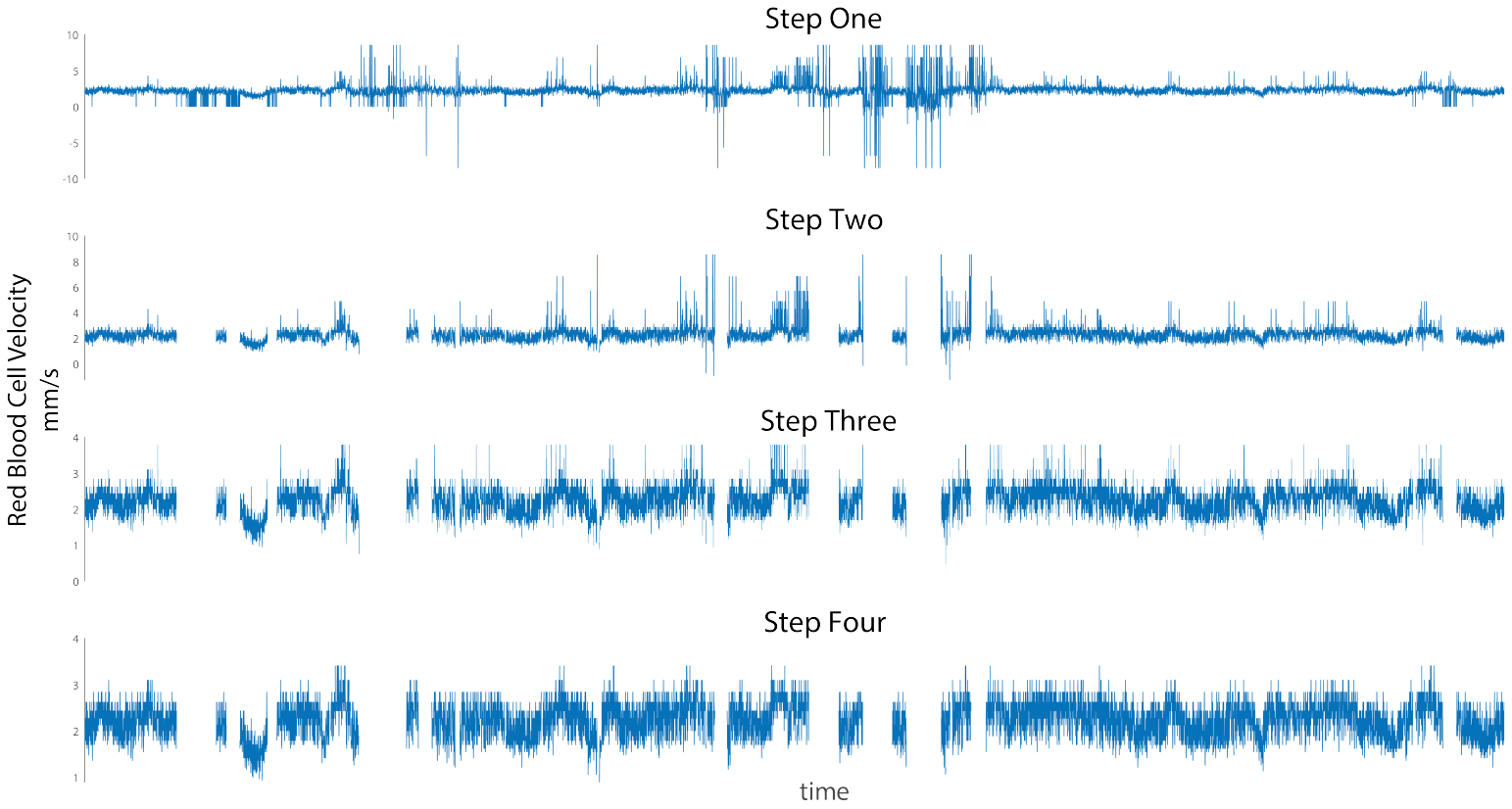

Figure 2.6: **Line scan data processing steps** Step One: Raw Data trace. Step Two: Angles that are very large or very small are removed. Step Three: First iteration. All Values greater than 3 standard deviations above or below the mean were removed. Step Four: Second iteration of step 3.

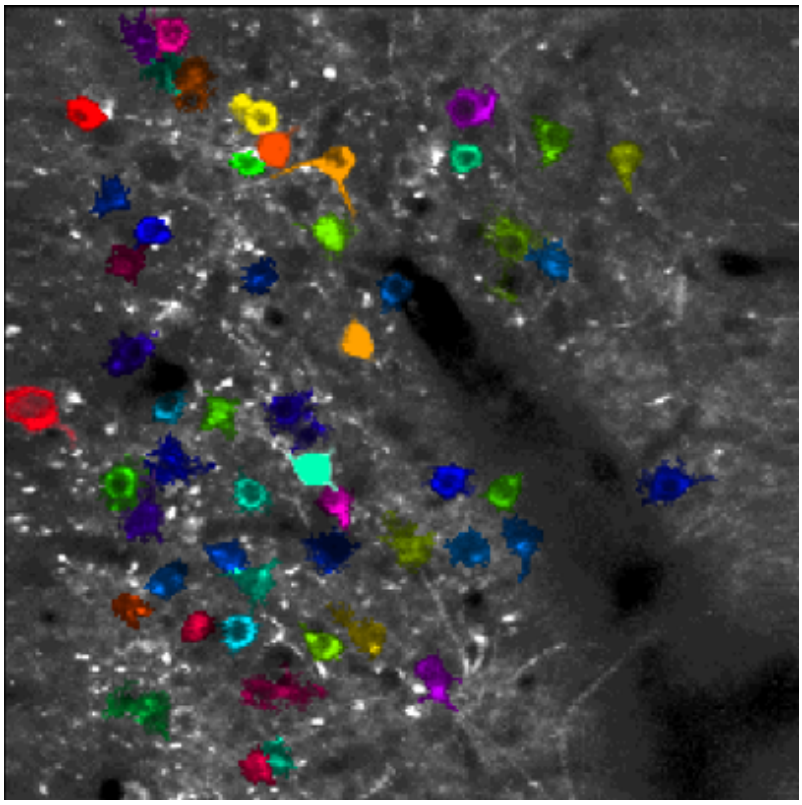

Figure 2.7: **Automated ROI finder, suite2P** An representative image obtained using two-photon microscopy, maximally projected to show fluorescent neurons. Coloured ROIs denote cells detected by Suite2P.

Net haemodynamic parameters

Traces for each of the haemodynamic parameters outlined previously were collected by VMS4.0 (Moor Instruments) at 40Hz. Traces were then exported and loaded directly into MATLAB as a 2D matrix.

Area Under Curve Measurements

Where appropriate, data were analysed to determine the area under the curve (AUC) during visual stimulation. This was calculated using the inbuilt MATLAB function "trapz" which utilised trapezoidal numerical integration.

2.5 Ex Vivo Experiments

As well as in vivo studies, a small number of ex vivo studies were also carried out using brain slices. Fixed slices were used to characterise vascular anatomy and levels of inflammation and detailed experimental procedures are outlined in chapter 3.

2.6 Behavioural Testing

Behavioural tests were conducted by Laura Bell on mice that had undergone surgery. Tests were conducted over three consecutive days and care was taken to maintain consistency across the three days. Mice were placed in the same position in the same experimental box at the same time each day and cages were not cleaned throughout the three day period. On day one, mice were placed in an empty experimental arena for 10 minutes in order to become familiar with the environment. A measure of locomotion was obtained from recordings made on day one, where a 3x3 grid was placed over the arena and the number of times the mouse crossed a grid line was recorded. The following day, animals underwent a spatial object recognition task where a pair of objects was placed in the arena. After 10 minutes of exploring the environment, mice were returned to the home cage for 5 minutes, before returning to the arena, where one of the objects was moved to a novel position. Animals were then permitted to explore this environment for a further 10 minutes before being returned to the home cage. On day three, mice were again placed in the arena with the same pair of objects for 10 minutes with a 5 minute return to the home cage, however instead of the object being moved to a novel position, it was replaced by a novel object in the same position (see figure 2.8). This combination of tests helped to examine spatial and short term memory as mice were expected to spend more time with the novel object/at the novel position than with the familiar object/position. The amount of time mice spent interacting with each object was hand scored using a macro in Excel (Microsoft). Interaction was classed as sniffing, touching or rearing up at an object. A ratio of time spent exploring the novel versus familiar object/position was calculated (discrimination ratio) and any animals that spent less than 15 seconds exploring were excluded from further analysis.

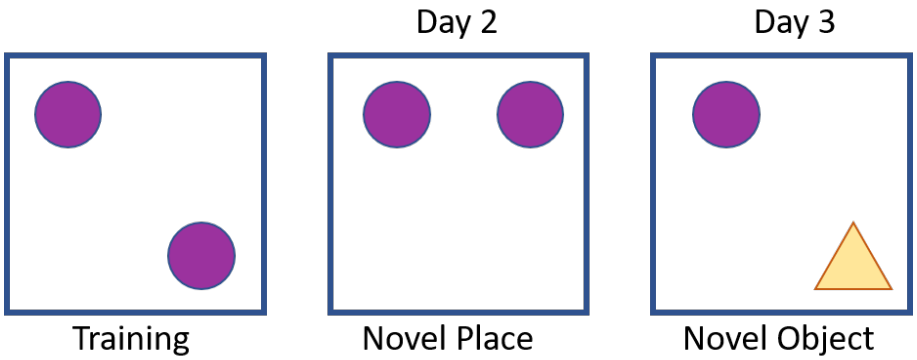

Figure 2.8: **Behavioural Assays** On both days mice were free to explore the arena for 10 minutes. Day 2: Familiar object was moved to a novel location. Day 3: Novel object was placed in a familiar location.

2.7 Statistical Analysis

Linear mixed models were carried out as described in the text in R, ANOVAs in SPSS and all other analyses in GraphPad Prism 8. Detailed statistical output and group sizes for each graph can be found in Appendix A .

Chapter 3

Effect of ApoE4 on Resting State Neurovascular Parameters in Young Mice

3.1 Introduction

Animal models expressing human APOE have been reported to have reduced CBF, increased BBB permeability as well as pericyte and endothelial damage and human carriers display altered CBF many years before going on to develop AD (Bell et al., 2012; Koizumi et al., 2018; Tai et al., 2016). This evidence points towards vascular disruption associated with ApoE4, however little is known about the ability of carriers to elicit the neurovascular coupling response and therefore provide neurons with adequate energy supply. Impairments to this process could help to explain how APOE4 helps to promote the development of Alzheimer's disease, as hypoxic conditions have been shown to facilitate the aggregation of of beta amyloid and tau (Fang et al., 2010; Sun et al., 2006). To study whether ApoE4 does alter this ability of the vasculature to meet neuronal demand with adequate blood supply, I first investigated neurovascular function at rest in this chapter, before going on to study how the neurons and vasculature in APOE4 mice respond to visual stimulation (in Chapter 4).

The motivation behind the work in this chapter was two-fold. Firstly by examining the vascular anatomy, resting state neuronal characteristics and intrinsic vascular properties such as vasomotion, it was possible to garner enough information to determine if APOE4 mice were likely to be operating with a baseline neurovascular deficit. Examining these basal properties is important before going on to examine the ability of the NVU to elicit

functional hyperaemia responses in the next chapter. Secondly, by choosing a relatively young age point, this study helps to further understand the role of ApoE early in the disease process.

3.1.1 Resting state vascular deficits in AD

As discussed in detail in the main introduction, in those with Alzheimer's disease, and in various mouse models of AD, there have been reported alterations to the vasculature that are thought to have functional ramifications. Such alterations include loss of BBB integrity (Sweeney et al., 2019; Montagne et al., 2017), an increase in the number of string vessels (Brown, 2010), capillary constriction (Nortley et al., 2019), pericyte dysfunction (Sagare et al., 2013) as well as a number of functional studies showing an increase in capillary stalling (Cruz Hernández et al., 2019) and hypoperfusion (Love and Miners, 2016). These findings suggest that in AD, there is an impairment in the basal vascular function, that would likely be compounded when neurons become active and the vasculature is tasked with providing them with an influx of fresh blood. As well as studies carried out in AD mouse models, some work has been done to investigate the effect of ApoE4 on the neurovasculature. Although this work is limited compared to that carried out in AD models, similar findings have been reported in APOE4 mice, including a more permeable BBB (Bell et al., 2012; Halliday et al., 2016), a reduction in vascular density (Koizumi et al., 2018), endothelial and pericyte damage (Bell et al., 2012; Halliday et al., 2016) and hypoperfusion (Koizumi et al., 2018).

I investigated several of these features of the vasculature in young APOE4-TR mice, in order to determine the baseline state of vascular function, upon which the functional hyperaemia response would be added.

In addition to the vasculature, I assessed the neuronal activity in these mice, whilst at rest in the dark, allowing for an estimation of energy demand at baseline. It also began to answer the question of whether or not these young mice displayed any neuronal hyperactivity or seizure like activity (Hunter et al., 2012; Nuriel et al., 2017), as previously reported in older APOE4-TR mice.

3.1.2 Vasomotion

One property of the vasculature that was only briefly eluded to in the main introductory text, is vasomotion. This is the oscillation of the vascular diameter at a frequency of ~0.1Hz in arterioles and arteries (Auer and Gallhofer, 1981; Mayhew et al., 1996; Mateo

et al., 2017). Little is known about the specific drivers of this oscillatory behaviour. Several studies have reported it to be an intrinsic vascular property that occurs in the absence of neuronal input (Osol and Halpern, 1988; Gustafsson et al., 1994) or is minimally affected by large reductions in neuronal activity (Winder et al., 2017) , however others have shown, by optogenetically driving the envelope over γ band activity, they were able to drive these slow oscillations in vascular diameter, demonstrating that γ activity entrains vasomotion (Mateo et al., 2017). These two apparently opposing conclusions can be reconciled by the idea that, probably, vasomotion is indeed an intrinsic property of vessels that can be modulated by a number of other inputs, including neuronal activity. What is known, is that the fluctuation in vascular diameter occurs as a result of the hyperpolarisation and depolarisation of VSMCs (Gokina et al., 1996; Oishi et al., 2002), resulting in vascular dilation and constriction respectively. As previously discussed (section 1.1.2), VSMCs are coupled to endothelial cells via myoendothelial gap junctions, allowing for this electrical activity to be propagated along the vessel across reasonably long distances ($\sim 1mm$) and it may also be conducted by callosal projections (Mateo et al., 2017). This intrinsic nature of vessels to fluctuate, independently of neural input, has important implications for resting state fMRI studies, however that is beyond the scope if this body of work.

Vasomotion is thought to play a role in several brain processes. Firstly, it is important for the passive clearance of substances, such as Aβ, from the brain. Studies have shown that a decrease in arteriole pulsatility correlates with a decrease in the movement and clearance of substances along the vessels (Iliff et al., 2013; van Veluw et al., 2019). It is thought to play a role in tissue perfusion (Rücker et al., 2000) and oxygenation (Tsai and Intaglietta, 1989). Its involvement in these multiple processes means that vasomotion can also serve as a useful indicator of whether the vasculature is functioning properly.

In Alzheimer's disease, several studies suggest that aberrant vasomotion may be part of the disease pathology. van Veluw et al. (2019) showed that disruption to the VSMCs as a result of Aβ, meant that vessels were less able to be driven to oscillate at the vasomotion frequency and the clearance of dextran from the parenchyma was reduced accordingly. In addition, other studies have shown that dysregulation of neuronal Ca^{2+}, as a result of Aβ, can cause a disruption to the vascular tone (Di Marco et al., 2015). Other effects of Aβ on the vasculature can cause the release of ET-1 which is a vasoconstrictor (Nortley et al., 2019; Palmer et al., 2012) and the suppression the production of the vasodilator NO (Toda and Okamura, 2012). Paradoxically, the suppression of NO has been shown to enhance vasomotion (Dirnagl et al., 1993; Yuill et al., 2010) however in tandem with

the effects of ET-1, aberrant fluctuations could occur that are outside of the optimal vasomotion frequency range. Evidently, disruption of vasomotion could have multiple deleterious effects in AD, and its role in the disease process is important to consider. What is unknown however, is whether vascular interactions with ApoE can impact this process, and if they do so in an isoform dependent manner.

3.1.3 Aims

The aims of this chapter were to validate the 3-4 month age range as a suitable, pre-clinical time point and subsequently to understand how the baseline vascular properties might be altered in APOE4 mice. Specifically, it aimed to determine : **1) Are there deficits to the vascular anatomy and functionality in APOE4 mice, even in the absence of neuronal demand?** As aforementioned, gaining this knowledge will help to further the understanding of ApoE4 on the neurovasculature so a basal energy balance in the brain can be estimated. **2) Is neuronal activity in the absence of a sensory stimulus altered in these animals?** Any vascular alterations could be a response to altered energy demands, to rule out this possibility, neuronal activity, indicative of energy demand, at baseline was measured.

3.2 Methods

3.2.1 In Vivo Preparation

3.2.2 Data Collection

As previously explained in the main methods section, APOE3-TR and APOE4-TR animals that had undergone cranial window surgery were either imaged using two-photon microscopy or had net haemodynamic parameters recorded across the window using the OXY-CBF probe. Pial and capillary diameter measurements, capillary RBC velocity measurements and population neuronal activity was recorded and for all of these parameters, with the exception of the capillary recordings, dedicated "baseline" recordings were taken where visual stimuli were not presented. On average, recordings lasted for ∼4 minutes. Locomotion was recorded using a rotary encoder device.

Data analysis

Baseline vascular and haemodynamic measurements

Data was extracted as described in section 2.4.2 and rest epochs in each of these measurements were identified, i.e. periods when the mouse was not moving. For capillary diameter and RBC velocity traces, where there was also a visual stimulation, rest periods were selected only during the inter-stimulus interval, when there was no visual stimulation displayed.

Movement of any duration was classified as locomotion and was removed from the analysis along with a 1.5 second transition period on either side. Any epochs that were within 3 seconds of each other were classified as the same event and so the entire period was removed.

The remaining data was averaged together to provide average pial and capillary diameters and average RBC velocities per blood vessel and average net $CMRO_2$, SO_2 and flux per animal. The coefficient of variation was calculated for RBCV, SO_2 and flux measurements by dividing the standard deviation by the mean.

In vivo z-stacks were taken along the horizontal plane, as deep into the parenchyma as was possible while maintaining image quality. A pixel size of 1.28 μm was maintained across all stacks.

Vasomotion

Rest epochs of at least 10 seconds were detected as described above, and the corresponding pial and capillary diameter traces during these epochs were taken for further analysis. A fast Fourier transform (FFT) of vessel diameter was carried out for each epoch using the inbuilt MATLAB "FFT" function. The variation in epoch length and the subsequent effect on the power, was controlled for by dividing by length. To produce an average power spectrum for each vessel, non-linear interpolation was used to make all FFTs the median length of all rest epochs per vessel. To control for pink noise (Szendro et al., 2001) all traces were multiplied by the frequency, and to control for variations in the power arising from variations in vessel brightness, relative power was determined by dividing all traces by their sum.

Neuronal Data

Fluorescence traces were extracted from neuronal recordings, as previously described in section 2.4.2, and the number of peaks per minute during rest periods were detected. Rest epochs of a least 10 seconds were detected as outlined above and the corresponding fluorescence traces were stitched together. Peaks that were at least twice the standard deviation of the entire trace and were at least 0.25 seconds apart from each other were counted and converted into peaks per minute. The trace was normalised to the middle 1000 frames (∼2minutes) to give a $\Delta F/F$ trace and the size of each peak was determined.

3.2.3 Slice Preparation

Tissue Extraction

With the assistance of Dr Kira Shaw, NG2-DsRed positive animals were transcardially perfused with a fixative and a fluorescent gel to enable visualisation of the vasculature post-mortem (Lugo-Hernandez et al., 2017; Tsai et al., 2009b). Animals were injected intraperitoneally with pentobarbital which acted as a terminal anaesthesia. Once the animal was no longer responsive to a toe pinch and had no other reflexes, the chest cavity was opened and the heart exposed. A 25 gauge needle was inserted into the left ventricle and the right atrium cut to allow for blood drainage. Iced 0.1M phosphate buffer saline (PBS) was then perfused into the heart for 5 minutes at 5mL/min followed by 15 minutes of iced 4% paraformaldehyde (PFA - Sigma-Aldrich) in PBS to fix the tissue. This was followed by 5 minutes of PBS warmed in a water bath to 30 °C , and finally by 3 minutes of 5% gelatin (Sigma-Aldrich) containing 0.2% FITC-conjugated albumin (Sigma-Aldrich).

Animals were then kept on ice for a minimum of 30 minutes before the brain tissue was extracted and placed into 4% PFA for 24 hours at 4°C, after which it was transferred to 30% sucrose in PBS for a minimum of 3 days.

For tissue that underwent immunofluorescent staining, tissue was extracted fresh and placed directly into PFA, as animals were being imaged under terminal anaesthesia and therefore, transcardial perfusion was not possible. Tissue was stored overnight in 4% PFA at 4°C before being transferred to 30% sucrose in PBS for a minimum of 3 days.

For both experiments, brains were coronally sliced to 200μm on a vibratome (Vibratome®) and those slices containing the visual cortex (as per the Allen Brain Atlas) were selected and were either stained for microglia and astrocytes before mounting or else directly mounted onto slides (SuperFrost, Thermo Scientific) and covered with HardSet Vectashield (Vector Labaratories) and glass coverslips (Menzel 24 x 60 mm 0.13 - 0.16mm, Thermo Scientific).

Immunofluorescence Protocol

The immunofluorescence experiments and image capture was carried out by Laura Bell using the method outlined below.

All incubation and washing steps were done under gentle agitation of the slices on a shaker. Upon slicing, brain tissue was washed for 10 minutes in PBS, three times before being incubated in a blocking/permeabilisation solution (5% normal goat serum (Sigma-Aldrich), 0.3% Triton X-100 (Sigma-Aldrich) in PBS) for a minimum of 1 hour. Slices were then incubated in primary antibody for 36 hours at 4°C and washed in PBS, three times for 10 minutes. They were then incubated in secondary antibody for 24 hours at 4°C before being washed in PBS, three times for 10 minutes. Slices were then mounted as described above. See table 3.1 for antibody details.

Immunofluorescence Imaging

The primary visual cortex regions of slices were imaged using an inverted Leica SP8 TCS confocal microscope (Leica Microsystems) using a 20x air objective (HC PL APO CS2 20X/0.75, Leica Microsystems). Continuous wave lasers with excitation wavelengths of 488nm, 561nm and 633nm were used to visualise FITC, DsRed and AlexaFluor 647, respectively. Z-stack images were collected as a 1024 x 1024 pixel matrix, with a line average ranging between 3 - 4, a lateral pixel resolution ranging from0.45μm - 0.57μm, and a z-pixel depth ranging from 0.7μm -2.4μm. All imaging was carried out with the user

	Blocking/permeabilization solution	Primary Antibody	Secondary Antibody
Astrocytes	5% normal goat serum, 0.3% Triton X-100 in 1x PBS	Chicken anti-GFAP (1:500 in blocking /permeabilization solution, Abcam ab4674)	Goat anti-chicken Alexa Fluor 647 (1:600 in blocking /permeabilization solution, Invitrogen A-21449)
Microglia		Rabbit anti-iba1 (1:600 in Blocking /permeabilization solution, WAKO 019-19741)	Goat anti-rabbit Alexa Fluor 647 (1:600 in blocking /permeabilization solution, Invitrogen A-21245)

Table 3.1: **Antibody details**

blinded to animal genotype. Images were viewed and analysed using ImageJ (Schindelin et al., 2012). NG2-DsRed/APOE-TR mice were used throughout all experiments. In those used to characterise vascular anatomy, DsRed was used to mark pericyte locations and calculate the number of pericytes per mm of vessel, and the vasculature filled with the FITC-conjugated albumin was used to assess vascular morphology. To study the effect of cranial window surgery on the inflammatory markers microglia and astrocytes, slices were stained for Iba1 and GFAP respectively.

Image Analysis

To characterise the vasculature and pericytes, z-stacks were analysed in ImageJ using a macro built by Dr. Devin Clarke. Both in vivo stacks and slice stacks were analysed in this way. First, stacks were registered and averaged across imaging planes, any large patches of noise were manually selected and removed, before thresholding using the autothreshold function in ImageJ. In one case the stack was manually thresholded but otherwise the Default, Huang, Huang2 or Li thresholds were selected, based upon which one best represented the non-thresholded stack. The vasculature was then skeletonised in 3D, all skeleton co-ordinates and branch points were determined and a distance map created of the vasculature. Vessel length was then calculated from the branch skeletons, density was determined from these values and vessel radii were found by determining the grey value from the distance map at each skeleton point. Pericyte cell body locations were marked

using the imageJ multipoint tool and vessel diameter as function of distance from the cell body was computed. Vessel tortuosity was calculated by dividing branch length by the euclidean length. All values were averaged per slice.

Microglia and astrocytes were analysed by Harry Trewhitt by conducting cell counts in 35μm bins from the surface of the brain on the surgical and non-surgical hemispheres. The cell counts were normalised to the area of each bin and the surgical hemisphere was normalised to the non-surgical hemisphere.

3.2.4 Behavioural Testing

All behavioural testing and analyses were carried out as described in section 2.6.

3.3 Results

3.3.1 Effect of ApoE on spatial and short term memory

To test whether 3-4 month old animals exhibited cognitive deficits, three simple behavioural measures were obtained. To test short term memory (Clark et al., 2000), a novel object recognition task was carried out and similarly, a spatial object recognition task was carried out to assess hippocampal dependent spatial memory (Dix and Aggleton, 1999). As the hippocampus is especially vulnerable in AD, this task was of particular interest and is where any deficits might have been expected to be observed. A discrimination ratio (DR) was calculated for both, with a higher DR indicative of better short term / spatial memory. Finally, a measure of locomotion was obtained to asses how much the mice moved within the testing arena. Across all three behavioural measures, APOE3 and APOE4 mice displayed similar DRs (see figures 3.1A, B) and similar measures of locomotion (see figure 3.1C) suggesting that there were no impairments in the short term or spatial memory of APOE4 mice of this age. This is an important finding as young animals were chosen to study the interaction of ApoE and the vasculature, prior to any cognitive deficits and the findings of these tests confirm the suitability of this age point.

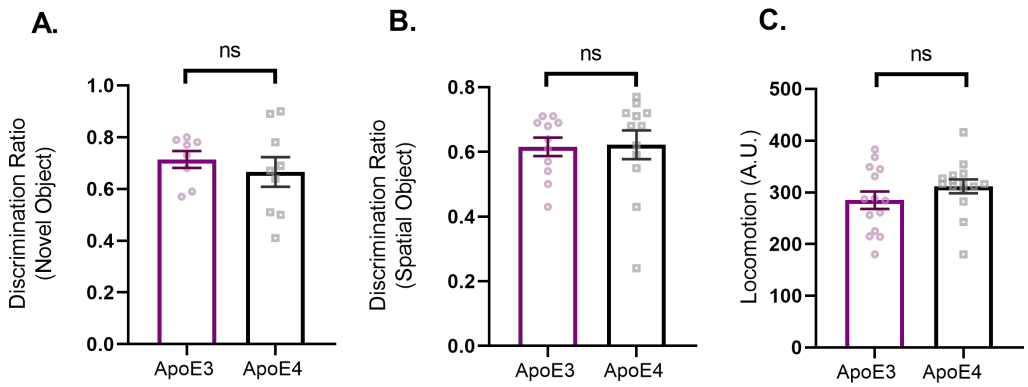

Figure 3.1: **Effect of ApoE on spatial and short term memory** A. Discrimination ratios for APOE3 and APOE4 mice during a novel object recognition task. B. Discrimination ratios for APOE3 and APOE4 mice during a spatial object recognition task. C. A measure of locomotion for APOE3 and APOE4 mice. Circles represent individual animal scores. Error bars represent SEM. For statistical outputs and n numbers see table A.1

3.3.2 Inflammation at the surgical site

ApoE4 has previously been associated with elevated inflammatory responses as a result of increased cytokine release (Fan et al., 2017; Ophir et al., 2005) and microglial activation (Safieh et al., 2019; Rodriguez et al., 2014). Although, in this study, every effort was taken to ensure mice were given sufficient time to recover from surgery (with a minimum recovery period of 2 weeks), it was still essential to ensure that neither genotype was disproportionally affected by the surgery, and therefore have the confounding effect of inflammation present. Sliced tissue was stained for microglia and astrocytes (figure 3.2A), as markers of inflammation. The number of cells as a function of distance from the surface of the brain was quantified from the surgical site and normalised to the non-surgical hemisphere. Results show that the normalised cell numbers did not differ over distance and at the surface of the brain, APOE4 animals did not show an increase in inflammatory markers (figures 3.2B, C). These data suggest that there were not increased levels of inflammation in APOE4 mice following recovery from the cranial window implantation.

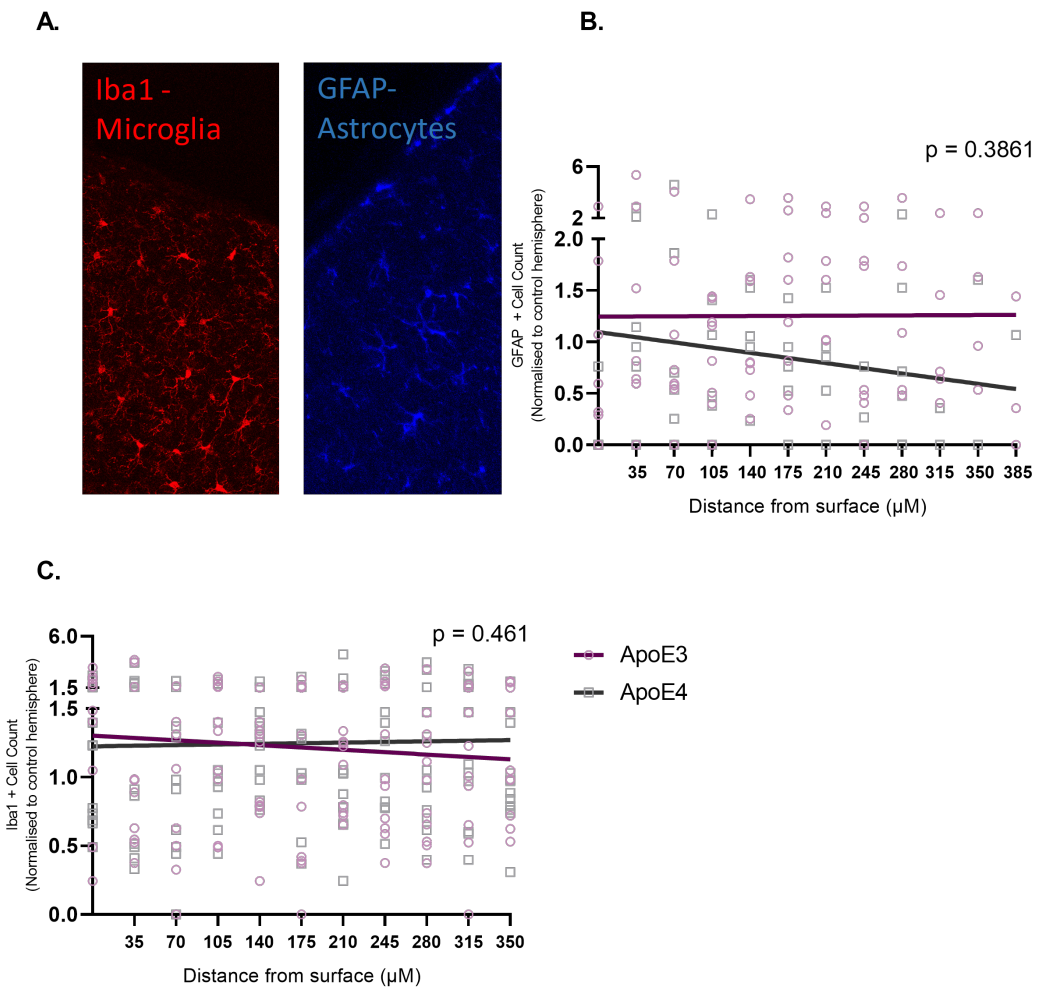

Figure 3.2: **Effect of ApoE on inflammatory responses post surgery** A. Example images of Iba1 positive cells (microglia) and GFAP positive cells (astrocytes) in brain slices. Taken using confocal microscopy. B. Number of GFAP positive cells in each distance bin (from the surface of the brain). Surgical hemisphere was normalised to non-surgical hemisphere. C. Number of Iba1 positive cells in each distance bin (from the surface of the brain). Surgical hemisphere was normalised to non-surgical hemisphere. Circles represent slice average at each distance point. p values reflect difference in the slopes. For detailed statistical output see table A.2.

3.3.3 Effect of ApoE on Vascular Anatomy

To characterise the vasculature in APOE3 and APOE4 mice, various parameters were measured across several platforms. These parameters included capillary density as an indicator of how well perfused the parenchyma was, capillary diameter as an indicator of blood volume that can reach the tissue, as well vascular tortuosity. Vessel tortuosity has previously been reported in AD where vessels have become twisted or kinked. This could result in a disruption to the network as a result of increased vascular resistance (Govindpani et al., 2019). Initially, these measures were obtained from in vivo z-stacks taken using two-photon microscopy (see figure 3.3A for an example image). No genotype differences were observed in the capillary density, diameter or tortuosity (figure 3.3B, C, D).

Whilst the in vivo approach was an attractive option as it measured from living tissue and was therefore not subject to post-mortem modifications and processing, the fact that the images were taken on a horizontal plane made it more difficult to gain information on the smaller capillaries that were deeper and therefore less bright. In addition, the imaging parameters used resulted in a relatively large pixel size (1.28 μm) making it difficult to pick out finer structures. This is evident from the observed average capillary diameter of $\sim$6μm which is larger than has previously previously reported (Koizumi et al., 2018).

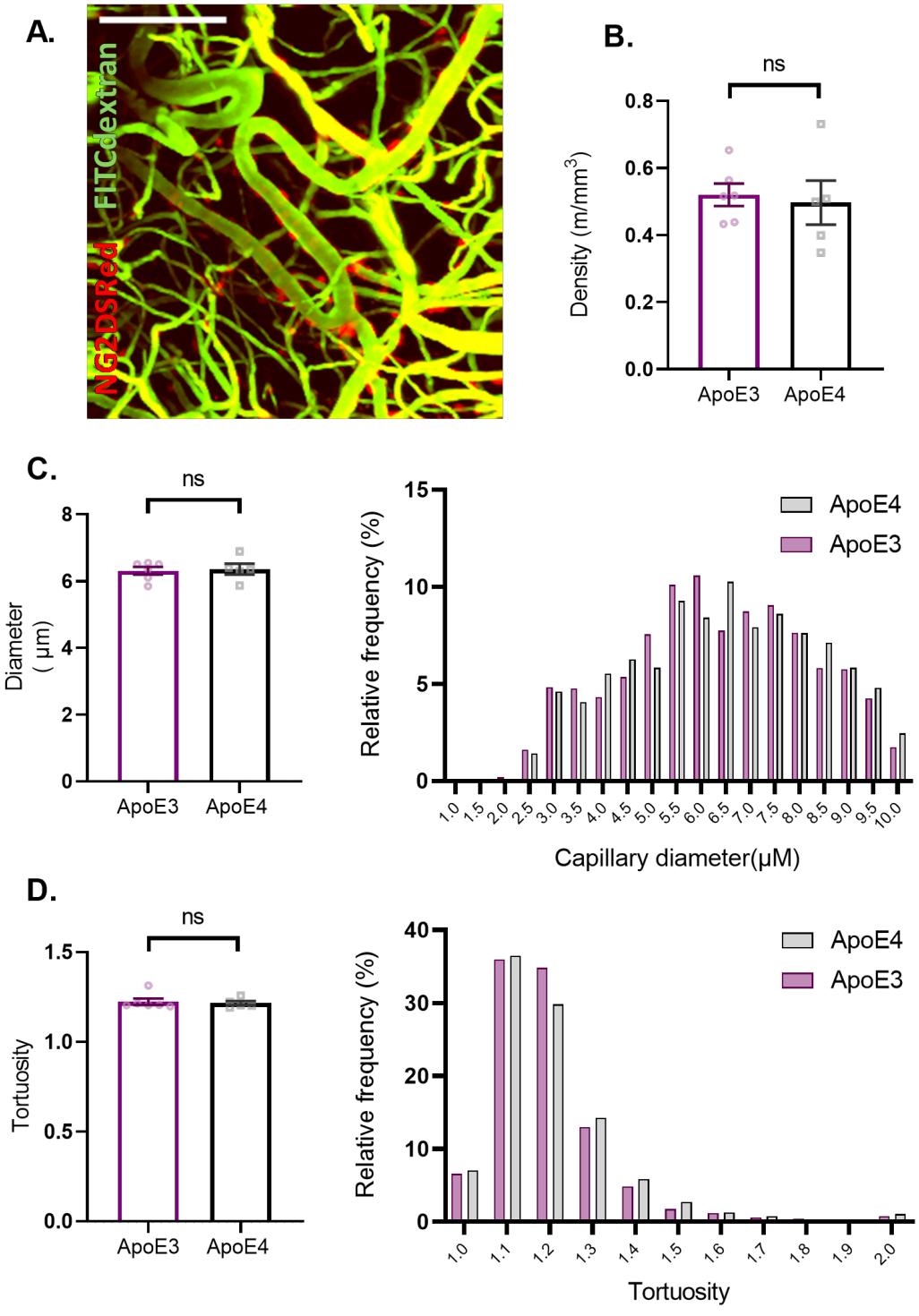

Figure 3.3: **In vivo vascular anatomy** A) An example horizontal z-stack taken from an APOE3 animal, using two-photon microscopy. Scale bar (white) = 100μm. B. In vivo capillary density in APOE3 and APOE4 mice. C. Average in vivo capillary diameter (left panel). Relative frequency distribution of all vessel diameters (right panel) D. Average in vivo capillary tortuosity (left panel). Relative frequency distribution of all vessel tortuosity measures (right panel). Circles represent individual animal averages. Error bars represent SEM. For detailed statistical output see table A.3

To overcome these difficulties in measuring from the smallest capillaries that were deep within the tissue, fixed coronal brain slices were taken from APOE3 and APOE4 animals and imaged using confocal microscopy. Animals had the vascular lumen filled with a fluorescent gel, allowing for the visualisation of the vascular network and the presence of DsRed in pericytes allowed for the examination and quantification of pericyte number. As is evident from figure 3.4A, this method allowed for easier visualisation of the smallest vessels, as well as for a smaller pixel size (0.57μm) than the in vivo images. This improved ability is also reflected in the lower capillary diameters measured across both genotypes (figure 3.4F, G) that better reflect the known range of capillary diameters (Koizumi et al., 2018; Shaw et al., 2019). Although with this method it is possible that some capillaries could have collapsed post mortem or were incompletely filled with gel.

These data from fixed tissue provided some interesting findings. In APOE4 animals the capillary density was reduced compared to APOE3 animals (figure 3.4B) which concurs with previous reports (Koizumi et al., 2018). Vessel tortuosity remained unchanged between genotypes (figure 3.4D), as did the number of pericytes per mm of vessel (figure 3.4C). Another intriguing difference between these data and the vivo recordings, was that the average capillary diameter in APOE4 mice, was greater than that in APOE3 mice. This has not previously been reported and was unexpected.

To further investigate this, capillary diameter as a function of distance from the pericyte soma, was calculated following findings by the Attwell group (Hall et al., 2014; Nortley et al., 2019) showing that pericytes can cause pathologic constriction in capillaries in response to ischaemia or Aβ. When considering the actual diameters along the vessel, it was apparent that the diameter at the soma was larger in APOE4 than in APOE3 mice (figure 3.4G, H), as found for the overall average diameters. However, normalising each vessel's diameter to that at the pericyte soma revealed that the diameter of APOE4 vessels increased with distance from the soma (the slope of the diameter as a function of distance from the soma was significantly different from zero), while APOE3 vessels had the same tone regardless of distance from the pericyte soma (figure 3.4I). These results suggest that there may be some dysfunction at the pericyte processes, resulting in the inability to maintain vascular tone. Important to note, is that these experiments show data from a relatively small experiential group (n = 3/4 animals per genotype) and replicates would be required to ensure these findings were sound.

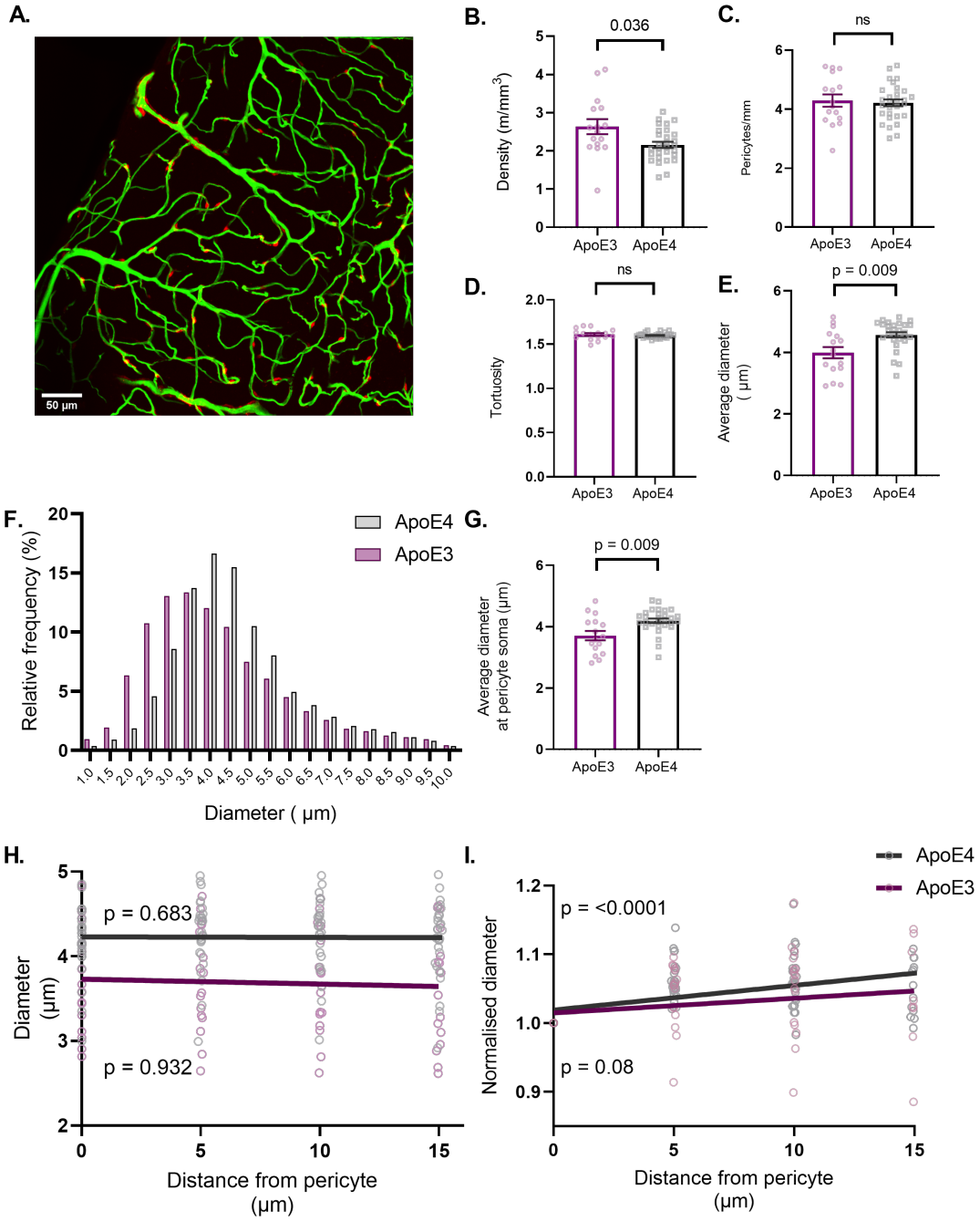

Figure 3.4: **Slice vascular anatomy** A. Example z-projection of a brain slice from an APOE3 animal with FITC-conjugated albumin (green) filled vasculature and DsRed positive pericytes and SMCs (red) taken using confocal microscopy. B. Capillary density measurements from APOE3 and APOE4 mice. C. Number of pericytes per mm of vasculature in APOE3 and APOE4 mice. D. Vessel tortuosity (branch length/euclidean length) from APOE3 and APOE4 mice. E. Average capillary diameter from APOE3 and APOE4 mice. F. Relative frequency distributions of all vascular diameters. G. Average capillary diameter at the pericyte soma in APOE3 and APOE4 mice. H. Absolute capillary diameter as a function of distance from the pericyte soma. I. Normalised capillary diameter as a function of distance from the pericyte soma. All circles represent a slice average and error bars represent SEM. For detailed statistical output and group sizes see table A.4

Individual vessels were sampled to further determine if there were any functional, as well as anatomical differences between genotypes. At an individual vessel level, the pial and capillary diameters did not differ between genotypes (figures 3.5A, B), nor did capillary RBC velocities (figures 3.5C). Some capillary diameters recorded in mice of both genotypes were smaller than expected (i.e. a minimum value of 1.7μm, as opposed to $\sim$3μm as seen in other studies (Koizumi et al., 2018; Shaw et al., 2019)). This is likely because of the passage of RBCs creating dark patches in the vessel and so decreasing the average diameter - it is therefore likely that the diameters obtained from the slice preparation were more accurate.

Resting net values across the visual cortex were compared between genotypes. It might have been expected to observe lower CBF (flux) or SO_2 values, as a result of the lower vascular density, however there was no genotype difference observed (figures 3.5D, E). In addition, the oxygen use in the brain ($CMRO_2$) was the same across genotypes (figure 3.5F).

The coefficient of variation (CV) provides a measure of temporal variability of each parameter, for flux and RBCV this measurement gives an indication of how oxygen delivery may, theoretically, be altered (Lu et al., 2019). Although there were no significant differences between genotypes across all three measures (figure 3.5G, H, I), there was a trend towards an increased CV in the RBCV in APOE4 mice ($p= 0.09$) suggesting that oxygen delivery may be mildly altered in APOE4 animals.

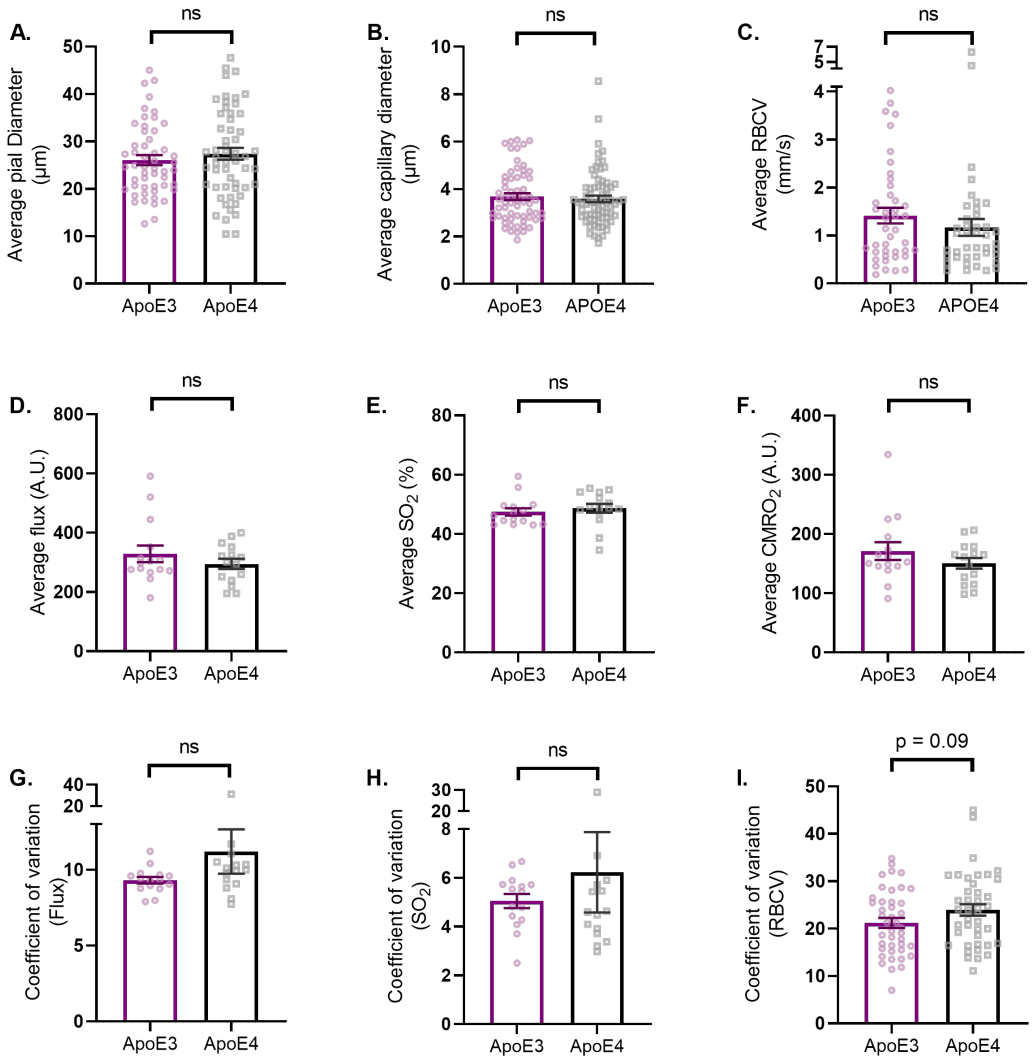

Figure 3.5: **In vivo resting state measurements** A. Average pial diameter during rest periods in APOE3 and APOE4 mice. B. Average capillary diameter during rest periods in APOE3 and APOE4 mice. C. Average capillary red blood cell velocity during rest periods in APOE3 and APOE4 mice. D. Average net flux (E) SO_2 and (F) $CMRO_2$ during rest periods in APOE3 and APOE4 mice. Coefficient of variation for net flux (G.) and SO_2 (H.) measurements, and for capillary RBC velocity measurements (I.) For A-C and I, circles represent individual vessel averages, for D-H circles represent animal averages. Error bars represent SEM. For statistical outputs see table A.5.

This examination of the vascular anatomy and functionality at rest, both in vivo and in slices, suggests that vascular properties were largely preserved in APOE4 mice, with the exception of the reduced vascular density and a trend suggesting the CV of RBC velocity might be higher in APOE4 mice. An increase in the CV of RBC velocity is thought to be reflective of an increased capillary transit time heterogeneity, an increase in which might suggest some alterations to oxygen extraction (Østergaard et al., 2013). In this case, these results were not significant and there was no corresponding change in resting SO_2, so it is likely that the trend level results were not having an significant impact on tissue oxygenation.

3.3.4 Examining Vasomotion in APOE-TR animals

As vasomotion is an important physiological process when considering clearance, tissue perfusion and oxygenation, it is an interesting parameter to explore in APOE-TR animals. Its role in these various processes means it can be useful in probing vascular health and indeed it has previously been found to be impaired in AD (Di Marco et al., 2015). In order to detect vasomotion, the time domain of vascular diameter traces during rest (see figure 3.6A) were converted to the frequency domain using a fast Fourier transform. Utilising this method, a peak was indeed observed in the vasomotion frequency range (∼0.1Hz) (See arrow in figure 3.6B). The power at the vasomotion frequency was determined for all APOE3 and APOE4 vessels during rest and the power (relative to the sum of the whole power spectrum) was determined across frequency bins of 0.1Hz. The relative power was found to be greater in APOE3 animals from 0.1-0.3Hz, with the 0.3- 0.4 Hz range almost reaching statistical significance ($p = 0.051$, figure 3.6C). When directly comparing the relative power at 0.1Hz, APOE3 mice exhibited statistically higher power at this frequency (figure 3.6D). As a further verification that power in the 0.1- 0.3Hz reflected vasomotion and not something else, I compared the power at the same frequencies in capillaries which do not exhibit vasomotion (Mateo et al., 2017; Di Marco et al., 2015). As can be seen in figure 3.6E, there was no peak at the vasomotion frequency, nor were there any differences in the relative power from 0.1Hz - 0.4Hz (figure 3.6E, F), confirming that the frequency bump observed in the pial diameter traces was not due to noise created during the FFT. These data point towards an intrinsic deficit within the APOE4 vasculature with possible consequences to the clearance and perfusion mechanisms in these animals, although further experiments would be needed to confirm the functional implications.

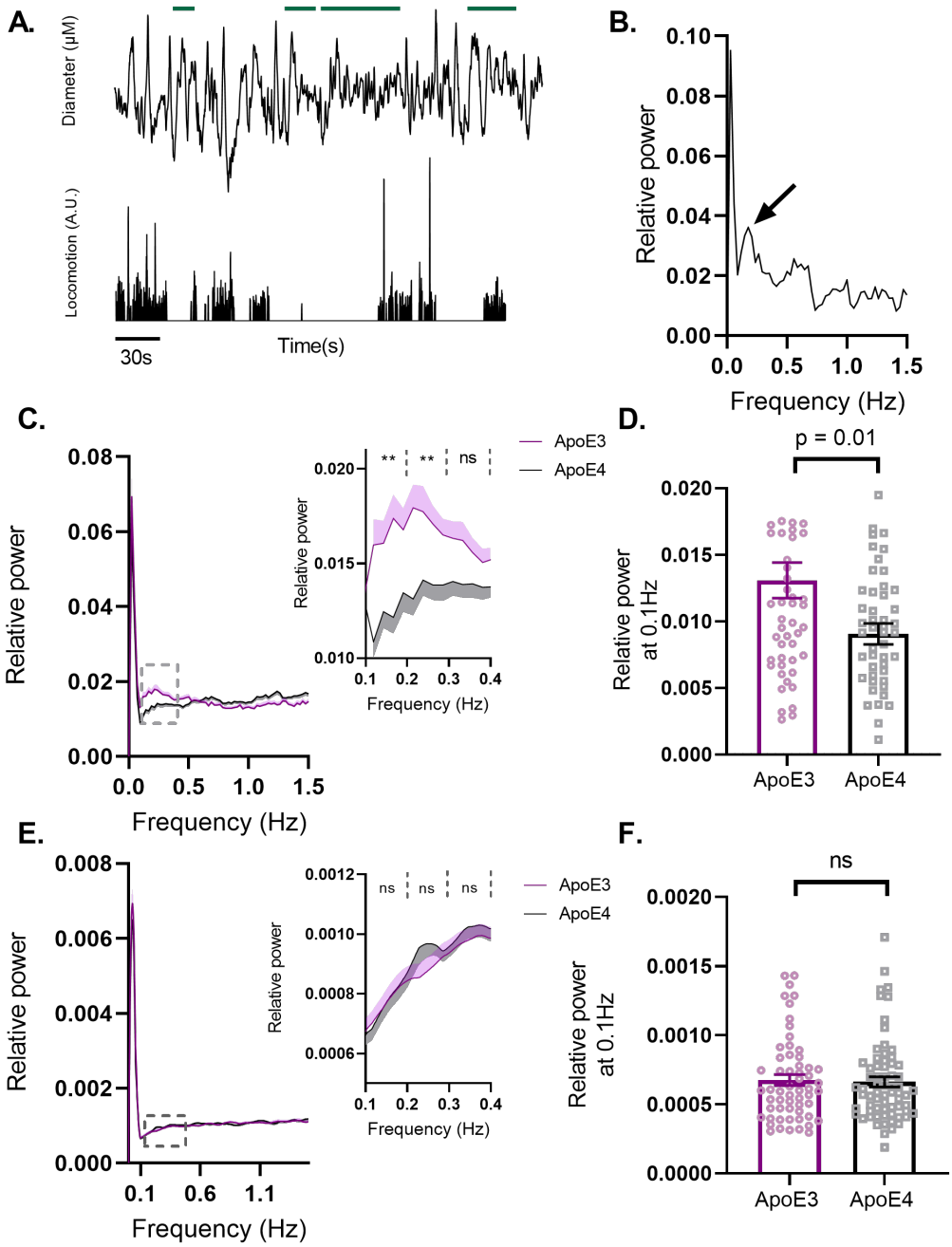

Figure 3.6: **Vasomotion during rest** A. An example diameter (top panel) and the corresponding locomotion (bottom panel) trace. Detected rest periods are represented by the green bars. B. Relative power spectrum of the vessel shown in A. Arrow denotes the peak in the vasomotion frequency range. C. Relative power spectra for all averaged APOE3 and APOE4 pial vessels. Upper right insert corresponds with the grey dashed box. Dashed grey lines on insert graph show the frequency bins that were compared. D. Relative power at 0.1Hz for APOE3 and APOE4 pial vessels. E. Relative power spectra for all averaged APOE3 and APOE4 capillaries. Upper right insert corresponds with the grey dashed box. Dashed grey lines on insert graph show frequency bins that were compared. F. Relative power at 0.1Hz for APOE3 and APOE4 capillaries. Circles represent vessel averages. Error bars represent SEM. For statistical outputs see table A.6.

3.3.5 Resting Neuronal Activity

In order to relate any vascular activity to neuronal demand, two-photon microscopy was used to examine the characteristics of fluorescent excitatory neurons. The number of peaks per minute has previously been used as an indicator of neuronal hyper- and hypoactivity (Busche et al., 2019) . Peaks were detected in the fluorescence traces (see figure 3.7A) and when averaged across animals, there was no observed difference between genotypes (see figure 3.7B). The correlation of neuronal firing was measured to determine if there were greater mass increases in neuronal activity in either genotype. The correlation coefficients that were measured were small, as to be expected when measuring sporadic firing in the absence of a stimulus. There was no difference in the average correlation of firing between genotypes (figure 3.7C), suggesting that the activity was equally "sporadic". Finally, the magnitude of detected peaks was determined. The amount of firing is tightly correlated to the magnitude of the GCaMP signal (Akerboom et al., 2012) and so is a useful measurement to gauge the amount of neuronal activity occurring. As with the other neuronal characteristics, there was no observed difference between genotypes (figure 3.7D). All data was averaged both by animal (as shown in figure 3.7) and across all cells. Data averaged across all cells (see figure B.1) showed the same pattern of results as seen in animal averages.

These data suggest that the neuronal characteristics were similar between genotypes and the basal energy requirements would therefore also be similar. This, coupled with the findings that the tissue in APOE4 mice had a less dense vascular network, less vasomotion and possibly a slight increase in temporal variability, suggests that there may be an energy imbalance in the tissue of APOE4 mice. However, this possible imbalance was not sufficient to alter resting SO_2 levels and is therefore likely to be subtle.

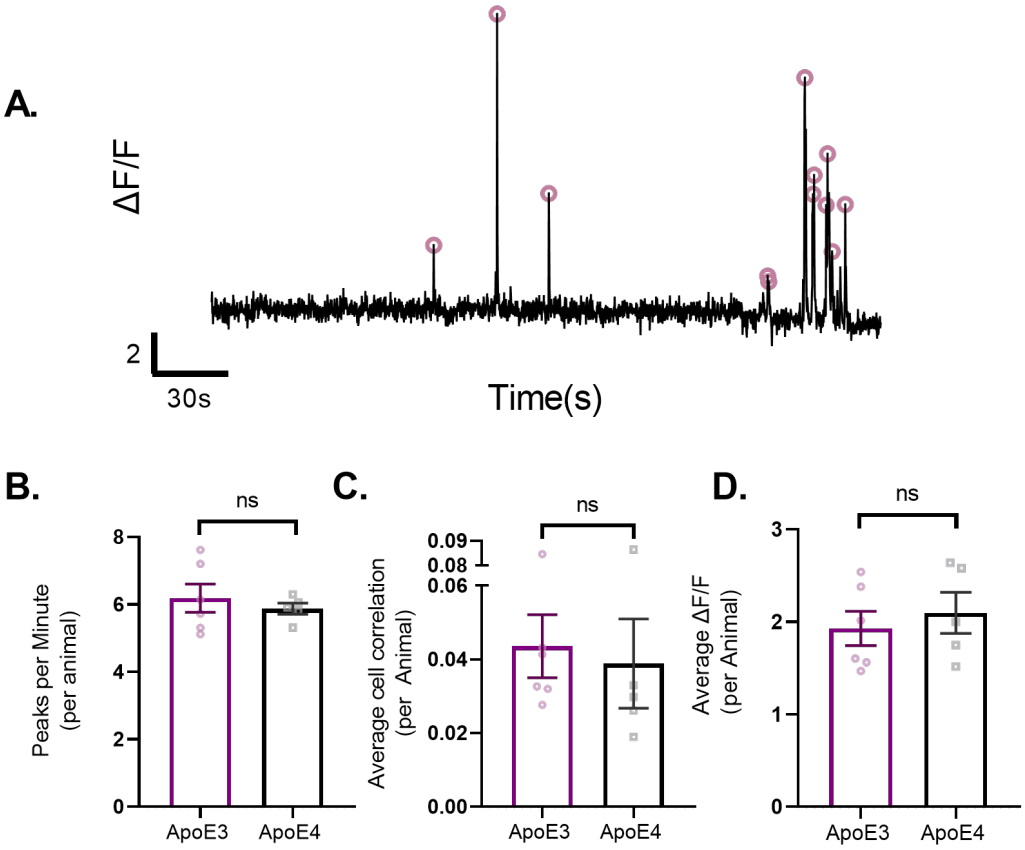

Figure 3.7: **Neuronal activity during rest**A. Example ΔF/F trace with detected peaks marked with purple circles. B. Average peaks per minute. C. Averaged correlation coefficient per animal. D. Average peak size per animal in APOE3 and APOE4 mice. Circles represent detected peaks (A) or individual animal averages (B, C, D). Error bars represent SEM. For detailed statistical output and n numbers see table A.7.

3.3.6 The Effect of ApoE4 and Sex on resting Neurovascular Parameters

Previous reports have suggested that female APOE4 carriers are more vulnerable to the pathological effects of the $\epsilon 4$ allele (Farrer, 1997) although it has been suggested by others that the risk of developing AD in APOE4 carriers is equal between males and females (Neu et al., 2017). Therefore, I wished to determine if there were any effects of sex on the data presented. For all the parameters analysed in figure 3.8, the effects of sex and genotype, as well as the sex*genotype interaction were elucidated. Across all parameters, bar neuronal PPM, there was no effect of sex, nor was there an interaction between sex and genotype in any of the measurements. In neuronal PPM measurements, there was an effect of sex, with females having a higher number of PPMs compared to males. These data indicate that sex does not have a robust effect on the results presented in this chapter and so grouping together both sexes was appropriate.

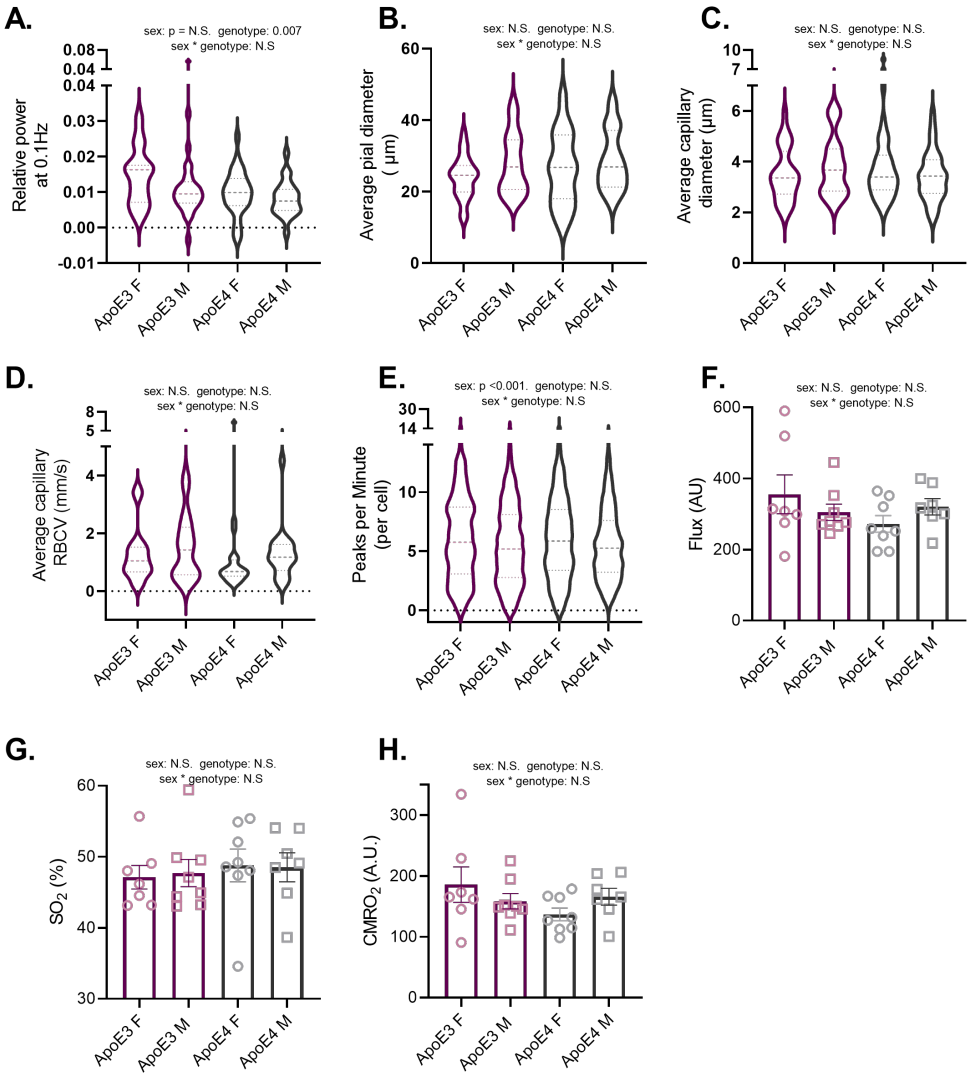

Figure 3.8: **Effect of sex on vascular and neuronal parameters** A.Relative power of pial diameter traces at 0.1Hz (vasomotion frequency), split by sex. B. Resting pial diameter, split by sex. C. Resting capillary diameter, split by sex. D. Resting capillary RBC velocity, split by sex. E. Neuronal peaks per minute during rest periods, split by sex. Net flux (F), SO_2 (G) and $CMRO_2$(H) , split by sex. A-D violin plots represent average values per vessel, E represents average value per cell and F-H represent average values per animals. Error bars represent SEM. For detailed statistical output and n numbers see table A.8.

3.4 Discussion

3.4.1 Results Summary and Interpretation

Young APOE4 animals do not display behavioural deficits

The insidious nature of AD, involving a prolonged pre-clinical period during which many pathophysiological events occur, means that the early stages of the disease are of great interest. Work from Iturria-Medina et al. (2016) has shown that vascular effects are one of the earliest deficits observed in AD patients, this in tandem with APOE4 being the most common genetic risk factor for going on to develop AD, makes studying the neurovasculature in young, APOE4 mice, an interesting and valuable research avenue. Critically, it is important to know more about what happens prior to the onset of cognitive decline so that a viable therapeutic target can eventually be identified.

In this study, 3-4 month old animals were chosen for several reasons, firstly, work from Koizumi et al. (2018) suggested that neuronal function was intact in animals of this age, but that there were already vascular deficits. In addition, practically speaking, to allow mice at least two weeks to recover, surgery needs to be carried out when mice are aged ∼8-10 weeks. Even at this age, mice (especially females) can be very small, so it would be difficult to obtain data on animals younger than this. The behavioural assays carried out in this chapter showed that there was no difference in the short term and hippocampal dependent spatial memory in young APOE4 animals, confirming this age as a suitable "young" time point to study. To fully assess cognitive function, a more thorough cognitive battery would be required, however this is outside of the scope of this work.

APOE4 mice have less perfused tissue but have larger capillary diameters

Although the in vivo approach had multiple advantages over a slice preparation in determining capillary density and diameter, the imaging parameters used, and the horizontal nature of the z-stacks made it difficult to collect information on the smallest vessels. Although one of the advantages of two-photon microscopy is the ability to penetrate relatively deep into living tissue (Shih et al., 2012), in this case, coronal slices offered a far superior look at the entire vascular tree. Therefore the data obtained from FITC-gel filled sliced was assumed to be more accurate than that obtained from the in vivo stacks. Congruent with work from Koizumi et al. (2018), APOE4 animals were shown to have a lower capillary density, when compared to APOE3 animals, suggesting that the tissue was generally less well perfused. On average neurons are $<15\mu$m from the nearest capil-

lary (Tsai et al., 2009a), allowing for the easy transmission of vasoactive messengers from neurons to the vessels (either directly or indirectly), as well as the provision of oxygen and glucose from the blood to these neurons. If these substrates have further to travel it could result in hypoxic pockets within the parenchyma or inadequate energy supply to the neurons. Paradoxically, the capillary diameters were larger in APOE4 animals, compared to APOE3 animals, coupled with this, it was found that the normalised capillary diameter increased further with increasing distance from the pericyte. There are a number of possibilities that could be at play, the pericytes could be dysfunctional and failing to maintain vascular tone - particularly at the processes. Alternatively, it could be a compensatory mechanism in place to allow a greater volume of blood to be delivered. Importantly these findings need to be replicated as they have currently been made in slices from a small number of animals.

APOE4 mice may have a larger degree of capillary RBC velocity heterogeneity

When individual pial and capillary diameters and capillary RBC velocities were measured during rest periods, they did not significantly differ between genotypes. Mathematical modelling has suggested that increased heterogeneity in the capillary bed could result in a lower oxygen extraction from the blood (Østergaard et al., 2013). In this study, the temporal variability in RBC velocity trended towards being higher in APOE4 animals, suggesting that less oxygen may be being extracted from the vasculature compared to APOE3 mice. As aforementioned, these changes were very small and may not have had any meaningful impact on the tissue oxygenation as resting SO_2 was not different between genotypes.

In light of the reduced vascular density observed in APOE4 mice, it would have been expected to detect a reduction in net CBF in these same animals. Unusually this was not the case, but a close look at the data might provide some insights as to why. APOE4 animals have a ∼18% reduction in vascular density, compared to APOE3 mice. In recent work from our group comparing the vascular density in the hippocampus and the visual cortex, there was a ∼47% reduction in vascular density that corresponded with a ∼25% reduction in net CBF (Shaw et al., 2019). Directly applying these findings to the data in this chapter, a ∼18% reduction in vascular density might be expected to result in a ∼9% reduction in CBF. In fact, the net CBF measurements in APOE4 mice were ∼11% lower that that measured in APOE3 mice, but due to the error present in the data, this was not significantly different. It is therefore likely that any resultant differences in CBF could

not be detected within the error of the data.

APOE4 mice exhibit a lower relative power at the vasomotion frequency

In what is, to my knowledge, the first look at vasomotion in APOE4-TR mice, a convincing reduction in the relative power from 0.1-0.3Hz was observed in APOE4 pial arterioles. Although vasomotion is classically at 0.1Hz, shifts from this frequency have previously been reported (van Veluw et al., 2019; Drew et al., 2010b). This fairly broad "peak" is therefore well within the vasomotion range, and further, the lack of a peak in capillary trace, buttresses the conclusion that it was vasomotion being observed. As previously discussed, vasomotion is an important indicator of vascular health as well as being a driver in clearance and perfusion mechanisms (Di Marco et al., 2015; Iliff et al., 2013; van Veluw et al., 2019) so this reduction in power is an interesting finding in APOE4 mice. At the very least it suggests some intrinsic vascular dysfunction at the pial level, and probably means there will be some disruption to the other, aforementioned, functions. APOE4 carriers already show slower clearance of Aβ due to the slower VLDL clearance pathway (discussed further in section 1.3), but this reduction in arteriolar pulsatility could be a additional contributing factor. Further experiments could be carried out to investigate the paravascular clearance of substances in APOE4 mice, such as monitoring the clearance of a fluorescent dye post vessel ablation, to determine the wider impact of the reduced oscillatory behaviour.

Neuronal characteristics are similar between genotypes

Using the number of peaks per minute, the size of these peaks and the correlation of neuronal firing, it was demonstrated that excitatory neuronal characteristics at rest and in the absence of visual stimulation, did not differ between genotypes. It was suggested by previous work that this would be the case in mice of this age and confirms that the observed vascular deficits in these baseline parameters are not as a result of reduced neuronal demand.

3.4.2 General Discussion

The overarching aim of this chapter was to determine if there were vascular deficits in APOE4 mice, even in the absence of a sensory stimulus. This allowed for an evaluation of how the NVU was operating at baseline and so when, in the following chapter, functional hyperaemia is investigated, it is known upon what baseline any deficits occur. The data

presented in this chapter demonstrate that, although subtle, there are several signs that the vasculature was impaired in APOE4 mice. Firstly, the tissue was less well perfused as a result of a less dense capillary bed, this could result in hypoxic brain tissue over time, which has been shown to have a role in the accumulation of Aβ and tau in AD (Fang et al., 2010; Sun et al., 2006). Compounding this effect, is the apparent increase in heterogeneity of flow within the blood vessels which is thought to reflect altered oxygen extraction from the blood to the parenchyma (Østergaard et al., 2013). As well at this, the reduced vasomotion signal in APOE4 mice is indicative of intrinsic vascular dysfunction and could have other functional consequences on perfusion and oxygenation as discussed above. What is unclear, is if the observed increase in vascular capillary diameter in APOE4 mice is a sign of pathological pericyte activity, or a compensatory mechanism to achieve a greater blood volume delivery. Although pericytes have been shown to die in rigour under pathological circumstances such as ischaemia (Hall et al., 2014), it is also possible that under certain conditions, such as inflammatory damage from the upregulation of the CypA-NF-κB-MMP9 pathway in APOE4 pericytes (Bell et al., 2012), contractile vascular tone might be lost (Mishra et al., 2014; Hartmann et al., 2020).

Either way, it is clear that there is some degree of vascular perturbation in these young animals, even in the absence of a stimulus. However, importantly, the dysfunction present in APOE4 animals was insufficient to alter resting net measurements and so is likely to be very subtle. It would be pertinent to study the consequence of these effects on the tissue, most notably to determine if hypoxic regions do exist using hypoxprobe staining (Aguilera and Brekken, 2014) or phosphorescence lifetime imaging (Sakadžić et al., 2010). Immunohistochemical staining for hypoxia markers (Aguilera and Brekken, 2014) has previously shown that there was indeed less oxygen in the tissue of 3-4 months APOE4 mice (Koizumi et al., 2018).

What has not been addressed in this chapter are the mechanisms underlying these deficits. Whether they are developmental or not is unknown, but various cells that make up the neurovascular unit have been found to be damaged as a result of ApoE4, including pericytes, endothelial cells and basement membrane (Montagne et al., 2020; Bell et al., 2012; Halliday et al., 2016), a reduction in the angiogenic factor, VEGF, has been reported (Salomon-Zimri et al., 2016), and in an APP mouse model, a disruption to SMC integrity was shown in relation to a reduction in vasomotion (van Veluw et al., 2019). In a study from Koizumi et al. (2018), it was suggested that ROS could be causing vascular disruption in APOE4-TR mice, so it is feasible that any, or more likely, a combination of

several of these factors are at play.

Examining each of these cell types morphologically and functionally, where possible, could help to untangle some of these effects. For example, the monitoring of calcium levels in SMCs as well as assessment of the structural integrity would demonstrate if the reduced vasomotion in APOE4 mice results from aberrant SMC signalling or a disruption to the structure. Similar experiments could be carried out to examine pericyte function.

.

3.4.3 Conclusion

In this chapter I have shown that the vasculature in young APOE4 animals is vulnerable to dysfunction, seen as reduced vasomotion, reduced vascular density and increased heterogeneity of RBC velocity. Although this did not manifest in alterations in blood SO_2, it is suggestive of subtle early changes to the energy delivery system in these young animals that could, over time, result in alterations in tissue oxygenation.

Chapter 4

Effect of ApoE4 on Neurovascular Coupling in Young Mice

4.1 Introduction

Following the exploration into neurovascular parameters under resting state conditions, allowing for a balance between baseline energy supply and demand to be estimated, this chapter investigates how these neurovascular parameters change under stimulus conditions. Importantly, it will elucidate whether or not the mild deficits observed in APOE4 mice under resting state conditions, continue to present when the primary visual cortex becomes active.

Neurovascular coupling is an essential brain function

As previously mentioned, one of the critical functions of the brain's vasculature is to provide energetically expensive neurons with oxygen and glucose to enable the generation of ATP by oxidative phosphorylation and glycolysis. ATP is primarily used to restore and maintain ions gradients in neurons (Attwell et al., 2010). The process by which the brain increases local blood supply following synaptic activation, is called neurovascular coupling and disruptions have been reported in various pathologies, including FTD, ALS, Parkinson's Disease and Alzheimer's Disease (Iadecola, 2017; Zlokovic, 2011; Kisler et al., 2017a; Sweeney et al., 2018a; Shabir et al., 2018).

Could perturbations to neurovascular coupling have a role in AD?

Something to note is that the neurovascular response has a considerable spatial spread (O'Herron et al., 2016), meaning that in some cases, a relatively local demand results in a widespread increase in net supply, sometimes lyrically described as "watering the entire garden for the sake of one thirsty flower" (Malonek and Grinvald, 1996). This leads to the question of whether or not disruptions to this system would have deleterious pathophysiological effects and could therefore play a role in AD.

As discussed extensively in chapter 1, evidence suggests that early perturbations to the vasculature are indeed of great importance in the disease progression (Iadecola, 2017; Zlokovic, 2011; Kisler et al., 2017a). Vascular dysregulation precedes many other deficits that present in the pre-clinical phase of AD, suggesting it may have a role in the earliest aspects of the disease, or may even be a driving factor (Iturria-Medina et al., 2016). The buffer of "watering the entire garden" does exist, and could therefore allow the brain to function normally for extended periods of time during the pre-symptomatic phase of the disease, but the effect of altered functional hyperaemia over time, and the exhaustion of any compensatory mechanisms, could have serious consequences for neuronal health and cognitive function. Work from Kisler et al. (2017b) utilising a phosphorescent probe that decays at rate proportional to the oxygen partial pressure, showed that perturbations in the functional hyperaemia response may contribute to the presence of hypoxic pockets in the parenchyma, particularly at 200μm below the surface, where the energy source is primarily the capillary bed. Hypoxic conditions have been shown to facilitate the formation of plaques and tangles in AD and so could be a key player in the disease process (Fang et al., 2010; Sun et al., 2006).

This finding, coupled with the knowledge that early vascular changes may be a driver of the disease pathogenesis, make investigating functional hyperaemia in young mice, as in this chapter, an important avenue of research.

The functional hyperaemia response has previously been shown to be defective in mouse models of AD, particularly as a result of Aβ deposition (van Veluw et al., 2019; Niwa et al., 2000; Iadecola et al., 1999; Zhang et al., 1997), however if NVC deficits could drive the onset of the disease, then it is also important to study NVC in the absence of Aβ, as in in this study. ApoE4 has previously been linked to decreases in NVC in an acute surgical preparation (Koizumi et al., 2018). These changes were observed in the endothelium-dependent component of the vascular response and were ameliorated upon superfusion of a ROS scavenger.

In this chapter I studied the NVC response more closely, in a chronic, awake preparation, to better understand the effect of ApoE4. To do so I investigated how individual neurons and blood vessels responded to sensory stimulation in APOE4 animals, and in addition, how any alterations were reflected in the net responses across the region.

4.2 Aims

In order to fully understand how neurovascular coupling mechanisms are affected by ApoE4, it is imperative to study both neuronal and vascular properties. The work in this chapter aimed to investigated these properties at a micro- and macroscopic level in order to address several key questions:

1. Does neuronal activity, in response to visual stimulation, differ in young APOE4 mice, compared to young APOE3 mice?

In order to assess the adequacy of the energy supply, it is also important to examine energy demand. APOE4 mice have previously been found to exhibit a hyperexcitable phenotype, thought to be as a result of the susceptibility of inhibitory GABA neurons to damage by ApoE4 fragments, however this was primarily found in aged mice (14- 20 months old) (Nuriel et al., 2017; Najm et al., 2019). Hyperactivity has also been demonstrated in human carriers, with default mode network hyperactivity observed in young healthy adults, as well as in AD patients (Najm et al., 2019; Filippini et al., 2009). Conversely, ApoE4 plays a role in synaptic failure, resulting in decreased spine density and reduced neurite outgrowth, compared to APOE3 carriers. These effects are thought to occur from a young age in APOE4-TR mice (Rodriguez et al., 2013; Dumanis et al., 2009), although not all studies were carried out in the cortex. Work from Bell et al. (2012) showed that neuronal responses to stimulation were reduced in ApoE4 mice. It was therefore possible that there would be a reduction in neuronal activity in the mice in this study, however limited evidence from previous work suggested that neural activity in APOE4 mice of this age would be similar to APOE3 responses (Koizumi et al., 2018). Nevertheless, characterising the neuronal response to visual stimulation allowed me to estimate energy demand, as well as study individual neuronal properties. To fulfil this aim, 3-4 month old APOE-TR mice with GCaMP6f in excitatory neurons, were imaged during visual stimulation using two-photon microscopy. Individual neuronal responses were recorded and the magnitude of response, the response frequency and cell characteristics were determined.

2. How do blood vessels respond to the neuronal demand?

In order to determine how much blood was delivered to the activated region, stimulus evoked blood vessel diameter changes, alongside red blood cell velocity changes, were measured across the vascular tree. Debate exists over the role of capillaries in the functional hyperaemia response with some arguing that they have a more passive role in NVC (Hill et al., 2015), whilst others suggest that they are critical players in this response (Hall et al., 2014) and may be the site of pathological changes in AD. Evidence from Bell

et al. (2012) points to pericytes present on capillaries as a possible site of dysfunction in APOE4-TR mice. In measuring these vascular parameters across the entire tree, it allowed for the evaluation of the role of capillaries in the NVC response in these mice, as well as determining if there were any vascular compartments particularly susceptible to ApoE4 mediated dysfunction. By comparing the neuronal energy demand with the blood supply, an estimation of energy balance in APOE4 mice, compared with APOE3 mice, could be elucidated.

3. Are there any perturbations to net haemodynamic properties in APOE4 mice? Net responses are invaluable for determining if any detected disruptions to individual vascular dynamics, have an impact on the global response. Haemoglobin spectroscopy offers the further advantage of showing the oxygenation state of the haemoglobin in the blood. During neuronal activation, the total haemoglobin (HbT) increases as the blood flow to the area increases. Along with this influx of fresh blood, is an influx of oxygenated haemoglobin (HbO) as deoxygenated haemoglobin (HbD) is washed away. An initial increase in HbD is sometimes observed in response to stimulation, as the Hb becomes deoxygenated before the influx of HbO arrives. As with the individual vessel responses, the magnitude of the vascular response should increase or decrease in concert with the neuronal demand, as has previously been demonstrated (Shabir et al., 2020). Stimulus triggered responses across the entire V1 area were recorded to asses the impact of any observed vascular and neuronal effects, on the overall regional activity.

4.3 Methods

4.3.1 In vivo data collection

Animals aged 3-4 months old were surgically prepared with a chronic cranial window as previously described (see section 2.2). The number of animals per experiment varied (see Appendix A for details) but were balanced according to APOE genotype and sex. A mixture of APOE-TR/DsRed and APOE-TR/Thy1GCaMP6f animals were used for all experiments recording from the vasculature, and APOE/Thy1GCaMP6f animals only were used for neuronal recordings. Recordings from each animal were made across 1-3 imaging sessions, with each session not exceeding four hours in duration, as per home office requirements.

Prior to two-photon experiments, mice were injected intravenously or subcutaneously with a fluorescent dye (FITC-dextran or Texas Red Dextran), allowing for the visualisation of the vascular lumen. Neuronal and vascular recordings were made in the same imaging sessions but haemoglobin spectroscopy/LDF measurements were taken on separate days to minimise interference from the fluorescent dye. Mice underwent the visual stimulation paradigm as previously described (see section 2.4.1), in brief, mice were head-fixed atop a running cylinder and visual stimuli consisting of drifting grating patterns were presented for 5 seconds with an interstimulus interval of 20 seconds. Mice were presented with 20 trials on average.

4.3.2 In vivo data analysis

Data processing

All data was extracted by the methods previously outlined in chapter 2 (see section 2.4.2), resulting in a continuous vessel diameter, red blood cell velocity, neuronal fluorescence or net haemodynamic trace. These traces were subsequently cut into visual stimulation trials to allow for the averaging across stimuli. Vascular responses were normalised to the four seconds prior to visual stimulation and multiplied by 100 to reflect percentage change. Neuronal trials were normalised in the same way (but without the conversion to a percentage change) to give a $\Delta F/F$ signal. Trials were classified according to the locomotion that occurred before and/or during the visual stimulation. Trials with no locomotion events in the two seconds preceding the visual stimulation or during the visual stimulation period were grouped together as "no locomotion trials" to undergo further analysis. A pre-stimulus period of two seconds was selected to allow for a return to baseline

following a locomotion epoch, before the presentation of a stimulus. All locomotion events that were less that one third of a second in length and were more than one second apart from adjacent epochs, were not counted as "true" locomotion, to allow for small jitters of the wheel.

As capillary measurements of diameter and RBCV were particularly susceptible to motion artefacts, large fluctuations were removed resulting in gaps in data as previously described. Trials missing more than 10% of the data during the stimulation period were excluded (see figure 4.1A) and those that remained were interpolated to fill in the missing values using a moving mean average (figure 4.1B). Traces were also smoothed using a loess smoothing method (smoothing range: 1-5% span of the total number of data points, depending on which best represented the shape of the data, (figure 4.1C)). Interpolated data was only used to determine area under curve (AUC) values, for all other analyses, either raw or smoothed traces were used.

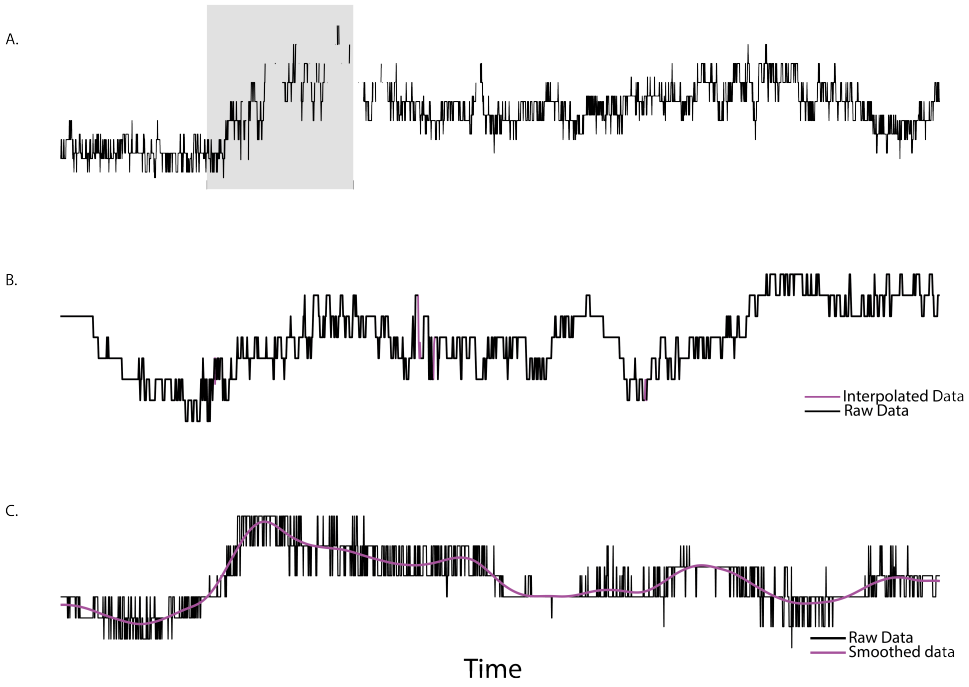

Figure 4.1: **Line scan processing during visual stimulation** A) An example trace with >10% of data missing during stimulation period (grey rectangle) that was excluded from further analysis. B) An example trace with missing values (black) that were interpolated using a moving mean average (pink). C) An example of a raw trace (black) and the same trace smoothed using a loess smoothing method (pink).

Response Size to visual stimulation

As outlined in the main methods section 2.4.2, in neuronal recordings, a region of interest (ROI) was placed over each individual cell. Trials were averaged across neuronal ROIs to give an average trace per ROI, which were subsequently averaged per animal. The AUC was measured per ROI and averaged per animal. All trials per vessel were averaged together to provide an average vessel trace. This was plotted and the AUC for each vessel was determined.

Average cell traces, and individual vessel trials, were then classified as responsive or non-responsive using custom written scripts in MATLAB. Traces were classified as responsive if the maximum peak (averaged over 0.5s around the true maximum peak to prevent single noise spikes resulting in a trace being incorrectly defined as responsive) of the trace during the visual stimulation period exceeded a predefined threshold. Thresholds of twice the standard deviation of the baseline period were applied to neuronal, pial diameter and capillary diameter traces and one times the standard deviation of the baseline period was applied to RBCV traces. Threshold values were decided for each data type based on the value that gave the most accurate results for a subset of each data type.

In neuronal data, AUC measurements were obtained from responsive cell traces that were subsequently averaged per animal. A response frequency was determined by calculating the percentage of responsive cells per animal.

All responsive trials per vessel were averaged to give an overall responsive trace per vessel. AUC measurements were made for each responsive trace. A response frequency was determined by calculating the percentage of responsive trials per vessel and grouping together vessels from animals of the same genotype.

Net haemodynamic traces were averaged per animal as the same region was measured across on each imaging session. AUC values were obtained from each average trace per animal.

In order to quantify how much vascular response there was per "unit" neuronal activity, a neurovascular coupling index (NVCi) was calculated, where vascular responses were normalised to neuronal responses. This was done in two different ways. First, the average neuronal AUC of responsive cells during visual stimulation was determined per animal, and subsequently divided into the average AUC of each vessel average from that animal. As the purpose was to glean how the energy balance differed across animals, only the AUC of responsive ROIs was used as this best reflects energy demand, and the AUC of

the vessel average across all trials (i.e. not just responsive trials) was used, as this is what best reflects energy delivery. Although this method is attractive as it allows for the vascular responses in each animal to be normalised to its own average neuronal response, it does mean vascular data from animals lacking GCaMP6f in their neurons (as is much of the data in this chapter) cannot be taken into account with this measure. In order to overcome this, a second NVCi method was utilised, where an average neuronal AUC per genotype was determined and all vessel AUCs in this genotype group were normalised to this value.

Neuronal characteristics

Neurons were classified as "on" , "off" , "both" or "neither" depending on whether they had a maximum peak two standard deviations above the baseline period during the stimulation (on), in the two seconds following the end of the visual stimulation (off), during both the stimulation and post-stimulation period (both) or not at all during either of these time periods (neither). In addition, the number of peaks above the specified threshold in the $\Delta F/F$ trace during visual stimulation were detected and converted to peaks per minute.

4.4 Results

4.4.1 Effect of APOE4 on neuronal responses to visual stimulation

In order to assess neuronal activity in the visual cortex of APOE4 mice compared to APOE3 mice, the magnitude of response sizes (i.e. the area under the curve of ΔF/F traces during the stimulus period) were compared. The magnitude of ΔF/F signals are tightly coupled with the number of spiking events (Akerboom et al., 2012), and so is an appropriate measure of neuronal activity and therefore energy demand.

Initially, all cells were analysed to compare response magnitudes between genotypes. APOE4 mice exhibited an increased response size during visual stimulation (figures 4.2A, B). Response frequency was then determined to establish whether or not one genotype was more likely to respond to visual stimulation than the other, however there was no observed effect of genotype (figure 4.2C). In order to better assess energy demand during the visual stimulation, responsive cells were analysed separately. In terms of energy use, this is likely to be a more accurate representation, as non-responsive cells will not require the oxygen and glucose delivered in the blood, but they will reduce the average ΔF/F signal. The magnitude of evoked responses of responsive cells only revealed the same results, APOE4 mice had a larger response size than APOE3 mice (figures 4.2D, E) reflecting an increase in stimulus triggered neuronal activity.

Rather than averaging across animals, I then used an alternative analysis, a linear mixed model, which analyses all data from individual cells while accounting for variance within animals. This yielded similar results as the animal average, with APOE4 cells showing larger response sizes to visual stimulation ($p = 0.0386$ (all cells), $p = 0.042$ (responsive cells only)).

To further probe for any differences in neuronal behaviour, I calculated the frequency of calcium transients during the stimulation period. An example of detected peaks can be seen in figure 4.2H. No difference in the number of transients per minute was found between genotypes (figure 4.2I), suggesting that it is only the magnitude of events that differs between the genotypes, driving the increased ΔF/F response observed. Although it is important to note that spikes occurring in quick succession (i.e. a spike train) will appear as only one peak in the trace, the magnitude of which will reflect the amount of spiking in this train. Therefore, in this case, it was the number of spikes in a burst of action potentials that was changing, not the frequency of the bursts themselves.

The classification of cells based on their response to visual stimulation has previously been used to probe for disruptions in visually evoked responses (van Veluw et al., 2019).

Neurons that responded exclusively to the visual stimulation were termed "on" cells (figure 4.2F, top panel). As well as this type of cell, there were others that responded exclusively to the offset of the visual stimulation, a previously established phenomenon (Liang et al., 2008; Jin et al., 2008). These cells were were termed "off" cells (figure 4.2F, second panel). Cells that exhibited both behaviours were termed "both" and those that did not exhibit any activity in response to visual stimulation were called "neither" (figure 4.2F, bottom two panels). "Neither" cells made up the majority of cells, and of those that responded, "on" cells were the most abundant. There was no observed difference in the distribution of cell types between genotypes (figure 4.2G). In addition all data was averaged per cell, rather than across animals and the same results were found across all parameters (see B.2).

Results appear to point towards a hyperactive phenotype of visually evoked responses in the visual cortex of APOE4 mice but also suggests that, in these same mice, there is an absence of a disruption to the overall network activity and that the cell firing patterns remain intact. In the context of energy demand, these data imply that APOE4 mice might have an increased demand for energy during visual stimulation.

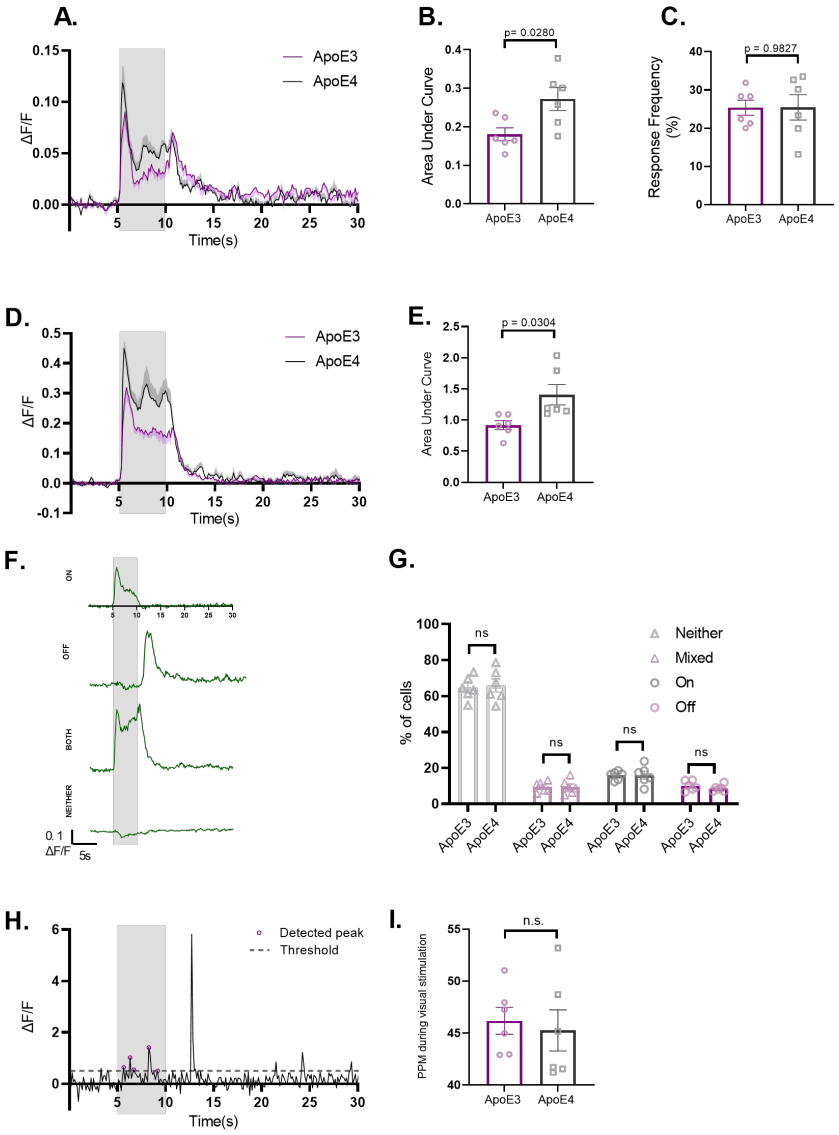

Figure 4.2: **Neuronal Responses to visual stimulation** A. Average ΔF/F traces of all cells averaged per animal in responsive to visual stimulation. B. AUC measurements for animal averages shown in A. C. Response frequency of cells per animal for APOE3 and APOE4 animals. D. Average ΔF/F trace of all responsive cells averaged per animal, in APOE3 and APOE4 mice during visual stimulation. E. Area under curve measurements for the responsive cells averaged per animal in D. F. Example ΔF/F traces for each cell type "On, Off, Both and Neither". G. The distribution of cell types outlined in F in APOE3 and APOE4 animals. H. Example ΔF/F trace during visual stimulation. Purple circles show peaks detected during stimulation and above threshold (dashed grey line). I. PPM values for all responsive APOE3 and APOE4 cells averaged per animal. Grey rectangles represent the onset and offset of visual stimulation. Individual points represent individual animal averages and error bars represent SEM. For detailed statistical outputs see table A.9

4.4.2 Vascular responses to visual stimulation

In order to assess if this increase in neuronal activity was being met with an increased blood supply in APOE4 mice, vascular responses to the same visual stimulation were determined.

The diameters of large pial blood vessels and small parenchymal capillary blood vessels, as well as capillary RBC velocity, were recorded over the course of the stimuli. A robust increase in diameter and RBC velocity was observed upon presentation of a visual stimulation (see figure 4.3). Increases in pial diameter and capillary RBCV in response to visual stimulation, were found to occur more frequently in APOE3 mice than in APOE4 mice (see figure 4.4A, G). The response frequency of stimulus evoked capillary diameter increases did not differ between genotypes (figure 4.4D).

As trials with significant amounts of locomotion were excluded from this analysis, some vessels had only very few contributing trials, meaning only very high or low response frequencies were possible. To examine the effect this might have on the results, the number of contributing trials per vessel was plotted against the response frequency (figures 4.4B, E, H). Indeed it can be seen that a large number of the extreme response frequencies (i.e. 0% and 100% response frequencies) were as a result of vessels with low numbers of trials. A cut off of a minimum of 10 trials was applied to eliminate this confound. This resulted in pial vessel diameter changes that were no longer significantly less responsive in APOE4 mice when compared to APOE3 mice, although they did trend towards significance (figure 4.4C, $p = 0.0824$). However, both capillary diameter increases (figure 4.4F) and RBC velocity increases (figure 4.4I) in response to stimulation, occurred more frequently in APOE3 mice when this threshold was applied. This presents a picture of vascular unreliability in the visual cortex of young APOE4 animals despite their elevated neuronal responses.

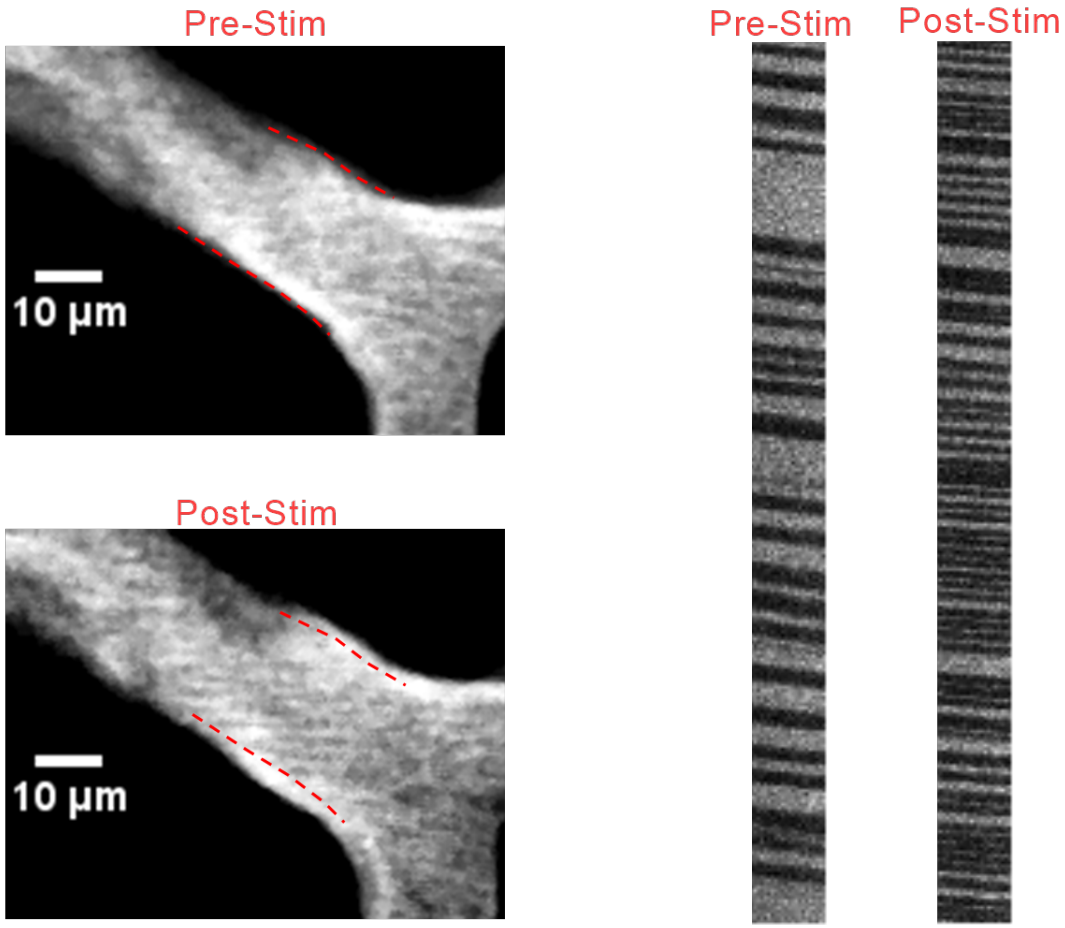

Figure 4.3: **Vascular responses to visual stimulation** Left panel: Example pial arteriole before and during stimulation. Red dashed lines show the outline of the vessel before stimulation. Right Panel: Example RBCV linescan showing the dark shadows cast by RBCs before and during visual stimulation. Flatter stripes represent cells that are travelling faster. Capillary diameter increases are generally small and difficult to see by eye, therefore an example is not shown.

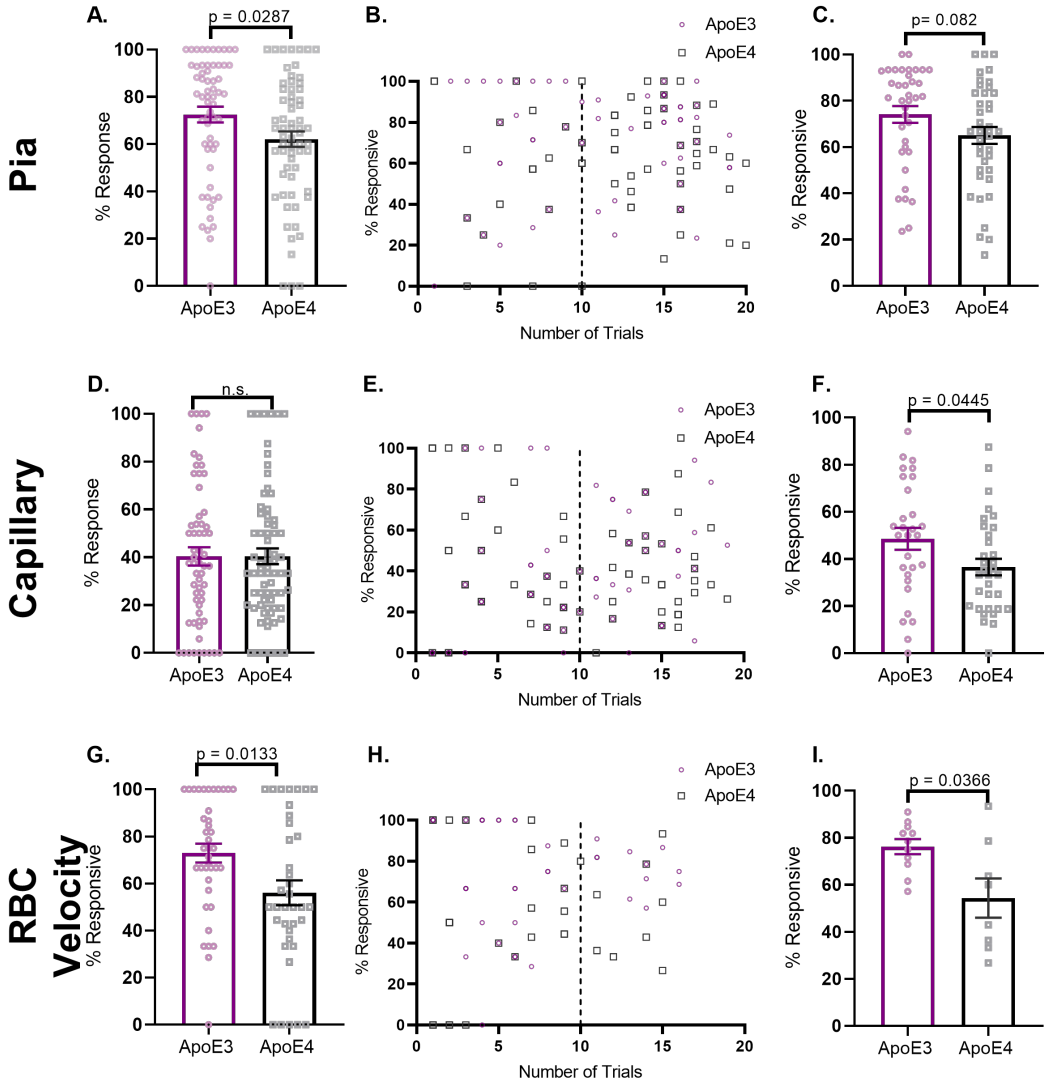

Figure 4.4: **Vascular response frequency to visual stimulation** A. Response frequency per vessel in pial arterioles. B. Response frequency plotted against the number of contributing trials per vessel in pial arterioles. C. Response frequency per vessel in pial arterioles with more than 10 contributing trials. D. Response frequency per vessel in capillaries. E. Response frequency plotted against the number of contributing trials per vessel in capillaries. F. Response frequency per vessel in capillaries with more than 10 contributing trials. G. Capillary RBCV response frequency per vessel. H. Capillary RBCV response frequency plotted against the number of contributing trials per vessel. I. Capillary RBCV response frequency per vessel in capillaries with more than 10 contributing trials. Grey line in B, E and H represents the 10 trial minimum threshold applied. Individual points represent vessels. Error bars represent SEM. For detailed statistical outputs and n numbers see table A.10

To continue the investigation into the ability of the vasculature to meet neuronal demands and following the finding that APOE4 animals have a less reliable energy supply, the size of the stimulus evoked vascular responses were studied. As mentioned, under physiological conditions, it would be expected that the vascular increases would be amplified to match the hyperexcitable neuronal responses. When looking at overall vessel averages, there was no significant difference between genotypes in the response magnitude of pial or capillary diameter changes, or in capillary RBC velocity changes (see figures 4.5A, B, E, F, I, J). As with the neuronal data, a more complex analysis was applied, a linear mixed model that accounted for the variability within each vessel. This analysis again showed that there was no effect of genotype on the magnitude of responses across all three measures (AUC: pia $p = 0.7059$, capillary diameter $p = 0.254$, capillary RBC velocity $p = 0.263$). Next, responsive trials only were averaged to give average vessel traces, the magnitude of which were then measured. As before, there was no effect of genotype on response size in any of the groups (figures 4.5, C, D, G, H, K, L), a finding that was confirmed with a linear mixed model (AUC: pia $p = 0.486$, capillary diameter $p = 0.7546$, capillary RBC velocity $p = 0.9604$). This failure of the blood vessels to dilate further to match the elevated levels of neuronal activity, coupled with the reduction in the reliability of responses, points towards a vascular insufficiency in APOE4 mice.

Vascular responses to visual stimulation A. Average stimulus induced diameter changes in pial arterioles, averaged per vessel. B. AUC measurements for the diameter changes shown in A. C. Average stimulus induced diameter changes in pial arterioles, responsive trials only averaged per vessel. D. AUC measurements for the diameter changes shown in C. E.Average stimulus induced diameter changes in capillaries, averaged per vessel. F. AUC measurements for the diameter changes shown in E. G. Average stimulus induced diameter changes in capillaries, responsive trials only averaged per vessel. H. AUC measurements for the diameter changes shown in G. I. Average stimulus induced velocity changes in capillaries, averaged per vessel. J. AUC measurements for the velocity changes shown in I. K. Average stimulus induced RBCV changes in capillaries, responsive trials only averaged per vessel. L. AUC measurements for the velocity changes shown in K. Grey rectangles represent the onset and offset of visual stimulation. Individual points represent individual vessels and error bars represent SEM. For detailed statistical outputs and n numbers see table: A.11

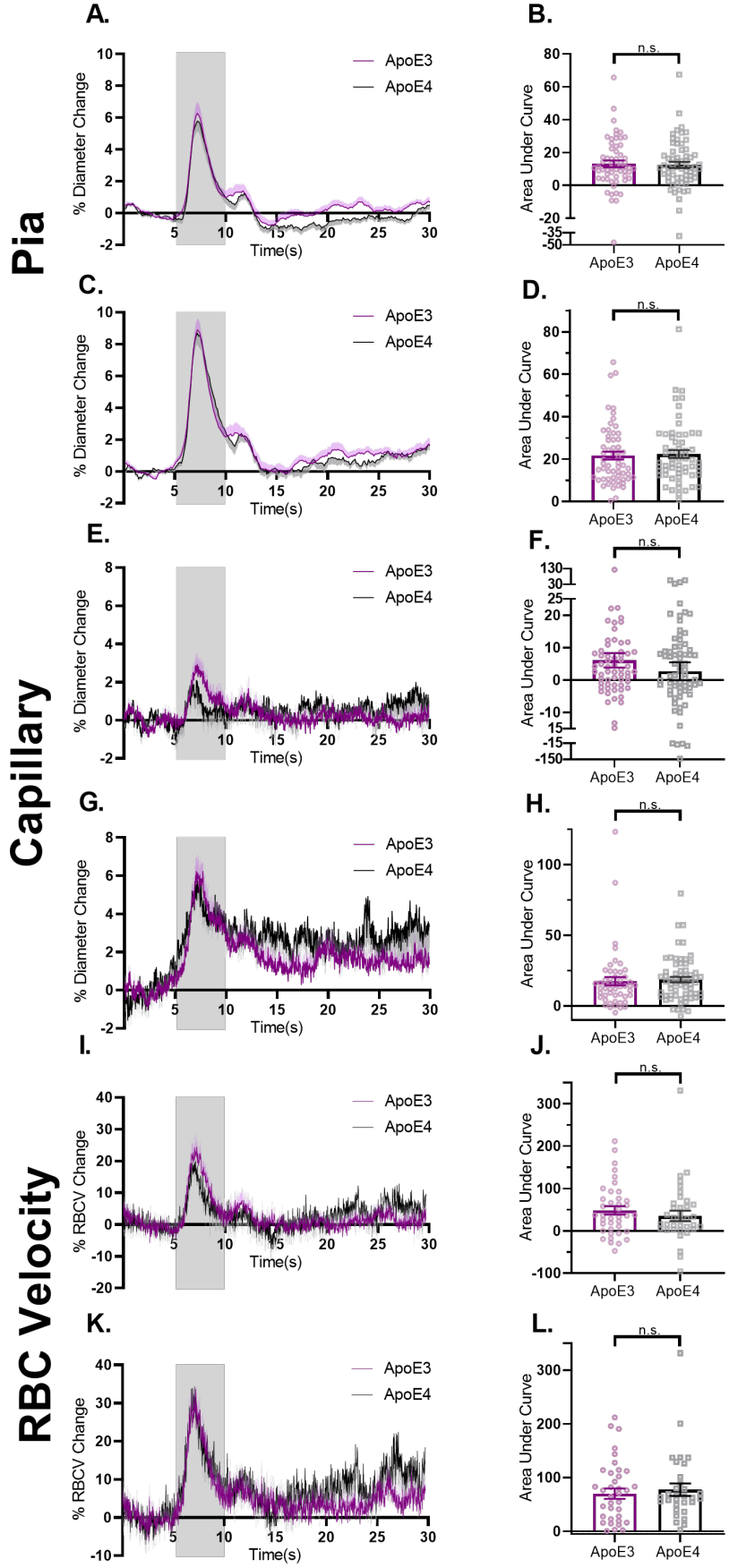

Figure 4.5: **Vascular responses to visual stimulation** Figure legend on previous page.

To quantify the amount of vascular response per "unit" neuronal activity, a neurovascular coupling index (NVCi) was created for each data set, where vascular responses were normalised to neuronal responses both within animals and across all vessels (see section 4.3.2)). A higher NVCi reflects a greater supply of blood (i.e. energy) in response to neuronal activity (i.e. demand). Pial vessels showed decreased NVC indices in APOE4 animals (figure 4.6A, B) and capillary RBC velocity NVC indices followed the same pattern, being lower in APOE4 animals ($p = 0.055$ (animal average), $p = 0.054$ (vessel average) (figure 4.6E, F). As the NVC indices for capillary diameters were not different between genotypes (figure 4.6C, D), it suggests that the RBC velocity differences were driven by upstream changes in flow, not downstream changes in resistance.

On the whole, vascular data suggests that the capillaries and possibly pial vessels are less likely to increase their diameters in response to neuronal activation in APOE4 mice. NVCi measurements imply that imbalances between the neuronal and vascular responses occur primarily at the pia, presumably as a result of the lower summed activity from the unreliable capillary bed. These pial effects may then drive the deficits observed in the RBC velocity increases. It is clear that there is a mild vascular deficit present in these young APOE4 animals, where there is a failure to meet increased neuronal activity with a corresponding increase in blood supply.

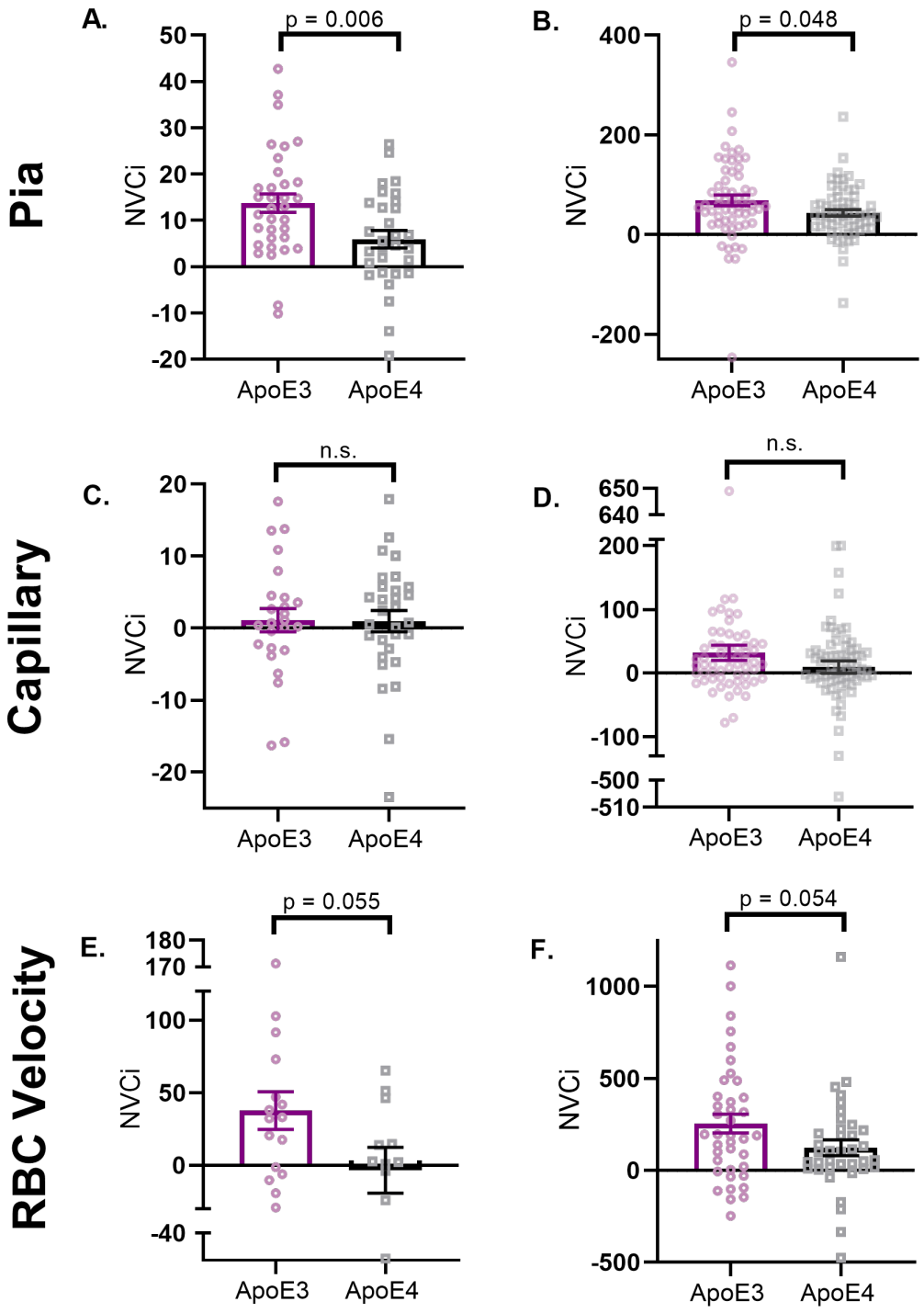

Figure 4.6: **Neurovascular coupling indices** A. Pial NVCi calculated using neuronal averages per animal. B. Pial NVCi calculated using neuronal averages per genotype. C. Capillary NVCi calculated using neuronal averages per animal. D. Capillary NVCi calculated using neuronal averages per genotype. E. Capillary RBCV NVCi calculated using neuronal averages per animal. F. Capillary RBCV NVCi calculated using neuronal averages per genotype. Individual points represent vessels. Error bars represent SEM. For detailed statistical outputs see table A.12.

4.4.3 Net responses to visual stimulation

Finally, subtle changes in the neurovascular coupling mechanisms at an individual neuronal and vascular level may or may not produce significant changes in regional measures of blood flow and haemodynamic responses. In order to investigate this, the Oxy-CBF probe utilised LDF and Hb spectroscopy, allowing for global responses from across the visual cortex to be determined. Example profiles of representative HbT, HbD, HbO and SO_2 responses to visual stimulation, as measured by Hb spectroscopy, are seen in figure 4.7A. The stimulus evoked increase in CBF (flux) as measured by LDF can be seen in figure 4.7B, and the $CMRO_2$, calculated from these parameters, can been seen in figure 4.7C. Increases in $CMRO_2$ are thought to be indicative of net increases in neuronal activity. When comparing all of these parameters, the response magnitude was not significantly different between genotypes. Nevertheless the direction of the differences in these net measures was generally in the direction that would be predicted by the measurements obtained from single cells and vessels. The traces show a slight, non-significant decrease in the APOE4 response to stimulation in HbT, HbO and SO_2 measurements (figures 4.7E, F, H), it seems that the subtle changes in the vasculature observed in two-photon experiments may have an impact on the macroscopic responses, although large variations in the data make this impossible to irrefutably conclude. Of particular interest is the apparent reduction in blood SO_2 in APOE4 mice, when compared with APOE3 mice. This may reflect a higher extraction of O_2 from the vessels in APOE4 mice, as a result of the increased neuronal activity, presumably resulting in larger energy demands in the tissue, coupled with the less reliable blood supply. In line with this, the HbO maximum appears to be somewhat lower in APOE4 mice, possibly reflecting the same scheme whereby more oxygen is being extracted from the blood in these animals. The small reduction in HbT magnitude, thought to be indicative of total blood volume, fits with the information gleaned from the previous chapter and this one, reduced vascular density coupled with an unreliable blood supply would lead to a reduction in the blood volume delivered. Surprising are the results for flux and $CMRO_2$ (figures 4.7D, I). An increase in neuronal demand would be expected to lead to an increase in $CMRO_2$, however it is possible that the large numbers of non-responsive neurons (>60% of all cells, figure 4.2F, G) meant that the $CMRO_2$ measurement cannot detect the increase in activity of the responsive "on" cells. In addition, as $CMRO_2$ combines the error from HbT, HbD and CBF measurements, it is often noisy. Finally, another unexpected outcome was the striking similarity of the CBF response in both genotypes (figure 4.7D). Individual capil-

lary measurements indicated that there might be a reduction in the response frequency of RBC velocity in APOE4 animals, that is not reflected in these net measurements. One speculation might be that the reduction in CBF as a result of the reduced responsiveness of the vessels is subtle and therefore cannot be detected within the error of these data.

Net haemodynamic responses to visual stimulation Figure on following page. A. Example haemodynamic parameters SO_2 (Oxygen Saturation), HbO (Oxygenated Haemoglobin), HbD (Deoxygenated haemoglobin), HbT (Total haemoglobin), B. Blood flow (Flux) and C. $CMRO_2$ responses to visual stimulation. D. Left panel: Average stimulus evoked changes in flux in APOE3 and APOE4 mice. Right panel: AUC measurements for flux changes represented in the left panel. E. Left panel: Average stimulus evoked changes in HbT in APOE3 and APOE4 mice. Right panel: AUC measurements for HbT changes represented in in the left panel. F. Left panel: Average stimulus evoked changes in HbO in APOE3 and APOE4 mice. Right panel: AUC measurements for HbO changes represented in the left panel. G. Left panel: Average stimulus evoked changes in HbD in APOE3 and APOE4 mice. Right panel: AUC measurements for HbD changes represented in the left panel. H. Left panel: Average stimulus evoked changes in SO_2 in APOE3 and APOE4 mice. Right panel: AUC measurements for SO_2 changes represented in the left panel. I. Left panel: Average stimulus evoked changes in $CMRO_2$ in APOE3 and APOE4 mice. Right panel: AUC measurements for $CMRO_2$ changes represented in the left panel. Grey rectangles represent the onset and offset of visual stimulation. Individual points represent individual animals and error bars represent SEM. For detailed statistical outputs see table A.13.

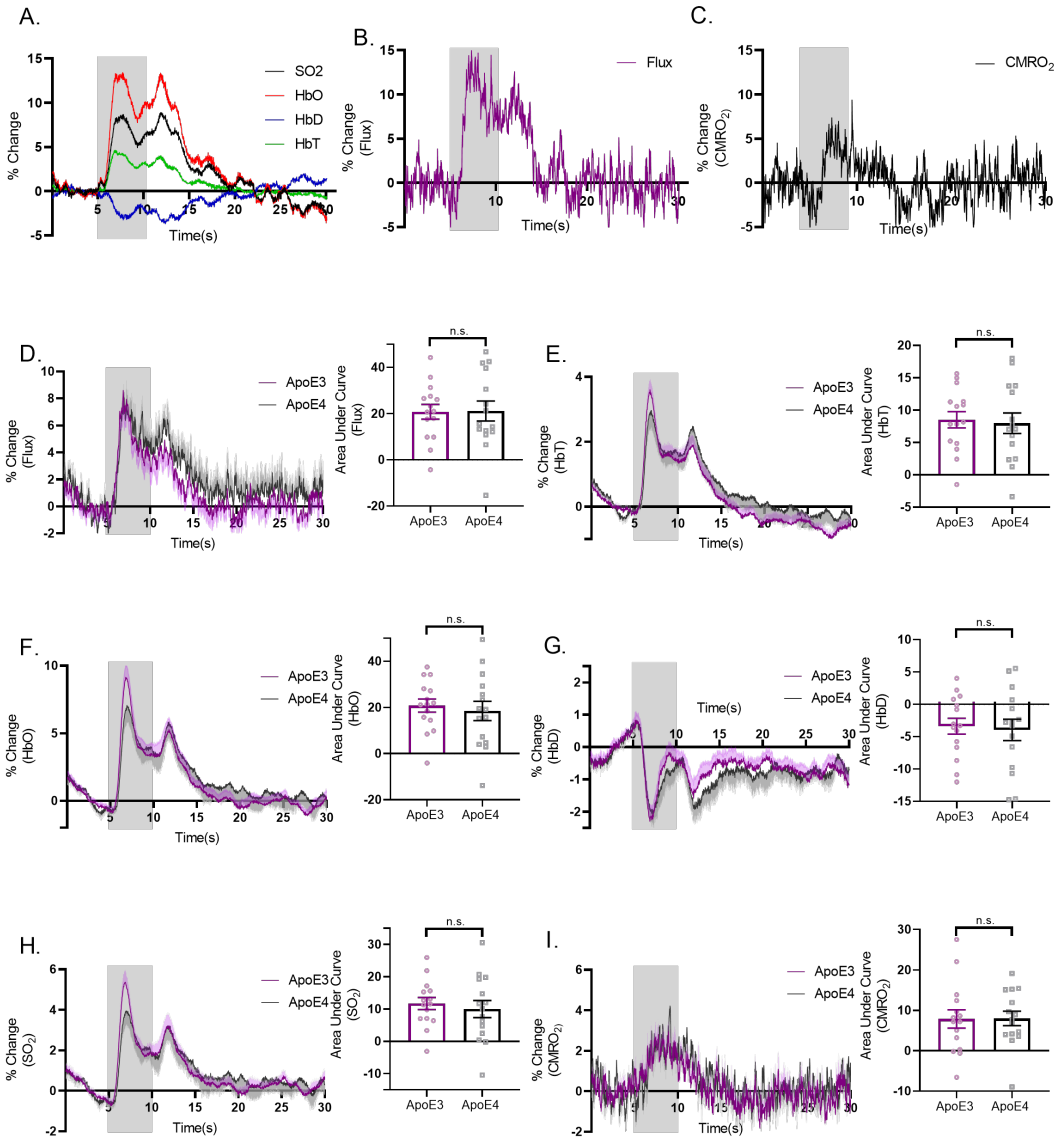

Figure 4.7: **Net haemodynamic responses to visual stimulation.** Figure legend on previous page.

4.4.4 The Effect of Sex and ApoE on Response Size and Frequency

As in chapter 3, the effect of sex on the NVC response was examined. AUC measurements for all vessels/cells were split by sex and APOE genotype to determine if there was any effect of sex or an interaction between sex and genotype. For pial and neuronal AUC measurements, there was no effect of sex (figure 4.8A, G). However for capillary diameter changes there was an observed interaction between sex and genotype (figure 4.8C), as well as an effect of sex on RBC velocity measurements (figure 4.8E). Males had smaller capillary responses in APOE4 mice, although it must be noted that a small number of extreme outliers do exist in the data.

Response frequency was also used to test for any effects of sex on the reliability of responses to stimulation. In pia and RBC velocity measurements, no effect was observed (figure 4.8B, F), however in the capillary diameter measurements, sex had a significant effect with females tending to respond more frequently than males (figure 4.8D). Similarly in the neuronal data, APOE4 females had neurons that fired more frequently than APOE3 females (figure 4.8H). Overall there appeared to be a mild effect of sex on some of these measures, however some of these effects were influenced by outliers. In addition the effects were not consistent or robust across all parameters.

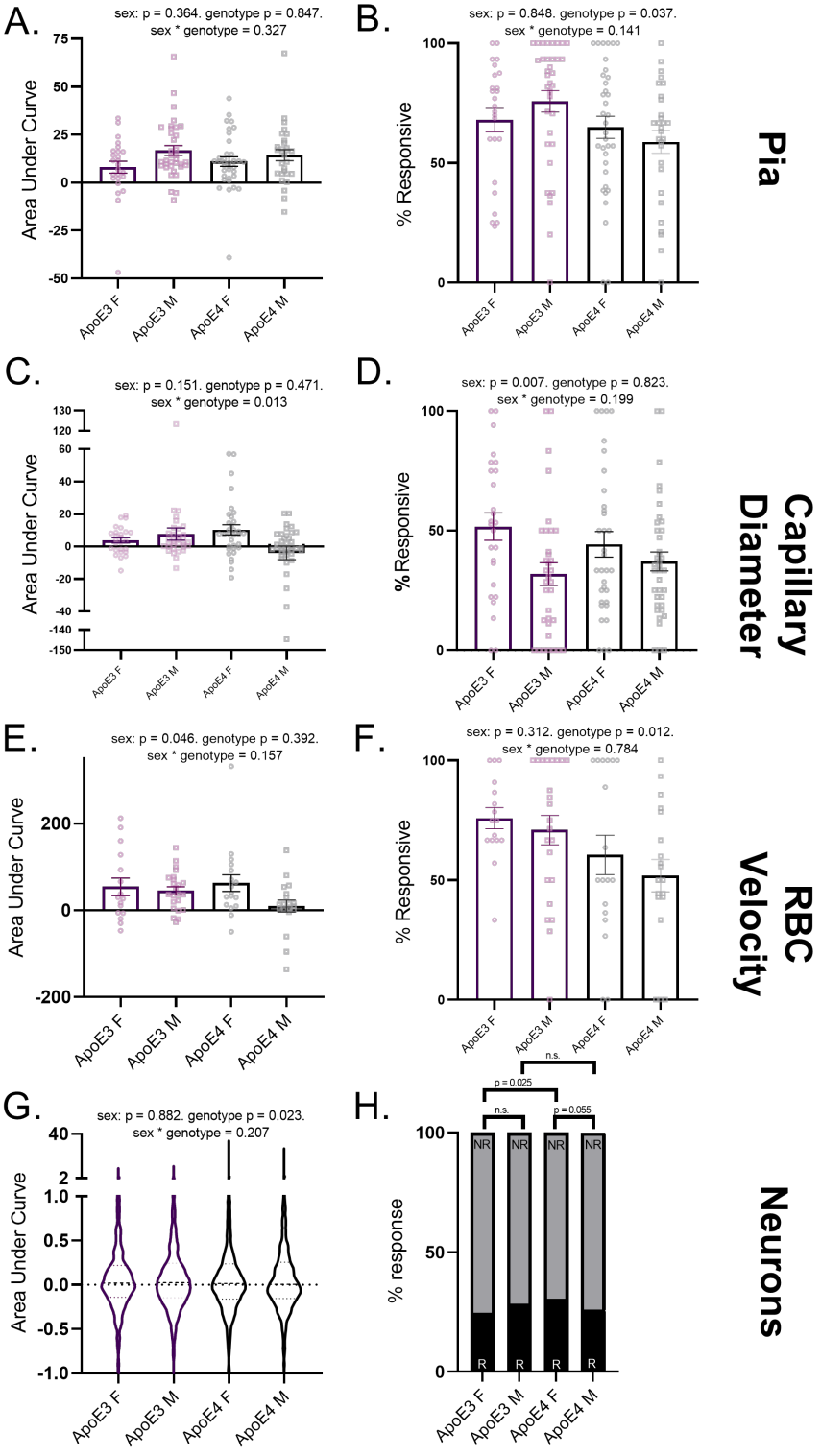

Figure 4.8: **The effect of sex on response size and frequency** A. Responsive pial vessel AUC, split by sex for APOE3 and APOE4 mice. B. Pial response rate, split by sex for APOE3 and APOE4 mice. C. Responsive capillary AUC, split by sex for APOE3 and APOE4 mice. D. Capillary response rate, split by sex for APOE3 and APOE4 mice. E. Responsive RBCV AUC, split by sex for APOE3 and APOE4 mice. F. Capillary RBCV response rate, split by sex for APOE3 and APOE4 mice. G. Responsive cells AUC, split by sex for APOE3 and APOE4 mice. H. Cell response rate, split by sex for APOE3 and APOE4 mice. Individual points represent vessel averages and violin plots show data across all cells. For detailed statistical outputs see table A.14.

4.5 Discussion

In this chapter, two-photon imaging, Hb spectroscopy and laser Doppler flowmetry were used to probe how the properties of individual elements of the neurovascular coupling response varied with APOE genotype and what effect this had on overall net activity.

4.5.1 Results Summary and Interpretation

Increased neuronal activity during visual stimulation in APOE4 mice

In APOE4 mice, neuronal responses to visual stimulation were increased. This finding is consistent with previous reports of hyperexcitability in APOE4 carriers as a result of the increased susceptibility of GABAergic inhibitory neurons to damage from neuronal ApoE4 fragments (Brecht et al., 2004; Li et al., 2009; Knoferle et al., 2014) and subsequent disinhibition of excitatory neurons. It was unclear whether or not we would observe this phenotype in such young animals as previous reports from APOE-TR mice suggested that neuronal responses should be intact or diminished at this age (Koizumi et al., 2018; Bell et al., 2012). In one such report, the investigators used a voltage-sensitive dye to measure voltage changes in 4 months old animals in response to a hindlimb stimulus and observed reduced activity in APOE4 mice (Bell et al., 2012). The animals used in this particular study were generated in house in the same way animals used in this thesis were generated and on the same background strain (Sullivan et al., 1997; Knouff et al., 1999), however one cannot rule this out as a source of variability. Another study using the same mouse model determined that neuronal activity was unlikely to be altered as Ca^{2+} increases in the neuron, as a result of NMDA application, were unaffected (Koizumi et al., 2018), but as this method was carried out in isolated neurons it would not capture the disinhibition that may be responsible for the hyperexcitability observed in this study. From the data outlined, it was evident that it was the response size that was increased in APOE4 animals (i.e. the amount of firing in a single burst), rather than the frequency of peaks (each representing a burst of action potentials) or the distribution of cell response types (i.e. On, Off, Both, Neither).

When comparing magnitudes of GCaMP fluorescence it is important to be mindful of a number of factors. First is that the variation in the signal-to-noise ratio between animals could result in a variation in $\Delta F/F$ signals. In this study, a background signal for each cell was generated and subtracted as outlined in the main methods section (2.4.2), which would diminish this variability and have the added benefit of removing any light artefacts

arising from the visual stimulation. Another important consideration, is the supralinearity of GCaMP (Akerboom et al., 2012). This means the values obtained when measuring the magnitude of the $\Delta F/F$ signals are not entirely quantitative, so we can be confident that there was more activity in APOE4 mice, just not precisely how much more.

With all of this in mind, we can conclude from the data presented in this chapter that there was increased neuronal activity in APOE4 mice during visual stimulation. From this we can speculate that APOE4 animals might have a greater demand for oxygen and glucose during sensory stimulation, in which case, it would expected to see a corresponding increase in the blood supply in APOE4 animals to meet this demand.

Reduced response frequency in APOE4 vasculature

Vascular data was then analysed to determine if the expected increase in vascular activity to meet the neuronal demand, was present. Initially the response frequency was analysed and a cut off of a minimum of 10 contributing trials per vessel was set. Without an applied threshold of ten trials, the pial and RBCV responses occurred less frequently in APOE4 mice, whereas the capillary diameter responses were not different between the two genotypes. The application of the cut off, in order to abrogate the extreme influence of vessels with a small number of trials, did alter the findings. After this application, the pia was no longer significantly less responsive (although the data trended in this direction), but the capillary diameters and RBCVs were. This reduction in response frequency demonstrates a degree of vascular unreliability in APOE4 animals, particularly when it comes to the capillary bed.

Failure of APOE4 mice to elevate vascular responses to match elevated neuronal activity

In conjunction with the disruption to response frequencies, further vascular insufficiency in APOE4 mice was evident from the discovery that there was an inability of blood vessels to increase their response size (i.e. the dilation or RBC velocity) to match the increased neuronal activity. Vasodilations at the pia are as a result of propagated responses from downstream vessels that are closer to neurons (Iadecola et al., 1997; Chen et al., 2014; Longden et al., 2017; Rungta et al., 2018). Therefore, a plausible scheme is one whereby there are less reliable responses in the capillary bed of APOE4 mice and these summate upstream at the pia at an insufficient magnitude to match the increased neuronal response. This was reflected in the reduced pial and capillary RBCV NVCi measurements in APOE4

animals.

Net haemodynamic measurements show trends that reflect, in part, two-photon observations

Net haemodynamic measurements offer a valuable insight into the overall, macroscopic effects of the microscopic observations. As discussed, some results obtained from these net readings were surprising, there was no observed increase in the magnitude of CBF responses in APOE3 mice, nor was there an increase in the $CMRO_2$ measurement in APOE4 mice. Despite this, the net recordings have offered some insights into the NVC process in APOE4 animals. In the absence of an increased blood supply in APOE4 animals, the pattern towards slightly reduced HbO and SO_2 levels during stimulation, could reflect a greater oxygen extraction fraction (OEF) from the blood in an attempt to meet the increased energy demands in the parenchyma. Perhaps this is a compensatory measure in these young animals that allows them to continue to function at a physiologically "normal" level despite the increased neuronal activity and reduced vascular reactivity. Alternatively, the possible reduction in HbO levels could purely reflect the trend towards a reduced blood volume delivery during visual stimulation, probably as a result of both a reduced vascular density and a less reliable NVC mechanism in APOE4 mice. What was clearly not present, as with the two-photon experiments, was an increase in net responses in APOE4 animals to match the increase in neuronal activity.

A different study in APOE4-TR mice reported a net decrease in CBF in response to a sensory stimulation when compared to APOE3-TR or WT mice (Koizumi et al., 2018). Some key experimental differences might explain why this result is inconsistent with our measurements. Firstly, the use of anaesthesia in these experiments could account for the differing results, as the increase in energy use by the tissue during activation compared to during rest, is greater in anaesthetised animals than in awake animals (Shulman et al., 1999). This is as a result of a lower resting energy use in anaesthetised animals and would therefore result in a larger percentage increase from baseline in response to stimulation. Conversely, another study has shown that haemodynamic responses can be preserved whilst mice are under anaesthesia (Sharp et al., 2015). It is likely that these effects vary with regime and whether APOE4 can modulate this in any way is unknown, but it nevertheless an interesting experimental difference to consider. Another possible explanation is that the experiments carried out by Koizumi et al. (2018) utilised an acute, rather than a chronic preparation. It is now well documented that APOE4 carriers have

an increased response to inflammatory stimuli due to mechanisms that involve enhanced microglial activation (Safieh et al., 2019; Rodriguez et al., 2014) and increased levels of pro-inflammatory cytokines (Fan et al., 2017; Ophir et al., 2005) and so a reasonably invasive procedure, such as a craniotomy with dura removal, may have acute effects on the NVC response in APOE4 mice as a result of increased inflammation, rather than as a direct interaction between the vasculature and APOE4.

4.5.2 Overall discussion

The results presented in this chapter show APOE4 animals to have increased neuronal activity coupled with subtle, yet robust vascular deficits. This could, over time lead to an energy imbalance, where increased neuronal energy demands are not met with adequate energy supply, although such a deficit is not yet present in the global measurements. As both the pia and capillaries are affected, and as mentioned the pial dilations are propagated from downstream vessels, perhaps the capillary bed is the initial site of dysfunction. Certainly, the idea that capillary dysfunction may be an important driver in the AD process is not a new one, with mathematical models suggesting that perturbations in capillary blood flow in AD could be the first step in a series of deleterious events, resulting in a degree of tissue hypoxia (Østergaard et al., 2013) and the aforementioned work from Nortley et al. (2019) showing convincing evidence that Aβ interacts with capillary pericytes, inducing constrictions as a result of reactive oxygen species production (Nortley et al., 2019). Specifically with reference to ApoE, there is evidence pointing towards capillary pericytes as key sites for ApoE4 meditated dysfunction. Studies from the Zlokovic group have shown there to an upregulation of a pro-inflammatory CypA-NF-κB-MMP9 mediated pathway in the pericytes and endothelial cells of APOE4 carriers (Bell et al., 2012; Halliday et al., 2016) that results in DNA damage in both these cell types. Indeed a recent study from the same group showed that human ApoE4 carriers have markers of pericyte injury in the cerebrospinal fluid and that the severity of this injury correlates with the cognitive trajectory of these patients, as well as with BBB permeability (Montagne et al., 2020).

A very interesting research question is what role do endothelial cells play in this dysfunction? The endothelial damage described by Bell et al. (2012) and Halliday et al. (2016), compliments the findings from Koizumi et al. (2018) showing it was the endothelium-dependent compartment of functional hyperaemia that was attenuated in

APOE4 animals. It would also be consistent with some of our findings in chapter 3 and in this current chapter. Endothelial cells are essential for the propagation of vasodilatory signals from downstream vessels to the pia (Chen et al., 2014; Longden et al., 2017) as well as for the conductance of vasomotion via gap junctions. Damage to endothelial cells could therefore result in dysfunctional signal conductance as well as aberrant endothelial signalling to the vasculature, resulting in less reliable responses at the capillary bed that are ineffectively propagated to the pia and therefore do not match the increased neuronal demand. Not only this, but endothelial damage could also account for the reduced vasomotion observed in APOE4 mice, if oscillations are not being effectively conducted along the vasculature. Future work, studying the endothelium of APOE4 mice would help to answer this question. Such experiments could include an investigation into the conductance of the endothelium in APOE4-TR mice as well as the physical properties of the cells such as the morphology or luminal coverage.

The work from Koizumi et al. (2018) pointed towards ROS as a potential reason for the vascular dysfunction. Studies suggest that ROS and CypA exist in a cycle, at least in VSMCs, where an increase in one, leads to an increase in the other (Satoh et al., 2010), so it is plausible that this pro-inflammatory pathway in pericytes and endothelial cells involving CypA, also involves ROS production. This could result in the damage of key cells in the neurovascular unit, pericytes and endothelium, but also a reduction of NO availability as it interacts with the ROS, superoxide, to produce peroxynitrite (Garthwaite, 2018), itself a molecule that exerts vascular damage (Girouard et al., 2007). ROS damage to VSMCs could also account for the reductions in vasomotion and the reduced NVCi in pial vessels, so an interesting future experiment could involve co-staining tissue for endothelial cells, pericytes or VSMCs with dihydroethidium to measure ROS levels(Dikalov et al., 2007). This would show if there are high levels of ROS in a specific cell type in APOE4 mice and so help to identify where the dysfunction is occurring (Dikalov et al., 2007).

4.5.3 Future work and limitations

In addition to the future work already mentioned throughout this chapter, an experiment to determine if the vasomotor apparatus is functionally intact, such as a hypercapnia challenge, would be suitable. It would test the ability of the vasculature to dilate, without modulating neuronal input (Jones et al., 2005) and would also not depend on the propagation of dilations, a process that could be defective if endothelial damage has taken place (Chen et al., 2014; Longden et al., 2017). This experiment would also shed light on whether or not APOE4 vessels posses the ability to dilate any further or if they are maximally dilated during the functional hyperaemia response.

4.5.4 Conclusion

In summary, the work in this chapter shows increased neuronal activity and mild vascular dysfunction in APOE4 mice. Over time this could produce a mismatch in energy supply and demand. Although the underlying mechanisms in these experiments are unclear, evidence from previous studies point towards endothelial and pericyte dysfunction as possible candidates. Over time this energy imbalance could worsen and eventually result in a chronic hypoxia in the brain, which could facilitate the formation of the hallmark pathologic features of AD, Aβ deposition and the hyperphosphorylation of tau (Fang et al., 2010; Sun et al., 2006).

Chapter 5

Effect of ApoE4 and Age on Neurovascular Properties

5.1 Introduction

The previous work in this study has provided an in depth look into the neurovascular coupling properties in young APOE4 and APOE3 mice. As previously mentioned, this young time point is important as it shows the early effects of ApoE4, before cognitive decline and AD would develop in humans. In addition to this age, two additional time points were studied, to determine how the effects found in young animals might evolve across a section of the lifespan.

5.1.1 Ageing and the neurovasculature

Age remains the single greatest risk factor for developing AD, and with APOE4 being the greatest genetic risk factor for going on to develop AD (Corder et al., 1993), the interaction and interplay between the two is of great interest. Ageing exerts a multitude of deleterious effects on the neurovasculature (for full reviews see: Iadecola et al. (2009); Brown and Thore (2011); Farkas and Luiten (2001)), including a thickening of the basement membrane that correlates with atherosclerosis (Farkas et al., 2006; Farkas and Luiten, 2001), capillary loss (Bell and Ball, 1981; Farkas and Luiten, 2001), pericyte degeneration (Iadecola et al., 2009), reduced CBF (Kalaria, 2009) and attenuated blood flow increases in response to sensory stimulation as a result of ROS produced from NADPH oxidase (Park et al., 2007). These deficits could result in an inadequate energy supply to active neurons which can have serious implications for neuronal health and cognitive function. Conversely, at least one study has found the NVC response to be preserved in animals >19 months old (unpublished

data - personal communication with Dr Kira Shaw).

5.1.2 ApoE and age

Consistent patterns of age dependent cognitive decline have been observed in APOE4 carriers compared to APOE3 carriers (Davies et al., 2014; Caselli et al., 2009), alongside various structural and functional age dependent effects such as a decline in functional connectivity and CBF in APOE4 carriers compared to WT controls (Zerbi et al., 2014) and increased seizure activity in APOE-TR mice (Hunter et al., 2012). Although very few longitudinal studies have been carried out investigating the effect of ApoE4 and age on the neurovasculature, existing evidence suggests that age exacerbates multiple deficits that exist in APOE4 mice. One such study is from Bell et al. (2012), where it was found that pericyte coverage of the microvasculature, as well as microvascular length decreased, and blood brain barrier permeability increased, in an age dependent manner from 2 weeks to 12 months in APOE4 mice.

5.2 Aims

This chapter aimed to fill in some of the existing knowledge gaps on the age dependent effects of ApoE4 on neurovascular function. Animals were studied longitudinally at 3-4 months of age (young time point) and at 6-7 months (middle age point). In addition, a separate small cohort of mice aged 12-13 months (old age point) were also tested. According to the Jackson laboratory, mice at 1 year of age better represent the middle aged human, rather than an elderly adult (Hagan, 2017). Therefore to gain further information on the effect of ApoE4 in later life, an additional time point could be considered e.g. 18- 24 months, however time constraints in this project meant that 12-13 month old mice were the oldest cohort that were tested. Despite this, the 6-7 month old range was still referred to as the "middle" age point in this chapter, as it was the middle relative to the other age points.

This chapter aimed to elucidate the neurovascular impact of age in APOE4 compared to APOE3 animals. Specifically to determine:

1. Are neurovascular resting state parameters altered in middle aged and old mice? Some deficits were observed in the baseline parameters in young animals and so investigating these properties across a section of the lifespan will help to determine if they are phenomena that exist only at young age or alternatively, if they continue to present with, or are modulated by age. The resting state parameters are of interest as they shed light on the baseline neurovascular conditions upon which the neurovascular coupling response is elicited. In addition to this, I also wished to determine:

2. Are neurovascular coupling responses to visual stimulation altered in middle aged and old mice? It has been reported that age alone can result in smaller NVC responses to sensory stimulation (Park et al., 2007) and so, in combination with ApoE4, attenuated responses to a sensory stimulation might be expected in older animals.

3. Do APOE4 mice exhibit any cognitive deficits at these age points? Conducting some behavioural assays at each time point provides valuable information on whether or not any neurovascular alterations are observed prior to behavioural effects.

5.3 Methods

5.3.1 Animal Ageing

As described in the main methods section, animals had a cranial window implanted at ∼8 weeks of age and were imaged between 3-4 months of age as described in the two previous experimental chapters. The majority of these mice were then aged to 6-7 months and imaged again, according to the same experimental paradigms. A separate cohort of mice were surgically prepared at ∼ 11 months of age, and imaged at 12-13 months of age. Unfortunately it was impractical to track the same animals from young to old due to the decreasing viability of the cranial window, and so separate cohorts were necessary.

5.3.2 Data Collection

All data collection was carried out in the same manner as described in the main methods section and in the methods outlined in chapters 3 and 4.

5.3.3 Data Analysis

All data was analysed in the same way as described in the main methods section and in chapters 3 and 4. All "young" data presented in this chapter is the same as that shown in chapters 3 and 4.

5.3.4 Statistical analysis

Statistical analysis was carried out in SPSS. To determine the effect of age on each parameter, two-way ANOVAs were carried out. As primarily vessels or neurons were used as subjects and crucially, old animals were a separate cohort, independent sample ANOVAs were carried out, rather than repeated measures. All error bars represent SEM and detailed statistical outputs, as well as sample sizes can be found in Appendix A .

5.4 Results

5.4.1 Effect of ApoE4 and Age on short term and spatial memory

Three behavioural assays were carried out to determine if the age points selected in this study were accompanied with cognitive changes. A novel object recognition task was performed to test short term memory (Clark et al., 2000) and a discrimination ratio was calculated to quantify the amount of time spent with the novel object, compared to the familiar object (figure 5.1A). There was no effect of age or genotype, nor was there an interaction between age and genotype. Similarly, a spatial object recognition task was carried out to assess hippocampal-dependent spatial memory (Dix and Aggleton, 1999). There was no observed effect of age or genotype and no interaction between the two (figure 5.1B). In both tasks, across all age groups, some animals failed to engage with the task for long enough (i.e. did not spend more than 15 seconds exploring) and so were excluded from the analysis. In the old cohort, APOE4 mice were unable to be statistically analysed due to a small sample size (post-exclusion) in both tasks, and similarly, data from APOE3 animals could not be analysed in the spatial object recognition task. Although this may suggest that the animals were less engaged in the task at this time point, it's important to be mindful of the fact the the cohorts were small to begin with (n=3-4 animals per genotype). Larger sample sizes would be required to determine if a reduction in task engagement is a feature of age or not. Using the data available, it appears that animals at these age points do not display any cognitive deficits. Using a measure of locomotion (as described in section 2.6), the activity of the mice was measured. Older mice were less active than younger mice, but there was no interaction of age with genotype, nor a difference between genotypes (figure 5.1C). In general, these results suggest there were no genotype dependent effects on cognitive performance, however the small sample sizes (post-exclusion) in the old cohort of mice means that larger group sizes would be required in order to be certain that this finding extended into mice aged 12-13 months.

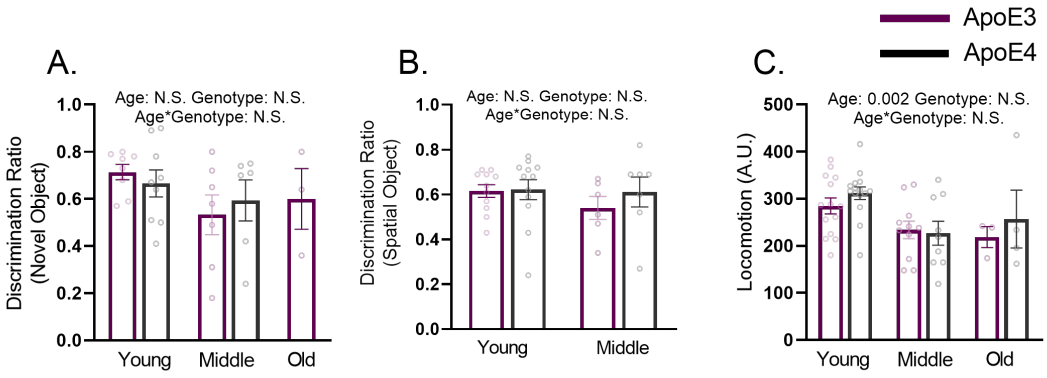

Figure 5.1: **Effect of ApoE on spatial and short term memory** A. Novel object recognition task: Discrimination ratio of amount of time spent with novel object:familiar object in young, middle aged and old mice. B. Spatial object recognition task: Discrimination ratio of amount of time spent in novel location:familiar location in young and middle aged mice. C. Locomotion measure in young, middle aged and old mice. Purple bars represent APOE3 and black bars represent APOE4. Circles represent individual animal averages and error bars represent SEM. For detailed statistical outputs see table A.15

5.4.2 Effect of ApoE4 and Age on resting state neuronal activity

In order to assess baseline energy demands in these mice over time, neuronal activity at rest and in the dark was recorded, however due to time constraints only data for young and middle aged groups were collected. The number of peaks per minute (PPM) was calculated and no genotype or age effect was observed (figure 5.2A). The correlation of firing was not affected by age or genotype under resting conditions (figure 5.2B) and finally, the size of the peaks did not differ with genotype or age (figure 5.2C). As well as averaging data across animals as in figure 5.2, it was also averaged across all cells (figure B.3). When averaging using this method there was an effect of age on the number of PPM as well as on the size of the peaks. Interestingly, middle aged animals displayed higher numbers of PPM but with lower magnitudes than young animals. However, as with animal averages, there was no effect of genotype.

In conclusion, when considering animal averages, age and genotype do not appear to interact at these age points to modulate resting neuronal activity, and so the neuronal characteristics and therefore presumably energy demand, in the absence of a visual stimulation, is likely be similar across all animals.

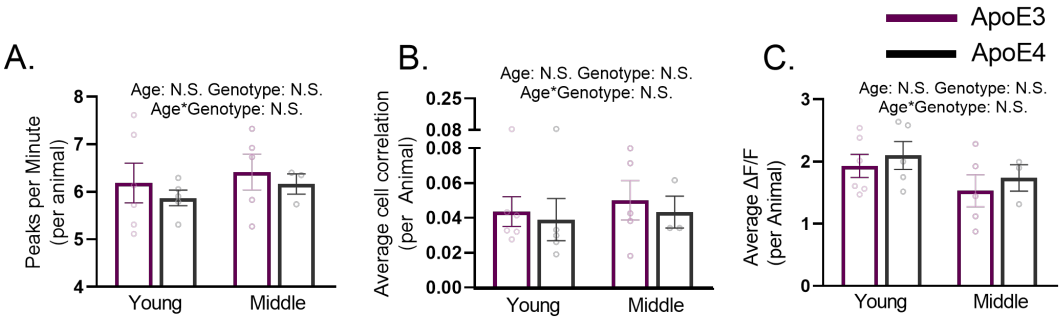

Figure 5.2: **Resting state neuronal activity** A. Peaks per minute. B. Cell correlation averaged per animal. C. Average ΔF/F of peaks. Purple bars represent APOE3 and black bars represent APOE4. Circles represent individual animal averages and error bars represent SEM. For detailed statistical outputs see table A.16

5.4.3 Effect of ApoE4 and Age on resting state haemodynamic parameters

In order to assess the tissue energy delivery in APOE3 and APOE4 mice, and how this was modulated by age, various parameters were investigated at both an individual vessel level and at a more global level across the region. Resting pial and capillary diameters were measured across all age points and there was no effect of age or genotype observed (figures 5.3A, B), although the data shows a trend towards reduced pial diameters in old APOE4 animals. Resting RBCV was measured across all three age points and it was found that the average RBCV remained similar across genotypes and age points (figures 5.3C). Net haemodynamic measurements were then analysed to look for global differences across age and genotype. Neither flux, SO_2 or $CMRO_2$ showed any effect of genotype or age, suggesting that these parameters also remained stable across the lifespan in both genotypes (figures 5.3D, E, F). Finally, the coefficient of variation was determined, to gain a measure of temporal fluctuations in the net flux, SO_2 and RBCV measurements. There was no observed effect of age or genotype on net flux or SO_2 measurements (figures 5.3G, H), but there was a significant effect of genotype in RBCV measurements. Data suggests that RBCV CV in APOE4 vessels was not differently affected across all three age points as there was no interaction between age and genotype, however, post hoc multiple comparisons with Bonferroni's correction, would suggest that this effect was present only at middle age.

These data demonstrate that the measured parameters remained mostly preserved across all age points, with APOE4 only resulting in an increased heterogeneity of velocity, which could result in altered oxygen extraction from the blood to the tissue (Østergaard et al., 2013). An interesting adjunct to these findings, would be a measure of vascular morphology in fluorescent gel filled brain slices, as was carried out in chapter 3. Vascular density was reduced in young APOE4 mice, however this was not reflected in the net CBF readings, possibly because of the subtlety of the effect. So despite there being no differences in the net haemodynamic measurements, there may be more subtle changes in older animals that can only be detected by studying the vasculature directly.

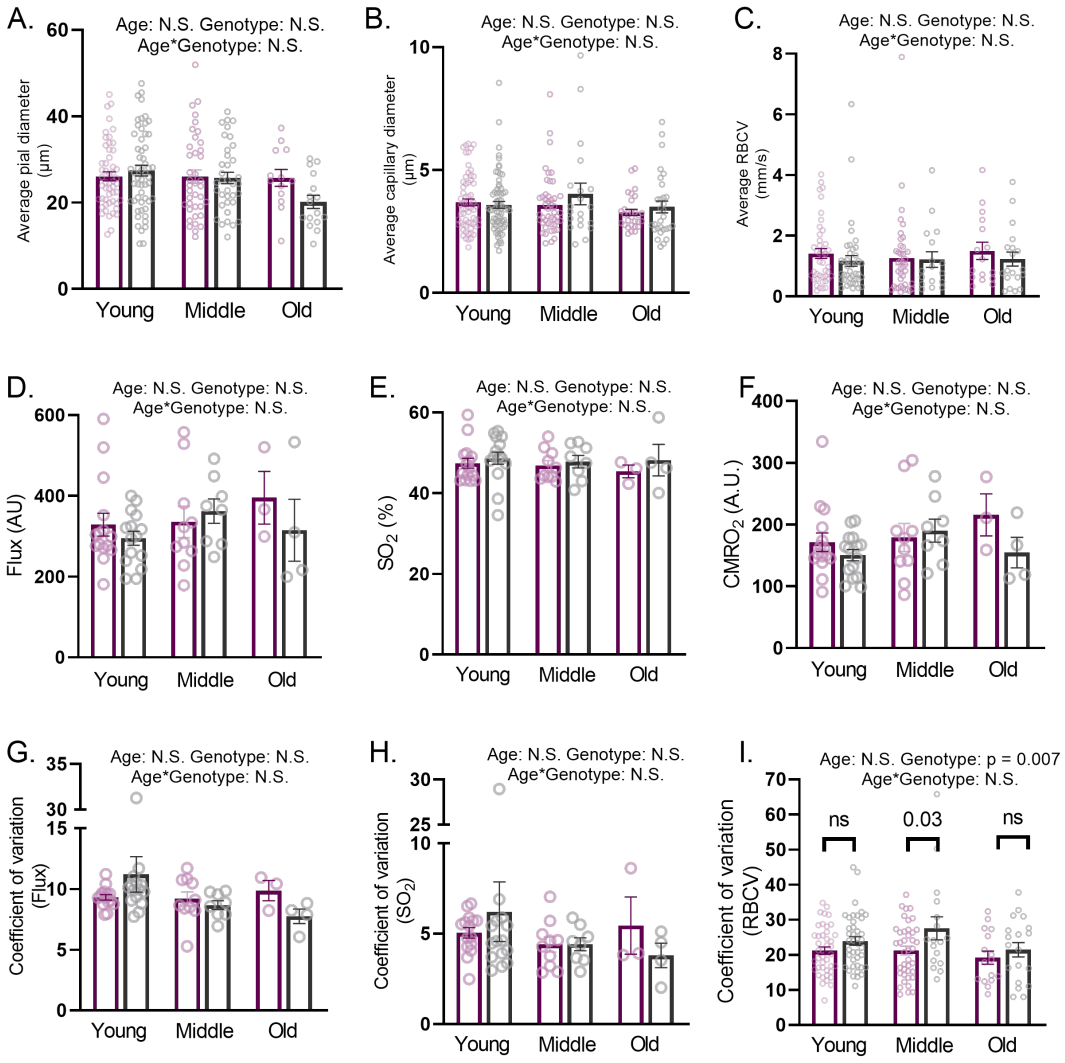

Figure 5.3: **Resting net haemodynamic parameters** A. Resting pial diameter. B. Resting capillary diameter. C. Resting red blood cell velocity (RBCV). D. Resting net flux, E. SO_2 and F. $CMRO_2$ measurements. G. Coefficient of variation of flux, H. SO_2 and I. RBCV measurements. All measurements were made across young, middle and old time points, in both APOE3 and APOE4 animals. Purple bars represent APOE3 and black bars represent APOE4. Circles in A-C and I represent individual vessel averages, and in D-H, circles represent individual animal averages. Error bars represent SEM. For detailed statistical outputs see table A.17

In addition to the above resting state parameters, vasomotion was measured at all three age points. A reduction in vasomotion was observed in young APOE4 animals in chapter 3 (figure 5.4A) and this pattern appeared to continue across all age points. Although the difference between the traces did not reach significance in middle aged animals (figure 5.4B), there was a trend towards there being a lower relative power in the 0.1-0.2Hz and 0.2 - 0.3Hz range in APOE4 mice ($p = 0.077$, 0.07 respectively). In old animals, there was significantly lower relative power in APOE4 vessels in the 0.1-0.2Hz frequency range (figure 5.4C), and although the relative power difference in the 0.2-0.3Hz frequency range, failed to reach statistical significance, it trended strongly towards being lower in APOE4 animals ($p = 0.06$). Finally, when purely considering the relative power at 0.1Hz, the classic vasomotion frequency, an effect of genotype was observed (figure 5.4D). The absence of an age by genotype effect suggests that the mean relative power was greater in APOE3 vessels across all three age points and that this effect remained stable across this section of the lifespan. Whilst when multiple comparisons were conducted, they suggested that differences existed in only young animals, in the absence of an age by genotype interaction we cannot conclusively say there is a difference in effects across age groups.

As previously mentioned vasomotion is thought to be not only a valuable indicator of vascular health, but also important for the clearance of substances from the brain (van Veluw et al., 2019) and possibly also for perfusion and oxygenation (Rücker et al., 2000; Tsai and Intaglietta, 1989). These data show a consistent deficit in the oscillatory properties of APOE4 blood vessels, suggesting that there may be deficits in the aforementioned clearance, perfusion and oxygenation mechanisms at each of these age points.

The examination of these baseline parameters across age yielded similar results to those found in chapter 3. Despite similar neuronal activity and therefore energy demands at rest, there appeared to be some subtle vascular deficits such as an increase in RBCV CV as well as reduced vasomotion in APOE4 mice. This suggests that there may have been a small imbalance in energy supply and demand across all age points, although not at sufficient levels to impact SO_2 or $CMRO_2$ measurements. Without neuronal data for old animals it's impossible to be certain of this conclusion in that age group. It does appear however, that there was no robust effect of age in these animals in either the neuronal or vascular properties at rest.

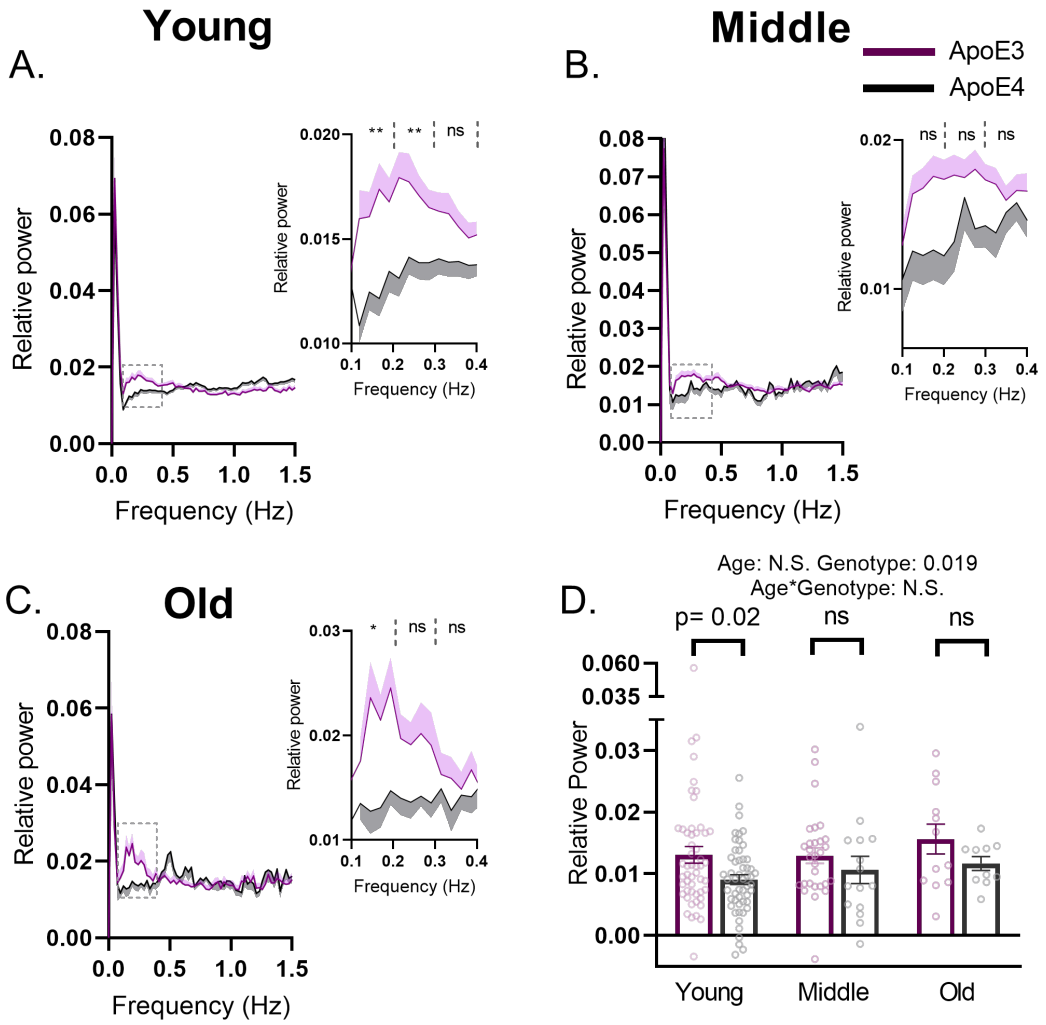

Figure 5.4: **Effect of ApoE and age on vasomotion** A. Relative power spectra for all averaged APOE3 and APOE4 pial vessels from young animals. Upper right insert corresponds with the grey dashed box. Dashed grey lines on insert graph show the frequency bins that were compared. B. Relative power spectra for all averaged APOE3 and APOE4 pial vessels from middle aged mice. Upper right insert corresponds with the grey dashed box. Dashed grey lines on insert graph show the frequency bins that were compared. C. Relative power spectra for all averaged APOE3 and APOE4 pial vessels from old animals. Upper right insert corresponds with the grey dashed box. Dashed grey lines on insert graph show the frequency bins that were compared. D. Average relative power at 0.1Hz across all age points. Circles represent individual vessel averages, and error bars represent SEM. For detailed statistical outputs see table A.18

To better understand how energy supply and demand was balanced across the three age points, neurovascular activity in response to visual stimulation was assessed.

5.4.4 Effect of ApoE4 and Age on neuronal responses to visual stimulation

When the neuronal response magnitude was compared across young and middle aged animals, there was a consistent pattern of increased response sizes to visual stimulation in APOE4 mice. This was observed when all cells were taken into account (figure 5.5A) and when only responsive cells were considered (figure 5.5C). Although the genotype effect was not statistically significant when all cells were averaged per animal (figure 5.5A), it almost reached statistical significance with $p = 0.055$. When considering responsive cells only, there was no interaction between age and genotype suggesting that the two age groups were not differently affected. However, when multiple comparisons were made with a Bonferroni correction, only the middle aged response size was significantly larger.

There was no observed difference in the response frequency in APOE3 and APOE4 animals (figures 5.5 B). The number of peaks per minute of responsive cells was calculated during visual stimulation and compared across genotypes and age points. Although there was no effect of genotype, there was a robust effect of age (figure 5.5D). As animals got older, the number of peaks during the stimulation appeared to reduce, although the magnitude of these events remained the same, as seen in figure 5.5C. As with all neuronal data, in addition to averaging by animal, data was also averaged across all cells (figure B.4) where the same effects were observed.

These data suggest that the overall energy demand was likely slightly lower at middle age when compared with young age, but that this was not genotype dependent and energy demand continued to be higher in APOE4 mice at both age points.

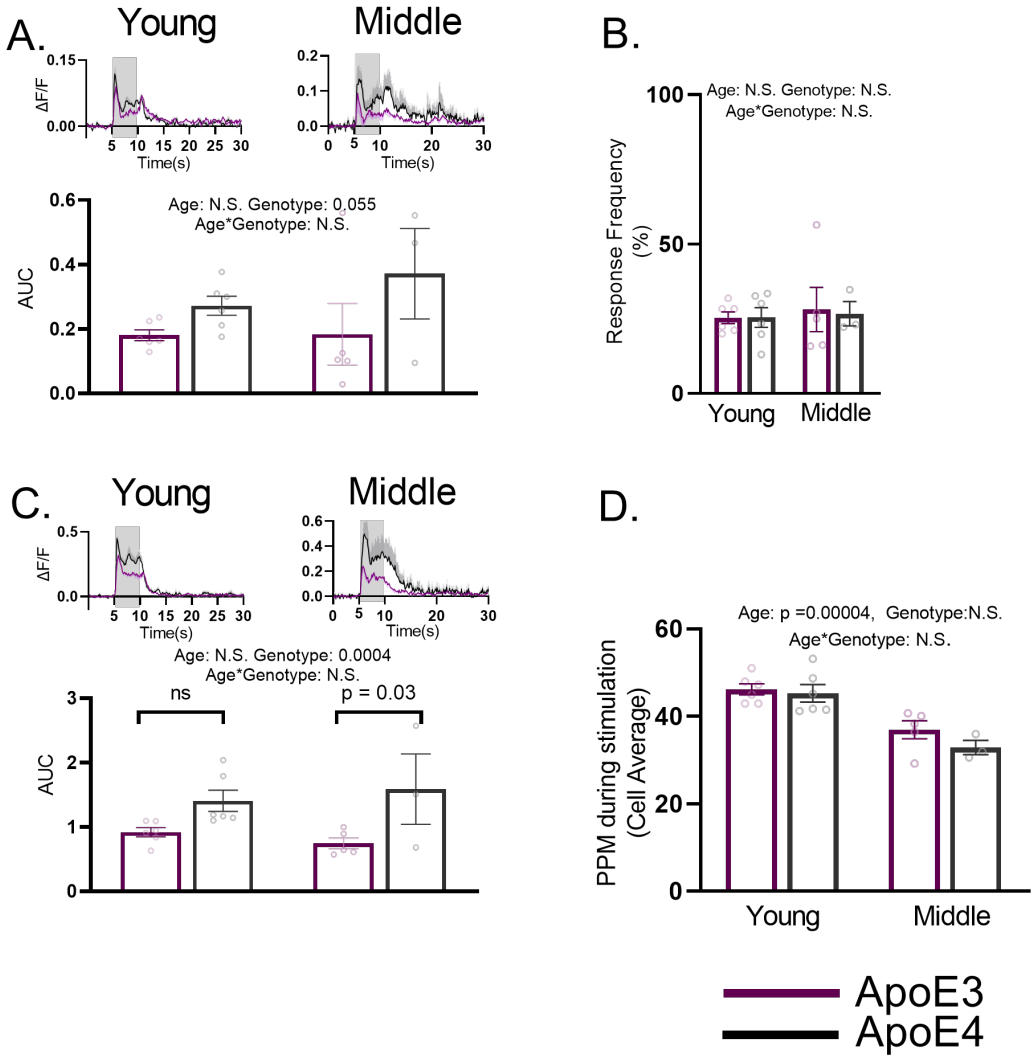

Figure 5.5: **Neuronal responses to visual stimulation** A. Top panels show average ΔF/F traces across all cells, in response to visual stimulation in young and middle aged mice, averaged per animal. Bottom panel shows AUC measurements for each ΔF/F trace during visual stimulation, averaged per animal. B. Response frequency of cells to visual stimulation, averaged per animal at both young and middle age points. C. Top panels show average ΔF/F traces across responsive cells only, in response to visual stimulation in young and middle aged mice, averaged per animal. Bottom panel shows AUC measurements for each responsive ΔF/F trace during visual stimulation, averaged per animal. D. Number of peaks per minute for each cell during visual stimulation, averaged per animal. Grey boxes represent visual stimulation. Circles represent individual animal averages, and error bars represent SEM. For detailed statistical outputs see table A.19

5.4.5 Vascular responses to visual stimulation

In order to assess how energy delivery was modulated by age, the vascular responses to visual stimulation were measured at the pia and in the capillary bed. Like in the previous chapter, vessel response frequency was measured across all age points, considering all vessels, as well as only those with greater than 10 contributing trials. Some vessels had only a small number of contributing trials, meaning only very low or very high response frequencies were possible. To eliminate this effect, subgroups containing only vessels with greater than 10 contributing trials were analysed separately. The response frequency across age points painted a mixed picture. In chapter 4 there was a consistent trend showing a reduction in the responsiveness of APOE4 vessels across all diameter and RBCV measurements, however this did not continue across the age points. Pial responsiveness did not show any effect of genotype when considering all vessels (figure 5.6A) or when considering only those with greater than 10 trials (figure 5.6B). However there was an effect of age when all vessels were considered, where old animals appeared to be more responsive than young or middle aged animals. Capillary diameter responsiveness, which was decreased in young APOE4 animals in vessels with more than 10 trials, did not display this patten across all age points. There was no effect of genotype on either data set (figure 5.6C, D), however when all vessels were considered there was again an effect of age, where old APOE4 animals were most responsive (figure 5.6C). This effect was lost when only vessels that had greater than 10 contributing trials were considered (figure 5.6D). RBC velocity responsiveness also did not continue with the effect observed at young age, where the RBC velocity increased less reliably in response to visual stimulation in APOE4 animals. In fact, there was again, no effect of genotype in either analysis but there was an effect of age where old animals appeared to be more responsive (figure 5.6E). Too few vessels had greater than 10 contributing trials at the old age point for statistical comparisons to be made (figure 5.6F).

Overall these data do not paint a clear picture, however the reduced responsiveness that was observed at a young age was not robust across all age points, suggesting that this may be only a feature that presents in young animals. The apparent increase in responsiveness in old animals was not present when the threshold of a minimum of 10 trials was applied, so likely appeared as a result of vessels with only few contributing trials.

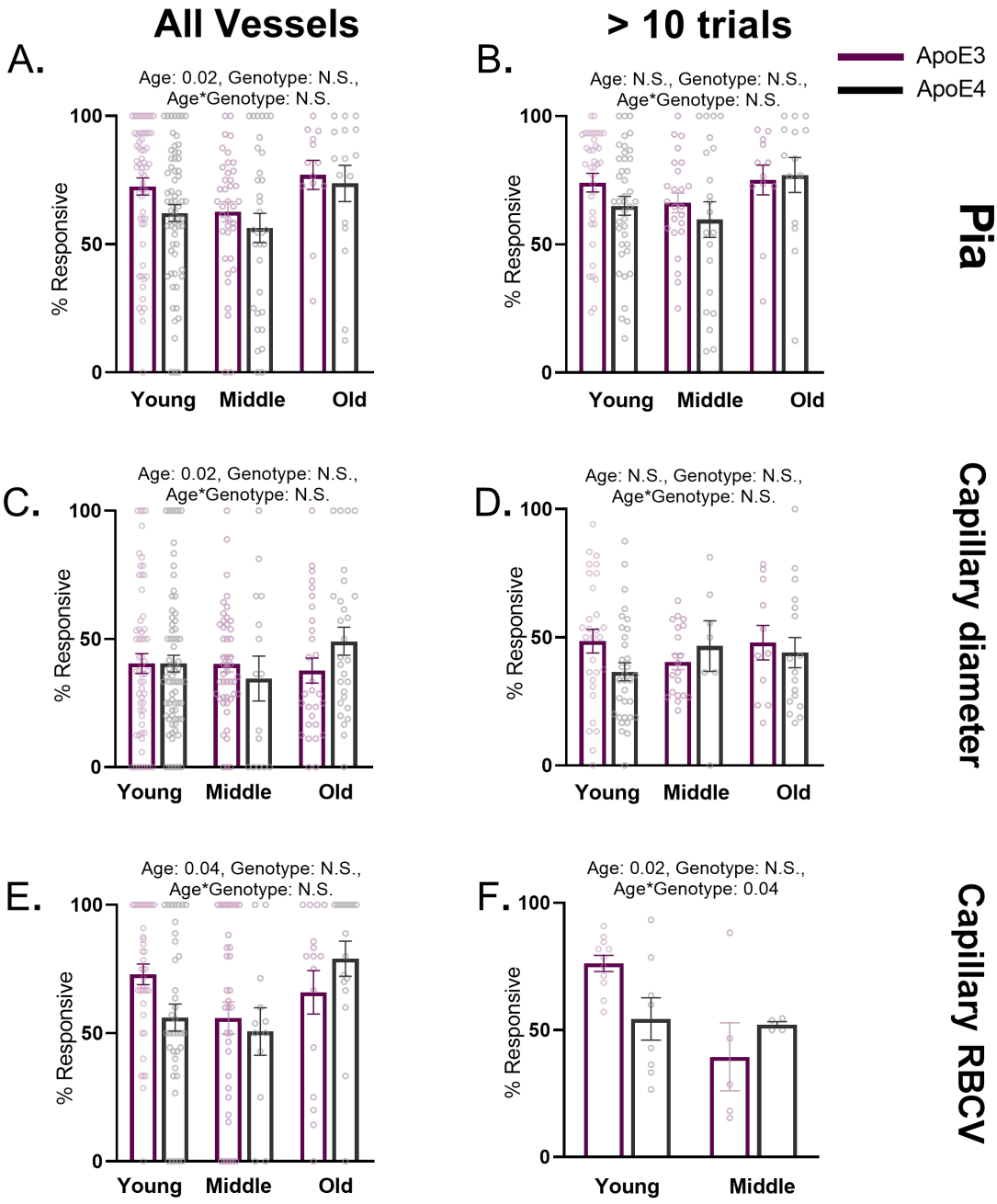

Figure 5.6: **Vascular response frequency** A. Pial vessels response frequency to visual stimulation, all vessles. B. Response frequency of pial vessels with greater than 10 trials. C. Capillary diameter response frequency to visual stimulation, all vessels. D. Response frequency of capillary diameters with greater than 10 trials. E. Capillary RBCV response frequency to visual stimulation, all vessels. F. Capillary RBCV response frequency in vessels with greater than 10 trials. Circles represent individual vessel averages, and error bars represent SEM. For detailed statistical outputs see table A.20.

The response magnitudes were then compared to determine if there was an effect of genotype or age on response size in these older animals. As with chapter 4, all trials per vessel were initially analysed (figure 5.7 left panel), then responsive trials only (figure 5.7 right panel). Vessel averages for responsive trials only, better reflect the response magnitude as averaging all trials together confounds response rate with response size. Pial response sizes showed an effect of age in both analyses (figures 5.7A, B), where the response sizes appeared to be smaller in middle aged animals, however there was no effect of genotype across any age points. Capillary diameters showed a slightly different pattern, where there was no effect of age or genotype when all trials were analysed (figure 5.7C), however when only responsive trials were taken into consideration, there was a genotype effect (figure 5.7D). This appeared to be driven by an increased response size in APOE4 animals at old age, this was confirmed with a multifactorial ANOVA split by age (middle age: $F = 1.493$, $p = 0.227$, old age: $F= 10.1$, $p = 0.002$). Finally, RBC velocity displayed similar results, with no effects present when considering all trials (figure 5.7E), but when looking at responsive trials only, there was an effect of age where, again, middle aged animals appeared to have smaller response sizes (figure 5.7F).

These results, alongside the response frequency data in figure 5.6, cast some confusion over the idea that blood vessels were less responsive in APOE4 animals and that this may have been expected to deteriorate further with age, or that the magnitude of responses may decrease with age. It still remains however, vascular responses did not increase in response frequency or size, in concert with increased neuronal demand at either the young or middle age time point. Capillary diameter responses increased in old APOE4 animals, suggesting some degree of recovery from the subtle deficits observed in younger animals.

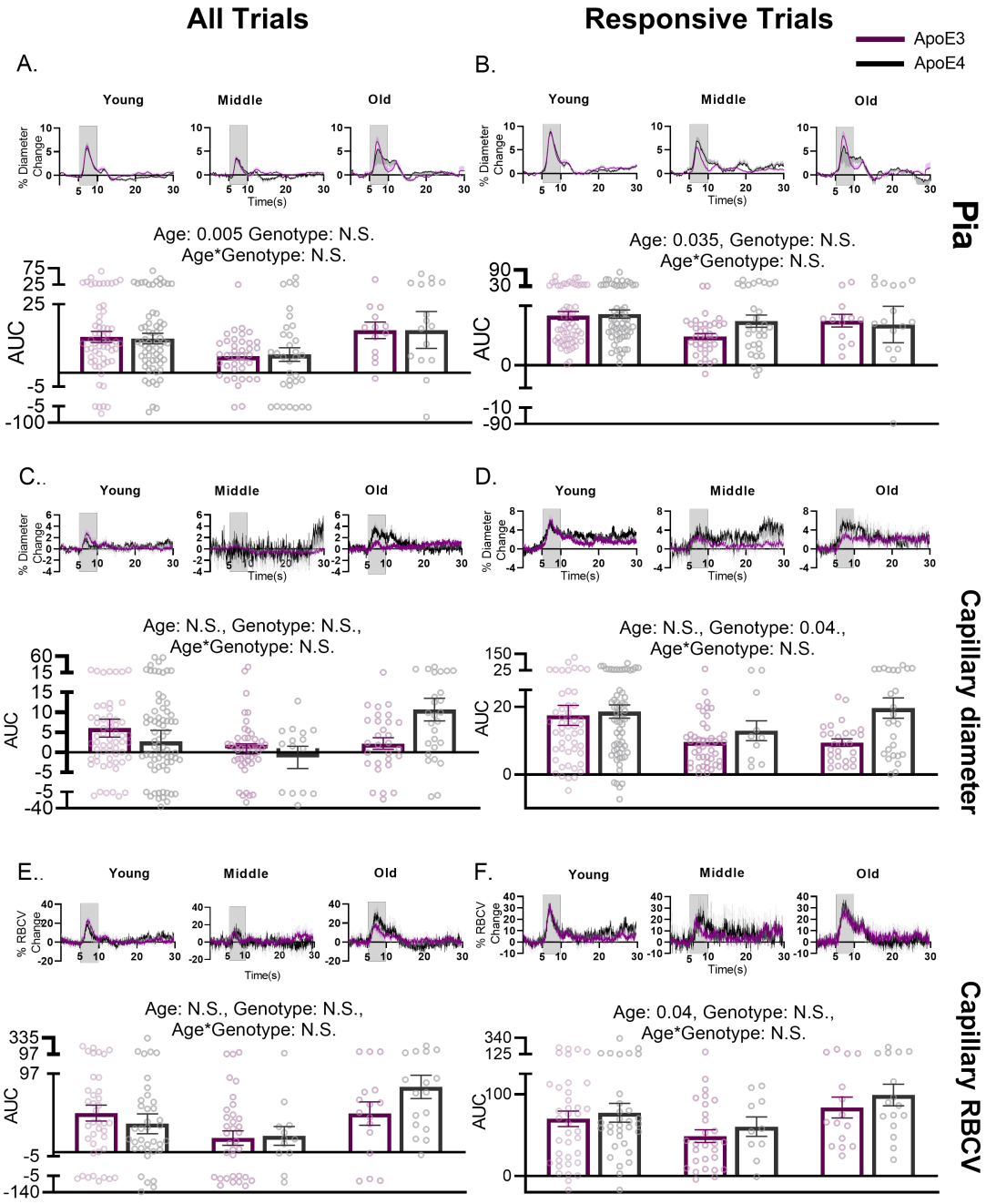

Figure 5.7: **Vascular responses to visual stimulation** A. Top panels show average pial vessel diameter traces in response to visual stimulation in young, middle aged and old animals. Bottom panel shows each vessel AUC during visual stimulation. B. Top panels show average pial vessel diameter traces of responsive trials only during visual stimulation in young, middle aged and old animals. Bottom panel shows the AUC of the vessel average of responsive trials only during visual stimulation. C. Top panels show average capillary diameter traces in response to visual stimulation in young, middle aged and old animals. Bottom panel shows each vessels AUC during visual stimulation. D. Top panels show average capillary diameter traces of responsive trials only during visual stimulation in young, middle aged and old animals. Bottom panel shows the AUC of the vessel average of responsive trials only during visual stimulation. E. Top panels show average capillary RBC velocity traces in response to visual stimulation in young, middle aged and old animals. Bottom panel shows each vessel AUC during visual stimulation. F. Top panels show average RBC velocity traces of responsive trials only during visual stimulation in young, middle aged and old animals. Bottom panel shows the AUC of the vessel average of responsive trials only during visual stimulation. Grey rectangles represent visual stimulation. Circles represent individual vessel averages, and error bars represent SEM. For detailed statistical outputs see table A.21.

5.4.6 Net haemodynamic responses to visual stimulation

In order to assess the haemodynamics across the entire region, net measurements were taken in response to visual stimulation across all three age points. As before, measurements were taken for flux, total haemoglobin (HbT), oxygenated haemoglobin (HbO), deoxygenated haemoglobin (HbD), oxygen saturation (SO_2) and cerebral metabolic rate of oxygen consumption ($CMRO_2$), which is indicative of net neuronal energy use. Across all parameters there was no effect of genotype, although as discussed in chapter 4, there appeared to be small genotype differences in some of these parameters at young age (figure 5.8). In HbT, HbO and SO_2 AUC measurements, there was an effect of age which appeared to be driven primarily by increases in the AUC of old animals (figure 5.8B, C, E). This was an interesting finding, and contrary to what might be expected from existing literature. It is important to remember however, that the group sizes were much smaller in older animals, and so were strongly influenced by outliers, it would be pertinent to increase the group sizes for these measurements in the future, to determine if these results are reproducible.

Net haemodynamic responses to visual stimulation Figure on following page. A. Top panels show average flux responses to visual stimulation in young, middle aged and old animals. Bottom panel shows AUC for the flux responses during visual stimulation shown in the top panel. B. Top panels show average HbT responses to visual stimulation in young, middle aged and old animals. Bottom panel shows AUC for the HbT responses during visual stimulation shown in the top panel. C. Top panels show average HbO responses to visual stimulation in young, middle aged and old animals. Bottom panel shows AUC for the HbO responses during visual stimulation, shown in the top panel. D. Top panels show average HbD responses to visual stimulation in young, middle aged and old animals. Bottom panel shows AUC for the HbD responses during visual stimulation, shown in the top panel. E. Top panels show average SO_2 responses to visual stimulation in young, middle aged and old animals. Bottom panel shows AUC for the SO_2 responses during visual stimulation shown in the top panel. F. Top panels show average $CMRO_2$ responses to visual stimulation in young, middle aged and old animals. Bottom panel shows AUC for the $CMRO_2$ responses during visual stimulation, shown in the top panel. Circles represent individual animal averages, and error bars represent SEM. For detailed statistical outputs see table A.22.

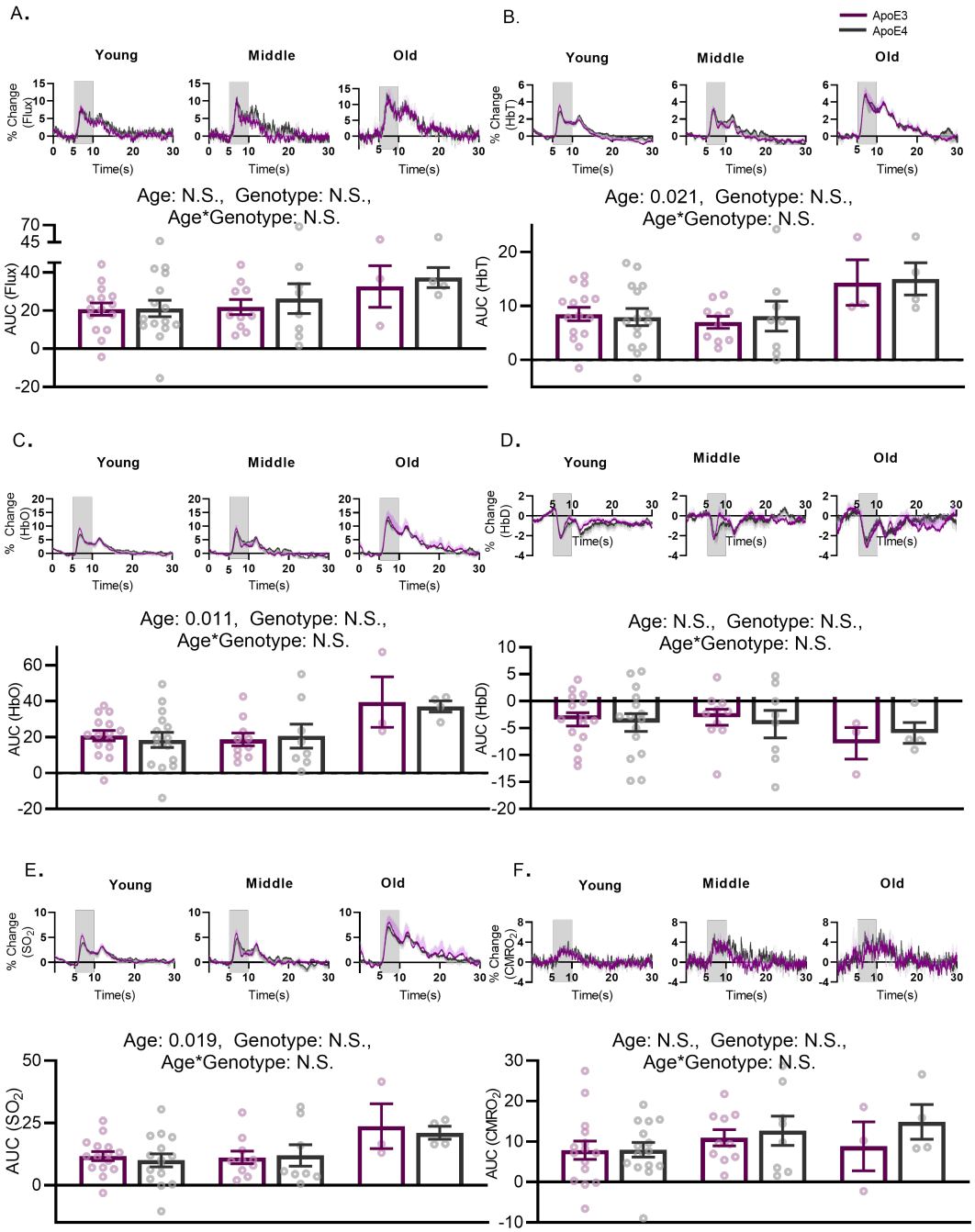

Figure 5.8: **Net haemodynamic responses to visual stimulation**. Figure legend on previous page.

5.5 Discussion

5.5.1 Results Summary and Interpretation

APOE4 animals do not display behavioural deficits at any of the examined age points

These animals were examined for impairments in spatial and short term memory and no deficits were detected in APOE4 animals at either the young or middle age point. Although, as aforementioned, the tests carried out are simple and a thorough cognitive battery would be required to detect more subtle behavioural changes, these results do suggest that the effects observed in young and middle aged time points, occur prior to global cognitive changes. Further work is required to determine if this is also the case with old animals.

Resting state parameters were then examined so that a baseline energy balance could be determined. Not only is this interesting to examine in its own right, it also allows for a greater understanding of the energy balance during the functional hyperaemia response as it may be acting on top of an already energy deficient system. As a result of delayed access to Th1-GCaMP6f animals (those with a genetically encoded calcium indicator in excitatory neurons), neuronal data was only collected for young and middle aged animals.

Resting state neuronal characteristics do not differ by genotype

Across all three resting state measurements, peaks per minute, cell correlation and average $\Delta F/F$, there was no effect of genotype or age. This suggests that at both age points, the energy requirements of APOE3 and APOE4 animals were similar.

Resting state vascular characteristics are modulated by genotype but not age

Although many of the baseline parameters such as blood vessel diameter and net haemodynamic parameters, remained unaffected by age and genotype, the trend towards increased CV in APOE4 RBCV, observed at young age, continued across the other age points and was particularly increased at middle age. As previously discussed, mathematical modelling from the Østergaard group has suggested that such temporal variation in the velocity of RBCs could result in a reduction in oxygen extraction from the blood to the tissue (Østergaard et al., 2013), implying that there could be deficits in

this mechanism in APOE4 mice, across all age points. In addition to this observation in APOE4 mice, there was also a reduction in vasomotion in these animals, across all age points. Together these alterations could result in basal reductions in tissue oxygenation and perfusion, as well as a reduction in clearance.

Neuronal and vascular responses to visual stimulation were then investigated to examine the ability of the local blood supply to increase energy delivery to active neurons. As APOE4 animals already appeared to be operating with a deficit under resting conditions, further alterations could enhance any energy insufficiencies.

Neuronal responses to visual stimulation are larger in APOE4 mice across age groups

The magnitude of the neuronal response to visual stimulation was increased in middle aged animals, as was observed in young animals. The $\Delta F/F$ of the GCaMP signal is closely coupled with the number of spiking events (Akerboom et al., 2012) and so is a valuable measure of neuronal activity and is therefore indicative of energy demand. Data shows that young mice had more frequent calcium transients and so presumably also had higher energy demands than middle aged mice. What is clear is that at this middle age point, APOE4 mice continued to have increased response sizes compared to APOE3 mice, suggesting that they had higher energy requirements. It would therefore be expected that they would have an increased energy supply, either by accordingly increasing the response frequency to visual stimulation, or alternatively, the response size.

Vascular responses to visual stimulation suggest that vascular unreliability does not continue into older age

Although at young age there was a clear reduction in response frequency in APOE4 animals, this did not continue robustly across all age points. All age points considered, there was no effect of genotype on the vascular response frequency at the pia or capillary bed. If all vessels were taken into account there was an observed effect of age which primarily appeared to be driven by low response frequencies at the middle point. As well as this, there was no observed reduction in the response magnitude in APOE4 animals at the pia or the capillary bed. As the vessel averages for responsive trials only are more indicative of net energy supply, these are the data that were focused on primarily. There was no

difference in the size of responses at the pia or when considering capillary RBCV, as assessed by AUC measurements, nor any obvious deterioration with age. However capillary diameter responses to visual stimulation were increased in old APOE4 mice.
This evidence demonstrates that the deficits in young APOE4 animals, resolve somewhat with age, although there was no significant interaction between age and genotype, presumably as the effect was very subtle even in young animals. Despite the lack of clear vascular insufficiency at the later time points, its important to remember that APOE4 animals had a larger energy demand compared to APOE3 animals, and so in a healthy system an increased vascular response would be expected.

5.5.2 Overall Discussion

This chapter aimed to elucidate the effect of ApoE4 on neurovascular properties and how this interacted with age. Mice at 3-4 months, 6-7 months and 12-13 months were studied and termed young, middle aged and old respectively. The data in this chapter confirmed that some of the effects found at the young time point, continued into middle and older ages, such as the reduction in vasomotion and the increase in the heterogeneity of RBC velocity in APOE4 animals. These effects were robust and presented across all three age points. Although there was no neuronal data for the old age group, middle aged animals displayed the same hyperactive neuronal phenotype as young animals, suggesting that the increased energy demand, alongside some deficits in vasomotion and RBCV existed across age groups.
There was some degree of recovery with age in APOE4 animals, the reduction in vascular response frequency observed in young animals was no longer present and capillary diameter responses to stimulation were increased in old APOE4 animals. However in general, most parameters did not change and remained the same throughout all the measured age points.

In this study I did not observe a degenerative phenotype with age and there are several reasons why this may be the case. Firstly, it is important to consider the mouse model used in this study. APOE-TR mice are not models of AD, and observing the effects of ApoE4 alone and independent of the pathological hallmarks of AD is undoubtedly of value but likely to be much milder than AD mouse models, in terms of deficits observed. Future work should study how the observed changes in APOE4 animals might promote or interact with Aβ and pathological tau
In addition, although three age points were selected, they were fairly close together and

did not include a time point more representative of true old age in humans, such as 18-24 months. It is therefore possible that the middle aged and old time points actually both translate to middle age in humans. The antagonistic pleiotropy hypothesis states that APOE4 carriers have some cognitive benefits in early age, little or no difference at middle age due to the recruitment of compensatory mechanisms and finally, when these compensatory mechanisms are exhausted at old age, the deficits in APOE4 carriers are observed (Tuminello and Han, 2011; Han and Bondi, 2008). Although the described benefits at early ages are not observed in this study, it is possible that the inconsistent results observed at middle and old age are as such due to the recruitment of compensatory mechanisms and that large global deficits might not be observed until later in the mouse lifespan.

The data in this chapter showing increased neuronal activity in middle aged APOE4 animals, without robust increases in vasodilation, support the energy mismatch theory postulated in previous chapters to some extent. However it also demonstrates, at least in the absence of Aβ and pathological tau, that any energy imbalance is not sufficient to cause a progressive decline in neurovascular function.

5.5.3 Future work and limitations

In addition to the future experiments suggested throughout this chapter, there are some additional points to consider. It is impossible to be certain that the fact the same mice were imaged at young and middle age, whereas a separate cohort was used for old age, did not have had an impact on results, especially as the time post surgery would be greatest at middle age compared to the young and old age points. In order to improve this, a longitudinal study where the same mice were imaged throughout but with an extended recovery time could be considered. Although this would also be accompanied with problems arising from long term implantation of the cranial window, such as ill health and bone regrowth. Alternatively, three separate cohorts could be used for each age point, meaning they would be imaged under identical conditions, although improved recovery in young animals cannot be ruled out.

5.5.4 Conclusion

Although the data in this chapter did not display the degenerative phenotype that might be expected as these animals age, it provided some interesting insights into how the neurovascular properties in this mouse model change over time. The disruptions to basal energy supply initially observed in young animals, namely the reduced vasomotion and increased RBCV CV, continued into middle and old age points. Conversely, the reduced reliability of the vascular response observed in young animals was not seen in older animals, suggesting that vascular function was somewhat improved at these later time points. Nevertheless, the increase in neuronal energy demand in APOE4 animals was observed in middle aged animals, without a corresponding increase in energy supply, so it is likely that the proposed energy deficit observed in young animals might continue until at least the middle time points. Further experiments would be required to determine if this was also the case in animals that were 12-13 months old.

Chapter 6

General Discussion

6.1 General Discussion

This body of work sought to determine the effect of ApoE4 and age on the neurovasculature in the visual cortex. We found subtle, yet robust changes in young APOE4 animals that we speculate could be one of the early triggers in AD pathogenesis in humans. These findings included deficits in APOE4 animals across multiple vascular elements, including the microvascular density, vasomotion, baseline RBCV heterogeneity, as well as in the reliability of the blood supply increase in response to neuronal activity. These vascular deficits were accompanied by an enhanced neuronal response to visual stimulation in APOE4 animals, where the response magnitude was larger.

These results point towards an energy mismatch in APOE4 animals, where the hyperexcitable neuronal phenotype would presumably result in a larger energy demand during visual stimulation and in order to match this increased demand with adequate blood supply and therefore adequate energy delivery, an increase in response frequency or response size would be expected. However this was not observed, on the contrary, blood vessel diameters and RBC velocity increased less reliably in APOE4 animals, compared to APOE3, and the response magnitude was comparable across genotypes at both the pia and capillary bed. Could this mismatch be the first step in a chain of events that results in a suboptimal energy supply to APOE4 neurons, eventually resulting in hypoxia and AD pathology (see figure 6.1)?

It is probable that this imbalance is not resulting in harmful effects in the young APOE4 brain, considering the resting SO_2 and behavioural measurements were not

different between genotypes. Perhaps this is as a result of the "buffer" built into the functional hyperaemia response, described previously as "watering the entire garden for the sake of one thirsty flower" (Malonek and Grinvald, 1996). Interesting to note is previous work from our group, comparing neurovascular function in the visual cortex and the hippocampus which shows that the hippocampus has less of a buffer (Shaw et al., 2019), and so might explain its vulnerability to hypoxia (Michaelis, 2012) and in Alzheimer's Disease. An interesting research avenue would be an investigation into neurovascular coupling in the CA1 region of APOE4 mice to determine if the changes observed in the cortex are present in the hippocampus, and if there are any harmful implications as a result.

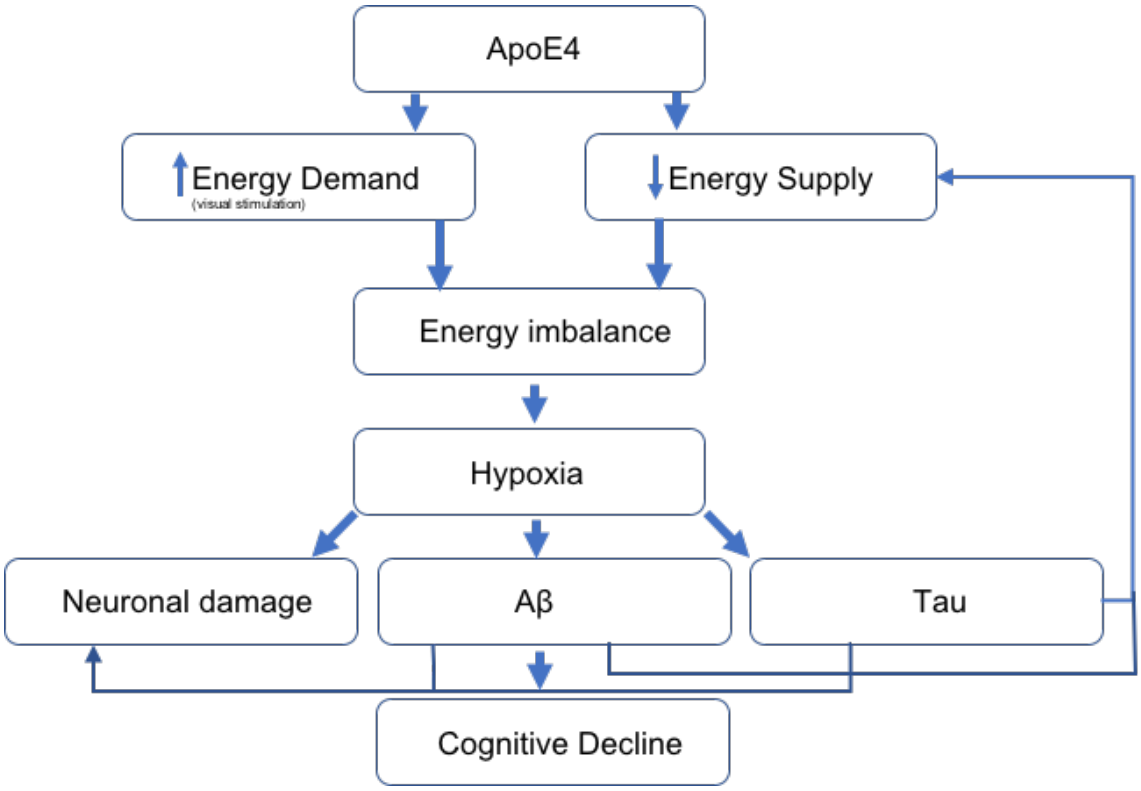

Figure 6.1: **Energy mismatch hypothesis of Alzheimer's Disease**. APOE4 carriers have an increased energy demand during stimulation, whilst having a less reliable blood supply. This could result in an energy imbalance which, over time could result in a chronic hypoxia in the brain. Hypoxia has been shown to play a role in neuronal damage as well as the facilitation of Aβ and tau accumulation. Aβ and tau can further diminish the ability of the brain to supply energy in response to synaptic activity, as well as contribute to neuronal death. Overtime this cycle could lead to the cognitive decline observed in Alzheimer's Disease

Although this study presents convincing evidence for a subtle yet robust alteration to neurovascular function in APOE4 animals, focusing on the largely preserved vascular function across different age points, offers an interesting perspective. As discussed, we found many vascular parameters unchanged in APOE4 animals, including neurovascular coupling response sizes, pericyte number, pial diameters, red blood cell velocity, net resting blood flow and net resting levels of SO_2. As some of these findings are contrary to previous work (Bell et al., 2012; Koizumi et al., 2018), it emphasises the inconsistencies that can arise between research groups, possibly as a result of differences in experimental preparation, therefore highlighting the importance of detailed methods information when reporting experimental outcomes.

These data, showing preserved function across many parameters, are testament to APOE4 being a risk factor for AD, rather than a causative factor. My data suggests that in the absence of additional factors, the effect of ApoE4 on the vasculature is present but mild, and perhaps relies on the compounding effects of these additional factors to elicit the more severe vascular impairment often seen in APOE4 carriers (Zlokovic, 2013). Perhaps the strictly controlled environment used in animal studies enhances this effect as human subjects are exposed to a more heterogeneous combination of pathological events that could potentially exacerbate vascular effects of ApoE4. Such factors could be any or several of: increased age, inflammation, traumatic injury, cardiovascular risk factors or the presence of Aβ and tau. Indeed, research from other groups shows there to be enhanced pathophysiology at the intersection between ApoE4 and features such as age (Bell et al., 2012), hypertension (Bender and Raz, 2012), traumatic head injury (Mayeux et al., 1995) and hyperphosphorylated tau (Shi et al., 2017), to name but a few. Interestingly, Montagne et al. (2020), showed BBB leakage in APOE4 carriers to be independent of vascular risk factors and the accumulation of Aβ and tau. This suggests that, alongside the findings in this study, loss of BBB integrity may be a key characteristic of ApoE4 pathophysiology that does not rely on the compounding effect of the aforementioned risks or pathologies.

My data show that vasomotion, neuronal responses to stimulation and RBCV heterogeneity are different in APOE4 carriers and this is stable across the section of the lifespan investigated in this study (in the absence of interacting factors). This is interesting both because it suggests additional factors/events are needed to push the functioning system into a pathological state and because these differences may well be one of the reasons why APOE4 carriers are more severely affected by such events. Therefore, studying how

vasomotion, neuronal responses to stimulation and RBCV heterogeneity are differentially affected by factors or events such as traumatic injury, inflammation, even older age or Aβ accumulation, will be informative about whether these long-standing differences do indeed mediate some of the increased risk of disease in APOE4 carriers.

This work has raised many important questions that should be answered in future studies, as discussed in each experimental chapter. In addition to the aforementioned experiments determining the effects of ApoE4 in combination with other, potentially exacerbating factors, these could include experiments to study the downstream effects of the proposed energy mismatch, such as tissue oxygenation, or of reduced vasomotion, such as clearance. Another interesting avenue would be to investigate the mechanism(s) underlying the effects observed in APOE4 mice and thus aid in the identification of a therapeutic target aiming reduce these observed functional differences.

In conclusion, it is hoped that this thesis can provide some valuable information to the field and will continue to be built upon in future studies. The more we further our understanding of the role of ApoE4 in the Alzheimer's disease process, particularly in the pre-clinical phase, the closer we come to identifying therapeutic targets and developing interventions that could benefit some of the many people currently living with Alzheimer's disease.

Chapter 7

References

Aguilera, K. and Brekken, R. (2014). Hypoxia Studies with Pimonidazole in vivo. *BIO-PROTOCOL*, 4(19).

Akerboom, J., Chen, T. W., Wardill, T. J., Tian, L., Marvin, J. S., Mutlu, S., Calderón, N. C., Esposti, F., Borghuis, B. G., Sun, X. R., Gordus, A., Orger, M. B., Portugues, R., Engert, F., Macklin, J. J., Filosa, A., Aggarwal, A., Kerr, R. A., Takagi, R., Kracun, S., Shigetomi, E., Khakh, B. S., Baier, H., Lagnado, L., Wang, S. S., Bargmann, C. I., Kimmel, B. E., Jayaraman, V., Svoboda, K., Kim, D. S., Schreiter, E. R., and Looger, L. L. (2012). Optimization of a GCaMP calcium indicator for neural activity imaging. *Journal of Neuroscience*, 32(40):13819–13840.

Alonzo, N. C., Hyman, B. T., Rebeck, G. W., and Greenberg, S. M. (1998). Progression of Cerebral Amyloid Angiopathy: Accumulation of Amyloid-ß40 in Affected Vessels. *Journal of Neuropathology and Experimental Neurology*, 57(4):353–359.

Andrews-Zwilling, Y., Bien-Ly, N., Xu, Q., Li, G., Bernardo, A., Yoon, S. Y., Zwilling, D., Yan, T. X., Chen, L., and Huang, Y. (2010). Apolipoprotein E4 causes age- and Tau-dependent impairment of GABAergic interneurons, leading to learning and memory deficits in mice. *The Journal of neuroscience : the official journal of the Society for Neuroscience*, 30(41):13707–17.

Arbel-Ornath, M., Hudry, E., Eikermann-Haerter, K., Hou, S., Gregory, J. L., Zhao, L., Betensky, R. A., Frosch, M. P., Greenberg, S. M., and Bacskai, B. J. (2013). Interstitial fluid drainage is impaired in ischemic stroke and Alzheimer's disease mouse models. *Acta Neuropathologica*, 126(3):353–364.

Arendt, T., Schindler, C., Brückner, M. K., Eschrich, K., Bigl, V., Zedlick, D., and

Marcova, L. (1997). Plastic neuronal remodeling is impaired in patients with Alzheimer's disease carrying apolipoprotein epsilon 4 allele. *The Journal of neuroscience : the official journal of the Society for Neuroscience*, 17(2):516–29.

ARUK (2019). Dementia Statistics Hub — Alzheimer's Research UK.

Attwell, D., Buchan, A. M., Charpak, S., Lauritzen, M., Macvicar, B. A., and Newman, E. A. (2010). Glial and neuronal control of brain blood flow. *Nature*, 468(7321):232–43.

Attwell, D. and Laughlin, S. B. (2001). An Energy Budget for Signaling in the Grey Matter of the Brain. *Journal of Cerebral Blood Flow & Metabolism*, pages 1133–1145.

Attwell, D., Mishra, A., Hall, C. N., O'Farrell, F. M., and Dalkara, T. (2016). What is a pericyte? *Journal of Cerebral Blood Flow & Metabolism*, 36(2):451–455.

Auer, L. M. and Gallhofer, B. (1981). Rhythmic Activity of Cat Pial Vessels in vivo. *European Neurology*, 20(6):448–468.

Bacyinski, A., Xu, M., Wang, W., and Hu, J. (2017). The Paravascular Pathway for Brain Waste Clearance: Current Understanding, Significance and Controversy. *Frontiers in Neuroanatomy*, 11:101.

Bell, M. A. and Ball, M. J. (1981). Morphometric comparison of hippocampal microvasculature in ageing and demented people: Diameters and densities. *Acta Neuropathologica*, 53(4):299–318.

Bell, R. D., Sagare, A. P., Friedman, A. E., Bedi, G. S., Holtzman, D. M., Deane, R., and Zlokovic, B. V. (2007). Transport pathways for clearance of human Alzheimer's amyloid β-peptide and apolipoproteins E and J in the mouse central nervous system. *Journal of Cerebral Blood Flow and Metabolism*, 27(5):909–918.

Bell, R. D., Winkler, E. A., Singh, I., Sagare, A. P., Deane, R., Wu, Z., Holtzman, D. M., Betsholtz, C., Armulik, A., Sallstrom, J., Berk, B. C., and Zlokovic, B. V. (2012). Apolipoprotein E controls cerebrovascular integrity via cyclophilin A. *Nature*, 485(7399):512–6.

Belloy, M. E., Napolioni, V., and Greicius, M. D. (2019). A Quarter Century of APOE and Alzheimer's Disease: Progress to Date and the Path Forward. *Neuron*.

Bender, A. R. and Raz, N. (2012). Age-related differences in memory and executive functions in healthy APOE e{open}4 carriers: The contribution of individual differences in prefrontal volumes and systolic blood pressure. *Neuropsychologia*, 50(5):704–714.

Bennett, R. E., Robbins, A. B., Hu, M., Cao, X., Betensky, R. A., Clark, T., Das, S., and Hyman, B. T. (2018). Tau induces blood vessel abnormalities and angiogenesis-related gene expression in P301L transgenic mice and human Alzheimer's disease. *Proceedings of the National Academy of Sciences of the United States of America*, 115(6):E1289–E1298.

Blair, L. J., Frauen, H. D., Zhang, B., Nordhues, B. A., Bijan, S., Lin, Y. C., Zamudio, F., Hernandez, L. D., Sabbagh, J. J., Selenica, M. L. B., and Dickey, C. A. (2015). Tau depletion prevents progressive blood-brain barrier damage in a mouse model of tauopathy. *Acta neuropathologica communications*, 3:8.

Bonnar, O. and Hall, C. N. (2020). First, tau causes NO problem. *Nature Neuroscience*.

Brecht, W. J., Harris, F. M., Chang, S., Tesseur, I., Yu, G. Q., Xu, Q., Fish, J. D., Wyss-Coray, T., Buttini, M., Mucke, L., Mahley, R. W., and Huang, Y. (2004). Neuron-Specific Apolipoprotein E4 Proteolysis Is Associated with Increased Tau Phosphorylation in Brains of Transgenic Mice. *Journal of Neuroscience*, 24(10):2527–2534.

Brown, W. R. (2010). A review of string vessels or collapsed, empty basement membrane tubes. *Journal of Alzheimer's Disease*, 21(3):725–739.

Brown, W. R. and Thore, C. R. (2011). Review: Cerebral microvascular pathology in ageing and neurodegeneration. *Neuropathology and Applied Neurobiology*, 37(1):56–74.

Bu, G. (2006). Apolipoprotein E and its receptors in Alzheimer's disease: pathways, pathogenesis and therapy. *Proceedings of the National Academy of Sciences of the United States of America*, 103(49):18727–32.

Busche, M. A., Wegmann, S., Dujardin, S., Commins, C., Schiantarelli, J., Klickstein, N., Kamath, T. V., Carlson, G. A., Nelken, I., and Hyman, B. T. (2019). Tau impairs neural circuits, dominating amyloid-β effects, in Alzheimer models in vivo. *Nature Neuroscience*, 22(1):57–64.

Busija, D. W., Bari, F., Domoki, F., and Louis, T. (2007). Mechanisms involved in the cerebrovascular dilator effects of N-methyl-d-aspartate in cerebral cortex. *Brain Research Reviews*, 56(1):89–100.

Cai, C., Fordsmann, J. C., Jensen, S. H., Gesslein, B., Lønstrup, M., Hald, B. O., Zambach, S. A., Brodin, B., and Lauritzen, M. J. (2018). Stimulation-induced increases in cerebral blood flow and local capillary vasoconstriction depend on conducted vascular

responses. *Proceedings of the National Academy of Sciences of the United States of America*, 115(25):E5796–E5804.

Cai, Z., Liu, N., Wang, C., Qin, B., Zhou, Y., Xiao, M., Chang, L., Yan, L.-J., and Zhao, B. (2016). Role of RAGE in Alzheimer's Disease. *Cellular and Molecular Neurobiology*, 36(4):483–495.

Calafate, S., Buist, A., Miskiewicz, K., Vijayan, V., Daneels, G., de Strooper, B., de Wit, J., Verstreken, P., and Moechars, D. (2015). Synaptic Contacts Enhance Cell-to-Cell Tau Pathology Propagation. *Cell Reports*, 11(8):1176–1183.

Carare, R. O., Aldea, R., Agarwal, N., Bacskai, B. J., Bechman, I., Boche, D., Bu, G., Bulters, D., Clemens, A., Counts, S. E., Leon, M., Eide, P. K., Fossati, S., Greenberg, S. M., Hamel, E., Hawkes, C. A., Koronyo-Hamaoui, M., Hainsworth, A. H., Holtzman, D., Ihara, M., Jefferson, A., Kalaria, R. N., Kipps, C. M., Kanninen, K. M., Leinonen, V., McLaurin, J., Miners, S., Malm, T., Nicoll, J. A. R., Piazza, F., Paul, G., Rich, S. M., Saito, S., Shih, A., Scholtzova, H., Snyder, H., Snyder, P., Thormodsson, F. R., Veluw, S. J., Weller, R. O., Werring, D. J., Wilcock, D., Wilson, M. R., Zlokovic, B. V., and Verma, A. (2020). Clearance of interstitial fluid (ISF) and CSF (CLIC) group—part of Vascular Professional Interest Area (PIA). *Alzheimer's & Dementia: Diagnosis, Assessment & Disease Monitoring*, 12(1).

Caselli, R. J., Dueck, A. C., Locke, D. E., Sabbagh, M. N., Ahern, G. L., Rapcsak, S. Z., Baxter, L. C., Yaari, R., Woodruff, B. K., Hoffman-Snyder, C., Rademakers, R., Findley, S., and Reiman, E. M. (2011). Cerebrovascular risk factors and preclinical memory decline in healthy APOE ϵ4 homozygotes. *Neurology*, 76(12):1078–1084.

Caselli, R. J., Dueck, A. C., Osborne, D., Sabbagh, M. N., Connor, D. J., Ahern, G. L., Baxter, L. C., Rapcsak, S. Z., Shi, J., Woodruff, B. K., Locke, D. E., Snyder, C. H., Alexander, G. E., Rademakers, R., and Reiman, E. M. (2009). Longitudinal modeling of age-related memory decline and the APOE ϵ4 effect. *New England Journal of Medicine*, 361(3):255–263.

Casey, C. S., Atagi, Y., Yamazaki, Y., Shinohara, M., Tachibana, M., Fu, Y., Bu, G., and Kanekiyo, T. (2015). Apolipoprotein E inhibits cerebrovascular pericyte mobility through a RhoA protein-mediated pathway. *Journal of Biological Chemistry*, 290(22):14208–14217.

Castano, E. M., Prelli, F., Wisniewski, T., Golabek, A., Kumar, R. A., Soto, C., and Frangione, B. (1995). Fibrillogenesis in alzheimer's disease of amyloid β peptides and apolipoprotein E. *Biochemical Journal*, 306(2):599–604.

Castellano, J. M., Kim, J., Stewart, F. R., Jiang, H., DeMattos, R. B., Patterson, B. W., Fagan, A. M., Morris, J. C., Mawuenyega, K. G., Cruchaga, C., Goate, A. M., Bales, K. R., Paul, S. M., Bateman, R. J., and Holtzman, D. M. (2011). Human apoE isoforms differentially regulate brain amyloid-β peptide clearance. *Science translational medicine*, 3(89):89ra57.

Castillo-Carranza, D. L., Nilson, A. N., Van Skike, C. E., Jahrling, J. B., Patel, K., Garach, P., Gerson, J. E., Sengupta, U., Abisambra, J., Nelson, P., Troncoso, J., Ungvari, Z., Galvan, V., and Kayed, R. (2017). Cerebral microvascular accumulation of tau oligomers in Alzheimer's disease and related tauopathies. *Aging and Disease*, 8(3):257–266.

Cauli, B. and Hamel, E. (2010). Revisiting the role of neurons in neurovascular coupling. *Frontiers in neuroenergetics*, 2:9.

Cauli, B., Tong, X. K., Rancillac, A., Serluca, N., Lambolez, B., Rossier, J., and Hamel, E. (2004). Cortical GABA interneurons in neurovascular coupling: Relays for subcortical vasoactive pathways. *Journal of Neuroscience*, 24(41):8940–8949.

Chen, B. R., Kozberg, M. G., Bouchard, M. B., Shaik, M. A., and Hillman, E. M. C. (2014). A critical role for the vascular endothelium in functional neurovascular coupling in the brain. *Journal of the American Heart Association*, 3(3):e000787.

Chen, G. J., Xu, J., Lahousse, S. A., Caggiano, N. L., and De la Monte, S. M. (2003). Transient hypoxia causes Alzheimer-type molecular and biochemical abnormalities in cortical neurons: Potential strategies for neuroprotection. *Journal of Alzheimer's Disease*, 5(3):209–228.

Chen, Q., Cichon, J., Wang, W., Qiu, L., Lee, S. J. R., Campbell, N. R., DeStefino, N., Goard, M. J., Fu, Z., Yasuda, R., Looger, L. L., Arenkiel, B. R., Gan, W. B., and Feng, G. (2012). Imaging Neural Activity Using Thy1-GCaMP Transgenic Mice. *Neuron*, 76(2):297–308.

Chow, B. W., Nuñez, V., Kaplan, L., Granger, A. J., Bistrong, K., Zucker, H. L., Kumar, P., Sabatini, B. L., and Gu, C. (2020). Caveolae in CNS arterioles mediate neurovascular coupling. *Nature*, 579(7797):106–110.

Clark, R. E., Zola, S. M., and Squire, L. R. (2000). Impaired recognition memory rats after damage to the hippocampus. *Journal of Neuroscience*, 20(23):8853–8860.

Coman, H. and Nemeş, B. (2017). New Therapeutic Targets in Alzheimer's Disease.

Cook, D. G., Leverenz, J. B., McMillan, P. J., Kulstad, J. J., Ericksen, S., Roth, R. A., Schellenberg, G. D., Jin, L. W., Kovacina, K. S., and Craft, S. (2003). Reduced hippocampal insulin-degrading enzyme in late-onset Alzheimer's disease is associated with the apolipoprotein E-ϵ4 allele. *American Journal of Pathology*, 162(1):313–319.

Corder, E. H., Saunders, a. M., Strittmatter, W. J., Schmechel, D. E., Gaskell, P. C., Small, G. W., Roses, a. D., Haines, J. L., and Pericak-Vance, M. a. (1993). Gene dose of apolipoprotein E type 4 allele and the risk of Alzheimer's disease in late onset families. *Science (New York, N.Y.)*, 261(5123):921–923.

Crous-Bou, M., Minguillón, C., Gramunt, N., and Molinuevo, J. L. (2017). Alzheimer's disease prevention: From risk factors to early intervention. *Alzheimer's Research and Therapy*, 9(1).

Cruchaga, C., Kauwe, J. S., Nowotny, P., Bales, K., Pickering, E. H., Mayo, K., Bertelsen, S., Hinrichs, A., Fagan, A. M., Holtzman, D. M., Morris, J. C., and Goate, A. M. (2012). Cerebrospinal fluid APOE levels: An endophenotype for genetic studies for Alzheimer's disease. *Human Molecular Genetics*, 21(20):4558–4571.

Cruz Hernández, J. C., Bracko, O., Kersbergen, C. J., Muse, V., Haft-Javaherian, M., Berg, M., Park, L., Vinarcsik, L. K., Ivasyk, I., Rivera, D. A., Kang, Y., Cortes-Canteli, M., Peyrounette, M., Doyeux, V., Smith, A., Zhou, J., Otte, G., Beverly, J. D., Davenport, E., Davit, Y., Lin, C. P., Strickland, S., Iadecola, C., Lorthois, S., Nishimura, N., and Schaffer, C. B. (2019). Neutrophil adhesion in brain capillaries reduces cortical blood flow and impairs memory function in Alzheimer's disease mouse models. *Nature Neuroscience*, page 1.

Dana, H., Chen, T.-W., Hu, A., Shields, B. C., Guo, C., Looger, L. L., Kim, D. S., and Svoboda, K. (2014). Thy1-GCaMP6 Transgenic Mice for Neuronal Population Imaging In Vivo. *PLoS hONE*, 9(9):e108697.

Davies, G., Harris, S. E., Reynolds, C. A., Payton, A., Knight, H. M., Liewald, D. C., Lopez, L. M., Luciano, M., Gow, A. J., Corley, J., Henderson, R., Murray, C., Pattie, A., Fox, H. C., Redmond, P., Lutz, M. W., Chiba-Falek, O., Linnertz, C., Saith, S.,

Haggarty, P., McNeill, G., Ke, X., Ollier, W., Horan, M., Roses, A. D., Ponting, C. P., Porteous, D. J., Tenesa, A., Pickles, A., Starr, J. M., Whalley, L. J., Pedersen, N. L., Pendleton, N., Visscher, P. M., and Deary, I. J. (2014). A genome-wide association study implicates the APOE locus in nonpathological cognitive ageing. *Molecular Psychiatry*, 19(1):76–87.

Deane, R., Sagare, A., Hamm, K., Parisi, M., Lane, S., Finn, M. B., Holtzman, D. M., and Zlokovic, B. V. (2008). apoE isoform-specific disruption of amyloid beta peptide clearance from mouse brain. *The Journal of clinical investigation*, 118(12):4002–13.

Deane, R., Wu, Z., Sagare, A., Davis, J., Du Yan, S., Hamm, K., Xu, F., Parisi, M., LaRue, B., Hu, H. W., Spijkers, P., Guo, H., Song, X., Lenting, P. J., Van Nostrand, W. E., and Zlokovic, B. V. (2004). LRP/amyloid β-peptide interaction mediates differential brain efflux of Aβ isoforms. *Neuron*, 43(3):333–344.

De Strooper, B. and Karran, E. (2016). The Cellular Phase of Alzheimer's Disease. *Cell*, 164(4):603–615.

Di Marco, L. Y., Farkas, E., Martin, C., Venneri, A., and Frangi, A. F. (2015). Is Vasomotion in Cerebral Arteries Impaired in Alzheimer's Disease? *Journal of Alzheimer's disease : JAD*, 46(1):35–53.

Diaz-Arrastia, R., Gong, Y., Fair, S., Scott, K. D., Garcia, M. C., Carlile, M. C., Agostini, M. A., and Van Ness, P. C. (2003). Increased risk of late posttraumatic seizures associated with inheritance of APOE ϵ4 allele. *Archives of Neurology*, 60(6):818–822.

Dickerson, B. C., Salat, D. H., Greve, D. N., Chua, E. F., Rand-Giovannetti, E., Rentz, D. M., Bertram, L., Mullin, K., Tanzi, R. E., Blacker, D., Albert, M. S., and Sperling, R. A. (2005). Increased hippocampal activation in mild cognitive impairment compared to normal aging and AD. *Neurology*, 65(3):404–11.

Dikalov, S., Griendling, K. K., and Harrison, D. G. (2007). Measurement of reactive oxygen species in cardiovascular studies. *Hypertension*, 49(4):717–727.

Dirnagl, U., Lindauer, U., and Villringer, A. (1993). Nitric oxide synthase blockade enhances vasomotion in the cerebral microcirculation of anesthetized rats. *Microvascular Research*, 45(3):318–323.

Dix, S. L. and Aggleton, J. P. (1999). Extending the spontaneous preference test of

recognition: Evidence of object-location and object-context recognition. *Behavioural Brain Research*, 99(2):191–200.

Dixit, R., Ross, J. L., Goldman, Y. E., and Holzbaur, E. L. (2008). Differential regulation of dynein and kinesin motor proteins by tau. *Science*, 319(5866):1086–1089.

Donahue, J. E., Flaherty, S. L., Johanson, C. E., Duncan, J. A., Silverberg, G. D., Miller, M. C., Tavares, R., Yang, W., Wu, Q., Sabo, E., Hovanesian, V., and Stopa, E. G. (2006). RAGE, LRP-1, and amyloid-beta protein in Alzheimer's disease. *Acta Neuropathologica*, 112(4):405–415.

Drew, P. J., Blinder, P., Cauwenberghs, G., Shih, A. Y., and Kleinfeld, D. (2010a). Rapid determination of particle velocity from space-time images using the Radon transform. *Journal of computational neuroscience*, 29(1-2):5–11.

Drew, P. J., Shih, A. Y., Driscoll, J. D., Knutsen, P. M., Blinder, P., Davalos, D., Akassoglou, K., Tsai, P. S., and Kleinfeld, D. (2010b). Chronic optical access through a polished and reinforced thinned skull. *Nature Methods*, 7(12):981–984.

Du, J., Chang, J., Guo, S., Zhang, Q., and Wang, Z. (2009). ApoE 4 reduces the expression of Aβ degrading enzyme IDE by activating the NMDA receptor in hippocampal neurons. *Neuroscience Letters*, 464(2):140–145.

Dumanis, S. B., Tesoriero, J. A., Babus, L. W., Nguyen, M. T., Trotter, J. H., Ladu, M. J., Weeber, E. J., Turner, R. S., Xu, B., Rebeck, G. W., and Hoe, H. S. (2009). ApoE4 decreases spine density and dendritic complexity in cortical neurons in vivo. *Journal of Neuroscience*, 29(48):15317–15322.

Esch, F. S., Keim, P. S., Beattie, E. C., Blacher, R. W., Culwell, A. R., Oltersdorf, T., McClure, D., and Ward, P. J. (1990). Cleavage of amyloid β peptide during constitutive processing of its precursor. *Science*, 248(4959):1122–1124.

Fan, Y. Y., Cai, Q. L., Gao, Z. Y., Lin, X., Huang, Q., Tang, W., and Liu, J. H. (2017). APOE ϵ4 allele elevates the expressions of inflammatory factors and promotes Alzheimer's disease progression: A comparative study based on Han and She populations in the Wenzhou area. *Brain Research Bulletin*, 132:39–43.

Fang, H., Zhang, L. F., Meng, F. T., Du, X., and Zhou, J. N. (2010). Acute hypoxia promote the phosphorylation of tau via ERK pathway. *Neuroscience Letters*, 474(3):173–177.

Farkas, E., de Vos, R. A., Donka, G., Jansen Steur, E. N., Mihály, A., and Luiten, P. G. (2006). Age-related microvascular degeneration in the human cerebral periventricular white matter. *Acta Neuropathologica*, 111(2):150–157.

Farkas, E. and Luiten, P. G. (2001). Cerebral microvascular pathology in aging and Alzheimer's disease. *Progress in Neurobiology*, 64(6):575–611.

Farrer, L. A. (1997). Effects of Age, Sex, and Ethnicity on the Association Between Apolipoprotein E Genotype and Alzheimer Disease. *JAMA*, 278(16):1349.

Fergus, A. and Lee, K. S. (1997). Regulation of cerebral microvessels by glutamatergic mechanisms. *Brain Research*, 754(1-2):35–45.

Fernández-Klett, F., Offenhauser, N., Dirnagl, U., Priller, J., and Lindauer, U. (2010). Pericytes in capillaries are contractile in vivo, but arterioles mediate functional hyperemia in the mouse brain. *Proceedings of the National Academy of Sciences of the United States of America*, 107(51):22290–5.

Filippini, N., MacIntosh, B. J., Hough, M. G., Goodwin, G. M., Frisoni, G. B., Smith, S. M., Matthews, P. M., Beckmann, C. F., and Mackay, C. E. (2009). Distinct patterns of brain activity in young carriers of the APOE-ϵ4 allele. *Proceedings of the National Academy of Sciences of the United States of America*, 106(17):7209–7214.

Filosa, J. A., Bonev, A. D., Straub, S. V., Meredith, A. L., Wilkerson, M. K., Aldrich, R. W., and Nelson, M. T. (2006). Local potassium signaling couples neuronal activity to vasodilation in the brain. *Nature Neuroscience*, 9(11):1397–1403.

Garcia-Alloza, M., Gregory, J., Kuchibhotla, K. V., Fine, S., Wei, Y., Ayata, C., Frosch, M. P., Greenberg, S. M., and Bacskai, B. J. (2011). Cerebrovascular lesions induce transient β-amyloid deposition. In *Brain*, volume 134, pages 3694–3704. Oxford University Press.

Garthwaite, J. (2018). Nitric oxide as a multimodal brain transmitter. *Brain and Neuroscience Advances*, 2:239821281881068.

Gerhard, A., Neumaier, B., Elitok, E., Glatting, G., Ries, V., Tomczak, R., Ludolph, A. C., and Reske, S. N. (2000). In vivo imaging of activated microglia using [11C]PK11195 and positron emission tomography in patients after ischemic stroke. *NeuroReport*, 11(13):2957–2960.

Girouard, H., Park, L., Anrather, J., Zhou, P., and Iadecola, C. (2007). Cerebrovascular nitrosative stress mediates neurovascular and endothelial dysfunction induced by angiotensin II. *Arteriosclerosis, Thrombosis, and Vascular Biology*, 27(2):303–309.

Goedert, M., Eisenberg, D. S., and Crowther, R. A. (2017). Propagation of Tau Aggregates and Neurodegeneration. *Annual Review of Neuroscience*, 40(1):189–210.

Gokina, N. I., Bevan, R. D., Walters, C. L., and Bevan, J. A. (1996). Electrical Activity Underlying Rhythmic Contraction in Human Pial Arteries. *Circulation Research*, 78(1):148–153.

Gordon, G. R., Choi, H. B., Rungta, R. L., Ellis-Davies, G. C., and MacVicar, B. A. (2008). Brain metabolism dictates the polarity of astrocyte control over arterioles. *Nature*, 456(7223):745–750.

Gould, I. G., Tsai, P., Kleinfeld, D., and Linninger, A. (2017). The capillary bed offers the largest hemodynamic resistance to the cortical blood supply. *Journal of Cerebral Blood Flow and Metabolism*, 37(1):52–68.

Govindpani, K., McNamara, L. G., Smith, N. R., Vinnakota, C., Waldvogel, H. J., Faull, R. L., and Kwakowsky, A. (2019). Vascular Dysfunction in Alzheimer's Disease: A Prelude to the Pathological Process or a Consequence of It? *Journal of Clinical Medicine*, 8(5):651.

Grant, R. I., Hartmann, D. A., Underly, R. G., Berthiaume, A.-A., Bhat, N. R., and Shih, A. Y. (2019). Organizational hierarchy and structural diversity of microvascular pericytes in adult mouse cortex. *Journal of cerebral blood flow and metabolism : official journal of the International Society of Cerebral Blood Flow and Metabolism*, 39(3):411–425.

Gustafsson, H., Bulow, A., and Nilsson, H. (1994). Rhythmic contractions of isolated, pressurized small arteries from rat. *Acta Physiologica Scandinavica*, 152(2):145–152.

Haass, C. (2004). Take five BACE and the γ-secretase quartet conduct Alzheimer's amyloid β-peptide generation. *The EMBO Journal*, 23(3):483–488.

Haass, C., Kaether, C., Thinakaran, G., and Sisodia, S. (2012). Trafficking and proteolytic processing of APP. *Cold Spring Harbor perspectives in medicine*, 2(5):a006270.

Hagan, C. (2017). When Are Mice Considered Old?

Hall, C. N., Reynell, C., Gesslein, B., Hamilton, N. B., Mishra, A., Sutherland, B. A., O'Farrell, F. M., Buchan, A. M., Lauritzen, M., and Attwell, D. (2014). Capillary pericytes regulate cerebral blood flow in health and disease. *Nature*, 508(7494):55–60.

Halliday, M. R., Rege, S. V., Ma, Q., Zhao, Z., Miller, C. A., Winkler, E. A., and Zlokovic, B. V. (2016). Accelerated pericyte degeneration and blood–brain barrier breakdown in apolipoprotein E4 carriers with Alzheimer's disease. *Journal of Cerebral Blood Flow & Metabolism*, 36(1):216–227.

Hamel, E. (2006). Perivascular nerves and the regulation of cerebrovascular tone. *Journal of Applied Physiology*, 100(3):1059–1064.

Han, S. D. and Bondi, M. W. (2008). Revision of the apolipoprotein E compensatory mechanism recruitment hypothesis. *Alzheimer's & Dementia*, 4(4):251–254.

Hardy, J. and Higgins, G. (1992). Alzheimer' s Disease : The Amyloid Cascade Hypothesis. *Science*, 256(5054):184–185.

Hartmann, D. A., Berthiaume, A.-A., Grant, R. I., Harrill, S. A., Noonan, T., Costello, J., Tieu, T., McDowell, K., Faino, A., Kelly, A., and Shih, A. Y. (2020). Brain capillary pericytes exert a substantial but slow influence on blood flow. *bioRxiv*, page 2020.03.26.008763.

Hauser, P. S., Narayanaswami, V., and Ryan, R. O. (2011). Apolipoprotein E: From lipid transport to neurobiology. *Progress in Lipid Research*, 50(1):62–74.

Hawkes, C. A., Sullivan, P. M., Hands, S., Weller, R. O., Nicoll, J. A., and Carare, R. O. (2012). Disruption of arterial perivascular drainage of amyloid-β from the brains of mice expressing the human APOE ϵ4 allele. *PLoS ONE*, 7(7).

Hill, R. A., Tong, L., Yuan, P., Murikinati, S., Gupta, S., and Grutzendler, J. (2015). Regional Blood Flow in the Normal and Ischemic Brain Is Controlled by Arteriolar Smooth Muscle Cell Contractility and Not by Capillary Pericytes. *Neuron*, 87(1):95–110.

Howarth, C., Gleeson, P., and Attwell, D. (2012). Updated energy budgets for neural computation in the neocortex and cerebellum. *Journal of cerebral blood flow and metabolism : official journal of the International Society of Cerebral Blood Flow and Metabolism*, 32(7):1222–32.

Huang, Y., Liu, X. Q., Wyss-Coray, T., Brecht, W. J., Sanan, D. A., and Mahley, R. W. (2001). Apolipoprotein E fragments present in Alzheimer's disease brains induce neurofibrillary tangle-like intracellular inclusions in neurons. *Proceedings of the National Academy of Sciences of the United States of America*, 98(15):8838–8843.

Hultman, K., Strickland, S., and Norris, E. H. (2013). The APOE $\epsilon 4/\epsilon 4$ genotype potentiates vascular fibrin(ogen) deposition in amyloid-laden vessels in the brains of Alzheimer's disease patients. *Journal of Cerebral Blood Flow and Metabolism*, 33(8):1251–1258.

Hunter, J. M., Cirrito, J. R., Restivo, J. L., Kinley, R. D., Sullivan, P. M., Holtzman, D. M., Koger, D., Delong, C., Lin, S., Zhao, L., Liu, F., Bales, K., and Paul, S. M. (2012). Emergence of a seizure phenotype in aged apolipoprotein epsilon 4 targeted replacement mice. *Brain Research*, 1467:120–132.

Iadecola, C. (2017). The Neurovascular Unit Coming of Age: A Journey through Neurovascular Coupling in Health and Disease. *Neuron*, 96(1):17–42.

Iadecola, C., Park, L., and Capone, C. (2009). Threats to the mind: Aging, amyloid, and hypertension. *Stroke*, 40(3 SUPPL. 1):S40.

Iadecola, C., Yang, G., Ebner, T. J., and Chen, G. (1997). Local and Propagated Vascular Responses Evoked by Focal Synaptic Activity in Cerebellar Cortex. *Journal of Neurophysiology*, 78(2):651–659.

Iadecola, C., Zhang, F., Niwa, K., Eckman, C., Turner, S. K., Fischer, E., Younkin, S., Borchelt, D. R., Hsiao, K. K., and Carlson, G. A. (1999). SOD1 rescues cerebral endothelial dysfunction in mice overexpressing amyloid precursor protein. *Nature Neuroscience*, 2(2):157–161.

Iliff, J. J., Wang, M., Liao, Y., Plogg, B. A., Peng, W., Gundersen, G. A., Benveniste, H., Vates, G. E., Deane, R., Goldman, S. A., Nagelhus, E. A., and Nedergaard, M. (2012). A paravascular pathway facilitates CSF flow through the brain parenchyma and the clearance of interstitial solutes, including amyloid β. *Science Translational Medicine*, 4(147).

Iliff, J. J., Wang, M., Zeppenfeld, D. M., Venkataraman, A., Plog, B. A., Liao, Y., Deane, R., and Nedergaard, M. (2013). Cerebral arterial pulsation drives paravascular CSF-Interstitial fluid exchange in the murine brain. *Journal of Neuroscience*, 33(46):18190–18199.

Iturria-Medina, Y., Sotero, R. C., Toussaint, P. J., Mateos-Pérez, J. M., Evans, A. C., and Alzheimer's Disease Neuroimaging Initiative, T. A. D. N. (2016). Early role of vascular dysregulation on late-onset Alzheimer's disease based on multifactorial data-driven analysis. *Nature communications*, 7:11934.

Ji, Y., Gong, Y., Gan, W., Beach, T., Holtzman, D. M., and Wisniewski, T. (2003). Apolipoprotein E isoform-specific regulation of dendritic spine morphology in apolipoprotein E transgenic mice and Alzheimer's disease patients. *Neuroscience*, 122(2):305–315.

Jiang, Q., Lee, C. Y., Mandrekar, S., Wilkinson, B., Cramer, P., Zelcer, N., Mann, K., Lamb, B., Willson, T. M., Collins, J. L., Richardson, J. C., Smith, J. D., Comery, T. A., Riddell, D., Holtzman, D. M., Tontonoz, P., and Landreth, G. E. (2008). ApoE Promotes the Proteolytic Degradation of Aβ. *Neuron*, 58(5):681–693.

Jin, J. Z., Weng, C., Yeh, C. I., Gordon, J. A., Ruthazer, E. S., Stryker, M. P., Swadlow, H. A., and Alonso, J. M. (2008). On and off domains of geniculate afferents in cat primary visual cortex. *Nature Neuroscience*, 11(1):88–94.

Johnson, E. L., Krauss, G. L., Lee, A. K., Schneider, A. L., Dearborn, J. L., Kucharska-Newton, A. M., Huang, J., Alonso, A., and Gottesman, R. F. (2018). Association between Midlife Risk Factors and Late-Onset Epilepsy: Results from the Atherosclerosis Risk in Communities Study. *JAMA Neurology*, 75(11):1375–1382.

Jones, M., Berwick, J., Hewson-Stoate, N., Gias, C., and Mayhew, J. (2005). The effect of hypercapnia on the neural and hemodynamic responses to somatosensory stimulation. *NeuroImage*, 27(3):609–623.

Kalaria, R. N. (2009). Linking cerebrovascular defense mechanisms in brain ageing and Alzheimer's disease. *Neurobiology of Aging*, 30(9):1512–1514.

Kanekiyo, T., Xu, H., and Bu, G. (2014). ApoE and Aβ in Alzheimer's disease: Accidental encounters or partners? *Neuron*, 81(4):740–754.

Karran, E., Mercken, M., and Strooper, B. D. (2011). The amyloid cascade hypothesis for Alzheimer's disease: An appraisal for the development of therapeutics. *Nature Reviews Drug Discovery*, 10(9):698–712.

Kisler, K., Nelson, A. R., Montagne, A., and Zlokovic, B. V. (2017a). Cerebral blood flow regulation and neurovascular dysfunction in Alzheimer disease. *Nature Publishing Group*, 18.

Kisler, K., Nelson, A. R., Rege, S. V., Ramanathan, A., Wang, Y., Ahuja, A., Lazic, D., Tsai, P. S., Zhao, Z., Zhou, Y., Boas, D. A., Sakadžić, S., and Zlokovic, B. V. (2017b). Pericyte degeneration leads to neurovascular uncoupling and limits oxygen supply to brain. *Nature Neuroscience*, 20(3):406–416.

Knoferle, J., Yoon, S. Y., Walker, D., Leung, L., Gillespie, A. K., Tong, L. M., Bien-Ly, N., and Huang, Y. (2014). Apolipoprotein E4 produced in GABAergic interneurons causes learning and memory deficits in mice. *The Journal of neuroscience : the official journal of the Society for Neuroscience*, 34(42):14069–78.

Knouff, C., Hinsdale, M. E., Mezdour, H., Altenburg, M. K., Watanabe, M., Quarfordt, S. H., Sullivan, P. M., and Maeda, N. (1999). Apo E structure determines VLDL clearance and atherosclerosis risk in mice. *Journal of Clinical Investigation*, 103(11):1579–1586.

Ko, K. R., Ngai, A. C., and Winn, H. R. (1990). Role of adenosine in regulation of regional cerebral blood flow in sensory cortex. *American Journal of Physiology - Heart and Circulatory Physiology*, 259(6 28-6).

Koffie, R. M., Hashimoto, T., Tai, H. C., Kay, K. R., Serrano-Pozo, A., Joyner, D., Hou, S., Kopeikina, K. J., Frosch, M. P., Lee, V. M., Holtzman, D. M., Hyman, B. T., and Spires-Jones, T. L. (2012). Apolipoprotein E4 effects in Alzheimer's disease are mediated by synaptotoxic oligomeric amyloid-β. *Brain*, 135(7):2155–2168.

Kohl-Bareis, M., Gürtler, R., Lindauer, U., Leithner, C., Sellien, H., Royl, G., and Dirnagl, U. (2005). System for the measurement of blood flow and oxygenation in tissue applied to neurovascular coupling in brain. *Optics InfoBase Conference Papers*.

Koizumi, K., Hattori, Y., Ahn, S. J., Buendia, I., Ciacciarelli, A., Uekawa, K., Wang, G., Hiller, A., Zhao, L., Voss, H. U., Paul, S. M., Schaffer, C., Park, L., and Iadecola, C. (2018). Apoϵ4 disrupts neurovascular regulation and undermines white matter integrity and cognitive function. *Nature Communications*, 9(1):3816.

Kok, E., Haikonen, S., Luoto, T., Huhtala, H., Goebeler, S., Haapasalo, H., and Karhunen, P. J. (2009). Apolipoprotein E-dependent accumulation of alzheimer disease-related lesions begins in middle age. *Annals of Neurology*, 65(6):650–657.

Lanctôt, K. L., Herrmann, N., Mazzotta, P., Khan, L. R., and Ingber, N. (2004). GABAergic function in Alzheimer's disease: evidence for dysfunction and potential as a thera-

peutic target for the treatment of behavioural and psychological symptoms of dementia. *Canadian journal of psychiatry. Revue canadienne de psychiatrie*, 49(7):439–53.

Lee, L., Boorman, L., Glendenning, E., Christmas, C., Sharp, P., Redgrave, P., Shabir, O., Bracci, E., Berwick, J., and Howarth, C. (2020). Key Aspects of Neurovascular Control Mediated by Specific Populations of Inhibitory Cortical Interneurons. *Cerebral Cortex*, 30(4):2452–2464.

Li, G., Bien-Ly, N., Andrews-Zwilling, Y., Xu, Q., Bernardo, A., Ring, K., Halabisky, B., Deng, C., Mahley, R. W., and Huang, Y. (2009). GABAergic Interneuron Dysfunction Impairs Hippocampal Neurogenesis in Adult Apolipoprotein E4 Knockin Mice. *Cell Stem Cell*, 5(6):634–645.

Liang, Z., Shen, W., Sun, C., and Shou, T. (2008). Comparative study on the offset responses of simple cells and complex cells in the primary visual cortex of the cat. *Neuroscience*, 156(2):365–373.

Lin, Y. T., Seo, J., Gao, F., Feldman, H. M., Wen, H. L., Penney, J., Cam, H. P., Gjoneska, E., Raja, W. K., Cheng, J., Rueda, R., Kritskiy, O., Abdurrob, F., Peng, Z., Milo, B., Yu, C. J., Elmsaouri, S., Dey, D., Ko, T., Yankner, B. A., and Tsai, L. H. (2018). APOE4 Causes Widespread Molecular and Cellular Alterations Associated with Alzheimer's Disease Phenotypes in Human iPSC-Derived Brain Cell Types. *Neuron*, 98(6):1141–1154.e7.

Lind, B. L., Brazhe, A. R., Jessen, S. B., Tan, F. C., and Lauritzen, M. J. (2013). Rapid stimulus-evoked astrocyte Ca2+ elevations and hemodynamic responses in mouse somatosensory cortex in vivo. *Proceedings of the National Academy of Sciences of the United States of America*, 110(48):E4678.

Lindauer, U., Leithner, C., Kaasch, H., Rohrer, B., Foddis, M., Füchtemeier, M., Offenhauser, N., Steinbrink, J., Royl, G., Kohl-Bareis, M., and Dirnagl, U. (2010). Neurovascular coupling in rat brain operates independent of hemoglobin deoxygenation. *Journal of cerebral blood flow and metabolism : official journal of the International Society of Cerebral Blood Flow and Metabolism*, 30(4):757–68.

Liraz, O., Boehm-Cagan, A., and Michaelson, D. M. (2013). ApoE4 induces Aβ42, tau, and neuronal pathology in the hippocampus of young targeted replacement apoE4 mice. *Molecular neurodegeneration*, 8(1):16.

Liu, J., Bartels, M., Lu, A., and Sharp, F. R. (2001). Microglia/macrophages proliferate in striatum and neocortex but not in hippocampus after brief global ischemia that produces ischemic tolerance in gerbil brain. *Journal of Cerebral Blood Flow and Metabolism*, 21(4):361–373.

Livingston, G., Sommerlad, A., Orgeta, V., Costafreda, S. G., Huntley, J., Ames, D., Ballard, C., Banerjee, S., Burns, A., Cohen-Mansfield, J., Cooper, C., Fox, N., Gitlin, L. N., Howard, R., Kales, H. C., Larson, E. B., Ritchie, K., Rockwood, K., Sampson, E. L., Samus, Q., Schneider, L. S., Selbæk, G., Teri, L., and Mukadam, N. (2017). Dementia prevention, intervention, and care. *Lancet (London, England)*, 390(10113):2673–2734.

Long, J. M. and Holtzman, D. M. (2019). Alzheimer Disease: An Update on Pathobiology and Treatment Strategies. *Cell*, 179(2):312–339.

Longden, T. A., Dabertrand, F., Koide, M., Gonzales, A. L., Tykocki, N. R., Brayden, J. E., Hill-Eubanks, D., and Nelson, M. T. (2017). Capillary K+-sensing initiates retrograde hyperpolarization to increase local cerebral blood flow. *Nature neuroscience*, 20(5):717–726.

Lovatt, D., Xu, Q., Liu, W., Takano, T., Smith, N. A., Schnermann, J., Tieu, K., and Nedergaard, M. (2012). Neuronal adenosine release, and not astrocytic ATP release, mediates feedback inhibition of excitatory activity. *Proceedings of the National Academy of Sciences of the United States of America*, 109(16):6265–6270.

Love, S. and Miners, J. S. (2016). Cerebrovascular disease in ageing and Alzheimer's disease. *Acta Neuropathologica*, 131(5):645–658.

Lu, X., Moeini, M., Li, B., Lu, Y., Damseh, R., Pouliot, P., Thorin, É., and Lesage, F. (2019). A Pilot Study Investigating Changes in Capillary Hemodynamics and Its Modulation by Exercise in the APP-PS1 Alzheimer Mouse Model. *Frontiers in Neuroscience*, 13:1261.

Lugo-Hernandez, E., Squire, A., Hagemann, N., Brenzel, A., Sardari, M., Schlechter, J., Sanchez-Mendoza, E. H., Gunzer, M., Faissner, A., and Hermann, D. M. (2017). 3D visualization and quantification of microvessels in the whole ischemic mouse brain using solvent-based clearing and light sheet microscopy. *Journal of Cerebral Blood Flow and Metabolism*, 37(10):3355–3367.

Ma, J., Yee, A., Brewer, H. B., Das, S., and Potter, H. (1994). Amyloid-associated proteins

α1-antichymotrypsin and apolipoprotein e promote assembly of Alzheimer β-protein into filaments. *Nature*, 372(6501):92–94.

Ma, Q., Zhao, Z., Sagare, A. P., Wu, Y., Wang, M., Owens, N. C., Verghese, P. B., Herz, J., Holtzman, D. M., and Zlokovic, B. V. (2018). Blood-brain barrier-associated pericytes internalize and clear aggregated amyloid-β42 by LRP1-dependent apolipoprotein E isoform-specific mechanism. *Molecular Neurodegeneration*, 13(1):57.

Mahley, R. W., Weisgraber, K. H., and Huang, Y. (2006). Apolipoprotein E4: A causative factor and therapeutic target in neuropathology, including Alzheimer's disease.

Malonek, D. and Grinvald, A. (1996). Interactions between electrical activity and cortical microcirculation revealed by imaging spectroscopy: Implications for functional brain mapping. *Science*, 272(5261):551–554.

Mandelkow, E., von Bergen, M., Biernat, J., and Mandelkow, E.-M. (2007). Structural Principles of Tau and the Paired Helical Filaments of Alzheimer's Disease. *Brain Pathology*, 17(1):83–90.

Mateo, C., Knutsen, P. M., Tsai, P. S., Shih, A. Y., and Kleinfeld, D. (2017). Entrainment of Arteriole Vasomotor Fluctuations by Neural Activity Is a Basis of Blood-Oxygenation-Level-Dependent "Resting-State" Connectivity. *Neuron*, 96(4):936–948.e3.

Mawuenyega, K. G., Sigurdson, W., Ovod, V., Munsell, L., Kasten, T., Morris, J. C., Yarasheski, K. E., and Bateman, R. J. (2010). Decreased clearance of CNS β-amyloid in Alzheimer's disease. *Science*, 330(6012):1774.

Mayeux, R., Ottman, R., Maestre, G., Ngai, C., Tang, M. X., Ginsberg, H., Chun, M., Tycko, B., and Shelanski, M. (1995). Synergistic effects of traumatic head injury and apolipoprotein-epsilon4 in patients with alzheimer's disease. *Neurology*, 45(3):555–557.

Mayhew, J. E., Askew, S., Zheng, Y., Porrill, J., Westby, G. W., Redgrave, P., Rector, D. M., and Harper, R. M. (1996). Cerebral vasomotion: A 0.1-Hz oscillation in reflected light imaging of neural activity. *NeuroImage*, 4(3):183–193.

Merlini, M., Wanner, D., and Nitsch, R. M. (2016). Tau pathology-dependent remodelling of cerebral arteries precedes Alzheimer's disease-related microvascular cerebral amyloid angiopathy. *Acta Neuropathologica*, 131(5):737–752.

Michaelis, E. K. (2012). Selective neuronal vulnerability in the hippocampus: Relationship to neurological diseases and mechanisms for differential sensitivity of neurons to stress.

In T. Bartsch (Ed.),. In *The clinical neurobiology of the hippocampus: An integrative view*, pages 54–76. Oxford University Press.

Mishra, A. (2017). Binaural blood flow control by astrocytes: listening to synapses and the vasculature. *The Journal of physiology*, 595(6):1885–1902.

Mishra, A., O'Farrell, F. M., Reynell, C., Hamilton, N. B., Hall, C. N., and Attwell, D. (2014). Imaging pericytes and capillary diameter in brain slices and isolated retinae. *Nature Protocols*, 9(2):323–336.

Mishra, A., Reynolds, J. P., Chen, Y., Gourine, A. V., Rusakov, D. A., and Attwell, D. (2016). Astrocytes mediate neurovascular signaling to capillary pericytes but not to arterioles. *Nature neuroscience*, 19(12):1619–1627.

Montagne, A., Nation, D. A., Sagare, A. P., Barisano, G., Sweeney, M. D., Chakhoyan, A., Pachicano, M., Joe, E., Nelson, A. R., D'Orazio, L. M., Buennagel, D. P., Harrington, M. G., Benzinger, T. L. S., Fagan, A. M., Ringman, J. M., Schneider, L. S., Morris, J. C., Reiman, E. M., Caselli, R. J., Chui, H. C., TCW, J., Chen, Y., Pa, J., Conti, P. S., Law, M., Toga, A. W., and Zlokovic, B. V. (2020). APOE4 leads to blood–brain barrier dysfunction predicting cognitive decline. *Nature*, 581(7806):1–6.

Montagne, A., Zhao, Z., and Zlokovic, B. V. (2017). Alzheimer's disease: A matter of blood-brain barrier dysfunction? *The Journal of experimental medicine*, 214(11):3151–3169.

Mosso, A. (1880). Sulla circolazione del sangue nel cervello dell'uomo. *Atti R Accad Lincei Mem Cl Sci Fis Mat Nat*, (3):237–358.

Najm, R., Jones, E. A., and Huang, Y. (2019). Apolipoprotein E4, inhibitory network dysfunction, and Alzheimer's disease. *Molecular Neurodegeneration*, 14(1).

Nathan, B. P., Jiang, Y., Wong, G. K., Shen, F., Brewer, G. J., and Struble, R. G. (2002). Apolipoprotein E4 inhibits, and apolipoprotein E3 promotes neurite outgrowth in cultured adult mouse cortical neurons through the low-density lipoprotein receptor-related protein. *Brain Research*, 928(1-2):96–105.

Nelson, P. T., Alafuzoff, I., Bigio, E. H., Bouras, C., Braak, H., Cairns, N. J., Castellani, R. J., Crain, B. J., Davies, P., Tredici, K. D., Duyckaerts, C., Frosch, M. P., Haroutunian, V., Hof, P. R., Hulette, C. M., Hyman, B. T., Iwatsubo, T., Jellinger, K. A., Jicha, G. A., Kövari, E., Kukull, W. A., Leverenz, J. B., Love, S., MacKenzie, I. R.,

Mann, D. M., Masliah, E., McKee, A. C., Montine, T. J., Morris, J. C., Schneider, J. A., Sonnen, J. A., Thal, D. R., Trojanowski, J. Q., Troncoso, J. C., Wisniewski, T., Woltjer, R. L., and Beach, T. G. (2012). Correlation of alzheimer disease neuropathologic changes with cognitive status: A review of the literature. *Journal of Neuropathology and Experimental Neurology*, 71(5):362–381.

Nelson, P. T., Pious, N. M., Jicha, G. A., Wilcock, D. M., Fardo, D. W., Estus, S., and William Rebeck, G. (2013). APOE-ϵ2 and APOE ϵ4 correlate with increased amyloid accumulation in cerebral vasculature. *Journal of Neuropathology and Experimental Neurology*, 72(7):708–715.

Neu, S. C., Pa, J., Kukull, W., Beekly, D., Kuzma, A., Gangadharan, P., Wang, L. S., Romero, K., Arneric, S. P., Redolfi, A., Orlandi, D., Frisoni, G. B., Au, R., Devine, S., Auerbach, S., Espinosa, A., Boada, M., Ruiz, A., Johnson, S. C., Koscik, R., Wang, J. J., Hsu, W. C., Chen, Y. L., and Toga, A. W. (2017). Apolipoprotein E genotype and sex risk factors for Alzheimer disease: A meta-analysis. *JAMA Neurology*, 74(10):1178–1189.

Nishitsuji, K., Hosono, T., Nakamura, T., Bu, G., and Michikawa, M. (2011). Apolipoprotein E regulates the integrity of tight junctions in an isoform-dependent manner in an in vitro blood-brain barrier model. *Journal of Biological Chemistry*, 286(20):17536–17542.

Niwa, K., Younkin, L., Ebeling, C., Turner, S. K., Westaway, D., Younkin, S., Ashe, K. H., Carlson, G. A., and Iadecola, C. (2000). Aβ1-40-related reduction in functional hyperemia in mouse neocortex during somatosensory activation. *Proceedings of the National Academy of Sciences of the United States of America*, 97(17):9735–9740.

Nizar, K., Uhlirova, H., Tian, P., Saisan, P. A., Cheng, Q., Reznichenko, L., Weldy, K. L., Steed, T. C., Sridhar, V. B., MacDonald, C. L., Cui, J., Gratiy, S. L., Sakadžić, S., Boas, D. A., Beka, T. I., Einevoll, G. T., Chen, J., Masliah, E., Dale, A. M., Silva, G. A., and Devor, A. (2013). In vivo stimulus-induced vasodilation occurs without IP3 receptor activation and may precede astrocytic calcium increase. *Journal of Neuroscience*, 33(19):8411–8422.

Nortley, R., Korte, N., Izquierdo, P., Hirunpattarasilp, C., Mishra, A., Jaunmuktane, Z., Kyrargyri, V., Pfeiffer, T., Khennouf, L., Madry, C., Gong, H., Richard-Loendt, A., Huang, W., Saito, T., Saido, T. C., Brandner, S., Sethi, H., and Attwell, D. (2019).

Amyloid β oligomers constrict human capillaries in Alzheimer's disease via signaling to pericytes. *Science*, 365(6450):eaav9518.

Nuriel, T., Angulo, S. L., Khan, U., Ashok, A., Chen, Q., Figueroa, H. Y., Emrani, S., Liu, L., Herman, M., Barrett, G., Savage, V., Buitrago, L., Cepeda-Prado, E., Fung, C., Goldberg, E., Gross, S. S., Hussaini, S. A., Moreno, H., Small, S. A., and Duff, K. E. (2017). Neuronal hyperactivity due to loss of inhibitory tone in APOE4 mice lacking Alzheimer's disease-like pathology. *Nature Communications*, 8(1):1464.

O'Herron, P., Chhatbar, P. Y., Levy, M., Shen, Z., Schramm, A. E., Lu, Z., and Kara, P. (2016). Neural correlates of single-vessel haemodynamic responses in vivo. *Nature*, 534(7607):378–382.

Oishi, H., Schuster, A., Lamboley, M., Stergiopulos, N., Meister, J. J., and Bény, J. L. (2002). Role of membrane potential in vasomotion of isolated pressurized rat arteries. *Life Sciences*, 71(19):2239–2248.

Ophir, G., Amariglio, N., Jacob-Hirsch, J., Elkon, R., Rechavi, G., and Michaelson, D. M. (2005). Apolipoprotein E4 enhances brain inflammation by modulation of the NF-κB signaling cascade. *Neurobiology of Disease*, 20(3):709–718.

Osol, G. and Halpern, W. (1988). Spontaneous vasomotion in pressurized cerebral arteries from genetically hypertensive rats. *American Journal of Physiology - Heart and Circulatory Physiology*, 254(1).

Østergaard, L., Aamand, R., Gutiérrez-Jiménez, E., Ho, Y. C. L., Blicher, J. U., Madsen, S. M., Nagenthiraja, K., Dalby, R. B., Drasbek, K. R., Møller, A., Brændgaard, H., Mouridsen, K., Jespersen, S. N., Jensen, M. S., and West, M. J. (2013). The capillary dysfunction hypothesis of Alzheimer's disease. *Neurobiology of Aging*, 34(4):1018–1031.

Owen, J. B., Sultana, R., Aluise, C. D., Erickson, M. A., Price, T. O., Bu, G., Banks, W. A., and Butterfield, D. A. (2010). Oxidative modification to LDL receptor-related protein 1 in hippocampus from subjects with Alzheimer disease: Implications for Aβ accumulation in AD brain. *Free Radical Biology and Medicine*, 49(11):1798–1803.

Pachitariu, M., Stringer, C., Schröder, S., Dipoppa, M., Rossi, L. F., Carandini, M., and Harris, K. D. (2016). Suite2p: beyond 10,000 neurons with standard two-photon microscopy. *bioRxiv*, page 061507.

Palmer, J. C., Barker, R., Kehoe, P. G., and Love, S. (2012). Endothelin-1 is Elevated in Alzheimer's Disease and Upregulated by Amyloid-β. *Journal of Alzheimer's Disease*, 29(4):853–861.

Park, L., Anrather, J., Girouard, H., Zhou, P., and Iadecola, C. (2007). Nox2-Derived Reactive Oxygen Species Mediate Neurovascular Dysregulation in the Aging Mouse Brain. *Journal of Cerebral Blood Flow & Metabolism*, 27(12):1908–1918.

Park, L., Anrather, J., Zhou, P., Frys, K., Pitstick, R., Younkin, S., Carlson, G. A., and Iadecola, C. (2005). NADPH oxidase-derived reactive oxygen species mediate the cerebrovascular dysfunction induced by the amyloid β peptide. *Journal of Neuroscience*, 25(7):1769–1777.

Park, L., Hochrainer, K., Hattori, Y., Ahn, S. J., Anfray, A., Wang, G., Uekawa, K., Seo, J., Palfini, V., Blanco, I., Acosta, D., Eliezer, D., Zhou, P., Anrather, J., and Iadecola, C. (2020). Tau induces PSD95–neuronal NOS uncoupling and neurovascular dysfunction independent of neurodegeneration. *Nature Neuroscience*, pages 1–11.

Park, L., Wang, G., Moore, J., Girouard, H., Zhou, P., Anrather, J., and Iadecola, C. (2014). The key role of transient receptor potential melastatin-2 channels in amyloid-β-induced neurovascular dysfunction. *Nature Communications*, 5:5318.

Peng, W., Achariyar, T. M., Li, B., Liao, Y., Mestre, H., Hitomi, E., Regan, S., Kasper, T., Peng, S., Ding, F., Benveniste, H., Nedergaard, M., and Deane, R. (2016). Suppression of glymphatic fluid transport in a mouse model of Alzheimer's disease. *Neurobiology of Disease*, 93:215–225.

Peppiatt, C. M., Howarth, C., Mobbs, P., and Attwell, D. (2006). Bidirectional control of CNS capillary diameter by pericytes. *Nature*, 443(7112):700–704.

Pfeifer, L. A., White, L. R., Ross, G. W., Petrovitch, H., and Launer, L. J. (2002). Cerebral amyloid angiopathy and cognitive function: The HAAS autopsy study. *Neurology*, 58(11):1629–1634.

Pluta, R. (2005). Pathological Opening of the Blood-Brain Barrier to Horseradish Peroxidase and Amyloid Precursor Protein following Ischemia-Reperfusion Brain Injury. *Chemotherapy*, 51(4):223–226.

Polvikoski, T., Sulkava, R., Haltia, M., Kainulainen, K., Vuorio, A., Verkkoniemi, A., Niin-

istö, L., Halonen, P., and Kontula, K. (1995). Apolipoprotein E, Dementia, and Cortical Deposition of β-Amyloid Protein. *New England Journal of Medicine*, 333(19):1242–1248.

Powers, W. J., Hirsch, I. B., and Cryer, P. E. (1996). Effect of stepped hypoglycemia on regional cerebral blood flow response to physiological brain activation. *American Journal of Physiology - Heart and Circulatory Physiology*, 270(2 39-2).

Price, J. L., McKeel, D. W., Buckles, V. D., Roe, C. M., Xiong, C., Grundman, M., Hansen, L. A., Petersen, R. C., Parisi, J. E., Dickson, D. W., Smith, C. D., Davis, D. G., Schmitt, F. A., Markesbery, W. R., Kaye, J., Kurlan, R., Hulette, C., Kurland, B. F., Higdon, R., Kukull, W., and Morris, J. C. (2009). Neuropathology of nondemented aging: Presumptive evidence for preclinical Alzheimer disease. *Neurobiology of Aging*, 30(7):1026–1036.

Price, J. L. and Morris, J. C. (1999). Tangles and plaques in nondemented aging and 'preclinical' alzheimer's disease. *Annals of Neurology*, 45(3):358–368.

Rodriguez, G. A., Burns, M. P., Weeber, E. J., and Rebeck, G. W. (2013). Young APOE4 targeted replacement mice exhibit poor spatial learning and memory, with reduced dendritic spine density in the medial entorhinal cortex. *Learning and Memory*, 20(5):256–266.

Rodriguez, G. A., Tai, L. M., LaDu, M. J., and Rebeck, G. W. (2014). Human APOE4 increases microglia reactivity at Aβ plaques in a mouse model of Aβ deposition. *Journal of Neuroinflammation*, 11.

Roy, C. S. and Sherrington, C. S. (1890). On the Regulation of the Blood-supply of the Brain. *The Journal of physiology*, 11(1-2):85–158.17.

Rücker, M., Strobel, O., Vollmar, B., Roesken, F., and Menger, M. D. (2000). Vasomotion in critically perfused muscle protects adjacent tissues from capillary perfusion failure. *American Journal of Physiology - Heart and Circulatory Physiology*, 279(2 48-2).

Rungta, R. L., Chaigneau, E., Osmanski, B.-F., and Charpak, S. (2018). Vascular Compartmentalization of Functional Hyperemia from the Synapse to the Pia. *Neuron*, 99(2):362–375.e4.

Ryu, J. K. and McLarnon, J. G. (2009). A leaky blood-brain barrier, fibrinogen infiltration and microglial reactivity in inflamed Alzheimer's disease brain. *Journal of Cellular and Molecular Medicine*, 13(9a):2911–2925.

Safieh, M., Korczyn, A. D., and Michaelson, D. M. (2019). ApoE4: an emerging therapeutic target for Alzheimer's disease. *BMC Medicine*, 17(1).

Sagare, A. P., Bell, R. D., Zhao, Z., Ma, Q., Winkler, E. A., Ramanathan, A., and Zlokovic, B. V. (2013). Pericyte loss influences Alzheimer-like neurodegeneration in mice. *Nature communications*, 4:2932.

Sakadžić, S., Roussakis, E., Yaseen, M. A., Mandeville, E. T., Srinivasan, V. J., Arai, K., Ruvinskaya, S., Devor, A., Lo, E. H., Vinogradov, S. A., and Boas, D. A. (2010). Two-photon high-resolution measurement of partial pressure of oxygen in cerebral vasculature and tissue. *Nature Methods*, 7(9):755–759.

Salloway, S., Gur, T., Berzin, T., Tavares, R., Zipser, B., Correia, S., Hovanesian, V., Fallon, J., Kuo-Leblanc, V., Glass, D., Hulette, C., Rosenberg, C., Vitek, M., and Stopa, E. (2002). Effect of APOE genotype on microvascular basement membrane in Alzheimer's disease. *Journal of the neurological sciences*, 203-204:183–7.

Salomon-Zimri, S., Glat, M. J., Barhum, Y., Luz, I., Boehm-Cagan, A., Liraz, O., Ben-Zur, T., Offen, D., and Michaelson, D. M. (2016). Reversal of ApoE4-Driven Brain Pathology by Vascular Endothelial Growth Factor Treatment. *Journal of Alzheimer's Disease*, 53(4):1443–1458.

Satoh, K., Shimokawa, H., and Berk, B. C. (2010). Cyclophilin A: Promising new target in cardiovascular therapy. *Circulation Journal*, 74(11):2249–2256.

Schindelin, J., Arganda-Carreras, I., Frise, E., Kaynig, V., Longair, M., Pietzsch, T., Preibisch, S., Rueden, C., Saalfeld, S., Schmid, B., Tinevez, J. Y., White, D. J., Hartenstein, V., Eliceiri, K., Tomancak, P., and Cardona, A. (2012). Fiji: An open-source platform for biological-image analysis. *Nature Methods*, 9(7):676–682.

Shabir, O., Berwick, J., and Francis, S. E. (2018). Neurovascular dysfunction in vascular dementia, Alzheimer's and atherosclerosis. *BMC neuroscience*, 19(1):62.

Shabir, O., Sharp, P., Rebollar, M. A., Boorman, L., Howarth, C., Wharton, S. B., Francis, S. E., and Berwick, J. (2020). Enhanced Cerebral Blood Volume under Normobaric Hyperoxia in the J20-hAPP Mouse Model of Alzheimer's Disease. *Scientific Reports*, 10(1).

Sharp, P. S., Shaw, K., Boorman, L., Harris, S., Kennerley, A. J., Azzouz, M., and Berwick,

J. (2015). Comparison of stimulus-evoked cerebral hemodynamics in the awake mouse and under a novel anesthetic regime. *Scientific Reports*, 5(12621).

Shaw, K., Bell, L., Boyd, K., Grijseels, D., Clarke, D., Bonnar, O., Crombag, H., and Hall, C. (2019). Hippocampus has lower oxygenation and weaker control of brain blood flow than cortex, due to microvascular differences. *bioRxiv*, page 835728.

Shi, Y., Yamada, K., Liddelow, S. A., Smith, S. T., Zhao, L., Luo, W., Tsai, R. M., Spina, S., Grinberg, L. T., Rojas, J. C., Gallardo, G., Wang, K., Roh, J., Robinson, G., Finn, M. B., Jiang, H., Sullivan, P. M., Baufeld, C., Wood, M. W., Sutphen, C., McCue, L., Xiong, C., Del-Aguila, J. L., Morris, J. C., Cruchaga, C., Fagan, A. M., Miller, B. L., Boxer, A. L., Seeley, W. W., Butovsky, O., Barres, B. A., Paul, S. M., and Holtzman, D. M. (2017). ApoE4 markedly exacerbates tau-mediated neurodegeneration in a mouse model of tauopathy. *Nature*, 549(7673):523–527.

Shibata, M., Yamada, S., Ram Kumar, S., Calero, M., Bading, J., Frangione, B., Holtzman, D. M., Miller, C. A., Strickland, D. K., Ghiso, J., and Zlokovic, B. V. (2000). Clearance of Alzheimer's amyloid-β1-40 peptide from brain by LDL receptor-related protein-1 at the blood-brain barrier. *Journal of Clinical Investigation*, 106(12):1489–1499.

Shih, A. Y., Driscoll, J. D., Drew, P. J., Nishimura, N., Schaffer, C. B., and Kleinfeld, D. (2012). Two-photon microscopy as a tool to study blood flow and neurovascular coupling in the rodent brain. *Journal of cerebral blood flow and metabolism : official journal of the International Society of Cerebral Blood Flow and Metabolism*, 32(7):1277–309.

Shulman, R. G., Rothman, D. L., and Hyder, F. (1999). Stimulated changes in localized cerebral energy consumption under anesthesia. *Proceedings of the National Academy of Sciences of the United States of America*, 96(6):3245–3250.

Silva, M. V. F., Loures, C. D. M. G., Alves, L. C. V., De Souza, L. C., Borges, K. B. G., and Carvalho, M. D. G. (2019). Alzheimer's disease: Risk factors and potentially protective measures. *Journal of Biomedical Science*, 26(1).

Sullivan, P. M., Mezdour, H., Aratani, Y., Knouff, C., Najib, J., Reddick, R. L., Quarfordt, S. H., and Maeda, N. (1997). Targeted replacement of the mouse apolipoprotein E gene with the common human APOE3 allele enhances diet-induced hypercholesterolemia and atherosclerosis. *Journal of Biological Chemistry*, 272(29):17972–17980.

Sun, X., He, G., Qing, H., Zhou, W., Dobie, F., Cai, F., Staufenbiel, M., Huang, L. E., and Song, W. (2006). Hypoxia facilitates Alzheimer's disease pathogenesis by up-regulating BACE1 gene expession. *Proceedings of the National Academy of Sciences of the United States of America*, 103(49):18727–18732.

Sweeney, M. D., Kisler, K., Montagne, A., Toga, A. W., and Zlokovic, B. V. (2018a). The role of brain vasculature in neurodegenerative disorders. *Nature Neuroscience*, 21(10):1318–1331.

Sweeney, M. D., Montagne, A., Sagare, A. P., Nation, D. A., Schneider, L. S., Chui, H. C., Harrington, M. G., Pa, J., Law, M., Wang, D. J., Jacobs, R. E., Doubal, F. N., Ramirez, J., Black, S. E., Nedergaard, M., Benveniste, H., Dichgans, M., Iadecola, C., Love, S., Bath, P. M., Markus, H. S., Salman, R. A., Allan, S. M., Quinn, T. J., Kalaria, R. N., Werring, D. J., Carare, R. O., Touyz, R. M., Williams, S. C., Moskowitz, M. A., Katusic, Z. S., Lutz, S. E., Lazarov, O., Minshall, R. D., Rehman, J., Davis, T. P., Wellington, C. L., González, H. M., Yuan, C., Lockhart, S. N., Hughes, T. M., Chen, C. L., Sachdev, P., O'Brien, J. T., Skoog, I., Pantoni, L., Gustafson, D. R., Biessels, G. J., Wallin, A., Smith, E. E., Mok, V., Wong, A., Passmore, P., Barkof, F., Muller, M., Breteler, M. M., Román, G. C., Hamel, E., Seshadri, S., Gottesman, R. F., van Buchem, M. A., Arvanitakis, Z., Schneider, J. A., Drewes, L. R., Hachinski, V., Finch, C. E., Toga, A. W., Wardlaw, J. M., and Zlokovic, B. V. (2019). Vascular dysfunction—The disregarded partner of Alzheimer's disease. *Alzheimer's & Dementia*, 15(1):158–167.

Sweeney, M. D., Sagare, A. P., and Zlokovic, B. V. (2018b). Blood-brain barrier breakdown in Alzheimer disease and other neurodegenerative disorders. *Nature Reviews Neurology*, 14(3):133–150.

Sweet, R. A., MacDonald, M. L., Kirkwood, C. M., Ding, Y., Schempf, T., Jones-Laughner, J., Kofler, J., Ikonomovic, M. D., Lopez, O. L., Garver, M. E., Fitz, N. F., Koldamova, R., and Yates, N. A. (2016). Apolipoprotein E4 (APOE4) genotype is associated with altered levels of glutamate signaling proteins and synaptic coexpression networks in the prefrontal cortex in mild to moderate Alzheimer disease. *Molecular and Cellular Proteomics*, 15(7):2252–2262.

Szendro, P., Vincze, G., and Szasz, A. (2001). Pink-noise behaviour of biosystems. *European Biophysics Journal*, 30(3):227–231.

Tai, L. M., Thomas, R., Marottoli, F. M., Koster, K. P., Kanekiyo, T., Morris, A. W., and Bu, G. (2016). The role of APOE in cerebrovascular dysfunction.

Tiraboschi, P., Hansen, L. A., Masliah, E., Alford, M., Thal, L. J., and Corey-Bloom, J. (2004). Impact of APOE genotype on neuropathologic and neurochemical markers of Alzheimer disease. *Neurology*, 62(11):1977–1983.

Toda, N. and Okamura, T. (2012). Cerebral blood flow regulation by nitric oxide in Alzheimer's disease. *Journal of Alzheimer's Disease*, 32(3):569–578.

Tsai, A. G. and Intaglietta, M. (1989). Local tissue oxygenation during constant red blood cell flux: A discrete source analysis of velocity and hematocrit changes. *Microvascular Research*, 37(3):308–322.

Tsai, P. S., Kaufhold, J. P., Blinder, P., Friedman, B., Drew, P. J., Karten, H. J., Lyden, P. D., and Kleinfeld, D. (2009a). Correlations of Neuronal and Microvascular Densities in Murine Cortex Revealed by Direct Counting and Colocalization of Nuclei and Vessels. *Journal of Neuroscience*, 29(46):14553–14570.

Tsai, P. S., Kaufhold, J. P., Blinder, P., Friedman, B., Drew, P. J., Karten, H. J., Lyden, P. D., and Kleinfeld, D. (2009b). Correlations of neuronal and microvascular densities in murine cortex revealed by direct counting and colocalization of nuclei and vessels. *Journal of Neuroscience*, 29(46):14553–14570.

Tuminello, E. R. and Han, S. D. (2011). The Apolipoprotein E Antagonistic Pleiotropy Hypothesis: Review and Recommendations. *International Journal of Alzheimer's Disease*, 2011.

Ueno, M., Tomimoto, H., Akiguchi, I., Wakita, H., and Sakamoto, H. (2002). Blood-brain barrier disruption in white matter lesions in a rat model of chronic cerebral hypoperfusion. *Journal of cerebral blood flow and metabolism : official journal of the International Society of Cerebral Blood Flow and Metabolism*, 22(1):97–104.

Uhlirova, H., Kılıç, K., Tian, P., Sakadžić, S., Gagnon, L., Thunemann, M., Desjardins, M., Saisan, P. A., Nizar, K., Yaseen, M. A., Hagler, D. J., Vandenberghe, M., Djurovic, S., Andreassen, O. A., Silva, G. A., Masliah, E., Kleinfeld, D., Vinogradov, S., Buxton, R. B., Einevoll, G. T., Boas, D. A., Dale, A. M., Devor, A., and Devor, A. (2016). The roadmap for estimation of cell-type-specific neuronal activity from non-invasive measurements. *Philosophical transactions of the Royal Society of London. Series B, Biological sciences*, 371(1705).

van Veluw, S. J., Hou, S. S., Calvo-Rodriguez, M., Arbel-Ornath, M., Snyder, A. C., Frosch, M. P., Greenberg, S. M., and Bacskai, B. J. (2019). Vasomotion as a Driving Force for Paravascular Clearance in the Awake Mouse Brain. *Neuron*.

Vinters, H. V. (1987). Cerebral amyloid angiopathy. A critical review. *Stroke*, 18(2):311–324.

Wang, C., Najm, R., Xu, Q., Jeong, D. E., Walker, D., Balestra, M. E., Yoon, S. Y., Yuan, H., Li, G., Miller, Z. A., Miller, B. L., Malloy, M. J., and Huang, Y. (2018). Gain of toxic apolipoprotein E4 effects in human iPSC-derived neurons is ameliorated by a small-molecule structure corrector article. *Nature Medicine*, 24(5):647–657.

Wang, C., Wilson, W. A., Moore, S. D., Mace, B. E., Maeda, N., Schmechel, D. E., and Sullivan, P. M. (2005). Human apoE4-targeted replacement mice display synaptic deficits in the absence of neuropathology. *Neurobiology of disease*, 18(2):390–8.

Wang, L., Benzinger, T. L., Su, Y., Christensen, J., Friedrichsen, K., Aldea, P., McConathy, J., Cairns, N. J., Fagan, A. M., Morris, J. C., and Ances, B. M. (2016). Evaluation of Tau imaging in staging Alzheimer disease and revealing interactions between β-Amyloid and tauopathy. *JAMA Neurology*, 73(9):1070–1077.

Wang, L., Jacques, S. L., and Zheng, L. (1995). MCML-Monte Carlo modeling of light transport in multi-layered tissues. *Computer Methods and Programs in Biomedicine*, 47(2):131–146.

Wang, R., Meschia, J. F., Cotter, R. J., and Sisodia, S. S. (1991). Secretion of the beta/A4 amyloid precursor protein. Identification of a cleavage site in cultured mammalian cells. *The Journal of biological chemistry*, 266(25):16960–4.

Watson, A. N., Berthiaume, A. A., Faino, A. V., McDowell, K. P., Bhat, N. R., Hartmann, D. A., and Shih, A. Y. (2020). Mild pericyte deficiency is associated with aberrant brain microvascular flow in aged PDGFRβ mice. *Journal of Cerebral Blood Flow and Metabolism*, page 271678X19900543.

Wei, H. S., Kang, H., Rasheed, I.-Y. D., Zhou, S., Lou, N., Gershteyn, A., McConnell, E. D., Wang, Y., Richardson, K. E., Palmer, A. F., Xu, C., Wan, J., and Nedergaard, M. (2016). Erythrocytes Are Oxygen-Sensing Regulators of the Cerebral Microcirculation. *Neuron*, 91(4):851–862.

Weingarten, M. D., Lockwood, A. H., Hwo, S. Y., and Kirschner, M. W. (1975). A protein factor essential for microtubule assembly. *Proceedings of the National Academy of Sciences of the United States of America*, 72(5):1858–1862.

Weller, R. O., Boche, D., and Nicoll, J. A. (2009). Microvasculature changes and cerebral amyloid angiopathy in Alzheimer's disease and their potential impact on therapy. *Acta Neuropathologica*, 118(1):87–102.

Wilhelmus, M. M. M. (2005). Apolipoprotein E Genotype Regulates Amyloid- Cytotoxicity. *Journal of Neuroscience*, 25(14):3621–3627.

Winder, A. T., Echagarruga, C., Zhang, Q., and Drew, P. J. (2017). Weak correlations between hemodynamic signals and ongoing neural activity during the resting state. *Nature Neuroscience*, 20(12):1761–1769.

Xu, Q., Bernardo, A., Walker, D., Kanegawa, T., Mahley, R. W., and Huang, Y. (2006). Profile and regulation of apolipoprotein E (ApoE) expression in the CNS in mice with targeting of green fluorescent protein gene to the ApoE locus. *Journal of Neuroscience*, 26(19):4985–4994.

Yamazaki, Y., Zhao, N., Caulfield, T. R., Liu, C. C., and Bu, G. (2019). Apolipoprotein E and Alzheimer disease: pathobiology and targeting strategies. *Nature Reviews Neurology*, 15(9):501–518.

Yuill, K. H., McNeish, A. J., Kansui, Y., Garland, C. J., and Dora, K. A. (2010). Nitric oxide suppresses cerebral vasomotion by sgc-independent effects on ryanodine receptors and voltage-gated calcium channels. *Journal of Vascular Research*, 47(2):93–107.

Zerbi, V., Wiesmann, M., Emmerzaal, T. L., Jansen, D., Beek, M. V., Mutsaers, M. P., Beckmann, C. F., Heerschap, A., and Kiliaan, A. J. (2014). Resting-state functional connectivity changes in aging apoe4 and apoe-ko mice. *Journal of Neuroscience*, 34(42):13963–13975.

Zhang, F., Eckman, C., Younkin, S., Hsiao, K. K., and Iadecola, C. (1997). Increased susceptibility to ischemic brain damage in transgenic mice overexpressing the amyloid precursor protein. *Journal of Neuroscience*, 17(20):7655–7661.

Zhang, X. and Le, W. (2010). Pathological role of hypoxia in Alzheimer's disease. *Experimental Neurology*, 223(2):299–303.

Zhao, N., Liu, C. C., Van Ingelgom, A. J., Linares, C., Kurti, A., Knight, J. A., Heckman, M. G., Diehl, N. N., Shinohara, M., Martens, Y. A., Attrebi, O. N., Petrucelli, L., Fryer, J. D., Wszolek, Z. K., Graff-Radford, N. R., Caselli, R. J., Sanchez-Contreras, M. Y., Rademakers, R., Murray, M. E., Koga, S., Dickson, D. W., Ross, O. A., and Bu, G. (2018). APOE $\epsilon 2$ is associated with increased tau pathology in primary tauopathy. *Nature Communications*, 9(1).

Zhu, X., Bergles, D. E., and Nishiyama, A. (2008). NG2 cells generate both oligodendrocytes and gray matter astrocytes. *Development*, 135(1):145–157.

Zipser, B. D., Johanson, C. E., Gonzalez, L., Berzin, T. M., Tavares, R., Hulette, C. M., Vitek, M. P., Hovanesian, V., and Stopa, E. G. (2007). Microvascular injury and blood-brain barrier leakage in Alzheimer's disease. *Neurobiology of Aging*, 28(7):977–986.

Zlokovic, B. V. (2011). Neurovascular pathways to neurodegeneration in Alzheimer's disease and other disorders. *Nature Reviews Neuroscience*, 12(12):723–738.

Zlokovic, B. V. (2013). Cerebrovascular effects of apolipoprotein E: implications for Alzheimer disease. *JAMA neurology*, 70(4):440–4.

Appendix A

Appendix A

A.1 Statistical outputs

Figure Label	n	Mean	SD	Test	Test statistic	P Value
A. NOR	n = 8/9 animals/ G (E3/E4)	APOE3: 0.708 APOE4: 0.663	APOE3 0.0822 APOE4:0. 155	Two – tailed unpaired t-test with Welch's Correction	t = 0.8486	0.477
B. SOR	n =11/12 animals/ G (E3/E4)	APOE3: 0.6192 APOE4: 0.6229	APOE3: 0.091 APOE4: 0.146	Two – tailed unpaired t-test with Welch's Correction	t = 0.9382	0.908
C. Locomotion	n = 14/15 animals/ G (E3/E4)	APOE3: 296.6 APOE4: 300.5	APOE3: 87.33 APOE4: 57.96	Two – tailed unpaired t-test with Welch's Correction	t = 0.1481	0.2214

Table A.1: **Statistical outputs for figure 3.1**

Figure Label	n	Mean	Standard Error	Test	Test Statistic	P Value
B. GFAP + cells	n = 8/6 slices n= 3 / 4 animals (E3/E4)	APOE3 slope: 0.0015 APOE4 slope: -0.05	APOE3 slope: 0.038 APOE4 slope: 0.042	Linear regression	ApoE3 R^2: 2.06e-005 ApoE4 R^2: 0.028	0.386
C. Iba1 + cells	n=11 /12 slices n = 3 / 4 animals (E3/E4)	APOE3 slope: -0.02 APOE4 slope: 0.005	APOE3 slope: 0.02 APOE4 slope: 0.02	Linear regression	ApoE3 R^2: 0.006 ApoE4 R^2: 0.0003	0.4616

Table A.2: **Statistical outputs for figure 3.2**

Figure Label	n	Mean	SD	Test	Test Statistic	95% CI	P Value
B. In vivo Capillary density	n = 6/5 animals (E3/E4)	APOE3: 0.5204 APOE4: 0.4971	APOE3: 0.0824 APOE4: 0.1472	Two – tailed unpaired t-test with Welch's Correction	t = 0.3161	-0.204 – 0.1573	0.7626
C. In vivo Capillary diameter	n = 6/5 animals (E3/E4)	APOE3:6.312 APOE4:6.357	APOE3: 0.281 APOE4: 0.3665	Two – tailed unpaired t-test with Welch's Correction	t = 0.2266	-0.422 – 0.5127	0.8268
D. In vivo Tortuosity	n = 6/5 animals (E3/E4)	APOE3: 1.224 APOE4:1.216	APOE3: 0.044 APOE4:0.0253	Two – tailed unpaired t-test with Welch's Correction	t = 0.3682	-0.0568 – 0.0411	0.7221

Table A.3: **Statistical outputs for figure 3.3**

Figure Label	n	Mean	SD	Test	Test Statistic	95% CI	P Value
B. Density	n= 3 / 4 animals (E3/E4) n = 16/29 slices (E3/E4)	APOE3: 2.634 APOE4: 2.157	APOE3: 0.7836 APOE4: 0.7269	Two – tailed unpaired t-test with Welch's Correction	t = 2.2254	-0.9172 - -.03561	0.0355
C. Pericytes per mm	n= 3 / 4 animals (E3/E4) n = 16/29 slices (E3/E4)	APOE3: 4.29 APOE4: 4.214	APOE3: 0.838 APOE4: 0.6280	Two – tailed unpaired t-test with Welch's Correction	t = 0.3158	-0.57 – 0.4185	0.7548
D. Tortuosity	n= 3 / 4 animals (E3/E4) n = 16/29 slices (E3/E4)	APOE3: 1.61 APOE4: 1.598	APOE3: 0.061 APOE4: 0.030	Two – tailed unpaired t-test with Welch's Correction	t = 0.4768	-0.046 – 0.022	0.4768
E. Capillary diameter	n= 3 / 4 animals (E3/E4) n = 16/29 slices (E3/E4)	APOE3: 3.99 APOE4: 4.569	APOE3 :0.7339 APOE4: 0.4558	Two – tailed unpaired t-test with Welch's Correction	t= 2.865	0.1594 – 0.999	0.009
G. Diameter at soma	n= 3 / 4 animals (E3/E4) n = 16/29 slices (E3/E4)	APOE3: 3.708 APOE4: 4.19	APOE3: 0.609 APOE4: 0.394	Two – tailed unpaired t-test with Welch's Correction	t= 2.852	0.1315 – 0.8321	0.009
H. Diameter as function pericyte distance (raw)	n= 3 / 4 animals (E3/E4) n = 16/29 slices (E3/E4)	APOE3 slope: -0.005 APOE4 slope: -0.0006	APOE3 slope: 0.014 APOE4 slope: 0.007	Simple linear regression (p assesses if slope significantly differs from zero)	APOE3 : R^2 = 0.003 APOE4 : R^2 = 6.36e-005	N/A	APOE3: 0.6832 APOE4: 0.9323
I. Diameter as function pericyte distance (normalised)	n= 3 / 4 animals (E3/E4) n = 16/29 slices (E3/E4)	APOE3 slope: 0.002 APOE4 slope: 0.0035	APOE3 slope: 0.0012 APOE4 slope: 0.0006	Simple linear regression (p assesses if slope significantly differs from zero)	APOE3 : R^2 = 0.048 APOE4 : R^2 = 0.217	N/A	APOE3: 0.0825 APOE4: <0.0001

Table A.4: **Statistical outputs for figure 3.4**

Figure Label	n	Mean	SD	Test	Test Statistic	P Value
A. Baseline Pia diameter	n = 15 animals per genotype n = 52/55 vessels (E3/E4)	APOE3: 26.06 APOE4: 27.39	APOE3: 7.589 APOE4: 9.337	Two – tailed unpaired t-test with Welch's Correction	t = 0.8089	0.4204
B. Baseline capillary diameter	n = 13 animals/ genotype n = 64/72 vessels (E3/E4)	APOE3: 3.679 APOE4: 3.582	APOE3: 1.119 APOE4: 1.172	Two – tailed unpaired t-test with Welch's Correction	t = 0.4931	0.6227
C. Baseline RBCV	n = 12/11 animals (E3/E4) n= 42/41 vessels (E3/E4)	APOE3: 1.415 APOE4: 1.168	APOE3: 1.05 APOE4: 1.128	Two – tailed unpaired t-test with Welch's Correction	t = 1.033	0.3047
D. Baseline Flux	n = 15 animals/ genotype	APOE3: 328.6 APOE4: 294.8	APOE3: 108.7 APOE4: 66.67	Two – tailed unpaired t-test with Welch's Correction	t = 1.028	0.3147
E. Baseline SO_2	n = 15 animals/ genotype	APOE3: 47.43 APOE4: 48.66	APOE3: 4.814 APOE4: 5.808	Two – tailed unpaired t-test with Welch's Correction	t = 0.6326	0.5323
F. Baseline $CMRO_2$	n = 15 animals/ genotype	APOE3: 171.3 APOE4: 150.5	APOE3: 58.15 APOE4: 35.01	Two – tailed unpaired t-test with Welch's Correction	t = 1.184	0.249
G. Flux CV	n = 15 animals/ genotype	APOE3: 9.313 APOE4: 11.20	APOE3: 0.842 APOE4: 5.651	Two – tailed unpaired t-test with Welch's Correction	t = 1.282	0.2197
H. SO_2 CV	n = 15 animals/ genotype	APOE3: 5.048 APOE4: 6.223	APOE3: 1.119 APOE4: 6.385	Two – tailed unpaired t-test with Welch's Correction	t = 0.7016	0.4938
I. RBCV CV	n = 12/11 animals (E3/E4) n= 42/41 vessels (E3/E4)	APOE3: 21.19 APOE4: 23.93	APOE3: 6.83 APOE4: 7.74	Two – tailed unpaired t-test with Welch's Correction	t = 1.706	0.092

Table A.5: **Statistical outputs for figure 3.5**

Figure Label	n	Mean	SD	Test	Test Statistic	P Value
C. Pia FFT traces	n= 52/53 vessels (E3/E4) n= 15 animals per genotype	**APOE3:** 0.1-0.2Hz: 0.0166 0.2-0.3Hz: 0.01731 0.3-0.4Hz: 0.01579 **APOE4:** 0.1-0.2Hz: 0.01223 0.2-0.3Hz: 0.01374 0.3-0.4Hz: 0.01390	**APOE3:** 0.1-0.2Hz: 0.0081 0.2-0.3Hz: 0.0068 0.3-0.4Hz: 0.0050 **APOE4:** 0.1-0.2Hz: 0.00597 0.2-0.3Hz: 0.00559 0.3-0.4Hz: 0.00479	Multifactorial ANOVA to compare the effect of genotype in each frequency bin	0.1-0.2Hz: F = 9.736972 0.2-0.3Hz: F = 8.611782 0.3-0.4Hz: F = 3.911150	0.1-0.2Hz: p = 0.0023 0.2-0.3Hz: p = 0.0041 0.3-0.4Hz : p = 0.051
D. Pia power at 0.1Hz	n= 52/53 vessels (E3/E4) N = 15 animals per genotype	**APOE3**:0.013 **APOE4**: 0.009	**APOE3:** 0.00965 **APOE4:** 0.00576	Two – tailed unpaired t-test with Welch's Correction	t-= 2.587	p = 0.0114
E. Capillary FFT traces	n= 58/68 vessels (E3/E4) n = 13 animals per genotype	**APOE3:** 0.1-0.2Hz: 0.00077 0.2-0.3Hz: 0.00088 0.3-0.4Hz: 0.00098 **APOE4:** 0.1-0.2Hz: 0.00077 0.2-0.3Hz: 0.00095 0.3-0.4Hz: 0.00101	**APOE3:** 0.1-0.2Hz: 0.00033 0.2-0.3Hz: 0.00034 0.3-0.4Hz: 0.00029 **APOE4:** 0.1-0.2Hz: 0.00033 0.2-0.3Hz: 0.00033 0.3-0.4Hz:0.00031	Multifactorial ANOVA to compare the effect of genotype in each frequency bin	0.1-0.2Hz: F= 0.000179 0.2-0.3Hz: F= 1.091452 0.3-0.4Hz: F= 0.394755	0.1-0.2Hz: p = 0.9894 0.2-0.3Hz: p = 0.2982 0.3-0.4Hz: p = 0.531
F. Capillary power at 0.1Hz	N = 58/68 vessels (E3/E4) N = 13 animals per genotype	**APOE3**:0.00068 **APOE4**:0.00066	**APOE3:** 0.0003 **APOE4**:0.0002	Two – tailed unpaired t-test with Welch's Correction	t = 0.2354	p = 0.8143

Table A.6: **Statistical outputs for figure 3.6**

Figure Label	n	Mean	SD	Test	Test Statistic	P Value
B. PPM An Avg.	n = 6/5 animals (E3/E4)	APOE3: 6.185 APOE4: 5.873	APOE3: 1.021 APOE4: 0.365	Two – tailed unpaired t-test with Welch's Correction	t = 0.645	p = 0.5349
C. Correlation Coefficient An Avg	n= 6/5 animals (E3/E4)	APOE3: 0.0436 APOE4: 0.0389	APOE3:0.0209 APOE4: 0.0270	Two – tailed unpaired t-test with Welch's Correction	t = 0.3180	p= 0.7592
D. Peak Size An Avg	n = 6/5 animals (E3/E4)	APOE3: 1.930 APOE4: 2.098	APOE3: 0.4557 APOE4: 0.4990	Two – tailed unpaired t-test with Welch's Correction	t = 0.5798	p = 0.5775

Table A.7: **Statistical outputs for figure 3.7**

Figure Label	n	Mean	SD	Test	Test Statistic (F)	P Value
A. Power at 0.1Hz	APOE3 F: 23 APOE3 M: 30 APOE4F: 29 APOE4M: 23	APOE3 F: 0.015 APOE3 M: 0.012 APOE4F: 0.0097 APOE4M: 0.008	APOE3 F: 0.008 APOE3 M: 0.011 APOE4F: 0.006 APOE4M: 0.005	Two-way ANOVA	G: 7.539 S: 1.888 G*S: 0.179	G: 0.007148 S: 0.172432 G*S: 0.672957
B. Pia Diameter	APOE3 F: 23 APOE3 M:31 APOE4F:29 APOE4M: 24	APOE3 F: 23.991 APOE3 M: 27.6995 APOE4F: 26.337 APOE4M: 28.743	APOE3 F: 5.915 APOE3 M: 8.433 APOE4F:10.058 APOE4M: 8.328	Two-way ANOVA	G: 1.054 S:3.431 G*S: 0.155	G: 0.307031 S: 0.066850 G*S: 0.694252
C. Capillary diameter	APOE3 F:26 APOE3M:38 APOE4F:35 APOE4M:37	APOE3 F: 3.489 APOE3 M: 3.809 APOE4F: 3.750 APOE4M: 3.4229	APOE3 F: 1.054 APOE3 M: 1.157 APOE4F: 1.339 APOE4M: 0.982	Two-way ANOVA	G: 0.099 S: 0.0003 G*S: 2.662	G: 0.754056 S: 0.986648 G*S: 0.105165
D. Capillary RBCV	APOE3 F:16 APOE3M:26 APOE4F:22 APOE4M:19	APOE3 F:1.257 APOE3 M: 1.513 APOE4F: 1.061 APOE4M: 1.291	APOE3 F:0.946 APOE3 M: 1.116 APOE4F: 1.297 APOE4M: 0.914	Two-way ANOVA	G: 0.726 S: 0.988 G*S: 0.003	G: 0.396746 S: 0.323257 G*S: 0.957770
E. PPM	ROIs APOE3 F: 795 APOE3 M: 973 APOE4F: 956 APOE4M: 720	APOE3 F: 6.116 APOE3 M: 5.620 APOE4F: 6.0460 APOE4M: 5.56	APOE3 F: 3.595 APOE3 M: 3.467 APOE4F: 3.481 APOE4M: 2.972	Two-way ANOVA	G: 0.288 S: 17.44 G*S: 0.004	G: 0.591696 S: 0.00003 G*S: 0.951984
F. Flux	Animals: APOE3 F: 7 APOE3 M: 8 APOE4F: 8 APOE4M:7	APOE3 F: 355.652 APOE3 M: 305.01 APOE4F:272.22 APOE4M: 320.62	APOE3 F: 145.07 APOE3 M: 65.06 APOE4F: 66.596 APOE4M: 61.145	Two-way ANOVA	G: 1.066 S: 0.001 G*S: 2.273	G: 0.311294 S:0.973020 G*S: 0.143676
G. SO_2	Animals: APOE3 F: 7 APOE3 M: 8 APOE4F: 8 APOE4M:7	APOE3 F: 47.118 APOE3 M: 47.695 APOE4F: 48.781 APOE4M: 48.52	APOE3 F: 4.412 APOE3 M: 5.430 APOE4F: 6.504 APOE4M: 5.415	Two-way ANOVA	G: 0.377 S:0.006 G*S: 0.0432	G: 0.544568 S:0.938898 G*S: 0.836898
H. $CMRO_2$	Animals: APOE3 F: 7 APOE3 M: 8 APOE4F: 8 APOE4M:7	APOE3 F: 185.91 APOE3 M: 158.482 APOE4F:137.07 APOE4M: 165.919	APOE3 F: 77.182 APOE3 M: 35.42 APOE4F: 29.531 APOE4M: 36.393	Two-way ANOVA	G: 1.420S:0.002 G*S: 2.624	G: 0.244117 S: 0.967487 G*S: 0.117326

Table A.8: **Statistical outputs for figure 3.8** G = Genotype, S = Sex, G*S = genotype* Sex

Figure Label	n	Mean	Standard Deviation	Test	Test Statistic	P Value
B. An Avg All Cells AUC	N = 6 animals/ genotype	APOE3:0.1806 APOE4:0.2722	APOE3: 0.0412 APOE4: 0.0727	Two – tailed unpaired t-test with Welch's Correction	t = 2.684	P = 0.0280
B. An Avg All Cells AUC	N = 6 animals/ genotype	-	-	Linear mixed model. Random factor: Animal ID	-	P = 0.03862
C. An Avg Response Frequency	N = 6 animals/ genotype	APOE3: 25.35 % R APOE4: 25.44% R	APOE3: 1.953 APOE4: 3.299	Two – tailed unpaired t-test with Welch's Correction	t = 0.022	P = 0.9827
E. An Avg Responsive Cells AUC	N = 6 animals/ genotype	APOE3: 0.9176 APOE4: 1.406	APOE3: 0.1742 APOE4:0.4029	Two – tailed unpaired t-test with Welch's Correction	t= 2.723	p = 0.0304
E. An Avg Responsive Cells AUC	N = 6 animals/ genotype	-	-	Linear mixed model. Random factor: Animal ID	-	P=0.0416
G. An Avg On/Off cells	N = 6 animals/ genotype	APOE3: 15.84/ 10.12/9.516/ 64.52% APOE4:16/8.71/ 9.43/65.84% on/off/mixed/ neither	APOE3: 2.39/2.66/2.84 /6.45 APOE4: 5.22/ 1.84/3.99 / 24.83	Multifactorial ANOVA	G: F = 0 CT: 368.4 G * CT: F= 0.16	G: p= 1 CT: p = 3.7E-29 G* CT: p = 0.923
I. An Avg Responsive PPM during stim	N = 6 animals/ genotype	APOE3: 46.18 APOE4: 45.26	APOE3: 3.172 APOE4: 4.854	Two – tailed unpaired t-test with Welch's Correction	t = 0.3896	p = 0.7603

Table A.9: **Statistical outputs for figure 4.2** G = Genotype, CT = cell type, G*CT = genotype*cell type

Figure Label	n	Mean	SD	Test	Test Statistic	P Value
A. Pia – Response frequency	n = 15 animals/G n = 60-64 vessels/ (E3/E4)	APOE3: 72.48 % R APOE4: 62.1% R	APOE3: 25.80 APOE4: 26.39	Two – tailed unpaired t-test with Welch's Correction	t = 2.214	p = 0.0287
C. Pia – Response frequency >10 trials	n = 15 animals/G n = 37-40 vessels/ g (E3/E4)	APOE3: 74.06 % R APOE4: 65.03% R	APOE3: 21.95 APOE4: 23.06	Two – tailed unpaired t-test with Welch's Correction	t = 1.761	p = 0.0824
D. Capillary Diameter – response frequency	n = 13 animals/G n = 60/71 vessels (E3/E4)	APOE3: 40.4 APOE4: 40.43	APOE3: 29.78 APOE4: 27.49	Two – tailed unpaired t-test with Welch's Correction	t = 0.005	p =0.9958
F. Capillary diameter – response frequency >10 trials	n = 13 animals/G n = 29/33 vessels (E3/E4)	APOE3: 48.53 APOE4:36.56	APOE3: 24.97 APOE4:20.21	Two – tailed unpaired t-test with Welch's Correction	t = 2.057	p = 0.0445
G. Capillary RBCV – response frequency	n = 12/11 animals (E3/E4) n = 39/37 vessels(E3/E4)	APOE3: 72.93% R APOE4: 56.05 % R	APOE3: 25.07 APOE4: 32.16	Two – tailed unpaired t-test with Welch's Correction	t= 2.543	p = 0.0133
I. Capillary RBCV – response frequency >10 trials	n = 12/11 animals (E3/E4) n = 11/8 vessels (E3/E4)	APOE3: 76.21% R APOE4: 54.35% R	APOE3: 10.6 APOE4: 23.57	Two – tailed unpaired t-test with Welch's Correction	t = 2.449	p = 0.0366

Table A.10: **Statistical outputs for figure 4.4**

Figure Label	n	Mean	SD	Test	Test Statistic	P Value
B. Pia –All Vessels AUC	n = 15 animals/ genotype n = 60-64 vessels/ genotype (E3/E4)	APOE3: 13.09 APOE4: 12.49	APOE3: 15.78 APOE4: 15.02	Two – tailed unpaired t-test with Welch's Correction	t = 0.2177	p = 0.8280
B. Pia –All Vessels AUC	-	-	-	Linear mixed model. Random factor: Vessel ID	-	0.7059
D. Pia – Responsive Trials AUC	n = 15 animals/genotype n = 59-61 vessels/ genotype (E3/E4)	APOE3: 21.69 APOE4: 22.39	APOE3: 14.26 APOE4: 14.38	Two – tailed unpaired t-test with Welch's Correction	t = 0.268	p=0.7891
D. Pia – Responsive Trials AUC	-	-	-	Linear mixed model. Random factor: Vessel ID	-	0.4861
F .Capillary Diameter – All Vessels AUC	n = 13 animals/genotype n = 60/71 vessels (E3/E4)	APOE3: 6.058 APOE4: 2.709	APOE3: 17.32 APOE4: 23.40	Two – tailed unpaired t-test with Welch's Correction	t = 0.9391	p = 0.3495
F. Capillary Diameter – All Vessels AUC	-	-	-	Linear mixed model. Random factor: Vessel ID	-	p= 0.254
H. Capillary Diameter – Responsive Vessels AUC	n = 13 animals/genotype n = 51/65 vessels (E3/E4)	APOE3: 17.49 APOE4:1 8.61	APOE3: 21.10 APOE4: 15.69	Two – tailed unpaired t-test with Welch's Correction	t = 0.3166	p = 0.7523
H. Capillary Diameter – Responsive Vessels AUC	-	-	-	Linear mixed model. Random factor: Vessel ID	-	P=0.7546
J. Capillary RBCV – All Vessels AUC	n = 12/11 animals (E3/E4) n = 39/37 vessels (E3/E4)	APOE3: 48.39 APOE4: 35.26	APOE3: 61.01 APOE4: 75.12	Two – tailed unpaired t-test with Welch's Correction	t = 0.8341	p = 0.4071
J. Capillary RBCV – All Vessels AUC	-	-	-	Linear mixed model. Random factor: Vessel ID	-	p = 0.263
L. Capillary RBCV – Responsive Vessels AUC	n = 12/11 animals (E3/E4) n = 38/32 vessels (E3/E4)	APOE3: 69.99 APOE4: 77.41	APOE3: 58.42 APOE4: 65.07	Two – tailed unpaired t-test with Welch's Correction	t = 0.4975	p= 0.6205
L. Capillary RBCV – Responsive Vessels AUC	-	-	-	Linear mixed model. Random factor: Vessel ID	-	0.9604

Table A.11: **Statistical outputs for figure 4.5**

Figure Label	n	Mean	SD	Test	Test Statistic	P Value
A. An Avg – Pia-NVCi	n = 6 animals/genotype n = 34/30 vessels (E3/E4)	APOE3: 13.7 APOE4: 5.944	APOE3: 11.6 APOE4: 10.37	Two – tailed unpaired t-test with Welch's Correction	t = 2.825	p = 0.0063
B. Vessel Avg – Pia-NVCi	n = 15 animals/genotype n = 60-64 vessels/ genotype (E3/E4)	APOE3: 68.88 APOE4: 43.70	APOE3: 83.02 APOE4: 52.57	Two – tailed unpaired t-test with Welch's Correction	t = 2.002	p = 0.0480
C. An Avg – Cap diameter-NVCi	n = 6/5 animals(E3/E4) n = 25/30 vessels (E3/E4)	APOE3: 1.107 APOE4: 0.9745	APOE3:8.05 APOE4:8.199	Two – tailed unpaired t-test with Welch's Correction	t = 0.06013	p = 0.9523
D. Vessel Avg – Cap diameter-NVCi	n = 13 animals/genotype n = 60/71 vessels (E3/E4)	APOE3: 31.87 APOE4: 9.481	APOE3:91.15 APOE4:81.90	Two – tailed unpaired t-test with Welch's Correction	t = 1.467	p = 0.1450
E. An Avg – Cap RBCV NVCi	n = 5/4 animals(E3/E4) n = 16/12 vessels (E3/E4)	APOE3: 37.74 APOE4: -3.446	APOE3: 52 APOE4: 54.53	Two – tailed unpaired t-test with Welch's Correction	t = 2.017	p = 0.055
F. Vessel Avg – Cap RBCV NVCi	n = 12/11 animals (E3/E4) n = 39/37 vessels(E3/E4)	APOE3: 254.6 APOE4: 123.4	APOE3: 321 APOE4:262.9	Two – tailed unpaired t-test with Welch's Correction	t = 1.954	p = 0.054

Table A.12: **Statistical outputs for figure 4.6**

Figure Label	n	Mean	Standard Deviation	Test	Test Statistic	P Value
D. Flux AUC	n = 15 animals/ genotype	APOE3: 20.76 APOE4: 21.13	APOE3: 12.42 APOE4: 16.76	Two – tailed unpaired t-test with Welch's Correction	t = 0.0679	P = 0.9464
E. SO_2 AUC	n = 15 animals/ genotype	APOE3: 11.68 APOE4: 9.976	APOE3: 7.214 APOE4: 10.23	Two – tailed unpaired t-test with Welch's Correction	t = 0.5271	P = 0.6027
F. HbO AUC	n = 15 animals/ genotype	APOE3: 20.82 APOE4: 18.45	APOE3:11.04 APOE4:16.24	Two – tailed unpaired t-test with Welch's Correction	t = 0.4669	P = 0.6447
G. HbD AUC	n = 15 animals/ genotype	APOE3: -3.380 APOE4: -3.951	APOE3:4.760 APOE4:6.397	Two – tailed unpaired t-test with Welch's Correction	t = 0.2773	P = 0.7837
H. HbT AUC	n= 15 animals/ genotype	APOE3: 8.513 APOE4: 7.962	APOE3: 4.883 APOE4: 6.152	Two – tailed unpaired t-test with Welch's Correction	t = 0.2716	P = 0.7880
I. $CMRO_2$ AUC	n = 15 animals/ genotype	APOE3:7.874 APOE4:8.002	APOE3:8.781 APOE4:6.964	Two – tailed unpaired t-test with Welch's Correction	t = 0.04426	P = 0.9650

Table A.13: **Statistical outputs for figure 4.7**

Figure Label	n	Mean	SD	Test	Test Statistic	P Value
A. Pia AUC.	APOE3 F: 25 APOE3 M: 34 APOE4 F:33 APOE4 M: 28	APOE3 F: 21.58 APOE3 M: 21.77 APOE4 F:24.69 APOE4 M: 19.69	APOE3F: 14.12 APOE3M:14.57 APOE4 F: 15.73 APOE4M:12.34	Two-way ANOVA	S: F= 0.831 G: F=0.037 S*G: F= 0.970	S: p = 0.364 G: p = 0.847 S*G: p = 0.327
B. Pia Response frequency	APOE3 F: 25 APOE3 M: 35 APOE4 F: 35 APOE4 M:29	APOE3 F: 67.85 APOE3M:64.86 APOE4 F:75.78 APOE4M:58.76	APOE3 F: 24.49 APOE3M:26.55 APOE4 F:27.41 APOE4M:25.16	Two-way ANOVA	S: F = 0.037 G: F = 4.47 S*G: F = 2.199	S: p = 0.848 G: p = 0.037 S*G: p = 0.141
C. Cap. Diameter AUC.	APOE3 F: 26 APOE3 M:34 APOE4 F: 33 APOE4 M: 38	APOE3 F: 3.86 APOE3 M: 7.74 APOE4 F: 10.33 APOE4 M: -3.91	APOE3 F: 8.34 APOE3M:21.84 APOE4 F: 17.73 APOE4M:25.84	Two-way ANOVA	S: F: = 2.091 G: F = 0.523 S*G: F = 6.412	S: p = 0.151 G: p = 0.471 S*G: p = 0.013
D. Cap. Diameter Response frequency	APOE3F:26 APOE3 M:34 APOE4 F:33 APOE4 M: 38	APOE3 F: 51.64 APOE3 M: 31.80 APOE4 F: 44.25 APOE4 M: 37.10	APOE3 F: 29.02 APOE3M:27.79 APOE4F: 30.70 APOE4M:24.28	Two-way ANOVA	S: 7.54 G: 0.045 S*G: 1.667	S: p = 0.007 G: p = 0.823 S*G: p =0.199
E. Cap. RBCV AUC.	APOE3 F: 16 APOE3 M: 23 APOE4 F: 18 APOE4 M: 19	APOE3 F: 53.81 APOE3 M: 44.62 APOE4 F: 62.57 APOE4 M: 9.38	APOE3 F: 80.25 APOE3M:44.74 APOE4 F: 81.37 APOE4M:59.83	Two-way ANOVA	S: 4.12 G: 0.742 S*G: 2.049	S: p = 0.046 G: p = 0.392 S*G: p =0.157
F. Cap. RBCV Response frequency	APOE3 F: 16 APOE3 M: 23 APOE4 F:18 APOE4 M: 19	APOE3 F: 75.87 APOE3 M: 70.89 APOE4 F: 60.49 APOE4 M: 51.84	APOE3 F: 17.67 APOE3M:29.36 APOE4F:34.999 APOE4M:29.54	Two-way ANOVA	S: F = 1.038 G: F = 6.62 S*G: F = 0.076	S: p = 0.312 G: p = 0.012 S*G: p =0.784
G. All ROIs AUC	APOE3 F: 914 APOE3 M: 1029 APOE4 F: 1045 APOE4 M: 1095	APOE3 F: 0.158 APOE3 M: 0.219 APOE4 F: 0.310 APOE4 M: 0.263	APOE3 F: 0.85 APOE3 M: 0.99 APOE4 F: 1.86 APOE4M:1.497	Two-way ANOVA	S: 0.022 G: 5.154 S*G: 1.591	S: p = 0.882 G: p = 0.023 S*G: p =0.207
H. All ROIs Response frequency	APOE3 F: 914 APOE3 M: 1029 APOE4 F:1045 APOE4 M:1095	APOE3 F: 24.62% APOE3 M: 28.38% APOE4 F: 30.52% APOE4 M: 25.84%	n/a	Pearson's Chi-squared, with post-hoc pairwise comparisons	Comparison	P value / Adjusted P value
					E3 F : E3 M	0.069 / 0.137
					E3 F : E4F	0.004 / 0.025
					E3 F : E4 M	0.563 / 0.563
					E3M : E4F	0.305 / 0.366
					E3M : E4M	0.206 / 0.309
					E3F : E4M	0.018 / 0.055

Table A.14: **Statistical outputs for figure 4.8**

Figure Label	n	Mean	SD	Test	Test Statistic	P Value
A. Novel object task	APOE3 Y: 8 APOE4 Y: 9 APOE3M: 7 APOE4M: 6 APOE3 O:3 APOE4 O: 0 n = animals	APOE3 Y: 0.71 APOE4 Y: 0.67 APOE3M: 0.53 APOE4M: 0.59 APOE3 O: 0.60	APOE3 Y: 0.09 APOE4 Y: 0.17 APOE3M: 0.22 APOE4M: 0.21 APOE3 O: 0.22	Two – tailed unpaired t-test with Welch's Correction	Age: 1.819 Genotype: 0.008 Age*Genotype: 0.660	Age: 0.181 Genotype: 0.928 Age*Genotype : 0.423
B. Spatial object task	APOE3 Y: 11 APOE4 Y: 12 APOE3M: 6 APOE4M: 7 APOE3 O: 0 APOE4 O: 0 n = animals	APOE3 Y: 0.615 APOE4 Y: 0.622 APOE3M: 0.54 APOE4M: 0.61	APOE3 Y: 0.09 APOE4 Y: 0.15 APOE3M: 0.13 APOE4M: 0.18	Two – tailed unpaired t-test with Welch's Correction	Age: 0.789 Genotype: 0.648 Age*Genotype: 0.457	Age: 0.381 Genotype: 0.427 Age*Genotype : 0.504
C. Locomotion measure	APOE3 Y: 14 APOE4 Y: 15 APOE3M: 11 APOE4M: 9 APOE3 O: 3 APOE4 O: 4 n = animals	APOE3Y:284.71 APOE4Y: 311.73 APOE3M: 233.73 APOE3M: 233.73 APOE4O: 218.33 APOE4O: 256.75	APOE3 Y: 63.43 APOE4 Y: 51.50 APOE3M: 61.02 APOE4M: 76.16 APOE3 O: 38.42 APOE4O: 122.41	Two – tailed unpaired t-test with Welch's Correction	Age: 6.882 Genotype: 0.841 Age*Genotype: 0.489	Age: 0.002 Genotype: 0.363 Age*Genotype : 0.616

Table A.15: **Statistical outputs for figure 5.1**

Figure Label	n	Mean	SD	Test	Test Statistic	P Value
B. An Avg. Peaks per min	APOE3 Y: 6 APOE4 Y: 5 APOE3M: 5 APOE4M: 3 n = animals	APOE3 Y: 6.19 APOE4 Y: 5.87 APOE3M: 6.41 APOE4M: 6.16	APOE3 Y: 1.02 APOE4 Y: 0.37 APOE3M: 0.84 APOE4M: 0.37	Two-way ANOVA	Age: F=0.519 Genotype: F = 0.603 Age*Genotype: F = 0.006	Age: 0.482 Genotype: 0.450 Age*Genotype: 0.938
D. An Avg. Correlation	APOE3 Y: 6 APOE4 Y: 5 APOE3M: 5 APOE4M: 3 n = animals	APOE3 Y: 0.04 APOE4 Y: 0.039 APOE3M: 0.05 APOE4M: 0.0433	APOE3 Y: 0.02 APOE4 Y: 0.027 APOE3M: 0.025 APOE4M: 0.016	Two-way ANOVA	Age: F = 0.239 Genotype: F = 0.269 Age*Genotype: F = 0.009	Age: 0.632 Genotype: 0.612 Age*Genotype: 0.927
F. An Avg. Average ΔF/F	APOE3 Y: 6 APOE4 Y: 5 APOE3M: 5 APOE4M: 3 n = animals	APOE3 Y: 1.93 APOE4 Y: 2.10 APOE3M: 1.53 APOE4M: 1.74	APOE3 Y: 0.456 APOE4 Y: 0.499 APOE3M: 0.576 APOE4M: 0.368	Two-way ANOVA	Age: F = 2.662 Genotype: F = 0.641 Age*Genotype: F = 0.006	Age: 0.124 Genotype: 0.436 Age*Genotype: 0.938

Table A.16: **Statistical outputs for figure 5.2**

Figure Label	n	Mean	SD	Test	Test Statistic	P Value
A. Pia baseline	APOE3 Y: 52 APOE4 Y: 55 APOE3M: 39 APOE4M: 36 APOE3 O: 13 APOE4 O: 16 n = vessels	APOE3 Y: 26.06 APOE4 Y: 27.39 APOE3M: 26.04 APOE4M: 25.68 APOE3 O: 25.7 APOE4 O: 20.15	APOE3 Y: 7.59 APOE4 Y: 9.34 APOE3M: 9.63 APOE4M: 7.97 APOE3 O: 7.06 APOE4 O: 6.10	Two-way ANOVA	Age: F =2.301 Genotype: F= 1.279 Age*Genotype: F=1.885	Age: 0.103 Genotype: 0.259 Age*Genotype: 0.154
B. Capillary diameter baseline	APOE3 Y:64 APOE4 Y:72 APOE3M: 47 APOE4M: 20 APOE3 O:29 APOE4 O: 30 n = vessels	APOE3 Y:3.68 APOE4 Y: 3.58 APOE3M: 3.57 APOE4M: 4.03 APOE3 O: 3.27 APOE4 O: 3.5	APOE3 Y: 1.12 APOE4 Y: 1.17 APOE3M: 1.18 APOE4M: 1.98 APOE3 O: 0.69 APOE4 O: 1.32	Two-way ANOVA	Age: F= 1.71 Genotype: F= 1.39 Age*Genotype: F= 1.14	Age: 0.183 Genotype: 0.239 Age*Genotype:0.323
C. Baseline capillary RBCV	APOE3 Y:42 APOE4 Y:41 APOE3M:40 APOE4M:17 APOE3 O: 16 APOE4 O:19 n = vessels	APOE3 Y:1.42 APOE4 Y: 1.17 APOE3M: 1.26 APOE4M: 1.22 APOE3 O: 1.50 APOE4 O: 1.23	APOE3 Y:1.05 APOE4 Y: 1.13 APOE3M: 1.36 APOE4M: 1.07 APOE3 O: 1.14 APOE4 O: 1.01	Two-way ANOVA	Age: F= 0.121 Genotype: F= 0.978 Age*Genotype: F= 0.138	Age: 0.886 Genotype: 0.324 Age*Genotype: 0.872
D. Baseline flux	APOE3 Y:15 APOE4 Y:15 APOE3M: 10 APOE4M: 8 APOE3 O: 3 APOE4 O: 4 n = animals	APOE3 Y:9.31 APOE4 Y: 11.20 APOE3M: 9.20 APOE4M: 8.68 APOE3 O: 9.87 APOE4 O: 7.76	APOE3 Y:0.84 APOE4 Y: 5.65 APOE3M: 1.85 APOE4M: 1.03 APOE3 O:1.45 APOE4 O: 1.2	Two-way ANOVA	Age: F = 1.208 Genotype: F = 0.056 Age*Genotype: F =1.490	Age: 0.308 Genotype: 0.814 Age*Genotype: 0.235
E. Baseline SO_2	APOE3 Y: 15 APOE4 Y: 15 APOE3M: 10 APOE4M: 8 APOE3 O:3 APOE4 O: 4 n = animals	APOE3 Y:47.43 APOE4 Y: 48.66 APOE3M: 46.87 APOE4M: 47.79 APOE3 O:45.4 APOE4 O: 48.18	APOE3 Y:4.81 APOE4 Y: 5.81 APOE3M: 3.81 APOE4M: 4.41 APOE3 O: 2.74 APOE4 O: 7.82	Two-way ANOVA	Age: F= 0.223 Genotype: F= 1.003 Age*Genotype: F = 0.086	Age: 0.801 Genotype: 0.322 Age*Genotype: 0.918
F. Baseline $CMRO_2$	APOE3 Y:15 APOE4 Y: 15 APOE3M: 10 APOE4M:8 APOE3 O:3 APOE4 O: 4 n = animals	APOE3 Y:171.3 APOE4 Y:150.53 APOE3M: 179.03 APOE4M: 190.17 APOE3 O: 215.74 APOE4 O: 154.55	APOE3 Y: 58.1 APOE4 Y: 35.01 APOE3M: 72.07 APOE4M: 53.16 APOE3 O:59.2 APOE4 O: 49.42	Two-way ANOVA	Age: F = 1.297 Genotype: F= 1.795 Age*Genotype: F = 1.170	Age: 0.283 Genotype: 0.187 Age*Genotype: 0.319
G. Flux CV	APOE3 Y:15 APOE4 Y:15 APOE3M:10 APOE4M:8 APOE3 O:3 APOE4 O:4 n = animals	APOE3 Y:9.31 APOE4 Y: 11.20 APOE3M: 9.20 APOE4M: 8.68 APOE3 O: 9.87 APOE4 O: 7.76	APOE3 Y: 0.84 APOE4 Y: 5.65 APOE3M: 1.85 APOE4M: 1.03 APOE3 O: 1.44 APOE4 O: 1.2	Two-way ANOVA	Age: F = 1.208 Genotype: F = 0.056 Age*Genotype: F = 1.49	Age: 0.308 Genotype: 0.814 Age*Genotype: 0.235
H. SO_2 CV	APOE3 Y:15 APOE4 Y:15 APOE3M:10 APOE4M: 8 APOE3 O: 3 APOE4 O: 4 n = animals	APOE3 Y: 5.05 APOE4 Y: 6.22 APOE3M: 4.41 APOE4M: 4.42 APOE3 O: 5.46 APOE4 O: 3.8	APOE3 Y:1.12 APOE4 Y: 6.39 APOE3M: 1.32 APOE4M: 1.01 APOE3 O: 2.75 APOE4 O: 1.35	Two-way ANOVA	Age: F = 0.72 Genotype: F = 0.018 Age*Genotype: F = 0.481	Age: 0.492 Genotype: 0.893 Age*Genotype: 0.621
I. RBCV CV	APOE3 Y:42 APOE4 Y: 41 APOE3M: 40 APOE4M: 17 APOE3 O:16 APOE4 O: 19 n = vessels	APOE3 Y:21.19 APOE4 Y: 23.93 APOE3M: 21.23 APOE4M: 27.57 APOE3 O:19.19 APOE4 O: 21.46	APOE3 Y:6.83 APOE4 Y: 7.74 APOE3M: 7.70 APOE4M: 13.55 APOE3 O:7.44 APOE4 O: 9.00	Two-way ANOVA (Multiple compar-ison with bonfferoni correction)	Age: F = 2.383 Genotype: F = 7.419 Age*Genotype: F = 0.856	Age: 0.095 Genotype: 0.007 (y = 0.4159, M = 0.0293, O = 0.99) Age*Genotype: 0.427

Table A.17: **Statistical outputs for figure 5.3**

Figure Label	n	Mean	SD	Test	Test Statistic	P Value
A. Pia Traces - young	N = 52/53 vessels (E3/E4) N = 15 animals per genotype	APOE3: 0.1-0.2Hz: 0.017 0.2-0.3Hz: 0.017 0.3-0.4Hz: 0.016 APOE4: 0.1-0.2Hz: 0.012 0.2-0.3Hz: 0.014 0.3-0.4Hz: 0.014	APOE3: 0.1-0.2Hz: 0.008076 0.2-0.3Hz: 0.006814 0.3-0.4Hz: 0.005004 APOE4: 0.1-0.2Hz: 0.005970 0.2-0.3Hz: 0.005590 0.3-0.4Hz: 0.004793	Multifactorial ANOVA to compare the effect of genotype in each frequency bin	0.1-0.2Hz: F = 9.736972 0.2-0.3Hz: F = 8.611782 0.3-0.4Hz: F = 3.911150	0.1-0.2Hz: p = 0.002343 0.2-0.3Hz: p = 0.004118 0.3-0.4Hz : p = 0.050639
B. Pia Traces - Middle	N = 29/15 vessels (E3/E4) N = animals per genotype	APOE3: 0.1-0.2Hz: 0.016 0.2-0.3Hz:0.018 0.3-0.4Hz: 0.017 APOE4: 0.1-0.2Hz: 0.012 0.2-0.3Hz: 0.014 0.3-0.4Hz: 0.015	APOE3: 0.1-0.2Hz: 0.007 0.2-0.3Hz: 0.006 0.3-0.4Hz: 0.005 APOE4: 0.1-0.2Hz: 0.007 0.2-0.3Hz: 0.006 0.3-0.4Hz: 0.004	Multifactorial ANOVA to compare the effect of genotype in each frequency bin	0.1-0.2Hz: F= 3.28 0.2-0.3Hz: F = 3.46 0.3-0.4Hz: F = 1.184	0.1-0.2Hz: p =0.077 0.2-0.3Hz: p =0.07 0.3-0.4Hz : p = 0.283
C. Pia Traces - Old	N =22/12 vessels (E3/E4) N = animals per genotype	APOE3: 0.1-0.2Hz: 0.022 0.2-0.3Hz: 0.195 0.3-0.4Hz: 0.016 APOE4: 0.1-0.2Hz: 0.014 0.2-0.3Hz: 0.014 0.3-0.4Hz: 0.014	APOE3: 0.1-0.2 Hz : 0.008 0.2-0.3Hz: 0.009 0.3-0.4Hz: 0.006 APOE4: 0.1-0.2Hz: 0.005 0.2-0.3Hz: 0.004 0.3-0.4Hz: 0.004	Multifactorial ANOVA to compare the effect of genotype in each frequency bin	0.1-0.2Hz: F= 7.52 0.2-0.3Hz: F = 3.79 0.3-0.4Hz: F = 0.723	0.1-0.2Hz: p = 0.013 0.2-0.3Hz: p = 0.06 0.3-0.4Hz : p = 0.405
D. FFTs power at 0.1Hz	APOE3Y:52 APOE4Y:53 APOE3M: 29 APOE4M: 15 APOE3 O: 12 APOE4 O: 10 n = vessels	APOE3 Y:0.013 APOE4 Y: 0.009 APOE3M:0.013 APOE4M: 0.011 APOE3 O: 0.016 APOE4 O: 0.012	APOE3 Y: 0.0097 APOE4 Y: 0.0058 APOE3M: 0.0068 APOE4M:0.0086 APOE3 O:0.008 APOE4 O: 0.004	Two-way ANOVA (Multiple comparison with bonfferoni correction)	Age: F = 1.046 Genotype: F =5.58 Age* Genotype: F = 0.187	Age: 0.354 Genotype:0.019 (y = 0.0239, M = 0.99, O = 0.687) Age*Genotype:0.830

Table A.18: **Statistical outputs for figure 5.4**

Figure Label	n	Mean	Standard Deviation	Test	Test Statistic	P Value
A. Animal Avg. AUC All cells.	APOE3 Y: 6 APOE4 Y: 6 APOE3M: 5 APOE4M: 3 n = animals	APOE3 Y: 0.18 APOE4 Y: 0.27 APOE3M: 0.18 APOE4M: 0.37	APOE3Y:0.041 APOE4Y:0.073 APOE3M: 0.21 APOE4M: 0.24	Two-way ANOVA	Age: 0.578 Genotype: 4.3 Age* Genotype: 0.511	Age: 0.458 Genotype: 0.055 Age*Genotype: 0.485
B. Animal Avg. Resp Frequency	APOE3 Y: 6 APOE4 Y: 6 APOE3M: 5 APOE4M: 3 n = animals	APOE3 Y: 25.35 APOE4 Y: 25.44 APOE3M: 28.13 APOE4M: 26.69	APOE3 Y: 4.78 APOE4 Y: 8.08 APOE3M: 16.6 APOE4M: 7.02	Two-way ANOVA	Age: 0.183 Genotype: 0.021 Age* Genotype: 0.026	Age: 0.674 Genotype: 0.888 Age*Genotype: 0.874
C. Animal Avg. AUC Responsive cells.	APOE3 Y: 6 APOE4 Y: 6 APOE3M: 5 APOE4M: 3 n = animals	APOE3 Y: 0.92 APOE4 Y: 1.41 APOE3M: 0.74 APOE4M: 1.59	APOE3Y:0.174 APOE4Y:0.40 APOE3M:0.19 APOE4M:0.95	Two-way ANOVA (Multiple comparison with bonfferoni correction)	Age: 0.0004 Genotype:11.28 Age* Genotype: 0.805	Age: 0.984 Genotype:0.004 (y = 0.1293, M = 0.0308) Age*Genotype: 0.383
D. Animal Avg. PPM during stimulation	APOE3 Y: 6 APOE4 Y: 6 APOE3M: 5 APOE4M: 3 n = animals	APOE3 Y: 46.18 APOE4 Y: 45.26 APOE3M: 36.93 APOE4M: 32.84	APOE3 Y: 3.17 APOE4 Y: 4.85 APOE3M: 4.65 APOE4M: 2.79	Two-way ANOVA	Age: 32.03 Genotype: 1.72 Age* Genotype: 0.689	Age: 0.000036 Genotype: 0.208 Age*Genotype: 0.419

Table A.19: **Statistical outputs for figure 5.5**

Figure Label	n	Mean	SD	Test	Test Statistic	P Value
A. Pia all vessels % Responsive	APOE3 Y:60 APOE4 Y: 64 APOE3M:38 APOE4M: 33 APOE3 O: 13 APOE4 O: 16 n = vessels	APOE3 Y:72.48 APOE4 Y:62.10 APOE3M: 62.60 APOE4M: 56.31 APOE3 O: 77.01 APOE4 O: 73.67	APOE3 Y: 25.80 APOE4 Y: 26.39 APOE3M: 24.16 APOE4M: 32.64 APOE3 O: 20.39 APOE4 O: 28.17	Two-way ANOVA	Age: F = 4.01 Genotype: F = 2.45 Age* Genotype: F = 0.266	Age: 0.019 Genotype: 0.119 Age* Genotype: 0.766
B. Pia diameter > 10 trials % Responsive	APOE3 Y:37 APOE4 Y: 40 APOE3M:24 APOE4M: 21 APOE3 O: 12 APOE4 O: 14 n = vessels	APOE3 Y:74.06 APOE4 Y: 65.03 APOE3M: 66.17 APOE4M: 59.65 APOE3 O:75.09 APOE4 O: 77.05	APOE3 Y: 21.95 APOE4 Y: 23.06 APOE3M: 18.83 APOE4M: 31.82 APOE3 O: 20.02 APOE4 O:25.42	Two-way ANOVA	Age: F = 2.651 Genotype: F = 1.119 Age*Genotype: F = 0.523	Age: 0.074 Genotype: 0.292 Age*Genotype: 0.594
C. Capillary diameter all vessels % Responsive	APOE3 Y:60 APOE4 Y:71 APOE3M:47 APOE4M: 15 APOE3 O: 29 APOE4 O: 28 n = vessels	APOE3 Y: 40.4 APOE4 Y: 40.42 APOE3M:40.12 APOE4M: 34.55 APOE3 O:37.66 APOE4 O:49.10	APOE3 Y: 29.78 APOE4 Y: 27.49 APOE3M:21.23 APOE4M:33.96 APOE3 O: 26.26 APOE4 O:28.80	Two-way ANOVA	Age: F = 0.615 Genotype: F = 0.243 Age*Genotype: F = 1.360	Age: 0.542 Genotype: 0.623 Age*Genotype: 0.259
D. Capillary diameter > 10 trials % Responsive	APOE3 Y:29 APOE4 Y:33 APOE3M:20 APOE4M: 7 APOE3 O: 11 APOE4 O: 17 n = vessels	APOE3 Y:48.53 APOE4 Y:36.56 APOE3M:40.44 APOE4M:46.60 APOE3 O:47.93 APOE4 O: 44.04	APOE3 Y: 24.97 APOE4 Y:20.21 APOE3M: 13.55 APOE4M: 26.06 APOE3 O: 22.44 APOE4 O: 24.26	Two-way ANOVA	Age:F = 0.234 Genotype: F = 0.489 Age*Genotype: F = 1.413	Age: 0.792 Genotype: 0.486 Age*Genotype: 0.248
E. RBCV all vessels % Responsive	APOE3 Y:39 APOE4 Y: 37 APOE3M:34 APOE4M: 12 APOE3 O: 16 APOE4 O: 17 n = vessels	APOE3 Y:72.93 APOE4 Y: 56.05 APOE3M: 55.90 APOE4M: 50.64 APOE3 O:65.90 APOE4 O: 79.00	APOE3 Y: 25.07 APOE4 Y:32.16 APOE3M: 36.5 APOE4M: 32.00 APOE3 O: 33.94 APOE4 O: 28.11	Two-way ANOVA	Age: F = 3.275 Genotype: F = 0.291 Age*Genotype: F = 2.654	Age: 0.041 Genotype: 0.590 Age*Genotype: 0.074
F. RBCV > trials % Responsive	APOE3 Y:11 APOE4 Y:8 APOE3M:5 APOE4M: 4 APOE3 O: 0 APOE4 O: 0 n = vessels	APOE3 Y:76.21 APOE4 Y: 54.35 APOE3M: 39.41 APOE4M: 52.10	APOE3 Y: 10.60 APOE4 Y: 23.57 APOE3M: 29.92 APOE4M: 2.44	Two-way ANOVA	Age: F = 6.38 Genotype: F = 0.352 Age*Genotype: F = 4.996	Age: 0.019 Genotype: 0.559 Age*Genotype: 0.035

Table A.20: **Statistical outputs for figure 5.6**

Figure Label	n	Mean	SD	Test	Test Statistic	P Value
A. Pia All Trials	APOE3 Y:60 APOE4 Y: 64 APOE3M:38 APOE4M: 33 APOE3 O: 13 APOE4 O: 16 n = vessels	APOE3Y:13.09 APOE4Y:12.49 APOE3M:6.08 APOE4M: 6.73 APOE3O: 15.51 APOE4O: 15.63	APOE3 Y: 15.78 APOE4 Y: 15.02 APOE3M: 7.03 APOE4M: 14.04 APOE3 O:10.86 APOE4 O:26.97	Two-way ANOVA	Age: F =5.47 Genotype: F = 0.001 Age* Genotype: F = 0.04	Age:0.005 Genotype: 0.982 Age* Genotype: 0.961
B. Pia Responsive Trials	APOE3 Y:59 APOE4 Y:61 APOE3M:36 APOE4M: 31 APOE3 O: 13 APOE4 O: 16 n = vessels	APOE3Y:21.69 APOE4Y:22.39 APOE3M: 12.65 APOE4M: 19.33 APOE3O: 19.51 APOE4 O: 17.83	APOE3 Y: 14.26 APOE4 Y:14.38 APOE3M:7.42 APOE4M:14.98 APOE3 O:10.06 APOE4 O: 31.97	Two-way ANOVA	Age: F = 3.407 Genotype: F = 0.593 Age* Genotype: F =1.084	Age:0.035 Genotype:0.442 Age* Genotype: 0.340
C. Capillary diameter All Trials	APOE3 Y:60 APOE4 Y:71 APOE3M:47 APOE4M: 15 APOE3 O: 29 APOE4 O: 28 n = vessels	APOE3 Y:6.06 APOE4 Y:2.71 APOE3M:0.86 APOE4M: -1.27 APOE3 O:2.19 APOE4 O:10.66	APOE3 Y: 17.32 APOE4 Y: 23.40 APOE3M: 8.44 APOE4M: 10.86 APOE3 O: 7.70 APOE4 O: 15.02	Two-way ANOVA	Age: 2.057 Genotype: 0.169 Age* Genotype: 2.548	Age: 0.130 Genotype: 0.681 Age* Genotype: 0.08
D. Capillary diameter Responsive Trials	APOE3 Y:51 APOE4 Y:65 APOE3M:44 APOE4M: 10 APOE3 O: 27 APOE4 O: 27 n = vessels	APOE3 Y:17.49 APOE4 Y: 18.61 APOE3M: 9.61 APOE4M: 12.92 APOE3 O:9.42 APOE4 O: 19.64	APOE3 Y: 21.1 APOE4 Y:15.7 APOE3M: 7.38 APOE4M:9.26 APOE3 O:5.65 APOE4 O:15.72	Two-way ANOVA	Age:2.987 Genotype: 4.17 Age* Genotype: 1.72	Age:0.053 Genotype: 0.042 Age* Genotype: 0.182
E. Capillary RBCV All Trials	APOE3 Y:39 APOE4 Y: 37 APOE3M:34 APOE4M: 12 APOE3 O: 16 APOE4 O: 17 n = vessels	APOE3 Y:48.39 APOE4 Y: 35.26 APOE3M:17.57 APOE4M:20.16 APOE3 O:47.91 APOE4 O:80.85	APOE3 Y: 61.01 APOE4 Y:75.12 APOE3M:51.63 APOE4M: 40.10 APOE3 O:58.15 APOE4 O:59.50	Two-way ANOVA	Age: 4.736 Genotype: 0.467 Age* Genotype: 1.632	Age: 0.10 Genotype: 0.495 Age* Genotype: 0.199
F. Capillary RBCV Responsive Trials	APOE3 Y:39 APOE4 Y:37 APOE3M:34 APOE4M: 12 APOE3 O: 16 APOE4 O: 17 n = vessels	APOE3 Y:72.93 APOE4 Y:56.05 APOE3M:55.90 APOE4M: 50.64 APOE3 O:65.90 APOE4 O: 79.00	APOE3 Y: 25.07 APOE4 Y: 32.16 APOE3M: 36.49 APOE4M: 32.00 APOE3 O: 33.9 APOE4 O: 28.11	Two-way ANOVA	Age:3.275 Genotype:0.291 Age* Genotype: 2.654	Age:0.041 Genotype:0.590 Age* Genotype:0.074

Table A.21: **Statistical outputs for figure 5.7**

Figure Label	n	Mean	SD	Test	Test Statistic	P Value
A. Flux AUC	APOE3 Y:15 APOE4 Y:15 APOE3M:10 APOE4M: 8 APOE3 O: 3 APOE4 O: 4 n = animal	APOE3Y:20.76 APOE4Y:21.13 APOE3M:21.83 APOE4M:26.23 APOE3O:32.60 APOE4 O: 37.27	APOE3 Y: 12.42 APOE4 Y:16.76 APOE3M:12.37 APOE4M:21.96 APOE3 O:18.86 APOE4 O:10.64	Two-way ANOVA	Age: F = 2.258 Genotype: F = 0.390 Age* Genotype: F =0.118	Age:0.115 Genotype: 0.535 Age* Genotype: 0.889
B. HbT AUC	APOE3 Y:15 APOE4 Y:15 APOE3M:10 APOE4M: 8 APOE3 O: 3 APOE4 O: 4 n = animal	APOE3 Y:8.51 APOE4 Y:7.96 APOE3M:6.998 APOE4M:8.130 APOE3 O:14.36 APOE4 O:15.03	APOE3 Y: 4.88 APOE4 Y:6.15 APOE3M:3.52 APOE4M:7.84 APOE3 O: 7.32 APOE4 O: 5.95	Two-way ANOVA	Age: F =4.16 Genotype: F =0.051 Age* Genotype: F= 0.128	Age:0.021 Genotype: 0.823 Age* Genotype: 0.880
C. HbO AUC	APOE3 Y:15 APOE4 Y:15 APOE3M:10 APOE4M: 8 APOE3 O: 3 APOE4 O: 4 n = animal	APOE3 Y:20.82 APOE4 Y: 18.45 APOE3M: 18.68 APOE4M: 20.56 APOE3 O: 39.5 APOE4 O: 37.07	APOE3 Y: 11.04 APOE4 Y: 16.24 APOE3M: 11.33 APOE4M: 19.0 APOE3 O: 24.23 APOE4 O:6.29	Two-way ANOVA	Age: 4.93 Genotype: 0.43 Age* Genotype: 0.129	Age: 0.011 Genotype: 0.837 Age* Genotype: 0.879
D. HbD AUC	APOE3 Y:15 APOE4 Y:15 APOE3M:10 APOE4M: 8 APOE3 O: 3 APOE4 O: 4 n = animal	APOE3 Y:-3.38 APOE4 Y: -3.95 APOE3M:-2.99 APOE4M: -4.25 APOE3 O:-7.80 APOE4 O: -5.90	APOE3 Y: 4.76 APOE4 Y: 6.4 APOE3M: 4.70 APOE4M: 7.2 APOE3 O: 5.06 APOE4 O: 3.84	Two-way ANOVA	Age: 0.976 Genotype:0.000172 Age* Genotype: 0.197	Age: 0.384 Genotype: 0.990 Age* Genotype: 0.821
E. SO_2 AUC	APOE3 Y:15 APOE4 Y:15 APOE3M:10 APOE4M: 8 APOE3 O: 3 APOE4 O: 4 n = animal	APOE3 Y:11.68 APOE4 Y: 9.98 APOE3M:11.14 APOE4M: 11.92 APOE3 O:23.72 APOE4 O: 21.04	APOE3 Y: 7.21 APOE4 Y: 10.23 APOE3M: 8.04 APOE4M: 12.16 APOE3 O: 15.56 APOE4 O: 5.22	Two-way ANOVA	Age: 4.311 Genotype: 0.154 Age* Genotype: 0.126	Age: 0.019 Genotype: 0.697 Age* Genotype: 0.882
F. $CMRO_2$ AUC	APOE3 Y:15 APOE4 Y:15 APOE3M:10 APOE4M: 8 APOE3 O: 3 APOE4 O: 4 n = animal	APOE3 Y:7.87 APOE4 Y: 8.001 APOE3M:10.94 APOE4M: 12.67 APOE3 O:8.84 APOE4 O: 14.87	APOE3 Y: 8.78 APOE4 Y: 6.96 APOE3M: 6.32 APOE4M:10.27 APOE3 O: 10.47 APOE4 O: 8.60	Two-way ANOVA	Age: 1.517 Genotype: 0.979 Age* Genotype: 0.366	Age: 0.229 Genotype: 0.327 Age* Genotype: 0.695

Table A.22: **Statistical outputs for figure 5.8**

Figure Label	n	Mean	Standard Deviation	Test	Test Statistic	P Value
A. PPM Cell Avg	n= 1769/1676 cells (E3/E4) n= 6/5 animals (E3/E4)	APOE3: 5.843 APOE4: 5.839	APOE3: 3.533 APOE4:3.279	Two – tailed unpaired t-test with Welch's Correction	t = 0.033	p = 0.9731
B. Correlation Coefficient FOV Avg	n = 6/5 animals (E3/E4) n = 35/33 FOV (E3/E4)	APOE3: 0.0438 APOE4: 0.0381	APOE3: 0.042 APOE4: 0.031	Two – tailed unpaired t-test with Welch's Correction	t = 0.6377	p = 0.526
C. Peak Size Cell Avg	n = 1729/1653 cells (E3/E4) n = 6/5 animals (E3/E4)	APOE3: 2.112 APOE4: 2.171	APOE3: 2.603 APOE4: 2.773	Two – tailed unpaired t-test with Welch's Correction	t= 0.5187	p = 0.5187

Table A.23: **Statistical outputs for figure B.1**

Figure Label	n	Mean	SD	Test	Test Statistic	P Value
B. Cell Avg- All Cells AUC	n = 6/6 animals n = 1943-2140 cells E3-E4	APOE3: 0.1901 APOE4: 0.2858	APOE3: 0.9235 APOE4: 1.686	Two – tailed unpaired t-test with Welch's Correction	t= 2.276	P = 0.0229
B. Cell Avg- All Cells AUC	n = 6/6 animals n= 1943-2140 cells E3-E4			Linear mixed model. Random factor: Cell ID		p=.0334
D. Cell Avg- Responsive Cells AUC	n = 6/6 animals n = 517-602 cells E3-E4	APOE3: 0.9547 APOE4:1.281	APOE3:1.487 APOE4: 2.927	Two – tailed unpaired t-test with Welch's Correction	t = 2.395	p= 0.0168
D. Cell Avg-Responsive Cells AUC	n = 6/6 animals n = 517-602 cells E3-E4			Linear mixed model. Random factor: Cell ID		p= 0.07578
E. Cell Avg – Response Frequency	n = 6/6 animals n = 1943-2140 cells E3-E4	APOE3: 26.6% R APOE4: 28.13 R	n/a	Pearson's Chi-squared test, 2x2 contingency table	X^2 = 1.187	P = 0.2760
F. Cell Avg – Responsive PPM during stim	n = 6/6 animals n = 517-602 cells E3-E4	APOE3: 45.81 APOE4: 45.22	APOE3: 25.83 APOE4: 26.41	Two – tailed unpaired t-test with Welch's Correction	t= 0.377	p = 0.7062
G. Cell Avg – On/off cells	n = /6 animals N = 1943-2140 cells E3-E4	APOE3: 16.26/ 10.55/10.34/62.84 APOE4: 17.29/ 9.16/10.84/62.71 % on/off/mixed/ neither	N/a	Chi-Square	2.886	p=0.4095

Table A.24: **Statistical outputs for figure B.2**

Figure Label	n	Mean	SD	Test	Test Statistic	P Value
A. Cell Avg. Peaks per min	APOE3 Y: 1768 APOE4 Y: 1676 APOE3M: 558 APOE4M: 500 n = cells	APOE3 Y: 5.84 APOE4 Y: 5.84 APOE3M: 6.56 APOE4M: 6.13	APOE3 Y: 3.53 APOE4 Y: 3.28 APOE3M: 3.93 APOE4M: 3.65	Two-way ANOVA	Age: 16.704 Genotype: 3.03 Age*Genotype: 2.92	Age: 0.000044 Genotype: 0.082 Age*Genotype: 0.088 :
B. FOV Avg. Correlation	APOE3 Y: 35 APOE4 Y: 33 APOE3M: 20 APOE4M: 14 n = FOVs	APOE3 Y: 0.044 APOE4 Y: 0.038 APOE3M: 0.054 APOE4M: 0.046	APOE3 Y: 0.042 APOE4 Y: 0.0307 APOE3M: 0.062 APOE4M: 0.051	Two-way ANOVA	Age: 0.906 Genotype: 0.537 Age*Genotype: 0.019	Age: 0.343 Genotype: 0.465 Age*Genotype: 0.891
C. Cell Avg. Average ΔF/F *	APOE3 Y: 1729 APOE4 Y: 1653 APOE3M: 544 APOE4M: 475 n = cells	APOE3 Y: 2.11 APOE4 Y: 2.17 APOE3M: 1.59 APOE4M: 1.76	APOE3 Y: 2.60 APOE4 Y: 2.77 APOE3M: 1.95 APOE4M: 2.29	Two-way ANOVA	Age: 26.13 Genotype: 1.532 Age*Genotype: 0.345	Age: 3.3295E-7 Genotype: 0.216 Age*Genotype: 0.557

Table A.25: **Statistical outputs for figure B.3**

Figure Label	n	Mean	Standard Deviation	Test	Test Statistic	P Value
A. Cell Avg. AUC All cells.	APOE3 Y: 1943 APOE4 Y: 2140 APOE3M: 666 APOE4M: 508 n = cells	APOE3 Y: 0.19 APOE4 Y: 0.29 APOE3M: 0.16 APOE4M: 0.40	APOE3 Y: 0.92 APOE4 Y: 1.69 APOE3M: 1.28 APOE4M: 1.84	Two-way ANOVA	Age: 0.830 Genotype: 12.57 Age*Genotype: 2.311	Age: 0.632 Genotype: 0.000397 Age* Genotype: 0.129
B. Cell Avg. Resp Frequency	APOE3 Y: 1943 APOE4 Y: 2140 APOE3M: 666 APOE4M: 508 N = cells	APOE3 Y: 26.6 R APOE4 Y: 28.13 R APOE3M: 27.02 R APOE4M: 27.56 R	N/A	Two-way ANOVA	$\chi 2$ = 1.306	P = 0.73
C. Cell Avg. AUC Responsive cells.	APOE3 Y: 517 APOE4 Y: 602 APOE3M: 180 APOE4M: 140 n = cells	APOE3 Y: 0.95 APOE4 Y: 1.28 APOE3M: 0.77 APOE4M: 1.62	APOE3 Y: 1.49 APOE4 Y: 2.93 APOE3M: 2.34 APOE4M: 3.15	Two-way ANOVA	Age: 0.236 Genotype: 14.12 Age*Genotype: 2.817	Age: 0.627 Genotype: 0.000178 Age* Genotype: 0.093
D Cell Avg. PPM during stimulation	APOE3 Y: 517 APOE4 Y: 602 APOE3M: 180 APOE4M: 137 n = cells	APOE3 Y: 45.81 APOE4 Y: 45.22 APOE3M: 37.51 APOE4M: 33.77	APOE3 Y: 25.83 APOE4 Y: 26.41 APOE3M: 21.17 APOE4M: 20.03	Two-way ANOVA	Age: 37.77 Genotype: 1.82 Age* Genotype: 0.963	Age: 1.0285E-9 Genotype: 0.178 Age* Genotype: 0.327

Table A.26: **Statistical outputs for figure B.4**

Figure Label	n	Mean	SD	Test	Test Statistic	P Value
A. Pia AUC	APOE3 DS: 19 APOE3 GMP: 34 APOE4 DS: 10 APOE4 GMP: 44 vessels	APOE3 DS:13.02 APOE3 GMP: 13.1 APOE4 DS: 28.97 APOE4 GMP: 8.76	APOE3 DS:12.69 APOE3 GMP:11.69 APOE4 DS: 17.46 APOE4 GMP: 12.94	Two – way ANOVA	G2: 11.736 APOE G: 3.914 G2 * APOE G: 11.92	G2: p = 0.001 APOE G: p = 0.051 G2 * APOE G: p =0.001
B. Pia Response Frequency	APOE3 DS:19 APOE3 GMP: 34 APOE4 DS:10 APOE4 GMP:44	APOE3 DS: 74.75 APOE3 GMP: 67.95 APOE4 DS:70.43 APOE4 GMP:58.27 % Responsive	APOE3 DS: 26.56 APOE3 GMP: 26.66 APOE4 DS:18.59 APOE4 GMP:26.52	Two – way ANOVA	G2: 2.602 APOE G: 1.419 G2 * APOE G:0.207	G2: p = 0.110 APOE G: p = 0.236 G2 * APOE G: p =0.650
C. Cap. Diameter AUC	APOE3 DS: 22 APOE3 GMP: 25 APOE4 DS:20 APOE4 GMP:40	APOE3 DS: 7.30 APOE3 GMP: 0.940 APOE4 DS: 8.20 APOE4 GMP: 1.61	APOE3 DS: 6.77 APOE3 GMP: 7.33 APOE4 DS: 40.65 APOE4 GMP: 9.89	Two – way ANOVA	G2: 2.873 APOE G: 0.042 G2 * APOE G:0.001	G2: 0.093 APOE G: p = p =0.837 G2 * APOE G: p =0.976
D. Cap. Diameter Response Frequency	APOE3 DS: 22 APOE3 GMP: 25 APOE4 DS: 20 APOE4 GMP:40	APOE3 DS: 35.84 APOE3 GMP: 35.63 APOE4 DS: 37.93 APOE4 GMP: 38.94 % Responsive	APOE3 DS: 29.20 APOE3 GMP: 26.95 APOE4 DS: 32.52 APOE4 GMP: 23.82	Two – way ANOVA	G2: 0.005 APOE G: 0.241 G2 * APOE G: 0.012	G2: p = 0.942 APOE G: p = 0.624 G2 * APOE G: p =0.913
E. Cap. RBCV AUC	APOE3 DS: 12 APOE3 GMP: 16 APOE4 DS:9 APOE4 GMP:19	APOE3 DS: 57.79 APOE3 GMP: 83.51 APOE4 DS:111.54 APOE4 GMP: 58.75	APOE3 DS: 65.02 APOE3 GMP: 64.65 APOE4 DS:98.20 APOE4 GMP: 38.68	Two – way ANOVA	G2: 0.577 APOE G: 0.662 G2 * APOE G: 4.85	G2: p = 0.451 APOE G: p = 0.419 G2 * APOE G: p =0.032
F. Cap. RBCV Response Frequency	APOE3 DS: 12 APOE3 GMP: 16 APOE4 DS: 11 APOE4 GMP: 20	APOE3 DS: 71.20 APOE3 GMP: 79.29 APOE4 DS: 62.47 APOE4 GMP: 54.21 % Responsive	APOE3 DS: 23.70 APOE3 GMP: 20.09 APOE4 DS: 37.74 APOE4 GMP: 26.38	Two – way ANOVA	G2: 0.0001 APOE G: 5.53 G2 * APOE G: 1.29	G2: p = 0.991 APOE G: p = 0.022 G2 * APOE g: p =0.261

Table A.27: **Statistical outputs for figure B.5** G2: Secondary genotype (NG2DsRed or Thy-GCaMP6f), APOE G: APOE genotype, G2 * APOE G: Secondary genotype * APOE genotype

Appendix B

Appendix B

B.1 Supplementary Figures

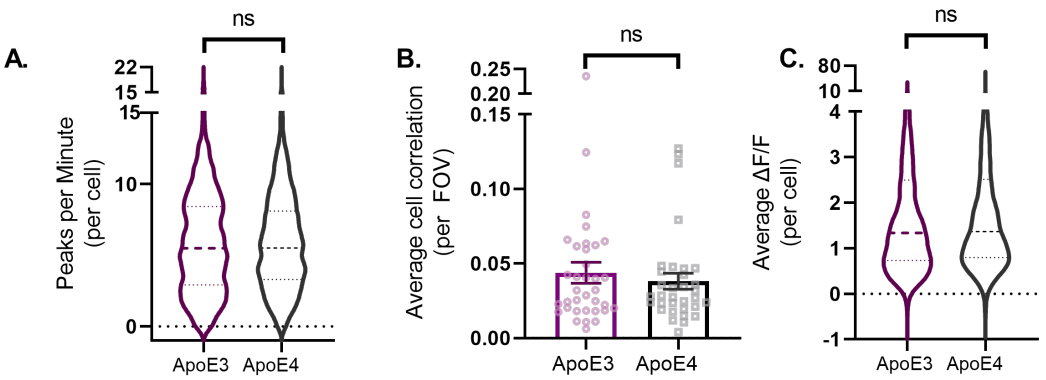

Figure B.1: **Neuronal activity during rest. Cell Average** A. Number of peaks per minute during rest. B. Average correlation of firing per field of view (FOV). C. Average ΔF/F of peaks during rest. Circles represent FOV and violin plots show data from all cells. Error bars represent SEM. For detailed statistical output see table A.23.

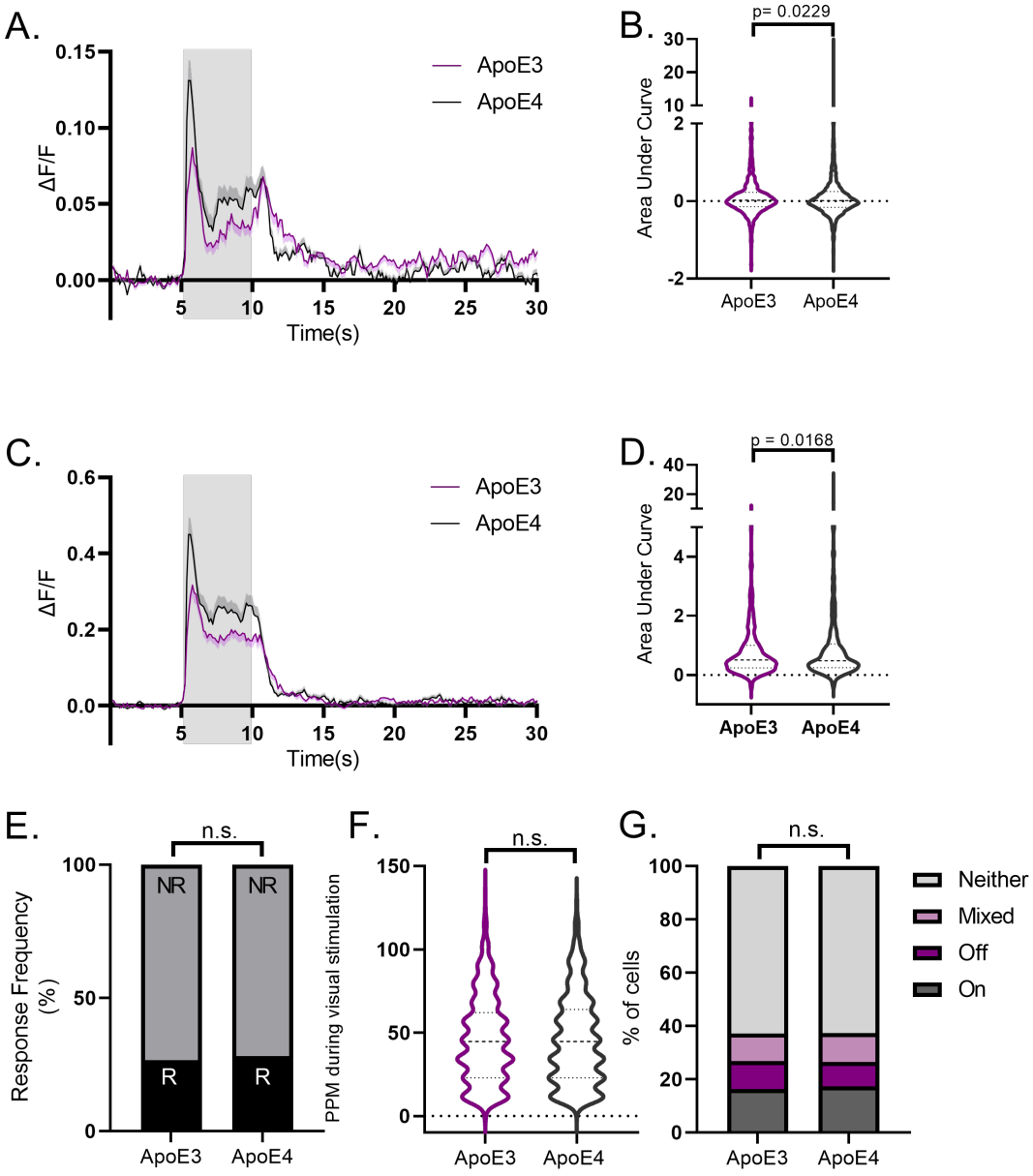

Figure B.2: **Neuronal activity during visual stimulation. Cell Average** A. Average ΔF/F traces of all cells in responsive to visual stimulation. B. AUC measurements for cell averages shown in A. C. Average ΔF/F trace of all responsive cells. D. Area under curve measurements for the responsive cells shown in C. E. Response frequency of cells in ApoE3 and ApoE4 animals. F. PPM values for all responsive ApoE3 and ApoE4 cells. G. The distribution of cell types in ApoE3 and ApoE4 animals. Grey rectangles represent the onset and offset of visual stimulation. Error bars represent SEM. For detailed statistical output see table A.24

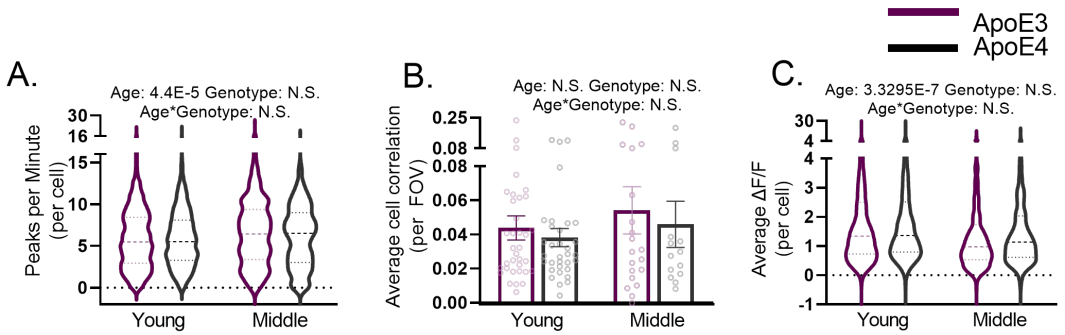

Figure B.3: **Effect of age and APOE on neuronal activity during rest. Cell average.** A. Number of peaks per minute during rest. B. Average correlation of firing per field of view (FOV). C. Average $\Delta F/F$ of peaks during rest. Circles represent FOV and violin plots show data from all cells. Error bars represent SEM. For detailed statistical output see table A.25

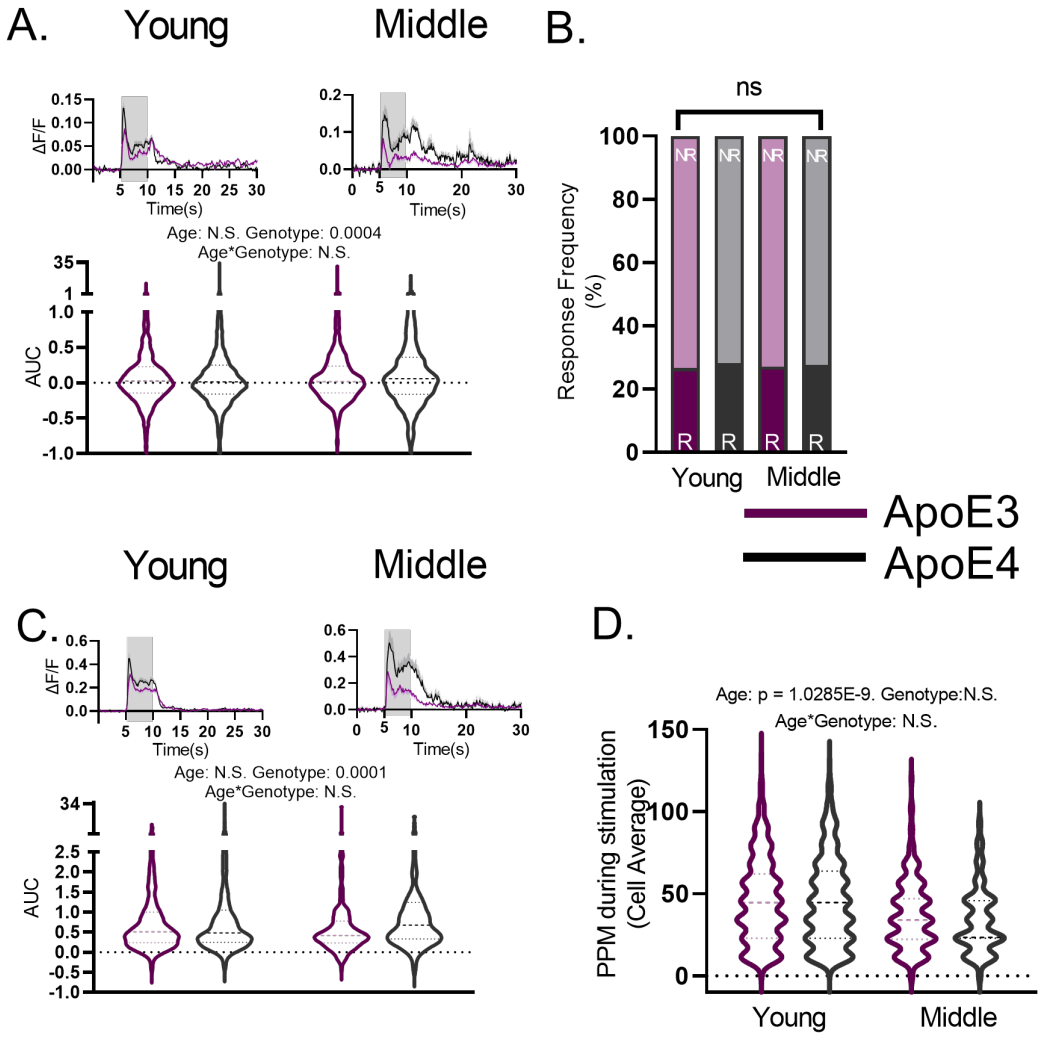

Figure B.4: **Effect of age and ApoE on neuronal responses to visual stimulation**. A. Top panels show average ΔF/F traces across all cells, in response to visual stimulation in young and middle aged mice, averaged per cell. Bottom panel shows AUC measurements for each cells ΔF/F trace during visual stimulation. B. Response frequency of cells to visual stimulation in both young and middle aged animals. R = responsive, NR = non-responsive. C. Top panels show average ΔF/F traces across responsive cells only, in response to visual stimulation in young and middle aged mice, averaged per cell. Bottom panel shows AUC measurements for each responsive cells ΔF/F trace during visual stimulation. D. Number of peaks per minute for each cell during visual stimulation. Error bars represent SEM and violin plots show data from all cells. For detailed statistical output see table A.26

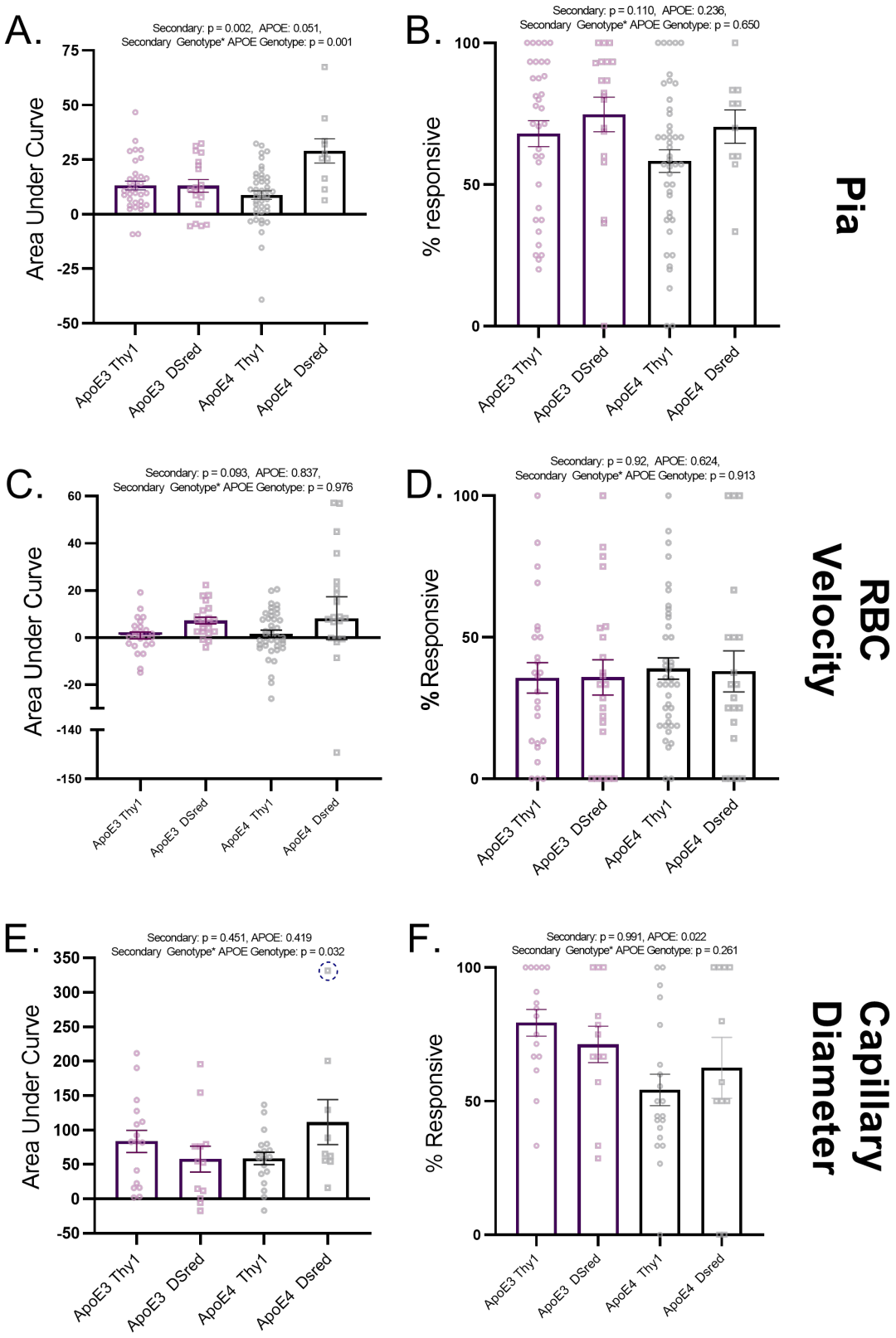

Figure B.5: **The effect of secondary genotype on response size and frequency**. A. Responsive pial vessel AUC, split by secondary genotype for ApoE3 and ApoE4 mice. B. Pial vessel response rate, split by secondary genotype for ApoE3 and ApoE4 mice. C. Responsive capillary RBCV AUC, split by secondary genotype for ApoE3 and ApoE4 mice. D. RBCV response rate, split by secondary genotype for ApoE3 and ApoE4 mice. E. Responsive capillary AUC, split by secondary genotype for ApoE3 and ApoE4 mice. F. Capillary response rate, split by secondary genotype for ApoE3 and ApoE4 mice. Individual points represent vessels, error bars represent SEM. For detailed statistical output see table A.27.